UNCLASSIFIED

AD NUMBER:	AD0809224

LIMITATION CHANGES

TO:

Approved for public release; distribution is unlimited.

FROM:

Distribution authorized to U.S. Gov't. agencies and their contractors; Export Controlled; 14 Feb 1967. Other requests shall be referred to Naval Air Systems Command, Washington, DC 20350.

AUTHORITY

THIS PAGE IS UNCLASSIFIED

PARAMETRIC INVESTIGATION OF VTOL
HOT GAS INGESTION AND
INDUCED JET EFFECTS
IN GROUND PROXIMITY

NOR 67-32

FINAL REPORT
14 FEBRUARY 1967

By
RAHIM LAVI

NORTHROP NORAIR

FOREWORD

CONTENTS

CONTENTS (continued)

TABLES

ILLUSTRATIONS

ILLUSTRATIONS (continued)

ILLUSTRATIONS (continued)

NOMENCLATURE

H	Vehicle height above ground
D	Nozzle diameter - 12.75 in.
P_N	Nozzle total pressure - psia
P_∞	Ambient pressure - psia
F	Installed thrust in ground effect - lbs.
F_{MAX}	Maximum engine thrust with no ingestion based on P_N/P_∞
N	Engine rpm
L_{JE}	Jet-induced lift - lbs
L	Net lift in ground effect ($L = F + L_{JE}$) - lbs
L_∞	Lift out of ground effect - lbs
P_S	Static pressure - psia
$\dfrac{\Delta M}{L_\infty \bar{C}}$	Pitching moment parameter $= \left(\dfrac{M}{L_\infty \bar{C}}\right)_{H/D = 8.7} - \left(\dfrac{M}{L_\infty \bar{C}}\right)$ in ground effect
V	Velocity - ft/sec
A_P	Plate area ft^2
A_j	Jet area ft.^{2}
$Y_{1/2}$	Height above ground at which $V = \frac{1}{2}\ V_{MAX}$
T	Temperature (F)
X	Radial distance from nozzle centerline
h	Thermocouple height above ground
$\dfrac{T - T_\infty}{T_{max} - T_\infty}$	: Ground jet temperature increment above ambient divided by the ground jet maximum temperature increment above ambient
α	Pitch attitude (degrees)
δ	$P_\infty/14.7$
θ	$T_\infty/518.7$
ρ	Density - lbs/ft^3

SUMMARY

A large-scale boiler-plate VTOL test bed designed around the Ames Lift Engine Pod was used for ground-proximity tests at the Ames Research Center VTOL test facility. The test program was conducted under the sponsorship of the Naval Air Systems Command, Washington, D. C. The primary program objectives were to obtain parametric data on gas ingestion and jet effects experienced by a number of jet-powered VTOL configurations.

The results showed, as expected, that both ingestion and induced-lift effects are strongly configuration- and time-dependent, and for many configurations the degree of ingestion experienced cannot be tolerated in operational aircraft. This contrasts with the results of recent small-scale tests, in which relatively uniform and low temperature rise resulted from hot gas ingestion.

The geometry effects are interdependent and their influence on ingestion characteristics cannot often be isolated. Wing geometry, size, location; engine arrangement; lift/cruise engine location and pitch attitude have a strong influence on ingestion tendencies and jet-induced effects. The severity of the near-field temperature environment appears to be strongly influenced by engine arrangement and to a lesser degree by the number of operating engines.

Rapid inlet temperature rise with a high temperature distortion at the compressor face sometimes resulted in engine stall. Also, internal hot gases expelled from the engine subsequent to stall occasionally caused stalling of adjacent engines. Large induced force levels and moments resulted from near-ground operation of many configurations; both positive- and negative-induced lift was measured.

Aerodynamic suckdown results obtained with a single jet-fundamental geometry configuration are in excellent agreement with an empirical correlation of small-scale tests.

The results also showed that transient measurements with rapid-response thermocouple and recording equipment are needed for realistic assessment of the VTOL environment and inlet temperature rise caused by ingestion.

I. INTRODUCTION

A potentially severe operational problem for jet lift VTOL aircraft in ground proximity is ingestion of hot exhaust gases by the engines, resulting in loss of net thrust. Jet-induced lift effects also pose a serious problem in near-ground operation in terms of aircraft net lift capability and moment imbalance. Lift loss due to ingestion and negative induced lift (suckdown) cannot be tolerated during lift-off since all lift is provided by the engines. Various investigations have shown (Refs. 1, 2, 3) in general that gas ingestion flow phenomena and jet-induced lift effects are configuration- and time-dependent. However, recently published small-scale tests (Ref. 4) show that gas ingestion is not time-dependent and is relatively insensitive to configuration changes.

Small-scale tests have been useful in providing indications of ground proximity jet effects, but not conclusive results applicable to full-scale configurations, or sufficient data upon which to base design decisions. Most were limited to a single jet, even though the majority of proposed VTOL designs required several lift engines (or composite arrangements of lift and lift/cruise engines). With the shortcomings of small-scale tests in mind, Northrop in cooperation with NASA-Ames embarked on a program to provide realistic hot-gas ingestion and jet-effects data on a full-scale vehicle. This program was organized around the NASA-Ames VTOL lift-engine pod, and conducted at the Ames outdoor VTOL test facility. The objective was primarily to obtain design data applicable to composite-configured (lift-plus-lift/cruise engines) supersonic VTOL fighter aircraft.

The modified Ames lift-engine pod with five in-line lift engines in the fuselage and two lift/cruise engines in the tail was an excellent tool for further investigations of ground-proximity effect beyond the previous Northrop-Ames cooperative test program (Ref. 5). In addition to providing realistic hot-gas ingestion data, the jet-lift engine arrangement in a full-scale test bed gave an insight into scaling effects by the comparison of full-scale data with the data obtained from similar small-scale models. Once scaling effects are understood, the value of small-scale tests may be determined, and may possibly be used to predict full-scale effects.

The Naval Air Systems Command authorized a full-scale test program as a follow-on to the Northrop-Ames cooperative program. The modified lift-engine pod was used to explore the influence of wing location and wing geometry as well as the influence of lift and lift/cruise engine location, on hot-gas ingestion and jet-induced ground effects at various heights above ground. To compare these results with previous small-scale results, certain selected configurations were geometrically similar to a 1/10th-scale model tested by Bell Aerosystems Company under a U.S. Navy sponsorship (Refs. 6, 7).

This report presents and discusses the results of the program conducted under sponsorship of Naval Air Systems Command, Washington, D. C.

1

II. PROGRAM OBJECTIVES

The primary objectives of the program were: (1) to obtain parametric design data on hot-gas ingestion experienced by a number of VTOL aircraft configurations powered by multijet propulsion systems, and to define engine inlet-temperature rise during ground-proximity operations; (2) to determine jet-induced force levels and characteristics during near-ground operation; (3) to explore scaling effects by comparing the results of full-scale tests with the results of small-scale tests of geometrically similar configurations.

III. MODEL DESCRIPTION

The test vehicle was designed around the Ames Lift Engine Pod. The basic Ames pod (Fig. 1) consisted of five interchangeable engine modules, each mounting a J85 dry engine with a bell-mouth inlet. The pod was supported from a stub wing. The lift-engine pod was modified (for a cooperative Northrop-Ames test program) to more closely simulate potential supersonic VTOL fighter configurations. The modified test model is shown in Fig. 2.

The design philosophy behind the Ames lift-engine pod modification was the creation of a basic test model from which a large number of jet-lift VTOL configurations could be evolved (Ref. 8). This flexibility was achieved by providing, (1) the capability for attaching various wing geometries at selected fuselage locations; (2) variable lift/cruise engine inlet locations; (3) the capability of employing various lift or lift/cruise engine arrangements; and (4) the thrust-vectoring capability to obtain representative VTOL operational environment. Modifications to the pod included a long, faired nose section, and an extension of the afterbody to provide realistic VTOL environment representative of actual airplane configurations. Two additional Y-J85 engines were mounted in the tail section to represent the lift/cruise engines of a typical composite VTOL airplane configuration. The engines were fitted with right-angle tailpipe and deflector doors to provide VTOL-mode exhaust environment.

Two lift/cruise inlet locations were provided, one on top of the aft fuselage (Figs. 3 and 4) and the second on the side of the fuselage (Figs. 3 and 5) just forward of the wing leading edge.

One delta and two swept-wing planforms were evaluated. The wings were mounted interchangeably at the three fuselage heights (low, mid, and high) shown in Figs. 6, 7 and 8. The wing geometries were the same as those evaluated in a 1/10-scale model by Bell Aerosystems (Ref. 6), and specifically selected to provide a geometrically similar model for scaling effects.

Remotely-actuated jet deflector doors (Fig. 9) were installed for all seven engines to provide full-scale simulation of an operational VTOL configuration, and to divert the hot exhaust gases aft and away from the vehicle prior to the start of a test run. The lift engines were mounted with a 10-degree incline aft; small exhaust control doors (Fig. 9) were therefore provided, in addition to the deflector doors, to permit simulation of the downward exhaust flow of a vertically-mounted lift engine.

A 10'-by-10' flat plate was mounted flush to the exhaust nozzle of Number 4 Engine (Fig. 10) for a special test series to evaluate jet-induced lift effects scaling factors. The hydraulic actuators used for thrust vectoring are also shown. (The hydraulic equipment on the right-hand side created an asymmetrical airplane configuration.)

5

The test configurations in Table 1 were selected to obtain parametric ground proximity data as well as basic design information. Each configuration was selected to obtain such desired effects as the influence of wing geometry, size, location, and also to establish specific configuration trends. Not all evaluated configurations were therefore necessarily potential and workable VTOL configurations; some were selected to obtain parametric data as well as data for scaling-effect studies.

IV. STATIC TEST FACILITY

The test program was conducted at the NASA-Ames Research Center Static Test Facility. This is an outdoor complex designed to support powered models and aircraft at varying ground heights and angles of attack for hover tests. Within this complex, Ames maintains a VTO Thrust Stand incorporating: (1) A fixed ground plane test site; (2) a towable trailer containing the motorized model support struts; (3) an office-type instrumentation trailer. The support trailer and ground plane formed a flat 80-by-90-foot area, providing an adequate expanse for the selected model. The test vehicle was mounted on the thrust stand by three beams, two extending from opposite sides of the fuselage just forward of the wing, and the third extending below the nose to take out pitch loads via a toggle mechanism (Fig. 11). The engines exhausted aft of the primary mounting struts, minimizing flow interference by the struts. Two-axis load cells were located on each side of the main support beam; the third was attached through the load cell at the nose. All power to, and instrumentation from, the vehicle was routed either under the ground plane or along the top of one of these support arms. Tests were conducted at vehicle heights varying between approximately 3.2 and 11 feet, and pitch attitudes of -4 to +4 degrees.

A small office trailer, located approximately 50 feet from the stand, served as a control room containing all data-recording equipment and the two engine-run consoles, one controlling the five lift engines, the other the two lift/cruise engines. All engine instrumentation (rpm, exhaust gas temperature, throttle position indicator, etc.) as well as throttle actuator control switches, and controls for starter, ignition, deflector doors, and hydraulics were installed in this trailer.

Electrical and hydraulic power, cooling water, fuel, and compressed air were supplied to the test stand.

V. INSTRUMENTATION

The test instrumentation was designed to obtain realistic data representative of an operational VTOL aircraft. Sensing and recording devices to obtain transient measurements were therefore employed to the greatest extent possible, to show the characteristics of the vehicle, its environment as well as engine performance. The instrumentation was as follows:

1. Vehicle Force and Moments. The model was mounted on three biaxial load cells, one at each tip of the main support beam, and one at the nose support point (Fig. 3). The main beam load cells recorded both normal and axial force measurements, and the nose beam cell, normal only. This was possible because the upper end of the support stand nose beam was connected to the load cell through a toggle arm, to allow the vehicle to be pitched. The toggle also served, however, to transmit only vertical loads (plus small horizontal loads resulting from its inclination from the vertical) to the load cell. These horizontal interaction loads were accounted for in the data reduction equations. The five force-data channels were recorded on a CEC oscillograph and reduced to three components: normal force, axial force, and pitching moment. The vehicle/load cell system was calibrated to 8,000-pound total axial force, 16,000-pound total normal force, and 1,000,000-pound-inch pitching moment. All first-order interactions were considered in the equations.

2. Engine Performance Parameters. Engine rpm and exhaust-nozzle total pressure and temperature of each engine were recorded continuously on an oscillograph during each test. Indications of engine speed and exhaust-gas temperature for all engines were also provided in the engine-control console, and monitored by the operators during each test.

3. Engine Inlet Temperatures and Pressures. To reproduce the actual temperature transients in the inlet, highly responsive thermocouples would have been required. However, those of sufficiently small thermal mass might not have survived the hostile vibration and acoustic environment of the engine inlet. In view of these practical limitations, and the large number of thermocouples needed to define the inlet temperature field, some compromise had to be made.

The objective was a capability for measuring inlet temperature rise causing engine thrust loss under quasi-steady conditions. To determine thrust degradation resulting from hot gas ingestion, measurements of short-duration pulses of the order of a few milliseconds are not required because of the relatively low thrust response of the engine to changes in inlet temperature (time constant of the order of 100 milliseconds). For an evaluation of this type, some damping of the instantaneous temperature field is acceptable. On the other hand, configurations developing exhaust-gas ingestion severe enough to result in engine stall, from rapid localized temperatures within the engine inlet, would have required undamped measurements of these temperature pulses for evaluation of engine stall characteristics.

9

Iron-Constantan (30-gage) 0.01-inch diameter thermocouples were used to evaluate the inlet temperature history. These have adequate response characteristics for determining the quasi-steady thrust degradation, although not the required response time to accurately assess the large, rapid temperature rises experienced prior to engine stall.

Eight thermocouples were installed in the inlets of all engines. The installation consisted of two rakes with three thermocouples each, located on the forward and left side radii, and single thermocouples near the outer wall on the aft and right side. The thermocouple installation of Number 1 Engine was later modified to incorporate four rakes with three thermocouples each, to obtain a better definition of inlet-temperature distortion. The rake thermocouples were spaced to define inlet temperatures over approximately equal flow areas. The inlet thermocouple arrangement is shown in Fig. 12. A high-temperature (150°F) reference system was used, and the outputs of the thermocouples continuously recorded by color traces on oscillographs to obtain response within the limitations of the thermocouple junction and distinction of traces for easy identification. The time constant for the thermocouple-recording system combination was of the order of 100 milliseconds. A detailed evaluation of thermocouple response characteristics is presented in Appendix A.

Inlets of Number 1 and 2 Engines were instrumented for measurements of total and static pressures. The pressure instrumentation was added during the test program to obtain an insight into the level of pressure distortion and its influence on engine stall. Fig. 12 shows the pressure rake and static and total probe arrangement. The inlet pressures were measured on a manometer board and recorded photographically.

4. Vehicle Pressures. Static pressure taps were located on the underside of the fuselage, wings and horizontal tail (Fig. 13). These pressures were also measured on a water manometer board and recorded photographically. In addition, transient static pressure measurements from transducers at four locations on the wing lower surface were oscillographically recorded for transient comparisons with steady-state manometer measurements.

5. Vehicle Proximity Pressures and Temperatures.

    a. Temperature Field. Eleven I/C thermocouples measured near-ground temperature field in the proximity of the vehicle. Seven were installed on a plate which could be mounted at selected locations on the ground plane. The remaining four were mounted on a rake at a distance of 1.75 to 18.75 inches off the ground. Fig. 14 shows the typical location of ground-proximity instrumentation. Ground plane thermocouples (Locations 1, 2, 3, 4, 5, 7, 8) and the thermocouple rake (Location 6) are shown in Fig. 14.

    Three additional rakes, each with four thermocouples, (30-gage) were permanently fixed at Locations 11, 12, and 13, from 48 to 120 inches from the vehicle center line. Location 11 was chosen closer to the model to avoid interference from the vehicle main mounting strut. Two other thermocouples (30-gage) were installed 45 inches above the lift engines 1 and 5, as shown in Fig. 14. The four-thermocouple rakes were installed in locations comparable to small-scale test rakes (Ref.

6), to specifically obtain temperature-scaling data. Measurements of all thermocouples were obtained on color oscillograph traces.

    b.   <u>Pressure Field.</u> Eleven static probes, to map the ground-plane pressure environment, were installed adjacent to the ground plane thermocouples at Locations 1 through 8 shown in Fig. 14. The pressures were measured on a manometer board and photographically recorded.

6.   <u>Vehicle Temperatures.</u> Thermocouples installed in selected locations monitored temperatures in the hydraulic system, on heat-sensitive electrical equipment, engine accessories and vehicle structure (Fig. 15). The vehicle temperatures were monitored on a Brown Multipoint recorder; each location was sampled once every 15 seconds.

7.   <u>Ambient Instrumentation.</u> Prior to each run, readings of ambient temperature, barometric pressure, and wind velocity and direction were hand recorded. Ground-plane anemometer locations are shown in Fig. 16.

8.   <u>Special Tests Instrumentation.</u> For the special test of Configuration A_1, to determine jet-induced lift effect and ground jet velocity profiles and velocity decay for comparison with small-scale data, the following instrumentation was employed:

    a.   Sixteen static-pressure taps were installed on the 10-by-10-foot plate (Fig. 17) attached to the nozzle exit. Nine were located on a radius from the nozzle to the edge of the plate. Two rows of static probes were also located at 45 and 90 degrees from the initial radial location, at selected distances from the nozzle edge, to check circumferential pressure distortions on the plane.

    b.   A total-pressure rake of 11 probes (Fig. 17) located between 0.2 and 10 inches from the ground plane, and a static-pressure rake of six probes similarly located, were used to define ground jet velocity profiles. The rakes were mounted on the ground plane at various distances from the nozzle centerline.

    c.   A temperature rake (Fig. 17) with six thermocouples ranging from 0.2 to 10 inches from the ground plane was also used to map the near-ground temperature field. The thermocouple and the two pressure rakes were mounted on the same stand at various distances from the nozzle centerline. The thermocouple measurements were oscillographically recorded.

VI. TEST PROCEDURE

The test procedures were designed to yield meaningful data representative of an operational VTOL aircraft. Quick thrust-vectoring techniques may be employed in such an aircraft to preclude rapid inlet-temperature rise at takeoff, and this technique was therefore employed in all test runs. The normal procedure was to start and stabilize the engines at 70 percent rpm, with the exhaust vectored rearward by the exhaust deflector doors to preclude ingestion prior to the start of the run. An effective vectoring angle of 50 degrees from vertical was selected as operationally representative. The initial engine speed of 70 percent rpm which is greater than the normal idle speed for a J85 was selected to allow engine accelerations to 100 percent rpm in one second. On signal, the vectoring doors were rotated and downward flow was achieved in one second. Subsequent to door deflection, approximately two seconds were allowed for flow stabilization prior to acceleration of the engines to maximum rpm. Maximum power was held for approximately 15 seconds for each run. The selected test duration was longer than usual for a typical VTOL aircraft rising to a height beyond ground effect. This longer time, however, might be experienced during hover and landing operations. Data recording began when the engines were stabilized at 70 percent rpm, and continued to the end of the run.

Each configuration was evaluated at heights of 3.2 to 11 feet above ground plane corresponding to (H/D) values of 2.5, 3.5, 4.5, 6.0 and 8.7. Selected configurations were evaluated at pitch attitudes from -4 to +4 degrees.

VII.   DATA REDUCTION

To present the vast amount of test data in useful engineering form, mechanized data reduction was extensively used.   The oscillograph traces were read on an Oscillograph Automatic Reader (OSCAR) to obtain data in digitized form.   Each trace was read at preselected location at approximately one second intervals.   Some traces, however, were read more frequently to obtain detailed information on engine thrust, inlet temperature rise and other pertinent parameters.   Pressure data were read on a film reader, and digitized data in card form were obtained.   Digitized oscillograph and manometer data were used in computer programs to obtain the various parameters of interest in tabular form.   In addition, selected parameters were machine-plotted.

The data reduction was directed toward defining the maximum performance degradation for a test condition resulting from hot-gas ingestion and jet-induced effects. The character of the transient data (Fig. 21) was such that a considerable degree of engineering judgment was needed to establish realistically the various trends and effects.   It is therefore pertinent to discuss the methods utilized so the reader may interpret the presented data.   The data reduction methods are delineated below.

1.   Inlet Temperature Rise

For ingestion-prone configurations a sporadic inflow of hot exhaust gases, causing inlet temperature rise, generally occurred shortly after engine acceleration to 100 percent rpm.   The magnitude and duration of temperature rise varied considerably over the compressor face.   The criterion for reading the transient inlet temperature data was to select times at which the spatial average inlet temperature rise appeared to be high, and for which the duration of the temperature rise was at least 100 m.s.   Although higher spatial average inlet temperature rises could be found to exist for periods less than 100 m.s., full response of the engine (in terms of thrust loss) to inlet temperature transients requires approximately 100 m.s.   This interval, however, was not always detectable by inspection of the inlet temperature data, since all temperature traces did not necessarily rise at the same time. Since the maximum value of the spatial average temperature rise was not usually discernible by inspection -- because of the generally out-of-phase characteristics of individual thermocouples -- several time-intervals, representing a high average inlet temperature rise, were selected.   The engine thrust parameter (exhaust gas total pressure) was also inspected to insure that the minimum thrust point (corresponding to maximum average inlet temperature rise) had been properly identified.   The measured local inlet temperatures were area-weighted to obtain an average inlet airflow temperature.

For multiengine configurations the thrusts of all operating engines were added at the point at which the total thrust was minimum.   The representative inlet temperature rise, thrust loss, and pitching moment parameters for a given H/D and α were then presented at this point.   It is emphasized that the highest inlet temperature rise of an individual engine did not necessarily occur at this point; rather, the overall combined temperature rise for all engines was highest at this time.   Additional data showing the maximum inlet temperature rise for each engine were calculated and machine-plotted automatically.

15

2. Engine Parameters

Engine rpm, exhaust gas temperatures, and pressures were read on the OSCAR at the preselected time intervals described above. The engine thrust at each point was calculated from the exhaust gas pressure (P_N/P_∞) and known nozzle area. The thrust-loss parameter ($F/F_{MAX.}$) was machined-calculated and plotted versus time. The maximum engine-corrected thrust (F_{MAX}/δ) corresponding to maximum corrected rpm ($N/\sqrt{\theta}$) obtained from engine performance curves was selected by the computer for each engine. This procedure was used to accurately establish maximum total thrust which could have been achieved with no ingestion during the run. Thus, the thrust degradations due to low rpm or lag in rpm could be identified and separated from vehicle lift losses due to ingestion and jet-induced effects. The total available thrust ($\Sigma F_{MAX.}$) was used in evaluations of vehicle net-lift capability in ground effect.

3. Vehicle Pressure Data

The static pressure data from wings and fuselage were read on a film reader to obtain tabulated digitized data. The static pressures were then integrated by the computer over the wing and fuselage areas (area of the underside of the wing and fuselage) to obtain jet-induced force levels.

The jet-induced force levels (L_{JE}) obtained from the integration of vehicle pressures were used together with the thrust data based on measured P_N/P_∞ to obtain vehicle net lift in ground proximity ($L = \Sigma F + L_{JE}$).

4. Load Cells

The cantilever arrangement of the vehicle on the thrust stand resulted in oscillation of the vehicle about the main beam, which was reflected in the load cell data. The load cell traces, in general, were oscillatory and the amplitude of the oscillations varied with number of operating engines as well as engine locations. Generally, the amplitude and frequency of the oscillations were such that a mean line could be easily drawn through the traces. The mean load cell values were read on the OSCAR at the preselected points corresponding to the point where inlet temperatures and engine data were also evaluated. The load cell data were used to determine vehicle net lift (L), jet-induced effects ($L_{JE} = L - \Sigma F$), and pitching moment effects. The net lift obtained by this method was used to supplement the combined thrust-pressure integration method described in (2) and (3), above. The data presented in various plots (L/L_∞), (L_{JE}/L_∞), and data of Table II are based on the thrust and pressure integration method.

VIII RESULTS

The near-ground characteristics of the various configurations were evaluated on the basis of average inlet-temperature rise due to ingestion, and jet-induced force and moments. In addition, detailed analyses of selected configurations were made to determine inlet-temperature distortion level, inlet-temperature rise resulting in engine stall, and local forces created by jet-induced flow or jet impingement on the lower vehicle surfaces. In general, the data are presented in terms of performance degradation due to: (1) gas ingestion; (2) jet-induced force and moments; and (3) combined effects of ingestion and jet-induced force levels. This will permit independent evaluation of the configurations of interest by the reader beyond the analyses made in this section.

A. General

1. Character of data - basically two types of inlet-temperature rise were observed:

   (1) relatively flat temperature traces with very little distortion, associated with configurations having little or no ingestion; and (2) temperature traces of a highly transient character, with localized temperature peaks as high as 200 F associated with ingestion-prone configurations. The lift-engine inlet temperature rise for ingestion-prone configurations was generally localized, and occurred over time intervals ranging from a few milliseconds to several seconds. This is in sharp contrast to the small-scale ingestion data presented in Ref. 6, in which gradual inlet temperature rise with time is exhibited. The lift/cruise engines exhibited the same transient characteristics, but the temperature rise was uniform over the compressor face, resulting in a minimum distortion level. This was due to the mixing of the ingested gases in the long ducts before reaching the thermal instrumentation immediately ahead of the compressor face. A comparison of the typical distortion levels between lift and lift/cruise engine inlets is shown in Figs. 18 and 19.

   In view of the highly transient nature of the temperature rise and distortion level of ingestion-prone configurations, it was desirable to determine the repeatability of the temperature data. Configuration C_4 was tested three times at H/D = 4.5 and $\alpha = 0$, at a wind velocity of approximately 5 feet/second. The temperature-time histories of (Fig. 20) the three runs showed the same general transient characteristics, although variations in the maximum value of the spatial average inlet-temperature rise was observed. Engines 1 and 2 developed relatively lower temperature rise during the first 8 seconds of runs 1 and 3. However, higher ingestion levels (similar to run 2) occurred during the latter portion of the run. The following table shows maximum spatial average inlet temperature rise calculated for each engine for the three runs.

TEMPERATURE RISE~°F

RUN	ENGINE 1	ENGINE 2	ENGINE 3	ENGINE 6	ENGINE 7
1	17	28	33	74	51
2	26	24	38	118	46
3	15	43	45	67	26

Based on the results of these and other data repeatability calibrations, it is apparent that inlet temperature data must be evaluated with discretion. This, however, should not be a reflection on data accuracy, but accepted as the variation one might expect from turbulent and unsteady flow in the proximity of the vehicle.

Repeatable data was obtained, however, for configurations in which ingestion was governed by buoyancy effects.

The engine exhaust-gas total pressure (representing engine thrust level) showed a transient characteristic that closely followed the average inlet-temperature rise (a thrust reduction proportional to the degree of gas ingestion was always observed).

The load-cell data and static-pressure measurements of the wing underside and fuselage showed that jet-induced effects for multiengine configurations were strongly time-dependent.

2. Governing phenomena

The test results indicate that the hot-gas ingestion is highly dependent on configuration and is dominated by either a buoyancy effect or a "fountain" effect. The buoyancy effect is characterized by the hot exhaust gases of a single engine, or two or more closely spaced, extending along the ground for an appreciable distance while mixing with the ambient air, then rising as a result of buoyancy forces, with subsequent ingestion by the engines. This type of hot gas ingestion usually occurs an appreciable time after the initial downward flow of the exhaust gases. The time lag from downward flow of the jet to ingestion is strongly influenced by the exhaust gas velocity, temperature, relative strength, and the location of the inlet. Hot gas ingestion associated with buoyancy effect is usually small (generally on the order of 10F) and strongly influenced by wind conditions in the proximity of the vehicle. The vehicle height above the ground appears to have very little effect on ingestion associated with buoyancy for the evaluated range of conditions (H/D of 2.5 to 8.7).

Hot gas ingestion due to buoyancy effects is not critical during aircraft takeoff, since enough altitude should be gained in about 5 to 10 seconds to put the vehicle above the hot-temperature environment. During vertical landing, however, the ingestion could be an increasing influence as the distance to ground decreases and the vehicle is exposed considerably longer to the hot environment.

For the case of two or more engines widely spaced (the jets do not merge before reaching the ground plane), the hot exhaust gases impinge on the ground plane and spread radially, subsequently meeting to create an upward

flow of hot gases. This is the "fountain" effect, and can cause substantial ingestion of hot exhaust gases if it occurs in the vicinity of the engine inlet. The buoyancy effect is also present, although small compared to the upward deflected gases from the "fountain" effect.

A typical inlet temperature-time history representing the "fountain" effect for a configuration employing a split arrangement of lift engines is shown in Fig. 21. The traces show typical temperature variation for ingestion-prone configurations. The exhaust gases of Lift Engines 1 and 2 spread parallel to the ground in all directions. The gases produced by Engines 1 and 2, flowing aft along the ground, meet those from Lift Engine Number 5 flowing forward, creating an upward flow of hot gases. The portion of the gases not deflected by the wing reach the inlets and are ingested by the lift engines. Configurations employing a split arrangement of life and/or lift plus lift/cruise engines can produce similar ingestion tendencies, the severity of ingestion being a function of the number of engines, distance between the engines and vehicle height above ground.

3. Induced Lift Effects

The jet-induced lift effects are also strongly configuration- and time-dependent. For a few configurations the induced effects varied by a factor of 3 to 4 during the test; many configurations, however, exhibited near-constant force levels. Jet-induced lift effects resulted in positive or negative lift forces depending primarily on engine arrangement and vehicle height above ground. In general, negative induced lift was associated with configurations exhibiting buoyancy effects, i.e., single engine or multiengine arrangements with engines closely spaced. Negative induced lift was approximately 4 to 6 percent, and increased with reduced height above ground. For some configurations negative force levels as high as 15 percent were recorded in close ground proximity.

Positive induced lift was, in general, associated with propulsion arrangements producing the "fountain" effect, and increased with reduced height above ground. Some configurations showed negative lift at H/D of 8.7 but developed a positive trend as H/D was reduced. A detailed evaluation of the data indicates that at lower heights (H/D $\approx$ 2.5) the lift/cruise engines produced a strong "fountain" where the jets did not have sufficient distance to merge before reaching the ground plane. As an example, the static pressure probe located between the lift/cruise engines of configuration E, recorded a pressure differential ($\Delta P = P_s - P_\infty$) of -0.053 psia at H/D of 8.7 and $\alpha = +4°$; at H/D of 2.5 and $\alpha = +1°$ the probe indicated a ΔP of +0.70 psia. It should be noted that at positive pitch attitudes and H/D = 2.5, the lift/cruise engines were very close to the ground plane; at zero or negative pitch attitude, for which the lift-cruise engines were further from the ground, the static pressure was considerably lower. Other pressure probes located between the lift engines disclosed similar trends, although the level of pressure was not as high as the pressure recorded between the lift/cruise engines.

Positive induced lift levels as high as 18 percent were calculated at H/D of 2.5 for configuration C_2, which employs a split arrangement of three lift engines in addition to the two lift/cruise engines. The positive lift created

19

by similar configurations should not be regarded as added or reserve lift in ground proximity; it diminishes very rapidly with increased height above ground. Also, this type of effect can cause an adverse pitching moment in near-ground operations.

4.   Engine Characteristics

Ingestion of hot exhaust gases resulted in engine thrust loss which closely followed the J85 performance characteristics shown in Fig. 22. The thrust loss due to ingestion fell within the limits shown. The transient thrust of each engine was calculated for all test runs. Figs. 23 and 24 show the average temperature-time history and the associated thrust-time history for two selected configurations. The thrust loss occurred within a few milliseconds of inlet temperature rise, and the degree of loss is about one percent for every 3 to 4F temperature rise. The dash line of Figs. 23 and 24 represents thrust loss based on data of Fig. 22, while the solid line shows the thrust calculated from tailpipe pressure measurements during the run. Similar correlations were obtained for most configurations. In a few, however, the engine temperatures deviated from this trend; close evaluation of the data, generally showed that the temperature rise was highly distorted, indicating that the inlet temperature-averaging method for highly distorted temperature field might have been inadequate. For these cases it was also observed that the calculated thrust loss based on Fig. 22 was generally higher than the actual measured thrust. This small difference, however, does not affect realistic evaluation of configurations effects and trends.

Rapid inlet temperature rise and/or high inlet-temperature profile can cause engine stall. Fig. 25 shows a typical temperature-time history for Engine Number 1 resulting in engine stall. The rapid and large temperature rise subsequent to engine stall is caused by the back-flow of hot internal gases expelled from the engine. The gases expelled from one lift engine occasionally stalled the adjacent engines, although not during the particular run under consideration.

Engine stall was not necessarily associated with ingestion-prone configurations; several stalls occurred in configurations exhibiting moderate to low ingestion tendencies. It would therefore appear that a potential stall condition exists as long as a random transient mass of hot exhaust gases can enter an unobstructed engine inlet. However, no stalls occurred in lift/cruise engines with long ducts.

B.   Configuration Effects

The test results of various configurations are compared in this section to show configuration effects and trends. Although sufficient data were obtained in general to establish statistical trends, deviations from established trends often occurred. The data analyses were directed toward identifying the influence of configuration variations on hot gas ingestion and jet-induced lift effects rather than detailed evaluations of each configuration.

Summary results of the pertinent performance parameters are presented in Table 2. The data are taken from the measurements of inlet temperature rise (as defined in Section VII) and associated thrust loss, and generally represent the maximum observed performance degradation for each test run. With the data of Table 2,

20

and the detailed data presented for selected configurations, independent evaluation of various configurations by the reader is possible.

1. **Single Engine Operation** - Hot gas ingestion associated with single-engine operation was governed by the buoyancy effect, and resulted in an average temperature rise less than 10F. Single-engine operations were conducted with the large swept wing at mid-fuselage position (Configuration B_1, B_2, and B_3) and the half-size swept wing at the same location (Configurations D_1 and D_2). The average inlet temperature increases for these configurations are presented at various heights above ground in Figs. 26 and 27. The variations are quite small, and no significant trend due to engine location and wing size or H/D is apparent. The data are taken from inlet temperature-time histories during a 15-second test run. High levels of ingestion might be expected for extended engine operations near ground, since the hot buoyant gases would have sufficient time to rise and recirculate to the vicinity of the inlets.

Entrainment of ambient air during single-engine operation resulted in negative induced-force levels (suckdown) at all heights. The force was generally evenly distributed between the wings and fuselage for configurations B_1, B_2 and B_3, and increased with decreasing H/D. The induced-force levels of Configurations D_1 and D_2 were mainly due to the large negative pressures of fuselage lower surfaces, and the wings usually contributed less than 20 percent of the total force. Inspections of the static pressure measurements from the fuselage and wing lower surfaces indicated that the force levels were highly transient and varied considerably with changes in H/D and wing planform. No significant trends in induced-force levels were observed as a function of engine location, although definite shifts in fuselage and wing static pressures were recorded.

2. **Multiengine Operations**

a. **Lift engines only.** Multi-engine tests of lift engines were conducted with both the large and the small wings at mid-fuselage location. Configurations employing a split arrangement of engines produced varying degrees of ingestion strongly influenced by engine spacing, wing planform and size, and relative locations of the engines with respect to the wing root. Configuration D_3 used the same engine arrangement as B_4 but employed the half-size swept wing. This resulted in very little ingestion at all H/D's shown in Fig. 28a and data of Table 2. The engines in both configurations were well protected by the wings, and not exposed to the upward flow of gases. Further separation of the engines resulted in a significant inlet temperature rise for a configuration in which the hot gases were not effectively blocked and reached the engine inlet. Configuration D_4 employing a split arrangement of engines 1 and 5 developed average inlet temperature rise as high as 120F, as shown in Fig. 28b. By contrast, Configuration B_5, employing the same engine arrangement, showed only moderate temperature rise (Fig. 29b). The difference may be attributed to the effectiveness of the large swept wing of Configuration B_5 in blocking the upward flow of hot exhaust gases.

Other lift-engine groupings with the large swept wing were also investigated. One employed a three-engine Configuration (B_6) of Engines 1 and 2 with Engine 5. This was similar to B_5 with Engine 2 added, and resulted in a large inlet temperature

rise for all engines at lower H/D's. Engines 1 and 5, located near the wing leading and trailing edge respectively, suffered more than Engine 2, which was protected by the wing. Comparing Configurations B_5 and B_6 (Fig. 30), one might expect B_6 to be somewhat more ingestion-prone if only because an additional engine contributed to the strength of the "fountain." The marked difference between the two, however, suggests wide differences in the flow-field characteristics.

Increasing ingestion at reduced heights above ground is indicated for Engine 5 by Figure 30b. It should be pointed out, however, that an ingestion-prone configuration, once in ground-effect (H/D<6), exhibits similar transient inlet-temperature characteristics with H/D, but with varying inlet temperature rise as illustrated previously in Fig. 20 (i.e., the turbulent nature of the flow associated with ingestion-prone configuration is such that, once in ground-effect (H/D<6), no definite ingestion trend with H/D variation can be established). A conservative approach to assigning an inlet temperature level to a configuration is to select the highest inlet-temperature rise recorded at any H/D as a guide to what might be expected for the configuration.

The effect of engine spacing on ingestion and induced-force levels was further investigated by Configuration B_7, employing 5 in-line lift engines. This configuration developed no ingestion at any height, as shown in Fig. 31. The close spacing of the engines results in coalescence of adjacent jets before they reached the ground plane, creating a single-engine effect. It is apparent that to minimize ingestion, closely-spaced engines are preferable.

The multi-lift-engine configurations generally created negative induced lift at various H/D locations (Table 2), although many of the split-engine arrangements created local areas of positive pressure under the wing and fuselage, particularly at lower H/D locations. Positive pressure areas on the fuselage existed between the operating engines. The positive pressure areas under the wing were located at or near the wing root and trailing edge. The magnitude and location of the high pressure regions under the wing appeared to correlate with severity of ingestion. High pressure areas result from the up-flow of high velocity hot gases created by two or more intersecting jets. Only small areas of high pressure were observed at H/D = 8.7 for Configuration B_6 ($\alpha = 4$), even though severe ingestion was experienced. This is believed attributable to reduced velocity of hot gases under the wing at higher H/D's. These gases were not deflected by the wing, as a more energetic stream would be, and consequently found their way into the engine inlet.

High pressure areas were observed between the engines of Configuration B_7 at H/D = 2.5. This suggests that at lower heights the jets did not have sufficient opportunity to merge, and consequently created a "fountain" between them.

b. <u>Lift plus lift/cruise engines</u>. Configurations employing composite arrangements of lift and lift/cruise engines generally created a high-temperature and turbulent flow environment which, when not blocked or deflected by the wing, resulted in ingestion of hot gases by one or more engines. The "fountain" between the lift and lift/cruise engine exhaust gases was always a large factor in promoting ingestion, and significantly influenced the level of jet-induced force and moments. In addition, interactions between split lift engines, when operating with lift/cruise engines, contributed to the unsteadiness of the flow field and ingestion level. Since the performance characteristics of various configurations were largely controlled by wing geometry, location, and other configuration peculiarities, these effects are discussed separately below.

3.   Wing Geometry Effects

The influence of wing geometry is shown by direct comparisons of Configurations B_8 with C_3, and E_1 with G_1. Configuration B_8 employs three lift engines closely spaced ahead of the wing box, with the top location of the lift/cruise engine inlet and swept wing planform at mid-fuselage height. C_3 employs a delta-wing planform with the other variables similar to B_8 Configuration. The same propulsion and lift/cruise-engine-inlet arrangements are used in E_1 and G_1, but the wings have been moved to the high fuselage locations.

Comparisons of average inlet temperature increases for Configurations B_8 and C_3 at various H/D locations (Fig. 32) show that B_8 experienced a temperature rise between 10 and 40F; Configuration C_3 was also ingestion prone and exhibited similar temperature rise. The lift/cruise engines of both configurations showed low and comparable ingestion levels.

Fig. 33 shows the influence of wing geometry with the wing in the high fuselage position. The overall ingestion level did not alter appreciably with the swept wing in the higher location. The delta wing in this location (Configuration G_1) significantly reduced ingestion level at H/D<6, although at higher values of H/D the change was minor. The reason for this significant reduction in ingestion for values of H/D<6 is not readily apparent. Possibly the delta wing gives better shielding capability when located close to the inlets. Wing geometry effects are closely tied to wing height and relative location with respect to the local "fountain" effects. One cannot readily assign a figure of merit to a wing geometry without adequate information on the jet-flow field, possible location of the wing with respect to the operating engines, and other configuration specifics. However, gross comparisons of various wing geometries may be made in terms of their potentials for shielding the inlets from the hot exhaust gases (i.e., a longer wing root would appear to offer better shielding than a wing of similar geometry having smaller root).

The influence of wing geometry on vehicle net-lift capability and jet-induced force and moments are presented in Figs. 34 and 35. Similar jet-induced force levels (L_{JE}/L_∞) for B_8 and C_3 are shown; however, B_8 has slightly better overall performance in terms of net lift (L/L_∞) in ground proximity, where (L/L_∞) includes thrust loss due to ingestion as well as the effect of jet-induced force levels. Higher wing locations did not affect the overall jet-induced force levels, even though the wing contribution at higher fuselage height was somewhat reduced. The engine thrust loss due to ingestion may be obtained by $\frac{F}{L_\infty} = \frac{L}{L_\infty} - \frac{L_{JE}}{L_\infty}$. The favorable trend of jet-induced lift forces with reduced H/D was found to be due to the high-pressure field created under the fuselage by intersecting jets from the lift and lift/cruise engines. At H/D of 2.5, a high positive-pressure area was created between the two lift/cruise engines, and accounted for the sharp increase in jet induced forces. This effect was also observed for all other configurations employing lift and lift/cruise engine arrangements.

The configurations under comparison experienced a total lift loss of 10 percent or more during ground operations. A loss of this magnitude would of course not be

acceptable for an operational aircraft. The moment inbalance $\frac{\Delta M}{L_\infty \bar{C}}$ created by each
configuration may or may not be a critical design factor, depending on the design
ground rules and engine-out capability requirements. It is therefore left to the reader
to determine the pitching moment effects and consequences.

4. Wing Size Effects

The large and half-size swept-wing planforms were used to investigate wing size
effects. Single jet (B_1, B_3 and D_1, D_2) and two-jet (B_4, B_5 and D_3, D_4) configurations,
similar to the small-scale test models, were selected for these evaluations. The
results of these tests, presented in Figs. 26 through 29, have already been discussed
from the standpoint of flow field created by single and multi-engine operation.

Definite conclusions cannot be reached by comparisons of single jet Configura-
tions B_1 and B_3 with D_1 and D_2 respectively, since very little or no interference by
the wings is anticipated for single-jet flow field. The influence of wing size however,
is readily apparent by comparisons of Configuration B_4 with D_3 (Fig. 36) and B_5 with
D_4 (Fig. 37). Very little ingestion was experienced by Configurations B_4 and D_3 at all
H/D heights. Engines 2 and 4 were effectively shielded by the wings; the half-size
swept wing provided adequate or at least as effective protection as the large-size wing.
For the greater engine spacing of Configuration D_4, where the engines were located
away from the shielding influence of the small-swept wing, severe ingestion was
experienced by Engine 1. Average inlet temperature rise as high as 120F was cal-
culated for Engine 1 at H/D = 6, and the level of ingestion was severe at all other
heights except at H/D = 2.5. By contrast, Configuration B_5 showed very little effect
from greater engine spacing, since better protection was provided by the wings.

Further investigations of the influence of wing size were made by employing
test Configurations A_2 and A_3 with no wings and the same engine arrangements as
B_4 and B_5. Configurations A_2 and A_3 suffered excessive temperature rise at all
H/D's. As shown in Figs. 36 and 37, large and highly distorted temperature rise
caused Engine Number 4 of Configuration A_2 to stall at H/D of 3.5 and 2.5. The in-
fluence of wing size and presence are more graphically illustrated by inlet-temperature
time histories of Figs. 38, 39, and 40 (Configurations B_5, D_4 and A_3). Similar
transient temperature characteristics were obtained at H/D<6 for these configurations.
These results indicate the shielding capability of properly located wings, and point out
the potential advantages to be gained from consideration of these factors in prelimi-
nary configurations design studies.

5. Wing Location Effects

The influence of wing location on ingestion and induced effects was investigated
by selective tests of delta- and large swept-wing planforms at three fuselage heights.
Each wing height was evaluated with respect to the same engine arrangement and lift/
cruise engine inlet locations. Comparisons of similar configurations are presented in
the following.

Configurations B_9 and E_2 (Figs. 41 and 42) show the influence of swept-wing height on ingestion and induced forces. Configuration B_9 with mid-wing location showed excessive ingestion at all heights above ground, and Engines 5 and 7 appeared to be severely affected, particularly at $H/D = 4.5$. Moving the wing to higher locations resulted in improvement only at $H/D = 6$; at lower heights, however, Engine 5 stalled prior to or shortly after reaching 100 percent rpm. Temperature rise prior to stall is not shown on Figure 41b for H/D of 4.5, 3.5, and 2.5, since sufficient data were not taken to the point of stall. Data obtained subsequent to engine stall are not realistic, since a change in the number of operating engines resulting from stall represents a configuration variation. Induced-force levels and moments for these configurations are presented in Figure 42. A slight improvement in "suckdown" due to higher location of the wings was apparent.

The swept-wing height effects were also evaluated by comparisons of Configuration B_{10} with E_3, both employing a composite arrangement of five lift and two lift/cruise engines. The wing locations did not significantly affect overall engine temperature rise, as shown in Fig. 43. However, at $H/D = 8.7$ the mid-wing location resulted in engine stall. Induced force levels and moments presented in Fig. 44 show similar trends and effects as B_9 and E_2 described previously.

A definite trend in hot gas ingestion due to delta wing height variation was not established. Comparisons of inlet temperature increases at various H/D's for configurations H_1, C_3 and G_1 (three lift and two lift/cruise engines with low, mid, and high wing locations respectively) showed that mid-wing location generally resulted in a higher lift-engine ingestion level than either low or high-wing positions (Fig. 45). High wing location, G_1, resulted in increased inlet-temperature rise with increasing H/D. However, the greatest ingestion-temperature rise was still less than the levels developed at low and mid-wing locations. The low wing location, H_1, showed very little or no ingestion at $H/D = 2.5$, 4.5, and 8.7, while temperature rise as high as 45F was recorded at $H/D = 6.0$.

Inlet temperature-time histories of Configurations H_1 and C_3 at $H/D = 3.5$ are presented in Figs. 46 and 47. The calculated maximum (spatial) inlet temperature rise for each engine, corresponding to the transient data at $H/D = 3.5$ is presented in Fig. 45.

The influence of wing height on ingestion level was not readily apparent on the basis of these data. Further analyses to determine wing height effects were made by comparisons of Configurations H_2, C_4, and G_2, employing the same wing geometry and engine arrangement as C_3, G_1, and H_1, but with the lift/cruise engine inlets located in the forward position. These comparisons (Fig. 48) show a definite trend of reduced ingestion with lowering of the wing. This effect is particularly evident in the severe ingestion level of lift/cruise engines at high wing location, compared to a considerably lower level with low-wing location. Similar ingestion characteristics would be expected for the lift/cruise engines with both high or mid-wing locations, since the inlets were located under the wings and exposed to the hot exhaust gases with either wing position. This similarity was observed in the oscillograph data although higher ingestion levels were recorded with high wing location. This similarity, however, is not evident in Fig. 48, since the temperature rise is taken at the point where the total

25

thrust of all engines is minimum and does not necessarily represent maximum temperature experienced by each engine. Highest temperature (average) recorded for each engine is shown in Table 2.

The jet-induced forces shown in Figs. 49 and 50 developed in a manner similar to other composite configurations evaluated. The lift/cruise engine inlet locations (forward versus top) had very little effect on the level of jet-induced forces, as might be expected.

Overall evaluations of all wing locations show no definite trend in engine ingestion level as a function of wing height. However, low or mid-wing locations more often resulted in a lower temperature rise than a high location. The results of previous tests conducted by Northrop (Ref. 5) show appreciable reduction in ingestion for a low wing positioned further aft (Fig. 1), compared to the wing locations evaluated in this program. It is believed that the aft location of the wing provided an effective shield in the area where the lift engine jets intersected with the lift/cruise engine exhaust gases, and deflected the upward-directed high velocity gases. It would therefore appear that a low wing location is more effective when it is positioned correctly (over the "fountain" of hot gases) with respect to the propulsion system arrangement.

Lower wing locations generally resulted in larger negative induced force levels (suckdown) at lower H/D's. The wing location with respect to engine arrangement (fore versus aft location) may, however, substantially alter this trend. A low wing positioned in the area where a "fountain" is present might be anticipated to exhibit positive induced forces due to the high pressure pockets created by the upflow of the hot gases. This effect, however, will diminish rapidly with increased H/D or during takeoff.

In summary, the wing height effects are closely tied to wing geometry and wing location with respect to the propulsion system arrangement. A low wing position, properly located, should offer better protection from hot gas ingestion but possibly at the expense of higher suckdown.

6. Lift/Cruise Engine Inlet Location

The influence of lift/cruise engine inlet location on ingestion and jet-induced effects was determined with respect to both swept and delta-wing planforms; each inlet location was evaluated with various engine arrangements and wing locations. Significantly smaller temperature rise was experienced by the lift/cruise engines with the top inlet location, compared to the forward position. The difference in ingestion level between the two locations was clearly evident for configurations with high and mid-wing location. These comparisons are shown for Configurations G_1 and G_2,

(Fig. 51); E_3 and E_4 (Fig. 52); C_3 and C_4 (Fig. 53); and E_1 and E_4 (Fig. 54). Little difference in ingestion characteristics should be expected between the high and mid-wing positions for the forward inlet location, since the inlet in both cases is located under and just ahead of the wing leading edge.

Although a reduction in ingestion level of the forward inlets was obtained with the low wing location (due to shielding effect of the wing at low height), the ingestion level still remained somewhat greater than experienced in the top inlet location. These effects are shown for Configuration H_1 and H_2 (Fig. 55).

Only a small difference in induced-lift effects was noticeable due to lift/cruise engine inlet locations, as shown in Fig. 56. This might be expected, since some flow disturbance occurs due to interference with the long duct, running on the side of the

fuselage. The variation in pitching moment shown in Fig. 56 is primarily due to thrust loss resulting from ingestion, rather than the induced effects.

In general, ingestion may be reduced or eliminated by proper shielding of the inlets with wings or auxiliary deflectors. Positioning of the inlets away from the hot exhaust gas sources by configuration arrangement is obviously a logical solution.

7.   Engine Arrangement Effects

Engine grouping affects exhaust gas ingestion primarily through changes in ground-jet characteristics and associated shifts or creation of local "fountain" effects. These were discussed previously for configurations employing lift engines only; analyses of composite configurations are now presented here. Comparisons of inlet temperature increases in ground proximity are presented for Configurations C_1 and C_2 in Fig. 57. Low to moderate ingestion levels were experienced by the lift engines C_1 at all H/D's. The "fountains" created by lift engines 1 and 5, and by lift engine 5 and lift/cruise engines, are primarily responsible for these temperature increases. Lift/cruise engine ingestion was negligible because of favorable top location.

Moderate to severe ingestion levels were experienced by Configuration C_2, a split arrangement of three lift engines and the lift/cruise engines. Operation at H/D less than 4.5 resulted in severe ingestion by the lift engines and repeated stall of Engine 1. The marked difference between the ingestion characteristics of these configurations is due to the undesirable arrangement of the lift engines of Configuration C_2, which created three separate "fountains." In addition, very little protection was provided by the wing for Engine 1 at this location.

Engine grouping effects with respect to the swept wing were similar. Comparison of Configurations E_4 and E_5 (Fig. 58) showed excessive ingestion by the lift engines of E_5, when all five lift engines were operating. Smaller temperature rise was generally experienced by the lift engines of Configuration E_4, although the degree of ingestion was still unacceptable.

The difference in ingestion level might be attributed to the unfavorable jet stagnation point with respect to the lift engine, as well as more severe temperature environment created by the seven-engine operation of E_5. The lift/cruise engines of both configurations exhibited similar characteristics, as might be expected with the forward inlet and high wing location.

Engine arrangements similar to E_4 and E_5, but with low swept-wing location, were also evaluated. Both Configurations F_1 and F_2 experienced unacceptable ingestion levels at all H/D's. However, configuration F_1, employing three lift engine arrangements, exhibited more serious ingestion tendencies than F_2 (Fig. 59), which employed seven engines. This is in sharp contrast to the expected trend just discussed. A possible explanation may lie in the better shielding effect of the high wing for conditions where little or no blockage of the hot gases is provided by the low-wing locations.

The engine arrangements under comparison disclosed few differences in jet-induced force levels, as shown in Figs. 60, 61 and 62. It should be noted that all configurations generated similar "fountain" characteristics between the lift and lift/cruise engines. Also, at low H/D's the contribution of the high pressure areas produced by the "fountain" effect between the lift/cruise engines predominates and overshadows small differences in induced effects due to lift engine geometry or wing location. Considerably larger differences in pitching moments resulted from different engine arrangements, primarily because of large thrust loss experienced in all configurations discussed.

8.   Influence of Pitch Attitude

No general trend was established in gas ingestion due to pitch attitude variation (-4 to +4 degrees). The influence of the pitch attitude appeared to be primarily due to the shift of the stagnation point created by the ground jets which in turn affected ingestion characteristics. Thus some configurations exhibited improved ingestion levels for positive (nose up) while others showed reduced ingestion for negative (nose down) pitch attitudes. In some cases both positive and negative pitch attitude variations resulted in increased ingestion of lift and lift/cruise engines. Generally pitch attitude effects were only significant at H/D < 6, and produced insignificant changes at higher H/D's.

The influence of pitch attitude variation on the ingestion behavior of various configurations is presented in Figs. 63 through 67. Configuration B6, employing a split arrangement of three lift engines, showed considerably better ingestion tendencies (Fig. 63) with positive pitch attitudes at lower H/D's. At H/D = 2.5 and α = -4, Engine Number 5 experienced a large temperature rise, which caused it to stall. A negative pitch attitude of Configuration B6 appears to have resulted in displacement of the ground jet stagnation point ("fountain") aft and closer to Engine 5. This effect, as might be expected, resulted in a greater ingestion by Engine 5 than the level experienced at α = 0, and led to engine stall. The increased ingestion exhibited by Engines 1 and 2 at this height was not expected, and might be attributed to the closeness of the Engine 1 and 2 inlets to ground plane at negative pitch attitude.

Reasons for ingestion tendencies exhibited by various configurations with pitch attitude (Figs. 63 and 67) might also be found through evaluation of near-field flow characteristics with respect to wing geometry, size, location and engine groupings. Small variations in pitch attitude might result in gross changes in ingestion tendencies as shown by comparisons presented in this section.

9.   Near-Field Temperature Environment

Ground-plane and vehicle-proximity temperatures are presented in Figs. 68 through 72 for selected engine groupings. Ground-plane and rake-thermocouple locations are shown in Fig. 14. Temperature environment data for single-engine operation are presented in Fig. 68 as a function of radial distance from nozzle centerline (X/D), vehicle height above ground (H/D), and thermocouple height above ground (h). Expected trends of decreasing temperature with increased X/D and h are shown. The local temperature appears to be less sensitive to H/D variations except at ground level. The effect of the jet growth with distance is indicated by the rate of temperature variation with h for each X/D.

Near-field temperature environment data with all five lift engines operating are shown in Fig. 69. Similar trends for single engine operation are shown with higher overall temperature levels at rake locations 12 and 13 (Fig. 14). The influence of lift/cruise engine operation on near-field temperature environment is shown in Fig. 70 for Configuration B10.

Generalized ground-plane temperature data for configurations employing lift and lift plus lift/cruise engines are presented in Figs. 71 and 72.

IX - SCALING EFFECTS*

A comparison of some of the results obtained in the subject investigation with the results of various small-scale tests follow. The comparisons include: (1), inlet temperature rise resulting from exhaust gas ingestion for both single jet and split-jet configurations; (2) aerodynamic suckdown forces and induced pressure distribution for a single jet fundamental geometry configuration; and (3) the ground jet flow field produced by a single jet configuration.

Ingestion Characteristics

The results of exhaust gas ingestion were compared to data from the small-scale tests of Ref. 7 for geometrically similar configurations. In general, both the present results and the results of Ref. 7 indicate steady low-level inlet temperature rise (approximately $10°F$ or less) for single engine configurations.

On the other hand, for split engine configurations, the results of the present investigation are of a completely different character from those of Ref. 7 for similar configurations and, as a result, have led to fundamentally different conclusions. That is, Ref. 7 shows low-level steady ingestion (similar to the results obtained for single engine configurations) similar to those of the current investigation which resulted in generally severe ingestion levels of a highly transient character (e.g. Fig. 39) representative transient data. As a result, Ref. 7 concludes that inlet temperature rise due to exhaust gas ingestion is low (approximately $10°F - 15°F$) and independent of aircraft configuration, while the present results indicate that inlet temperature rise due to exhaust gas ingestion is highly configuration dependent with inlet temperature rises over $100°F$ for many of the configurations tested.

Figs. 73 and 74 show some specific comparisons of inlet temperature rise for configurations of the small-scale tests of Ref. 7 to the data obtained in the current investigation for similar configurations. The data of Fig. 73a are for a single engine configuration with the large swept wing. The inlet temperature rise of the current investigation is negligible while that of Ref. 7 is encompassed within a band in the neighborhood of $10°F$. In turning to Fig. 73b, data are compared for a two engine split jet configuration with the large swept wing. Again, for this configuration, in which the wing is effective in blocking the exhaust gases from the inlet, the inlet temperature rise indicated by the data of Ref. 7 is comparable to that of the full-scale tests. The character of the temperature data of this comparison are different, however. The full-scale data were of a transient nature, with periods of negligible ingestion occurring within the run, while the data of Ref. 7 were steady.

Figs. 74a and 74b show the effects of reducing the wing size and eliminating the wing, respectively. For these cases the maximum spatial average temperature rise was in the neighborhood of $100°F$ for the full-scale configurations, with localized

---

temperatures as high as 200°F, and data were of a highly transient nature. On the other hand, the data of Ref. 7 remain steady and at the same low level as for the previous configurations.

In an effort to explain the differences between the small-scale data of Ref. 7 and the present full-scale data one might consider: (1) subtle, but possibly important differences in the geometry and nozzle exit flows between the models and full-scale test articles; (2) differences in instrumentation and data recording techniques between the model and full-scale test articles, and more basically; (3) the possibility that even with proper simulation of the model and instrumentation, there might be a fundamental difference in the flow fields produced by a small-scale model and that produced by a full-scale test article. Although at this time it is not possible to identify positively which one (or combination) of the above considerations has caused the differences in the small-scale and full-scale results to date, each of the above considerations warrants comment.

1. There is some evidence that the apparent problem of ingestion modeling may be attributed to differences in the nozzle exit flow conditions. Some of the differences between the nozzle exit flows of small-scale test and full-scale test to date are (1) exhaust gas swirl on the full-scale tests; (2) non-vertical (and non-parallel) jet exit conditions on small-scale tests due to insufficient lengths of the nozzle approach section (the "vertical" split jets of the small-scale tests were found to issue at 7° and 2°, respectively, from the vertical); (3) non-uniform jet exit conditions on small-scale tests due to sharp bends in the flow ducting system immediately upstream of the nozzle exit; and (4) differences in jet exit turbulence levels. Due to the unstable nature of the flow of a jet impinging upon a surface, one or a combination of the above biases in the jet exit conditions could result in an amplified effect in the proximity of the ground plane stagnation region and within the interacting interfaces of the flows from split jet VTOL configurations. As a example, previous Norair full-scale tests have shown a large reduction in ingestion levels for the jet exhaust vectored only 10° aft. As another example, NASA tests (Ref. 9) have shown a large effect in the jet decay rate for differences in the nozzle supply plenums.

2. Differences in instrumentation have been reviewed in detail. Although many differences exist(such as response times of thermocouple junctions, response times and damping characteristics of recorders, continuous data recording as compared to data sampling, etc.), none of these differences would account for the grossly different character of the data obtained from small-scale test from that obtained from the full-scale tests.

3. With proper simulation of the model and instrumentation one would expect to be able to reproduce the full-scale near flow field, where dynamic and viscous effects dominate, in small-scale. An exception might be a configuration in which boundary layer effects were important, in which case differences in Reynolds Numbers between the full-scale and small-scale could affect the model results. For split jet configurations, it is the near flow field which will dominate the ingestion characteristics of the configuration.

Due to the currently unresolved status of exhaust gas ingestion scaling, additional work is warranted in this area. For recommendations of the nature of such work the reader is referred to Section XI (Recommendations) and to Ref. 10 for additional detail.

Aerodynamic Suckdown

For the purpose of comparing the aerodynamic suckdown of a single jet configuration with the results obtained from small-scale tests, the fundamental geometry shown in Figs. 75 and 10 was selected. This configuration consisted of a single jet issuing from the center of a square plate attached to the nozzle exit. The ratio of the plate area to the jet area, A_p/A_j, was 142. The results obtained are compared to the data from the small-scale tests of Refs. 11 and 12 in which the nozzle exit areas were 4.4 inches and 1.0 inch, respectively, and were supplied by air at ambient temperature.

Fig. 76 shows the variation in thrust ratio, F/F_{MAX}, (defined as the ratio of the installed thrust in ground effect to the momentum flux of the isolated jet) with the non-dimensional height of the plate above the ground plane, H/D, for a nozzle pressure ratio of 1.45. Data from the current full-scale test and the small-scale tests of Ref. 12 are presented along with an empirical equation based on a rigorous correlation of the data of Ref. 11 in which the effects of A_p/A_j, plate planform shape, nozzle pressure ratio, and jet Reynolds number were successfully correlated for numerous single jet configurations. For the case of a square plate with a centrally located jet, the empirical equation of Reference 11 reduces to

$$\frac{F}{F_{MAX}} = \frac{F_{H/D\,=\,\infty}}{F_{MAX}} \quad .012 \left(\frac{H/D}{.994\,A_p/A_j - 1}\right)^{-2.30}$$

The full-scale values of F/F_{MAX} shown in Fig. 76 were obtained from integration of the measured pressure distribution over the plate area (see Fig. 17 for plate pressure instrumentation) along with the calculated value of jet momentum flux based on the measured nozzle pressure ratio. On the other hand, the data of Ref. 12 and the empirical correlation from Ref. 11 were obtained from direct thrust measurements, although pressure distributions were also measured in the tests of Ref. 12. The data from Ref. 12 have been reduced by 2 percent to reflect the "base loss" difference in the reference thrust, F_{MAX}, used in Fig. 76 compared to the reference thrust, $L\infty$, (installed thrust out of ground effect) adopted in Ref. 12. The value of 2 percent for the base loss was obtained from the experimental data of Ref. 11 for $A_p/A_j = 142$.

From Fig. 76 it is seen that the thrust loss data of the full-scale test are in excellent agreement with the generalized correlation curve of Ref. 11 in the range of practical values of H/D for VTOL aircraft (say, $H/D > 2$). On the other hand, the small-scale data of Ref. 12 indicate higher values of thrust loss than those of the full-scale tests. Fig. 77 shows a similar relation between the data of the full-scale test, Ref. 11, and Ref. 12 in demonstrating the independence of thrust ratio with nozzle pressure ratio.

Fig. 78 shows the plate pressure distributions obtained from the full-scale test and from Ref. 12. The reference for the pressure coefficient is taken as the jet dynamic pressure, $1/2\,\rho\,V^2$, rather than $P_N - P_\infty$ as in Ref. 12. As a result, the data

correlation becomes independent of pressure ratio. The pressure ratio independence when correlated with $1/2 \, \rho \, V^2$ rather than $P_N - P_\infty$ follows from Fig. 77 which shows the invariance of thrust ratio with pressure ratio. The data of Fig. 73 show close agreement between the pressure distribution of the full-scale tests and those of Ref. 12.

In summary, it would appear that valid aerodynamic suckdown data applicable to full-scale vehicles can be obtained from small-scale tests with cold jets for single jet (or closely spaced multiple jet) configurations. It should be pointed out, however, that extension of the above conclusion to include multiple split-jet configurations is a dangerous extrapolation due to fundamental differences in the flow phenomena between split-jet and single jet configurations, and therefore cannot be made on the basis of the data presented in this report. Finally it would appear that the small-scale data correlation of Ref. 11 is an excellent representation of aerodynamic suckdown for full-scale configurations of the same family evaluated in Ref. 11.

Ground Jet Flow Field

During the aerodynamic suckdown tests cited above, the ground jet pressure and temperature profiles were surveyed at distances of $r/D = 3.0$, 4.5, and 6.0 from the jet centerline for a value of $H/D = 5.0$. The results of these surveys are presented in Figs. 79 through 83. In general, the non-dimensional velocity profiles, the velocity decay rate with r/D, and the temperature decay rate with r/D were found to be in good agreement with the data of small-scale tests. On the other hand, the rate of growth of the full-scale hot jet was found to be significantly higher than the rate of growth of cold jets, either small or large scale.

Fig. 79 shows a sample of the ground jet velocity profiles for $r/D = 4.5$. The data are non-dimensionalized in the standard form of $Y/Y_{1/2}$ and V/V_{max}, where $Y_{1/2}$ is the height above the ground at which the velocity in the ground jet, V, is equal to one-half the maximum velocity in the ground jet, V_{max}. The profiles are seen to be independent of nozzle pressure ratio and are in excellent agreement with the small-scale cold flow results of Ref. 13. Similar agreement was obtained at the other values of r/D.

Fig. 80 shows the ground jet temperature profiles corresponding to the ground jet velocity profiles of Fig. 79. Again, the data are non-dimensionalized by the quantities $Y/Y_{1/2}$ as defined above and $T-T_\infty/T_{max}-T_\infty$, which is the ground jet temperature increment above ambient divided by the ground jet maximum temperature increment above ambient. From Fig. 80 it is seen that the ground jet thermal layer is independent of nozzle pressure ratio and is approximately twice the thickness of the velocity layer. This result is similar to the observation of more rapid growth of the thermal layer than the velocity layer for a free turbulent jet.

The rate of decay of maximum velocity within the ground jet (referenced to jet exit velocity) with distances from the nozzle centerline is shown in Fig. 81. Again, the data are independent of nozzle pressure ratio and are in excellent agreement with the small-scale results of Ref. 9 for which the jet exit temperature was 1200°F. Also shown in Fig. 81 are the results of the cold flow full-scale (12-inch diameter) nozzle from Ref. 12. It may be seen that the rate of decay for the 12-inch nozzle of Ref. 14 is similar to that of the full-scale data and small-scale results of Ref. 9, with the primary difference resulting from comparing the former data at $H/D = 4.0$ to the latter data at $H/D = 5.0$ for which the velocity of the jet at ground impingment is less.

34

The variation in maximum temperature within the ground jet (referenced to jet exit temperature), with distance from the nozzle centerline is shown in Fig. 82. The full-scale data are seen to be somewhat higher than the small-scale data of Ref. 9, for which the jet exit temperature was 1200°F.

The rate of growth of the ground jet is shown in Fig. 83. The data show a linear rate of growth with distance from the jet centerline. The data of the subject test indicate a growth rate significantly higher than the small-scale cold flow data of Ref. 13 and the large-scale cold flow data of Ref. 14. Once gain, it is noted that the growth rate of the thermal layer is considerably higher than that of the velocity layer as indicated by the comparison of Figs. 79 and 80.

X. CONCLUSIONS

1. The flow field created in the vicinity of the lift engine inlets by the combined effects of the engine exhausts and inlet airflows in close ground proximity resulted in intermittent and localized gas ingestion. The severe temperature environment often resulted in a large temperature distortion and rapid temperature rise at the compressor face.

2. Hot gas ingestion was highly time- and configuration-dependent. Wing geometry, size, location, engine arrangement; lift/cruise engine-inlet location; and pitch attitude have a strong influence on ingestion tendencies and jet-induced effects -- the geometry effects are particularly significant at close ground proximity ($H/D \leq 4.5$).

3. The geometry effects are interdependent and their influence on ingestion cannot often be isolated. Lower wing location, for example, appears to be more effective in reducing ingestion only if it is properly located with respect to the propulsion system arrangement to permit effective deflection and shielding of the hot exhaust gases. Pitch attitude effects are closely tied to the shift in local stagnation point of the ground jets and may reduce or aggravate ingestion depending on other geometrical variations such as wing location, size, geometry and lift/cruise engine-inlet location.

4. The severity of the near-field temperature environment is strongly influenced by the engine arrangement and to a lesser degree by number of operating engines. Single engine or engine groupings which behave similarly to a single engine (jets merge before reaching the ground plane) do not significantly alter temperature environment in the vicinity of the inlets (for duration of operation near ground required by a representative operational VTOL aircraft) and thus pose no serious problem. By contrast, engine arrangement or groupings which result in a "fountain" effect (widely spaced engines) create a severe temperature environment in the proximity of the vehicle, which if permitted to reach the vicinity of the inlet, will create an unacceptable configuration.

5. Small or subtle geometrical variations may significantly alter the ingestion level of a given configuration. Therefore, extrapolation of data to configurations other than those actually tested is unreliable; only gross prediction of ingestion tendencies of new configurations evolved from design studies can be made within the scope of the present data.

6. Rapid inlet-temperature rise with high-temperature distortion at the compressor face can result in engine stall. Engine stall is not necessarily associated with ingestion-prone configurations; several stalls occurred for configurations exhibiting little to moderate ingestion. Internal hot gases expelled from one engine subsequent to stall may stall adjacent engines.

7. Jet-induced force levels are of sufficient magnitude (6-10%) to be considered from the standpoint of required thrust and induced moment imbalance. However, hot gas ingestion which can result in considerably larger thrust loss, could be an overriding consideration.

8. The character of ingestion data and the severity of inlet temperature rise obtained in large-scale tests appears to be considerably different from the data of small-scale tests (Ref. 7).

9. Aerodynamic suckdown results obtained with a single jet-fundamental geometry configuration are in excellent agreement with an empirical correlation of small-scale results presented in Ref. 11.

10. The non-dimensional velocity profiles and the rate of velocity decay of the ground jet produced by a J85 engine is in good agreement with experimental results obtained for small-scale cold-flow ground jets. On the other hand, the rate of growth of the full-scale hot jet was found to be significantly higher than the rate of growth of cold jets, either small- or large-scale. The higher rate of growth and velocity decay is most likely a temperature effect rather than a size effect.

11. Fast-response sensing and recording equipment are required to assess realistically the VTOL ground proximity environment.

XI. RECOMMENDATIONS[1]

The results of this investigation have shown that the severity of exhaust gas ingestion is highly configuration dependent, with major changes in exhaust gas ingestion levels sometimes resulting from what would appear to be minor changes of configuration. Although the data serve as guidelines in synthesizing aircraft configurations, it is clear that extrapolation of the data to configurations other than those tested is unreliable. Each new configuration evolved from design studies must be tested to determine its exhaust gas ingestion characteristics. Obviously, if such evaluations are required for each candidate configuration, small-scale testing yielding meaningful results applicable to geometrically similar full-scale configurations is highly desirable in order to avoid full-scale testing during the preliminary design stages of a VTOL aircraft development. At present, however, there is no evidence that meaningful exhaust gas ingestion results can be obtained from small-scale tests. The question of whether or not such results can be obtained from small-scale tests should be resolved, and if positive, the techniques required for reliable modeling should be established.

Secondly, if it is not feasible to obtain generalized design data for exhaust gas ingestion, it is increasingly important to have a detailed understanding of the exhaust gas ingestion problem, to insure a more sound technical approach in synthesizing aircraft designs, thereby minimizing costly cut-and-try experimental approaches. Such an understanding is best provided by detailed investigations of the character of the flow field produced by various fundamental geometry models.

Finally, to alleviate some of the limitations imposed by reingestion considerations in the design of a VTOL aircraft, and thereby allow more freedom in accommodating other design considerations, potential methods of reducing exhaust gas ingestion should be investigated.

In summarizing, a series of VTOL exhaust gas ingestion technology investigations with the following objectives is recommended:

1. To determine whether exhaust gas ingestion data applicable to full-scale vehicles can be obtained from small-scale model tests, and if so, establish the important modeling criteria and techniques required to obtain such data.

2. To provide detailed data and understanding of the flow field produced by conceptual representations of potential split-jet VTOL configurations.

3. To investigate the effectiveness and application potential of various ingestion control devices with particular emphasis on continued investigation of the aerodynamic shield concept (Ref. 15).

---

[1]For further detail, see Ref. 10.

XII. REFERENCES
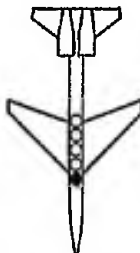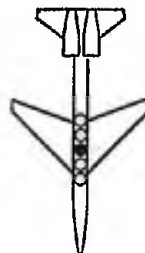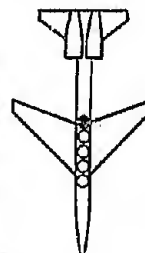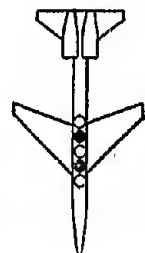
1. W.H. Tolhurst, Jr., and M.W. Kelley, "Characteristics of Two Large-Scale Jet-Lift Propulsion Systems," Ames Research Center, presented at Conference on V/STOL and STOL Aircraft - Ames Research Center, April 4-5, 1966.

2. H. Clyde McLemore, C.C. Smith, Jr., "Hot-Gas Ingestion of Large-Scale Jet VTOL Fighter Type Models," LWP-332, Langley Research Center, November 30, 1966.

3. F. Smith, "CL 747 Flight Test Results," Lockheed Aircraft Report, 28 April 1965.

4. R.F. Speth and P.E. Ryan, "A Generalized Experimental Study of Inlet Temperature Rise and Near Field Temperature Contours of Jet V/STOL Aircraft in Ground Proximity," AIAA Paper No. 66-740, Bell Aerosystems Company, Buffalo, New York.

5. W. Stark, et al., "Results of a Hot-Gas Ingestion and Jet Effects Test Program with a Large-Scale VTOL Test Vehicle in Ground Proximity," Northrop NOR 66-246.

6. B.A. Zeganoski, "A Generalized Experimental Study of Inlet Temperature Rise and Lift-Thrust of Jet VTOL Aircraft in Ground Effect," Bell Aerosystems Company Report No. 2099-928002.

7. Bell Aerosystems Company Report No. 2099-928003, "Generalized Study of Inlet Temperature Rise of Jet V/STOL Aircraft in Ground Effect," April 5, 1966.

8. W.W. Watson, Rahim Lavi, Haig Asdurian, "Design and Instrumentation of a Large-Scale VTOL Test Bed for Investigation of Ground Proximity Effects," AIAA Paper No. 67-181 presented at the AIAA 5th Aerospace Sciences Meeting, New York, January 23-26, 1967.

9. C.D. Higgins, et al., "Exhaust Jet Wake and Thrust Characteristics of Several Nozzles Designed for VTOL Downwash Suppression," NASA CR-373, January 1966.

10. G.R. Hall, "Recommended VTOL Exhaust Gas Ingestion Technology Investigations," Northrop NB 67-31, January 1967.

11. L.A. Wyatt, "Static Tests of Ground Effect on Planforms Fitted with a Centrally-Located Round Lifting Jet," Ministry of Aviation, C.P. No. 749, 1964.

12. K.P. Spreeman and I.R. Sherman, "Effects of Ground Proximity on the Thrust of a Simple Downward-Directed Jet Beneath a Flat Surface," NACA TN 4407, September 1958.

13. P. Bakke, "An Experimental Investigation of a Wall Jet," Journal of Fluid Mechanics, Volume 2, July 1957.

14. Cornell Aeronautical Laboratory, "Theoretical and Experimental Studies of Impinging Uniform Jets," April 1963.

15. G. R. Hall and Rahim Lavi, "Feasibility Investigation of an Aerodynamic Shield as a Means of Reducing Hot-Gas Ingestion in VTOL Aircraft," Northrop NB 66-291, September 1966.

TABLE 1 TEST·CONFIGURATIONS

BASIC CONFIGURATION	TEST NO.	CONFIG-URATION	OPERATING ENGINE (S)	PITCH ATTITUDE
LIFT ENGINES ONLY	1	A_1		0
		A_2		0
		A_3		

BASIC CONFIGURATION	TEST NO.	CONFIG-URATION	OPERATING ENGINE(S)			PITCH ATTITUDE
			WING LOCATION			α
			MID WING	HIGH WING	LOW WING	0
LIFT ENGINES ONLY	2	B_1				
		B_2				
		B_3				
		B_4				
		B_5				
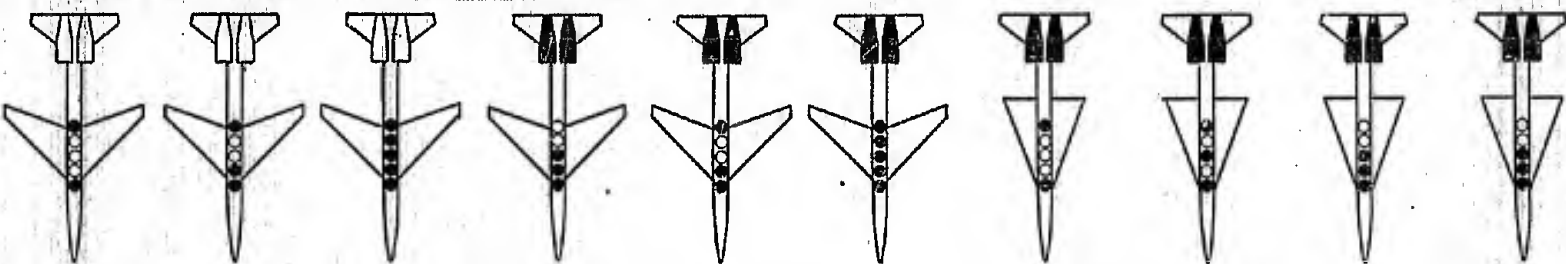
-4,0,+4   0   -4,0,+4   0   -4,0,+4   0

B5   B6   B7   B8   B9   B10   C1   C2   C3   C4

LIFT +
LIFT/CRUISE
TOP
INLET

LIFT +
LIFT/CRUISE
FORWARD
INLET

-4,0,+4 0 0 -4,0,+4 0

| C_4 | D_1 | D_2 | D_3 | D_4 | E_1 | E_2 | E_3 | E_4 | E_5 |

4 5

FORWARD
INLET

LIFT
ENGINES
ONLY

LIFT +
LIFT/CRUISE
TOP
INLET

LIFT +
LIFT/CRUISE
FORWARD
INLET

3

-4,0,+4

0

-4,0,+4

0

E3

E4

E5

F1

F2

G1

G2

H1

H2

6

7

8

LIFT + LIFT/CRUISE FORWARD INLET

LIFT + LIFT/CRUISE TOP INLET

LIFT + LIFT/CRUISE FORWARD INLET

LIFT + LIFT/CRUISE TOP INLET

LIFT + LIFT/CRUISE FORWARD INLET

EACH CONFIGURATION TESTED AT 5 (h/D) POSITIONS

DARKENED INLET INDICATES OPERATING ENGINE(S)

TABLE 2 - DATA SUMMARY

CONFIGURATION	FOR PLOTTED DATA SEE FIGURE NUMBER	α	$\dfrac{H}{D}$	WIND & DIRECTION	INLET TEMPERATURE RISE — ENGINE NUMBER 1 (± / ±±)	2	3	4	5	6	7	$\dfrac{L}{L}$
South ◄ A₂	36	0	8.7	7N		0		0				
			6.0	7NE		24		13				
			4.5	5N		15		37				
			3.5	6N		82		101*				
			2.5	6N		26		150*				
A₃	37	0	6.0	7N	45				22			-0.
			4.5	9N	40				40			-0.
			3.5	9N	35				25			-0.
			2.5	3N	60				85			
B₁	26	0	8.7	12NW	8 / 8							-0.
			6.0	10-15N	9 / 9							-
			4.5	5N	0 / 0							-
			3.5	5E	6 / 6							-0.
			2.5	5SE	4 / 4							-0.

± Inlet temperature rise at time where $\Sigma\, F_N$ = minimum
±± Maximum (spatial average) temperature rise during the run
* Engine stall

TABLE 2-DATA SUMMARY

FOR PLOTTED DATA SEE FIGURE NUMBER	α	$\frac{H}{D}$	WIND & DIRECTION	INLET TEMPERATURE RISE ENGINE NUMBER									$\frac{L_{JE}}{L\infty}$	$\frac{F.}{L\infty}$	$\frac{L}{L\infty}$
				1 ± / ±±		2	3	4	5	6	7				
	0	8.7	7N			0		0							
		6.0	7NE			24		13							
36		4.5	5N			15		37							
		3.5	6N			82		101*							
	↓	2.5	6N			26		150*							
	0	6.0	7N	45					22				-0.016		
		4.5	9N	40					40				-0.028		
37		3.5	9N	35					25				-0.037		
	▼	2.5	3N	60					85						
	0	8.7	12NW	8	8								-0.074	0.972	0.898
		6.0	10-15N	9	9								-	-	-
36		4.5	5N	0	0								-	-	-
		3.5	5E	6	6								-0.073	0.977	0.904
	▼	2.5	5SE	4	4								-0.093	0.988	0.895

± Inlet temperature rise at time where ΣF_N = minimum

±± Maximum (spatial average) temperature rise during the run

* Engine stall

TABLE 2 – DATA SUMMARY

CONFIGURATION	FOR PLOTTED DATA SEE FIGURE NUMBER	α	$\dfrac{H}{D}$	WIND & DIRECTION	INLET TEMPERATURE RISE ENGINE NUMBER 1 ±/±±	2 ±/±±	3	4 ±/±±	5 ±/±±	6	7
B₂	26	0	8.7	7N		0 / 0					
			6.0	4NE		2 / 2					
			4.5	7N		0 / 0					
			3.5	5NW		0 / 0					
			2.5	6NW		0 / 0					
B₃	26	0	8.7	10N					10 / 10		
			6.0	10-15NW					10 / 10		
			4.5	6N					0 / 0		
			3.5	5N					2 / 2		
			2.5	6N					0 / 0		
B₄	29	0	8.7	10N		4 / 4		7 / 7			
			6.0	10N		13 / 13		12 / 12			
	36		4.5	10-15N		9 / 9		9 / 9			
			3.5	10N		12 / 18		12 / 13			
			2.5	10N		0 / 0		2 / 2			

±Inlet temperature rise at time where ΣF_N = minimum

±±Maximum (spatial average) temperature rise during the run

*Engine stall

TABLE 2 – DATA SUMMARY

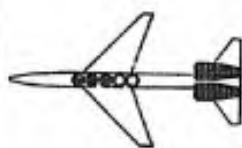| D E	α	$\dfrac{H}{D}$	WIND & DIRECTION	INLET TEMPERATURE RISE — ENGINE NUMBER							$\dfrac{L_{JE}}{L_\infty}$	$\dfrac{F}{L_\infty}$	$\dfrac{L}{L_\infty}$
				1 (± / ±±)	2	3	4	5	6	7			
0		8.7	7N		0 / 0						-0.088	0.988	0.900
		6.0	4NE		2 / 2						-	-	-
		4.5	7N		0 / 0						-	-	-
		3.5	5NW		0 / 0						-0.083	0.973	0.890
▼		2.5	6NW		0 / 0						-0.120	0.996	0.870
0		8.7	10N				10 / 10				-0.020	0.985	0.965
		6.0	10-15NW				10 / 10				-	-	-
		4.5	6N				0 / 0				-	-	-
		3.5	5N				2 / 2				-0.102	0.995	0.893
▼		2.5	6N				0 / 0				-0.146	1.000	0.854
0		8.7	10N		4 / 4		7 / 7				-0.080	0.982	0.902
		6.0	10N		13 / 13		12 / 12				-0.064	0.955	0.891
		4.5	10-15N		9 / 9		9 / 9				-0.063	0.967	0.904
		3.5	10N		12 / 18		12 / 13				-0.076	0.951	0.875
▼		2.5	10N		0 / 0		2 / 2				-0.071	0.993	0.922
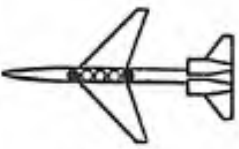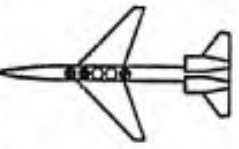
±Inlet temperature rise at time where ΣF_N = minimum

±±Maximum (spatial average) temperature rise during the run

*Engine stall

TABLE 2 - DATA SUMMARY

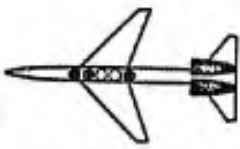| CONFIGURATION	FOR PLOTTED DATA SEE FIGURE NUMBER	α	$\frac{H}{D}$	WIND & DIRECTION	INLET TEMPERATURE RISE — ENGINE NUMBER 1 ($\pm$ / $\pm\pm$)	2	3	4	5	6	7
B5	29 30 37	0	8.7	8N	5				2		
			6.0	8NW	17				2		
			4.5	5W	8				2		
			3.5	5N	9				8		
			2.5	0	8				7		
B6	63	-4	8.7	5-10N	10 / 10	25 / 25			20 / 29		
			6.0	10NW	8 / 10	8 / 13			26 / 32		
			4.5	0-5SE	5	3			11		
			3.5	5N	25	35			32		
			2.5	5NW	34 / 34	43 / 43			60*		
	30 63	0	8.7	5-10N	10 / 15	13 / 15			15 / 20		
			6.0	5-10N	24 / 24	21 / 21			22 / 25		
			4.5	5N	42 / 47	5 / 22			4 / 6		
			3.5	5-7NE	59 / 104	30 / 39			22 / 22		
			2.5	5NE	0 / 10	3 / 20			75 / 75		

$\pm$ Inlet temperature rise at time where ΣF_N = minimum

$\pm\pm$ Maximum (spatial average) temperature rise during the run

*Engine stall

TABLE 2 - DATA SUMMARY

	α	$\dfrac{H}{D}$	WIND & DIRECTION	INLET TEMPERATURE RISE — ENGINE NUMBER 1	2	3	4	5	6	7	$\dfrac{L_{JE}}{L_\infty}$	$\dfrac{F}{L_\infty}$	$\dfrac{L}{L_\infty}$
				$\pm$ / $\pm\pm$									
	0	8.7	8N	5				2			-0.049	0.995	0.946
		6.0	8NW	17				2			-0.016	0.970	0.954
		4.5	5W	8				2			-0.031	0.980	0.949
		3.5	5N	9				8			-0.073	0.989	0.916
		2.5	0	8				7			-0.076	0.983	0.907
	-4	8.7	5-10N	10 / 10	25 / 25			20 / 29			-0.043	0.963	0.920
		6.0	10NW	8 / 10	8 / 13			26 / 32			-0.043	0.969	0.926
		4.5	0-5SE	5	3			11			-	-	-
		3.5	5N	25	35			32			-	-	-
		2.5	5NW	34 / 34	43 / 43			60*			-0.062	0.885	0.823
	0	8.7	5-10N	10 / 15	13 / 15			15 / 20			-0.044	0.967	0.923
		6.0	5-10N	24 / 24	21 / 21			22 / 25			-0.062	0.947	0.885
		4.5	5N	42 / 47	5 / 22			4 / 6			-0.054	0.956	0.902
		3.5	5-7NE	59 / 104	30 / 39			22 / 22			-0.054	0.896	0.842
		2.5	5NE	0 / 10	3 / 20			75 / 75			-0.061	0.919	0.858
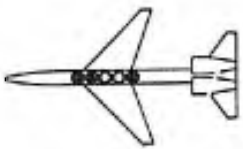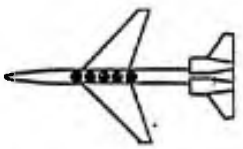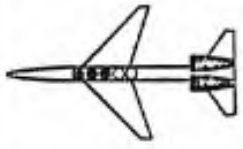
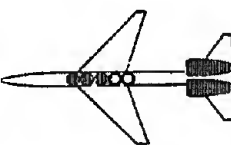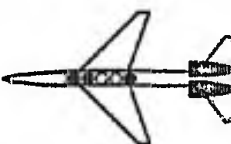$\pm$ Inlet temperature rise at time where ΣF_N = minimum

$\pm\pm$ Maximum (spatial average) temperature rise during the run

*Engine stall

TABLE 2–DATA SUMMARY

CONFIGURATION	FOR PLOTTED DATA SEE FIGURE NUMBER	α	$\dfrac{H}{D}$	WIND & DIRECTION	INLET TEMPERATURE RISE — ENGINE NUMBER 1	2	3	4	5	6	7
B₆	63	3.2	8.7	5-10N	68/83	29/44			34/35		
		4.0	6.0	5-10N	9/12	13/13			22/22		
		4.0	4.5	5N	31/31	2/2			0/0		
		4.0	3.5	5-7NE	0/7	7/7			0/3		
		1.0	2.5	5NE	15/15	4/4			4/4		
B₇	31	0	8.7								
		↓	6.0	5N	0	0	0	0	0		
			4.5	10S	0	0	0	0	0		
			3.5	5NE	0	0	0	0	0/0		
		▼	2.5	5NW	0	0/3	3	0	2/2		
B₈	34 64	-4	8.7	10-15N	11/12	3/3	9/16			4/6	7/32
		↓	6.0	8N	49/49	26/26	15/21			5/5	8/12
			4.5	10NW	14/26	10/26	29/32			13/18	58/62
			3.5	10NW	20/20	3/3	1/15			0/14	0/8
		▼	2.5	5-10W	24/37	28/38	49/49			13/25	13/32

± Inlet temperature rise at time where $\Sigma\,F_N$ = minimum

±± Maximum (spatial average) temperature rise during the run

*Engine stall

TABLE 2-DATA SUMMARY

R ...TED ...SEE ...RE ...BER	α	H/D	WIND & DIRECTION	INLET TEMPERATURE RISE — ENGINE NUMBER							$\frac{L_{JE}}{L_\infty}$	$\frac{F}{L_\infty}$	$\frac{L}{L_\infty}$
				1 (±/±±)	2	3	4	5	6	7			
	3.2	8.7	5-10N	68/83	29/44			34/35			-0.054	0.859	0.805
	4.0	6.0	5-10N	9/12	13/13			22/22			-0.057	0.960	0.903
	4.0	4.5	5N	31/31	2/2			0/0			-	-	-
	4.0	3.5	5-7NE	0/7	7/7			0/3			-0.062	1.000	0.938
	1.0	2.5	5NE	15/15	4/4			4/4			-0.063	0.985	0.922
	0 ↓	8.7									-	-	-
		6.0	5N	0	0	0	0	0			-	-	-
		4.5	10S	0	0	0	0	0			-	-	-
		3.5	5NE	0	0	0	0	0/0			-0.015	1.000	0.985
	▼	2.5	5NW	0	0/3	3	0	2/2			-0.027	0.990	0.971
	-4	8.7	10-15N	11/12	3/3	9/16			4/6	7/32	-0.064	0.969	0.905
		6.0	8N	49/49	26/26	15/21			5/5	8/12	-0.054	0.925	0.871
		4.5	10NW	14/26	10/26	29/32			13/18	58/62	-0.037	0.918	0.881
		3.5	10NW	20/20	3/3	1/15			0/14	0/8	-0.032	0.977	0.945
	▼	2.5	5-10W	24/37	28/38	49/49			13/25	13/32	-0.047	0.935	0.888

±Inlet temperature rise at time where $\sum F_N$ = minimum

±±Maximum (spatial average) temperature rise during the run

*Engine stall

2

TABLE 2 - DATA SUMMARY

CONFIGURATION	FOR PLOTTED DATA SEE FIGURE NUMBER	α	$\dfrac{H}{D}$	WIND & DIRECTION	INLET TEMPERATURE RISE — ENGINE NUMBER							
					1 ($\pm$ / $\pm\pm$)	2	3	4	5	6	7	
B8	32 64	0	8.7	10-15N	18/20	16/23	15/22			15/15	20/20	-0
			6.0	10-15NW	14/14	24/24	19/19			0/10	14/15	-0
			4.5	6NW	29/29	28/30	33/35			49/49	5/10	-0
			3.5	6NW	2/15	6/23	33/33			2/18	1/9	-0
			2.5	5NW	5/28	12/34	30/44			28/53	6/13	0
	64	3.2	8.7	5-10NW	11/11	21/21	15/15			5/6	11/11	-0.
		4.0	6.0	5-10N	2/20	5/20	20/29			22/22	21/44	-0.
		4.0	4.5	10N	0/23	0/20	20/36			36/36	70/70	-0.
		4.0	3.5	5-10N	56/56	42/45	46/46			0/28	10/65	0.
		1.0	2.5	5-10N	12/96	1/62	60*/			111/117	148/158	0.
B9	41 42	0	8.7	5-10N	14/15	16/18			20/21	19/23	26/26	-0.
			6.0	10N	15/40	29/29			50/50	15/25	58/58	-0.
			4.5	5N	29/97	33/89			67/90	43/55	63/105	-0.
			3.5	6NE	14/14	5/13			4/40	2/3	30/30	-0.
			2.5	5NE	14/14	36/58			51/71	5/18	53/80	+0.

$\pm$ Inlet temperature rise at time where $\sum F_N$ = minimum

$\pm\pm$ Maximum (spatial average) temperature rise during the run

* Engine stall

TABLE 2-DATA SUMMARY

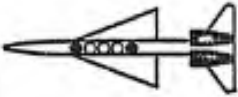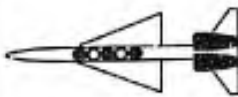| α	$\frac{H}{D}$	WIND & DIRECTION	1 (±/±±)	2	3	4	5	6	7	$\frac{L_{JE}}{L\infty}$	$\frac{F}{L\infty}$	$\frac{L}{L\infty}$
0	8.7	10-15N	18/20	16/23	15/22			15/15	20/20	-0.058	0.945	0.886
	6.0	10-15NW	14/14	24/24	19/19			0/10	14/15	-0.049	0.949	0.900
	4.5	6NW	29/29	28/30	35/35			49/49	5/10	-0.034	0.900	0.866
	3.5	6NW	2/15	6/23	33/33			2/28	1/9	-0.024	0.962	0.938
	2.5	5NW	5/28	12/34	30/44			28/53	6/13	0.043	0.961	1.004
3.2	8.7	5-10NW	11/11	21/21	15/15			5/6	11/11	-0.054	0.960	0.906
4.0	6.0	5-10N	2/20	5/20	20/29			22/22	21/44	-0.053	0.949	0.896
4.0	4.5	10N	0/23	0/20	20/36			36/36	70/70	-0.033	0.933	0.900
4.0	3.5	5-10N	56/56	42/45	46/46			0/28	10/65	0.062	0.907	0.969
1.0	2.5	5-10N	12/96	1/62	60*			111/117	148/158	0.147	0.777	0.924
0	8.7	5-10N	14/15	16/18			20/21	19/23	26/26	-0.032	0.938	0.906
	6.0	10N	15/40	29/29			50/50	15/25	58/58	-0.048	0.916	0.868
	4.5	5N	29/97	33/89			67/90	43/55	63/105	-0.047	0.840	0.793
	3.5	6NE	14/14	5/13			4/40	2/3	30/30	-0.018	0.973	0.955
	2.5	5NE	14/14	36/58			51/71	5/18	53/80	+0.001	0.915	0.916

±Inlet temperature rise at time where $\Sigma\ F_N$ = minimum

±±Maximum (spatial average) temperature rise during the run

*Engine stall

TABLE 2 - DATA SUMMARY

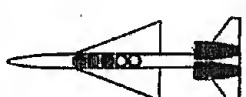| CONFIGURATION	FOR PLOTTED DATA SEE FIGURE NUMBER	α	$\dfrac{H}{D}$	WIND & DIRECTION	INLET TEMPERATURE RISE — ENGINE NUMBER						
					1 ($\pm$ / $\pm\pm$)	2	3	4	5	6	7
B8	32 / 64	0	8.7	10-15N	18 / 20	16 / 23	15 / 22			15 / 15	20 / 20
			6.0	10-15NW	14 / 14	24 / 24	19 / 19			0 / 10	14 / 15
			4.5	6NW	29 / 29	28 / 30	35 / 35			49 / 49	5 / 10
			3.5	6NW	2 / 15	6 / 23	33 / 33			2 / 28	1 / 9
			2.5	5NW	5 / 28	12 / 34	30 / 44			28 / 53	6 / 13
	64	3.2	8.7	5-10NW	11 / 11	21 / 21	15 / 15			5 / 6	11 / 11
		4.0	6.0	5-10N	2 / 20	5 / 20	20 / 29			22 / 22	21 / 44
		4.0	4.5	10N	0 / 23	0 / 20	20 / 36			36 / 36	70 / 70
		4.0	3.5	5-10N	56 / 56	42 / 45	46 / 46			0 / 28	10 / 65
		1.0	2.5	5-10N	12 / 96	1 / 62	60*			111 / 117	148 / 158
B9	41 / 42	0	8.7	5-10N	14 / 15	16 / 18			20 / 21	19 / 23	26 / 26
			6.0	10N	15 / 40	29 / 29			50 / 50	15 / 25	58 / 58
			4.5	5N	29 / 97	33 / 89			67 / 90	43 / 55	63 / 105
			3.5	6NE	14 / 14	5 / 13			4 / 40	2 / 3	30 / 30
			2.5	5NE	14 / 14	36 / 58			51 / 71	5 / 18	53 / 80

$\pm$Inlet temperature rise at time where $\Sigma\,F_N$ = minimum

$\pm\pm$Maximum (spatial average) temperature rise during the run

*Engine stall

TABLE 2-DATA SUMMARY

FOR PLOTTED DATA SEE FIGURE NUMBER	α	$\dfrac{H}{D}$	WIND & DIRECTION	INLET TEMPERATURE RISE — ENGINE NUMBER							$\dfrac{L_{JE}}{L_\infty}$	$\dfrac{F}{L_\infty}$	$\dfrac{L}{L_\infty}$
				1 ($\pm$/$\pm\pm$)	2	3	4	5	6	7			
	0	8.7	10-15N	18/20	16/23	15/22			15/15	20/20	-0.058	0.945	0.886
2, 4		6.0	10-15NW	14/14	24/24	19/19			0/10	14/15	-0.049	0.949	0.900
		4.5	6NW	29/29	28/30	35/35			49/49	5/10	-0.034	0.900	0.866
		3.5	6NW	2/15	6/23	33/33			2/28	1/9	-0.024	0.962	0.938
		2.5	5NW	5/28	12/34	30/44			28/53	6/13	0.043	0.961	1.004
	3.2	8.7	5-10NW	11/11	21/21	15/15			5/6	11/11	-0.054	0.960	0.906
	4.0	6.0	5-10N	2/20	5/20	20/29			22/22	21/44	-0.053	0.949	0.896
	4.0	4.5	10N	0/23	0/20	20/36			36/36	70/70	-0.033	0.933	0.900
	4.0	3.5	5-10N	56/56	42/45	46/46			0/28	10/65	0.062	0.907	0.969
	1.0	2.5	5-10N	12/96	1/62	60*			111/117	148/158	0.147	0.777	0.924
	0	8.7	5-10N	14/15	16/18			20/21	19/23	26/26	-0.032	0.938	0.906
		6.0	10N	15/40	29/29			50/50	15/25	58/58	-0.048	0.916	0.868
		4.5	5N	29/97	33/89			67/90	43/55	63/105	-0.047	0.840	0.793
		3.5	6NE	14/14	5/13			4/40	2/3	30/30	-0.018	0.973	0.955
		2.5	5NE	14/14	36/58			51/71	5/18	53/80	+0.001	0.915	0.916

$\pm$ Inlet temperature rise at time where $\Sigma\, F_N$ = minimum

$\pm\pm$ Maximum (spatial average) temperature rise during the run

* Engine stall

TABLE 2- DATA SUMMARY

CONFIGURATION	FOR PLOTTED DATA SEE FIGURE NUMBER	α	$\dfrac{H}{D}$	WIND & DIRECTION	INLET TEMPERATURE RISE — ENGINE NUMBER 1 (±/±±)	2	3	4	5	6	7
B_{10}	43 44	0	8.7	10-15N	16/21	15/23	21/25	22/27	25*	15/28	20/29
			6.0	7N	5/12	8/11	7/18	28/28	36/36	8/8	29/29
			4.5	7SE	3/24	4/41	14/54	38/66	68/74	18/42	46/46
			3.5	5NE	0/0	0/1	18/18	20/20	15/15	0/3	0/4
			2.0	5NW	16/16	11/11	8/16	15/18	10/20	0/10	0/7
C_1	57 60	0	8.7	5-10NW	22/32				19/20	0/0	0/0
			6.0	5-10N	30/30				9/12	0/0	0/0
			4.5	5-10NW	31/31				14/14	0/0	0/10
			3.5	5-10NW	54/54				25/25	0/7	0/5
			2.5	5-10	22/1				14/0	18/0	5/0
C_2	65	-4	8.7	5SE	9/15		27/27		30/30	0/0	0/7
			6.0	5NE	20/40		26/26		5/15	0/0	5/10
			4.5	5SE	55/65		52/71		34/196	10/35	23/46
			3.5	5NW*	110*/157		104*		71/81	20/29	76/80
			2.5	—							

±Inlet temperature rise at time where $\Sigma\, F_N$ = minimum

±±Maximum (spatial average) temperature rise during the run

*Engine stall

TABLE 2- DATA SUMMARY

ED EE E ER	α	$\dfrac{H}{D}$	WIND & DIRECTION	INLET TEMPERATURE RISE ENGINE NUMBER							$\dfrac{L_{JE}}{L_\infty}$	$\dfrac{F}{L_\infty}$	$\dfrac{L}{L_\infty}$
				1 $\pm$/$\pm\pm$	2	3	4	5	6	7			
	0	8.7	10-15N	16/21	15/23	21/25	22/27	25*/	15/28	20/29	-0.047	0.956	0.909
		6.0	7N	5/12	8/11	7/18	28/28	36/36	8/8	29/29	—	--	—
		4.5	7SE	3/24	4/41	14/54	38/66	68/74	18/42	46/46	—	—	—
		3.5	5NE	0/0	0/1	18/18	20/20	15/15	0/3	0/4	0.019	0.970	0.951
		2.0	5NW	16/16	11/11	8/16	15/18	10/20	0/10	0/7	0.005	0.964	0.969
	0	8.7	5-10NW	22/32				19/20	0/0	0/0	-0.026	0.961	0.935
		6.0	5-10N	30/30				9/12	0/0	0/0	-0.029	0.969	0.940
		4.5	5-10NW	31/31				14/14	0/0	0/10	-0.039	0.960	0.921
		3.5	5-10NW	54/54				25/25	0/7	0/5	-0.021	0.933	0.912
		2.5	5-10	22/1				14/0	18/0	5/0	0.023	0.952	0.975
	-4	8.7	5SE	9/15		27/27		30/30	0/0	0/7	-0.041	0.947	0.906
		6.0	5NE	20/40		26/26		5/15	0/0	5/10	-0.033	0.968	0.935
		4.5	5SE	55/65		52/71		34/196	10/35	23/46	-0.027	0.899	0.872
		3.5	5NW*	110*/157		104*/		71/81	20/29	76/80	0.011	0.768	0.779
		2.5	—								—	—	—

$\pm$Inlet temperature rise at time where $\Sigma \, F_N$ = minimum

$\pm\pm$Maximum (spatial average) temperature rise during the run
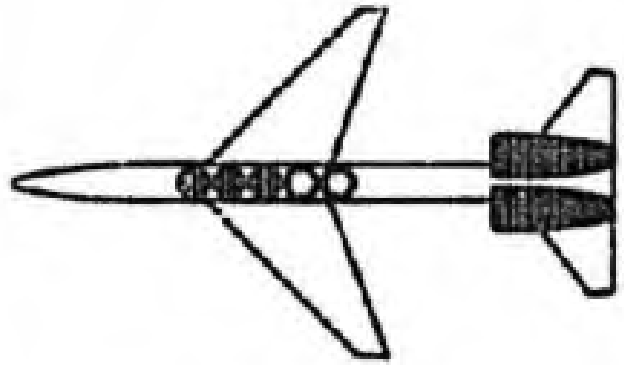
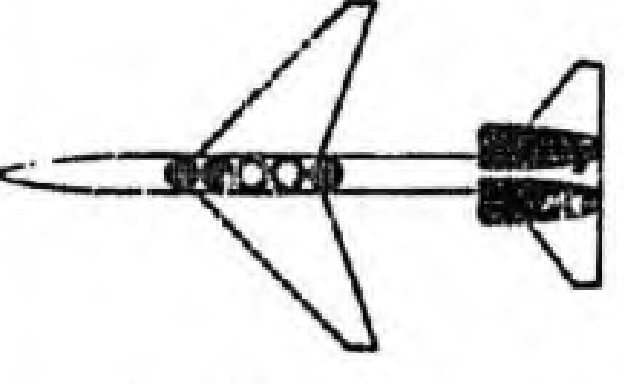*Engine stall

TABLE 2-DATA SUMMARY

CONFIGURATION	FOR PLOTTED DATA SEE FIGURE NUMBER	α	$\dfrac{H}{D}$	WIND & DIRECTION	INLET TEMPERATURE RISE ENGINE NUMBER						
					$\pm$ / $\pm\pm$ 1	2	3	4	5	6	7
C$_2$	57 60 65	0	8.7	5SE	3 / 3		6 / 6		8 / 8	0 / 0	0 / 0
			6.0	5NE	28 / 28		20 / 29		1 / 12	0 / 0	0 / 10
			4.5	5NE	27 / 47		42 / 54		30 / 39	0 / 4	15 / 15
			3.5	5SW	42 / 45		103*		57 / 57	31 / 35	69 / 70
	65	3.2	8.7	5S	10 / 15		8 / 10		2 / 5	0 / 0	0 / 0
		4.0	6.0	0	15 / 0		26 / 26		10 / 1	0 / 0	5 / 6
		4.0	4.5	5NE	25 / 33		50 / 51		61 / 61	0 / 0	41 / 41
		4.0	3.5	5-10N	8 / 8		24 / 24		24 / 24	0 / 0	1 / 7
		1.0	2.5	5NE	33*		4 / 10		20 / 20	2 / 8	26 / 35
C$_3$	32 34 49 45 53 57	0	8.7	5-10N	20 / 20	10 / 24	2 / 22			1 / 1	3 / 3
			6.0	5N	15 / 27	40 / 43	31 / 40			8 / 8	14 / 27
			4.5	5-10N	13 / 38	28 / 38	42 / 57			2 / 19	20 / 41
			3.5	5-10N	31 / 45	36 / 36	11 / 22			6 / 20	5 / 13
			2.5	5-10N	16 / 40	19 / 30	30 / 30			11 / 11	8 / 13

$\pm$Inlet temperature rise at time where $\Sigma\ F_N$ = minimum

$\pm\pm$Maximum (spatial average) temperature rise during the run

*Engine stall

51

TABLE 2-DATA SUMMARY

OR TTED SEE URE BER	α	$\dfrac{H}{D}$	WIND & DIRECTION	INLET TEMPERATURE RISE — ENGINE NUMBER 1	2	3	4	5	6	7	$\dfrac{L_{JE}}{L\infty}$	$\dfrac{F}{L\infty}$	$\dfrac{L}{L\infty}$
	0	8.7	5SE	3 / 3		6 / 6		8 / 8	0 / 0	0 / 0	-0.039	0.994	0.955
		6.0	5NE	28 / 28		20 / 29		1 / 12	0 / 0	0 / 10	-0.030	0.959	0.929
		4.5	5NE	27 / 47		42 / 54		30 / 39	0 / 4	15 / 15	-0.021	0.902	0.881
		3.5	5SW	42 / 45		103*		57 / 57	31 / 35	69 / 70	-0.002	0.820	0.818
	3.2	8.7	5S	10 / 15		8 / 10		2 / 5	0 / 0	0 / 0	-0.034	0.980	0.946
	4.0	6.0	0	15 / 0		26 / 26		10 / 1	0 / 0	5 / 6	-0.028	0.957	0.929
	4.0	4.5	5NE	25 / 33		50 / 51		61 / 61	0 / 0	41 / 41	-0.020	0.905	0.885
	4.0	3.5	5-10N	8 / 8		24 / 24		24 / 24	0 / 0	1 / 7	0.101	0.950	1.051
	1.0	2.5	5NE	33*		4 / 10		20 / 20	2 / 8	26 / 35	0.180	0.930	1.110
	0	8.7	5-10N	20 / 20	10 / 24	2 / 22			1 / 1	3 / 3	-0.056	0.981	0.925
		6.0	5N	15 / 27	40 / 43	31 / 40			8 / 8	14 / 27	-0.051	0.918	0.867
		4.5	5-10N	13 / 38	28 / 38	42 / 57			2 / 19	20 / 41	-0.038	0.899	0.861
		3.5	5-10N	31 / 45	36 / 36	11 / 22			6 / 20	5 / 13	-0.017	0.934	0.917
		2.5	5-10N	16 / 40	19 / 30	30 / 30			11 / 11	8 / 13	0.033	0.940	0.973

±Inlet temperature rise at time where ΣF_N = minimum

±±Maximum (spatial average) temperature rise during the run

*Engine stall

TABLE 2 - DATA SUMMARY

CONFIGURATION	FOR PLOTTED DATA SEE FIGURE NUMBER	α	$\frac{H}{D}$	WIND & DIRECTION	INLET TEMPERATURE RISE ENGINE NUMBER 1 (± / ±±)	2	3	4	5	6	7
C₄	48 50 53	0	8.7	5-NNE	15 / 15	12 / 16	27 / 28			13 / 20	15 / 18
			6.0	5-NNE	30 / 30	13 / 34	10 / 47			10 / 24	73 / 73
			4.5	5NE	30 / 45	41 / 50	43 / 60			79 / 80	33 / 40
			3.5	5NE	0 / 3	17 / 24	31 / 31			36 / 36	22 / 40
			2.5	5NE	23 / 23	16 / 16	14 / 18			18 / 18	22 / 22
D₁	27	0	8.7	0-5ESE	2 / 2						
			6.0	1-3SW	0 / 0						
			4.5	5E	1 / 1						
			3.5	3SE	0 / 0						
			2.5	0	0 / 0						
D₂	27	0	8.7	5SW						2 / 2	
			6.0	0-2SE						4 / 4	
			4.5	5SE						0 / 0	
			3.5	3ESE						0 / 0	
			2.5	3SE						0 / 0	

±Inlet temperature rise at time where $\Sigma \, F_N$ = minimum

±±Maximum (spatial average) temperature rise during the run

*Engine stall

TABLE 2—DATA SUMMARY

FOR PLOTTED DATA SEE FIGURE NUMBER	α	$\dfrac{H}{D}$	WIND & DIRECTION	INLET TEMPERATURE RISE — ENGINE NUMBER							$\dfrac{L_{JE}}{L_\infty}$	$\dfrac{F}{L_\infty}$	$\dfrac{L}{L_\infty}$
				1 (±/±±)	2	3	4	5	6	7			
	0	8.7	5-NNE	15 / 15	12 / 16	27 / 28			13 / 20	15 / 18	−0.063	0.963	0.900
8		6.0	5-NNE	30 / 30	13 / 34	10 / 47			10 / 24	73 / 73	−0.056	0.927	0.871
0		4.5	5NE	30 / 45	41 / 50	43 / 60			79 / 80	33 / 40	−0.044	0.851	0.807
3		3.5	5NE	0 / 3	17 / 24	31 / 31			36 / 36	22 / 40	−0.018	0.925	0.907
		2.5	5NE	23 / 23	16 / 16	14 / 18			18 / 18	22 / 22	0.006	0.957	0.963
	0	8.7	0-5ESE	2 / 2							−0.022	0.990	0.968
7		6.0	1-3SW	0 / 0							−0.029	1.000	0.971
		4.5	5E	1 / 1							−0.045	0.995	0.950
		3.5	3SE	0 / 0							−0.060	1.000	0.940
		2.5	0	0 / 0							−0.056	1.000	0.944
	0	8.7	5SW					2 / 2			−0.034	0.989	0.955
		6.0	0-2SE					4 / 4			−0.022	0.982	0.960
		4.5	5SE					0 / 0			−0.025	1.000	0.975
		3.5	3ESE					0 / 0			−0.057	1.000	0.943
		2.5	3SE					0 / 0			−0.104	1.000	0.896

±Inlet temperature rise at time where ΣF_N = minimum

±±Maximum (spatial average) temperature rise during the run

*Engine stall

TABLE 2–DATA SUMMARY

CONFIGURATION	FOR PLOTTED DATA SEE FIGURE NUMBER	α	$\dfrac{H}{D}$	WIND & DIRECTION	INLET TEMPERATURE RISE — ENGINE NUMBER						
					1 ($\pm$ / $\pm\pm$)	2	3	4	5	6	7
D_3	28 36	0	8.7	7N		0/0		0/0			
			6.0	6N		0/0		0/0			
			4.5	7NE		6/6		0/0			
			2.5	5N		0		18/18			
		↓	2.5	6NNW		0		33/33			
D_4	28 37	0	8.7	0-2S	102/102				10/32		
			6.0	0	120/120				20/20		
			4.5	5SE	100/100				14/14		
			3.5	3SE	58*				0/4		
		↓	2.5	3SE	13*				4/9		
E_1	66	-4	8.7	6N	8/22	8/26	21/34			55/55	42/56
			6.0	6NW	13/20	12/25	45/45			12/17	37/47
			4.5	7N	3/14	18/18	16/25			1/7	21/21
			3.5	5-10N	12/20	13/16	45/45			12/16	32/32
		↓	2.5	7N	40/40	32/40	31*			36/45	13/15

$\pm$ Inlet temperature rise at time where ΣF_N = minimum

$\pm\pm$ Maximum (spatial average) temperature rise during the run

* Engine stall

53

TABLE 2 - DATA SUMMARY

(OR TTED SEE URE BER)	α	$\frac{H}{D}$	WIND & DIRECTION	INLET TEMPERATURE RISE — ENGINE NUMBER 1 (±/±±)	2	3	4	5	6	7	$\frac{L_{JE}}{L_\infty}$	$\frac{F}{L_\infty}$	$\frac{L}{L_\infty}$
	0	8.7	7N		0/0		0/0				-0.032	1.000	0.968
		6.0	6N		0/0		0/0				-0.032	1.000	0.968
		4.5	7NE		6/6		0/0				-0.026	0.987	0.961
		3.5	5N		0		18/18				-0.050	0.980	0.930
		2.5	6NNW		0		33/33				-0.096	0.940	0.844
	0	8.7	0-2S	102/102				10/32			-0.028	0.796	0.768
		6.0	0	120/120				20/20			-0.022	0.753	0.731
		4.5	5SE	100/100				14/14			-0.024	0.792	0.768
		3.5	3SE	58*				0/4			-0.036	0.890	0.854
		2.5	3SE	13*				4/9			-0.049	0.963	0.914
	-4	8.7	6N	8/22	8/26	21/34			55/55	42/56	-0.057	0.918	0.861
		6.0	6NW	13/20	12/25	45/45			12/17	37/47	-0.048	0.943	0.895
		4.5	7N	3/14	18/18	16/25			1/7	21/21	-0.040	0.964	0.924
		3.5	5-10N	12/20	13/16	45/45			12/16	32/32	-0.028	0.951	0.923
		2.5	7N	40/40	32/40	31*			36/45	13/15	-0.027	0.883	0.856

±Inlet temperature rise at time where ΣF_N = minimum
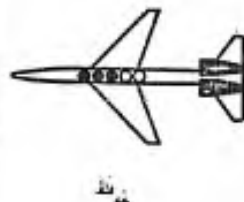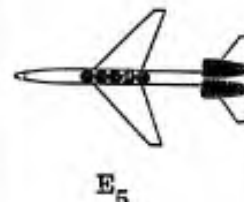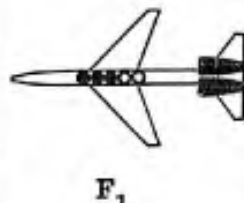
±±Maximum (spatial average) temperature rise during the run

*Engine stall

TABLE 2–DATA SUMMARY

CONFIGURATION	FOR PLOTTED DATA SEE FIGURE NUMBER	α	$\dfrac{H}{D}$	WIND & DIRECTION	INLET TEMPERATURE RISE — ENGINE NUMBER							$\dfrac{L}{L}$
					1 ±/±±	2	3	4	5	6	7	
E₁	33 35 54 66	0	8.7	5-10N	1/7	9/9	14/38			0/7	0/7	-0.0
			6.0	5-10NW	28/30	25/26	37/37			13/26	34/42	-0.0
			4.5	5-10N	4/14	2/12	6/20			8/19	0/19	-0.0
			3.5	5-10N	1/19	0/15	28/28			12/23	7/14	-0.0
		▼	2.5	7N	3/10	2/2	6/8			8/12	6/6	0.0
	66	3.2	8.7	5-10N	30/30	19/21	9/19			3/8	3/13	-0.0
		4.0	6.0	5-10N	55/60	29/39	44/48			20/32	44/56	-0.0
		4.0	4.5	5-10NW	3/10	5/11	8/28			47/47	4/10	-0.0
		4.0	3.5	5-10NW	26/26	30/30	26/32			9/21	11/22	0.0
		1.0	2.5	5-10NW	19/19	2/13	5/12			6/15	4/12	0.1
E₂	41 42	0	8.7	0	48/48	0/1			3/14	0/0	0/8	-0.0
			6.0	1-2N	60/60	9/17			15/39	5/5	16/38	-0.0
			4.5	5N	34*/	6/6			17*/17	5/8	0/10	-0.0
			3.5	0-5N	38/38	5/5			27*/0	0/0	13/13	-0.0
		▼	2.5	5N	51/51	53/53			91*	69/69	158/158	+0.0

±Inlet temperature rise at time where ΣF_N = minimum
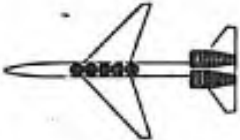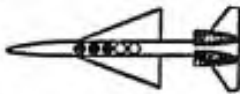
±±Maximum (spatial average) temperature rise during the run

*Engine stall

TABLE 2 - DATA SUMMARY

FOR PLOTTED DATA SEE FIGURE NUMBER	α	$\frac{H}{D}$	WIND & DIRECTION	INLET TEMPERATURE RISE — ENGINE NUMBER							$\frac{L_{JE}}{L_\infty}$	$\frac{F}{L_\infty}$	$\frac{L}{L_\infty}$
				1 ±/±±	2	3	4	5	6	7			
	0	8.7	5-10N	1/7	9/9	14/38			0/7	0/7	-0.065	0.976	0.911
33		6.0	5-10NW	28/30	25/26	37/37			13/26	34/42	-0.051	0.900	0.849
35		4.5	5-10N	4/14	2/12	6/20			8/19	0/19	-0.026	0.985	0.959
54		3.5	5-10N	1/19	0/15	28/28			12/23	7/14	-0.020	0.972	0.952
66		2.5	7N	3/10	2/2	6/8			8/12	6/6	0.042	0.984	1.026
	3.2	8.7	5-10N	30/30	19/21	9/19			3/8	3/13	-0.058	0.953	0.895
	4.0	6.0	5-10N	55/60	29/39	44/48			20/32	44/56	-0.044	0.889	0.845
66	4.0	4.5	5-10NW	3/10	5/11	8/28			47/47	4/10	-0.032	0.938	0.906
	4.0	3.5	5-10NW	26/26	30/30	26/32			9/21	11/22	0.024	0.927	0.951
	1.0	2.5	5-10NW	19/19	2/13	5/12			6/15	4/12	0.133	0.985	1.118
	0	8.7	0	48/48	0/1			3/14	0/0	0/8	-0.021	0.956	0.935
		6.0	1-2N	60/60	9/17			15/39	5/5	16/38	-0.041	0.916	0.875
41		4.5	5N	34*/	6/6			17*/17	5/8	0/10	-0.038	0.950	0.912
42		3.5	0-5N	38/38	5/5			27*/	0/0	13/13	-0.014	0.935	0.921
		2.5	5N	51/51	53/53			91*/	69/69	158/158	+0.018	0.608	0.626

±Inlet temperature rise at time where ΣF_N = minimum

±±Maximum (spatial average) temperature rise during the run

*Engine stall

TABLE 2-DATA SUMMARY

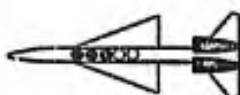| CONFIGURATION	FOR PLOTTED DATA SEE FIGURE NUMBER	α	$\dfrac{H}{D}$	WIND & DIRECTION	INLET TEMPERATURE RISE ENGINE NUMBER							
					1 ± / ±±	2	3	4	5	6	7	
E₃	43 44 52	0	8.7	2-3N	6/6	8/8	4/4	5/7	11/12	5/5	6/6	-0
			6.0	5NE	0/7	0/7	20/20	3/28	18/35	0/5	21/21	-0
			4.5	5NE	22/28	39/39	21/37	10/30	12/65	10/20	12/40	-0
			3.5	6-7N	0/10	15/25	8/22	14/14	35/23	12/18	0/0	-0
			2.5	6-7NW	10/10	16/8	18/13	16/11	7/14	3/10	3/3	0
E₄	67	-4	8.7	5ESE	10/18	10/22	21/21			30/50	52/52	-0
			6.0	5ESE	?/10	0/18	25/25			50/50	5/48	-0
			4.5	5NW	2/21	8/29	42*/84			10/84	94/94	-0
			3.5	6NNW	1/2	20/24	49*/84			60/84	76/76	-0
			2.5	5N	15/19	10/25	4/20			11/20	5/26	-
	54 61 67	0	8.7	5NE	2/10	9/14	20/20			8/32	37/37	
			6.0	5E	0/20	0/30	10/26			0/9	48/48	-
			4.5	6N	4/22	11/20	8/21			43/80	42/70	-
			3.5	5N	17/25	19/20	42/55			78/90	46/60	-
			2.5	5-7N	52/52	16/34	9/31			38/52	21/23	

±Inlet temperature rise at time where ΣF_N = minimum

±±Maximum (spatial average) temperature rise during the run
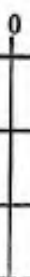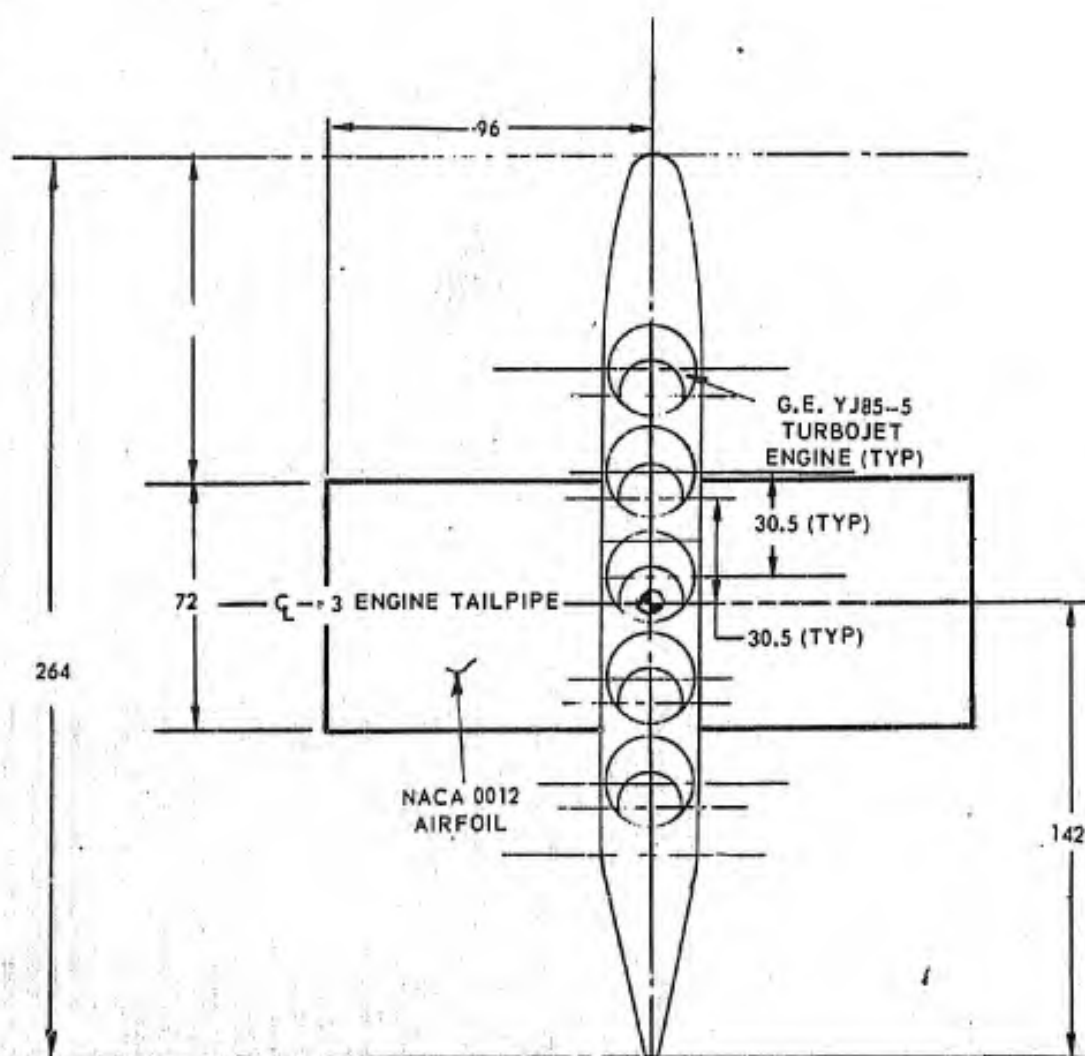
*Engine stall

TABLE 2-DATA SUMMARY

	α	$\dfrac{H}{D}$	WIND & DIRECTION	INLET TEMPERATURE RISE ENGINE NUMBER 1 (± / ±±)	2	3	4	5	6	7	$\dfrac{L_{JE}}{L_\infty}$	$\dfrac{F}{L_\infty}$	$\dfrac{L}{L_\infty}$
	0	8.7	2-3N	6/6	8/8	4/4	5/7	11/12	5/5	6/6	-0.049	0.965	0.916
		6.0	5NE	0/7	0/7	20/20	3/28	18/35	0/5	21/21	-0.046	0.977	0.931
		4.5	5NE	22/28	39/39	21/37	10/30	12/65	10/20	12/40	-0.026	0.949	0.923
		3.5	6-7N	0/10	15/25	8/22	14/14	35/23	12/18	0/0	-0.014	0.953	0.929
		2.5	6-7NW	10/10	16/8	18/13	16/11	7/14	3/10	3/3	0.004	0.954	0.958
	-4	8.7	5ESE	10/18	10/22	21/21			30/50	52/52	-0.061	0.885	0.824
		6.0	5ESE	2/10	0/18	25/25			50/50	5/48	-0.056	0.933	0.877
		4.5	5NW	2/21	8/29	42*/			10/84	94/94	-0.036	0.880	0.844
		3.5	6NNW	1/2	20/24	49*			60/84	76/76	-0.027	0.872	0.845
		2.5	5N	15/19	10/25	4/20			11/20	5/26	-0.032	0.958	0.926
	0	8.7	5NE	2/10	9/14	20/20			8/32	37/37	-0.057	0.944	0.887
		6.0	5E	0/20	0/30	10/26			0/9	48/48	-0.048	0.946	0.898
		4.5	6N	4/22	11/20	8/21			43/80	42/70	-0.033	0.917	0.884
		3.5	5N	17/25	19/20	42/55			78/90	46/60	-0.013	0.824	0.811
		2.5	5-7N	52/52	16/34	9/31			38/52	21/23	0.029	0.914	0.943

±Inlet temperature rise at time where ΣF_N = minimum

±±Maximum (spatial average) temperature rise during the run

*Engine stall

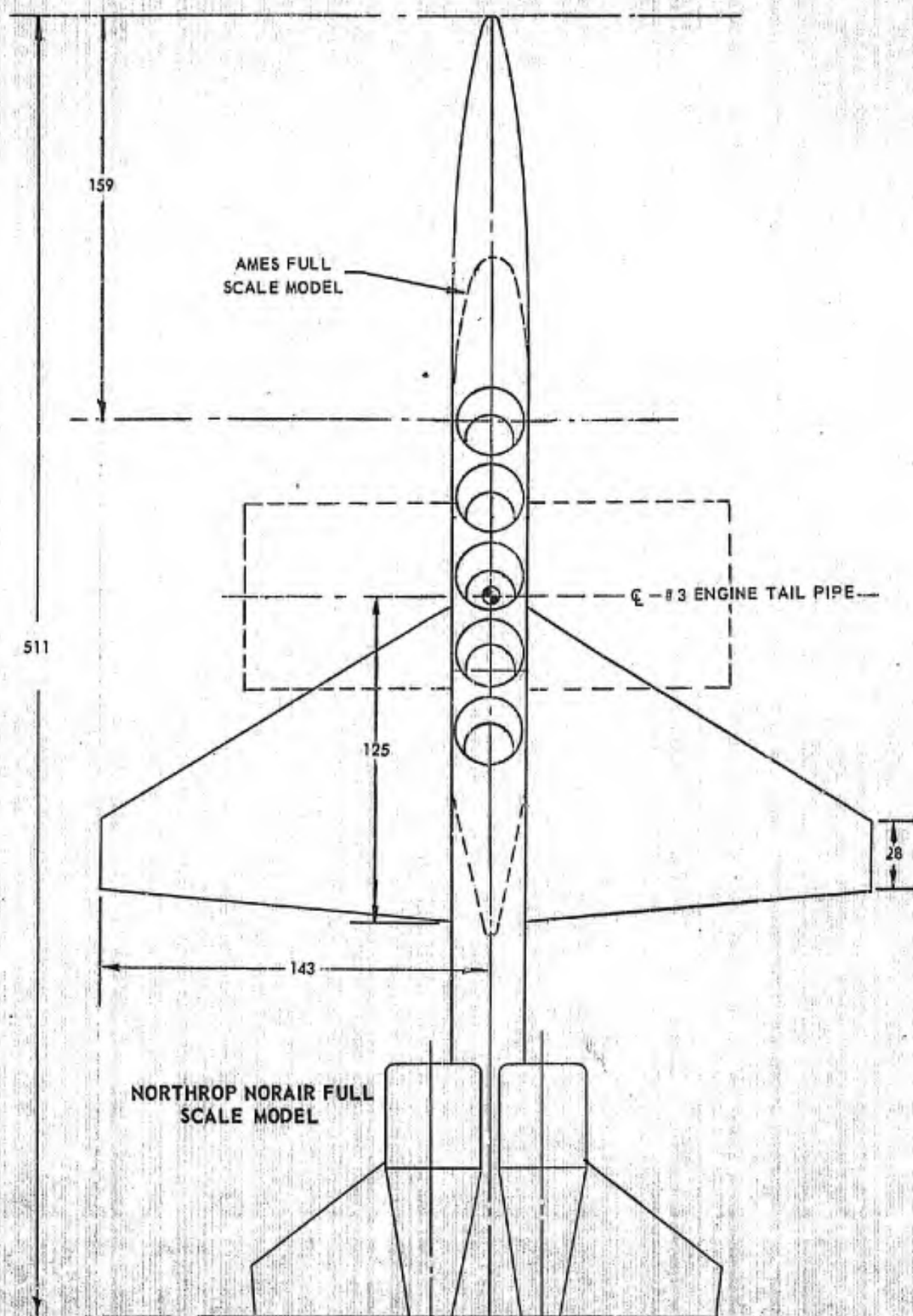TABLE 2-DATA SUMMARY

CONFIGURATION	FOR PLOTTED DATA SEE FIGURE NUMBER	α	$\frac{H}{D}$	WIND & DIRECTION	INLET TEMPERATURE RISE ENGINE NUMBER 1	2	3	4	5	6	7	$\frac{L}{L}$
E_4	67	3.2	8.7	5E	2/13	3/10	2/18			15/15	11/11	-0.
		4.0	6.0	5NW	0/10	0/2	0/12			36/36	37/61	-0.
		4.0	4.5	5NNW	2/20	0/15	0/30			74/74	15/35	-0.
		4.0	3.5	5NNW	0/10	0/15	1/20			70/70	5/15	0.
		1.0	2.5	5-7N	3/20	0/30	2/28			30/41	60/60	0.
E_5	52 58 61	0	8.7	7N	5/5	5/6	5/5	4/5	6/12	5/5	7/21	-0.
			6.0	7NE	4/11	7/12	7/19	5/24	5/15	30/30	40/40	-0.
			4.5	5N	0/13	0/12	9/26	43/45	52/61	6/34	11/47	-0.
			3.5	7NW	14/42	23/23	64/64	68/68	13/43	39/39	59/106	-0.
			2.5	8-10N	4/15	4/24	11*/37	36/37	20*/132	4/40	75/115	0.
F_1	59 62	0	8.7	7N	29/29	23/23	16/30			3/8	26/27	-0.
			6.0	5N	18/22	42/42	29*/43			8/15	33/39	-0.
			4.5	5-10N	38/50	67/67	73/73			57/71	32/58	-0.
			3.5	8NW	45/50	73/73	39/46			10/23	76/76	-0.
			2.0	8NW	75/75	73/73	30/51			84/84	21/40	0.

±Inlet temperature rise at time where ΣF_N = minimum

±±Maximum (spatial average) temperature rise during the run

*Engine stall

TABLE 2-DATA SUMMARY

(NUMBER – SEE FIGURE)	α	$\dfrac{H}{D}$	WIND & DIRECTION	INLET TEMPERATURE RISE — ENGINE NUMBER 1	2	3	4	5	6	7	$\dfrac{L_{JE}}{L_\infty}$	$\dfrac{F}{L_\infty}$	$\dfrac{L}{L_\infty}$
				±/±±									
	3.2	8.7	5E	2/13	3/10	2/13			15/15	11/11	-0.060	0.978	0.918
	4.0	6.0	5NW	0/10	0/2	0/12			36/36	37/61	-0.057	0.903	0.846
	4.0	4.5	5NNW	2/20	0/15	0/30			74/74	15/35	-0.016	0.944	0.928
	4.0	3.5	5NNW	0/10	0/15	1/20			70/70	5/15	0.063	0.930	0.993
	1.0	2.5	5-7N	3/20	0/30	2/28			30/41	60/60	0.126	0.955	1.081
0		8.7	7N	5/5	5/6	5/5	4/5	6/12	5/5	7/21	-0.049	0.976	0.927
		6.0	7NE	4/11	7/12	7/19	5/24	5/15	30/30	40/40	-0.046	0.956	0.910
		4.‹	5N	0/13	0/12	9/26	43/45	52/61	6/34	11/47	-0.029	0.930	0.901
		3.5	7NW	14/42	23/23	64/64	68/68	13/43	39/39	59/106	-0.011	0.837	0.826
		2.5	8-10N	4/15	4/24	11*/37	36/37	20*/132	4/40	75/115	0.012	0.919	0.931
0		8.7	7N	29/29	23/23	16/30			3/8	26/27	-0.082	0.944	0.862
		6.0	5N	18/22	42/42	29*/43			8/15	33/39	-0.074	0.951	0.877
		4.5	5-10N	38/50	67/67	73/73			57/71	32/58	-0.061	0.850	0.793
		3.5	8NW	45/50	73/73	39/46			10/23	76/76	-0.029	0.844	0.815
		2.0	8NW	75/75	73/73	30/51			84/84	21/40	0.003	0.835	0.838

± Inlet temperature rise at time where ΣF_N = minimum

±± Maximum (spatial average) temperature rise during the run

* Engine stall

TABLE 2 – DATA SUMMARY

CONFIGURATION	FOR PLOTTED DATA SEE FIGURE NUMBER	α	$\dfrac{H}{D}$	WIND & DIRECTION	INLET TEMPERATURE RISE ENGINE NUMBER 1 ($\pm$ / $\pm\pm$)	2	3	4	5	6	7	
F₂	59 62	0	8.7	5N	12 / 13	24 / 24	31 / 31	21 / 26	9 / 17	0 / 4	7 / 23	-0.
		0	6.0	5N	4 / 4	7 / 7	12 / 22	9 / 22	24 / 24	0 / 2	26 / 26	-0.
		0	4.5	5N	0 / 7	4 / 26	*33 / 33	42 / 42	14 / 14	2 / 2	30 / 36	-0.
		0	3.5	5N	15 / 27	16 / 42	39 / 61	37 / 47	0 / 49	2 / 2	75 / 75	-0.
		0	2.5	5N	23 / 24	10 / 19	5 / 12	0 / 0	0 / 7	1 / 6	32 / 32	0.
G₁	33 35 49 56 45 51	0	8.7	9N	19 / 21	30 / 30	20 / 20			5 / 13	7 / 20	-0.
		0	6.0	5E	38 / 59	41 / 47	45 / 46			2 / 8	32 / 32	-0.
		0	4.5	5SE	0 / 12	2 / 2	16 / 16			0 / 5	2 / 7	-0.
		0	3.5	1-2S	0 / 4	3 / 5	4 / 5			0 / 5	10 / 10	-0.
		0	2.5	5E	0 / 0	0 / 0	0 / 0			0 / 0	0 / 0	0.
G₂	48 50 51 56	0	8.7	5-7N	24 / 24	36 / 36	27 / 27			18 / 66	47 / 55	-0.
		0	6.0	0-10N	13 / 37	16 / 24	10 / 20			5 / 41	55 / 97	-0.
		0	4.5	0-10N	16 / 16	28 / 29	40 / 40			81 / 118	20 / 42	-0.
		0	3.5	0-5E	0 / 37	0 / 34	4 / 40			70 / 75	12 / 74	-0.
		0	2.5	5-10N	12 / 12	10 / 10	8 / 8			71 / 78	1 / 49	0.

$\pm$ Inlet temperature rise at time where $\Sigma\, F_N$ = minimum

$\pm\pm$ Maximum (spatial average) temperature rise during the run

*Engine stall

57

TABLE 2 -DATA SUMMARY

...ED EE E CR	α	$\dfrac{H}{D}$	WIND & DIRECTION	INLET TEMPERATURE RISE — ENGINE NUMBER 1 $\pm$ / $\pm\pm$	2	3	4	5	6	7	$\dfrac{L_{JE}}{L\infty}$	$\dfrac{F}{L\infty}$	$\dfrac{L}{L\infty}$
	0	8.7	5N	12/13	24/24	31/31	21/26	9/17	0/4	7/23	-0.067	0.966	0.899
	0	6.0	5N	4/4	7/7	12/22	9/22	24/24	0/2	26/26	-0.064	0.957	0.873
	0	4.5	5N	0/7	4/26	*33/33	42/42	14/14	2/2	30/36	-0.041	0.923	0.882
	0	3.5	5N	15/27	16/42	39/61	37/47	0/49	2/2	75/75	-0.017	0.909	0.892
	0	2.5	5N	23/24	10/19	5/12	0/0	0/7	1/6	32/32	0.005	0.948	0.953
	0	8.7	9N	19/21	30/30	20/20			5/13	7/20	-0.049	0.957	0.908
	0	6.0	5E	38/59	41/47	45/46			2/8	32/32	-0.040	0.909	0.869
	0	4.5	5SE	0/12	2/2	16/16			0/5	2/7	-0.036	0.986	0.950
	0	3.5	1-2S	0/4	3/5	4/5			0/5	10/10	-0.005	0.987	0.982
	0	2.5	5E	0/0	0/0	0/0			0/0	0/0	0.035	1.000	1.035
	0	8.7	5-7N	24/24	36/36	27/27			18/66	47/55	-0.058	0.923	0.865
	0	6.0	0-10N	13/37	16/24	10/20			5/41	55/97	-0.042	0.944	0.902
	0	4.5	0-10N	16/16	28/29	40/40			81/118	20/42	-0.027	0.939	0.843
	0	3.5	0-5E	0/37	0/34	4/40			70/75	12/74	-0.011	0.950	0.939
	0	2.5	5-10N	12/12	10/10	8/8			71/78	1/49	0.023	0.941	0.964

$\pm$ Inlet temperature rise at time where ΣF_N = minimum

$\pm\pm$ Maximum (spatial average) temperature rise during the run

*Engine stall

TABLE 2–DATA SUMMARY

CONFIGURATION	FOR PLOTTED DATA SEE FIGURE NUMBER	α	$\dfrac{H}{D}$	WIND & DIRECTION	INLET TEMPERATURE RISE ENGINE NUMBER ± / ±±							
					1	2	3	4	5	6	7	
H₁	45 49 55	0	8.7	5NNE	8/10	15/15	5/5			0/5	0/12	-0.
			6.0	5NE	20/43	28/30	43/43			10/10	27/32	-0.
			4.5	5E	2/2	10/10	11/11			7/7	20/24	-0.
			3.5	1-2SE	20/20	22/22	21/22			6/16	17/17	-0.
			2.5	0	0/0	0/0	0/0			0/0	0/0	0.
H₂	48 50 55	0	8.7	1-2N	0/1	3/3	1/1			0/2	0/2	-0.
			6.0	5SE	28/28	20/32	4/34			0/9	37/39	-0.
			4.5	5SE	1/2	1/3	2/2			14/20	0/12	-0.
			3.5	5ESE	4/8	3/10	2/15			0/4	34/41	-0.
			2.5	5N	0/0	1/1	2/2			0/0	0/0	-0.

± Inlet temperature rise at time where $\Sigma\, F_N$ = minimum

±± Maximum (spatial average) temperature rise during the run

* Engine stall

TABLE 2- DATA SUMMARY

R ED SEE RE ER	α	$\dfrac{\bar{H}}{D}$	WIND & DIRECTION	INLET TEMPERATURE RISE — ENGINE NUMBER 1 (± / ±±)	2	3	4	5	6	7	$\dfrac{L_{JE}}{L_\infty}$	$\dfrac{F}{L_\infty}$	$\dfrac{L}{L_\infty}$
	0	8.7	5NNE	8 / 10	15 / 10	5 / 5			0 / 5	0 / 12	-0.053	0.985	0.932
		6.0	5NE	20 / 43	28 / 30	43 / 43			10 / 10	27 / 32	-0.058	0.926	0.868
		4.5	5E	2 / 2	10 / 10	11 / 11			7 / 7	20 / 24	-0.045	0.964	0.919
		3.5	1-2SE	20 / 20	22 / 22	21 / 22			6 / 16	17 / 17	-0.010	0.931	0.921
		2.5	0	0 / 0	0 / 0	0 / 0			0 / 0	0 / 0	0.033	1.000	1.033
	0	8.7	1-2N	0 / 1	3 / 3	1 / 1			0 / 2	0 / 2	-0.059	0.990	0.931
		6.0	5SE	28 / 28	20 / 32	4 / 34			0 / 9	37 / 39	-0.065	0.960	0.895
		4.5	5SE	1 / 2	1 / 3	2 / 2			14 / 20	0 / 12	-0.055	0.978	0.923
		3.5	5ESE	4 / 8	3 / 10	2 / 15			0 / 4	34 / 41	-0.016	0.980	0.964
		2.5	5N	0 / 0	1 / 1	2 / 2			0 / 0	0 / 0	-0.016	0.998	0.982

± Inlet temperature rise at time where ΣF_N = minimum

±± Maximum (spatial average) temperature rise during the run

* Engine stall

G.E. YJ85-5
TURBOJET
ENGINE (TYP)

96

30.5 (TYP)

72 — C$_L$ – 3 ENGINE TAILPIPE

30.5 (TYP)

264

511

142

NACA 0012
AIRFOIL

159

NASA—AMES FULL
SCALE MODEL

0 20 40 60 80 100

SCALE   ALL DIMENSIONS IN INCHES

FIGURE 1   TEST MODEL EVOLUTION

59

AMES FULL
SCALE MODEL

¢ – #3 ENGINE TAIL PIPE

159

159

107

511

511

125

28

4

143

NORTHROP NORAIR FULL
SCALE MODEL

59

2

159

57

107

IL PIPE—

511

€ --# 3 ENGINE TAIL PIPE—

79

190

-4

28

SWEPT WING
CONFIGURATION

DELTA WING
CONFIGURATION

143

85

NAVY
TEST MODEL

3
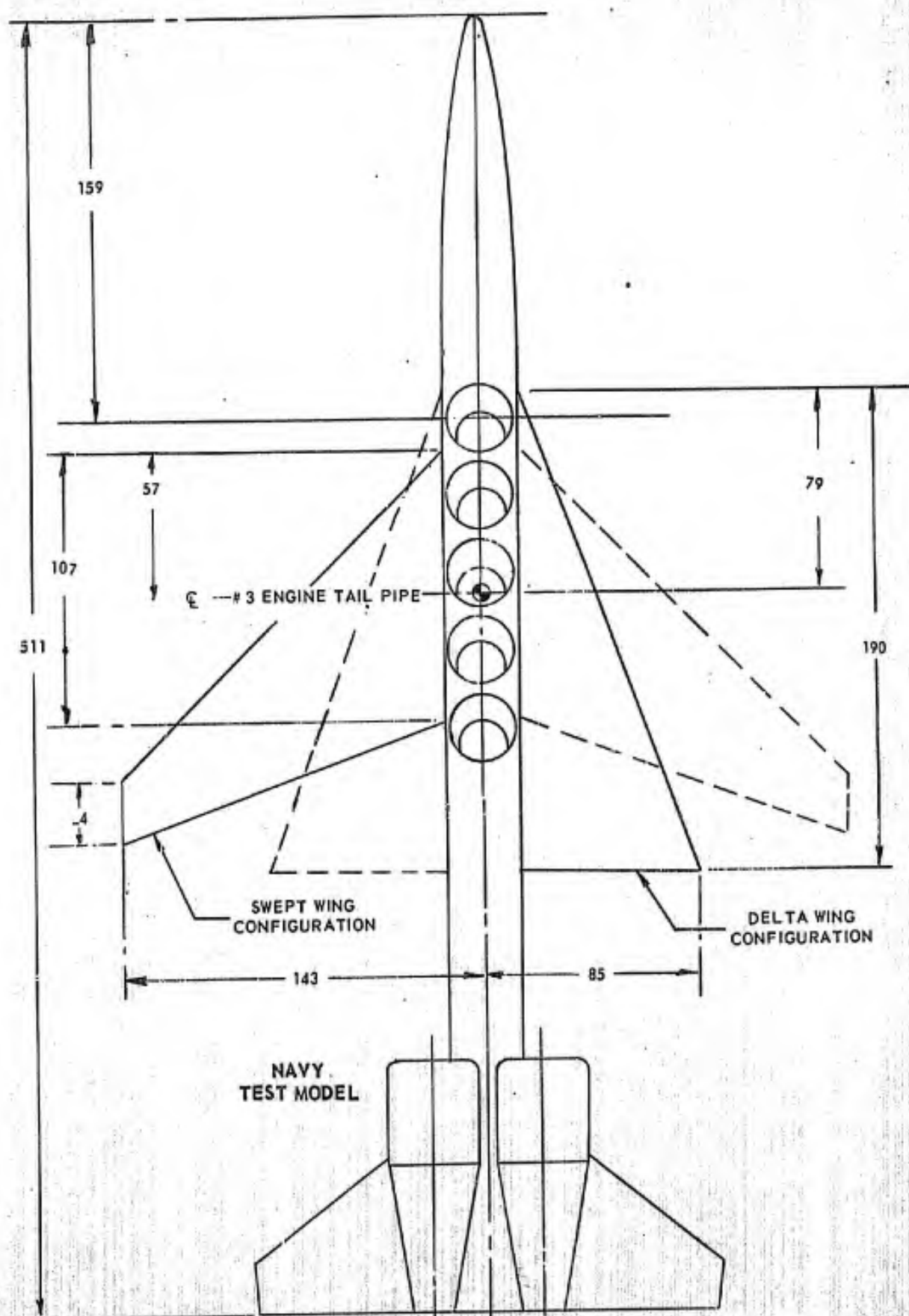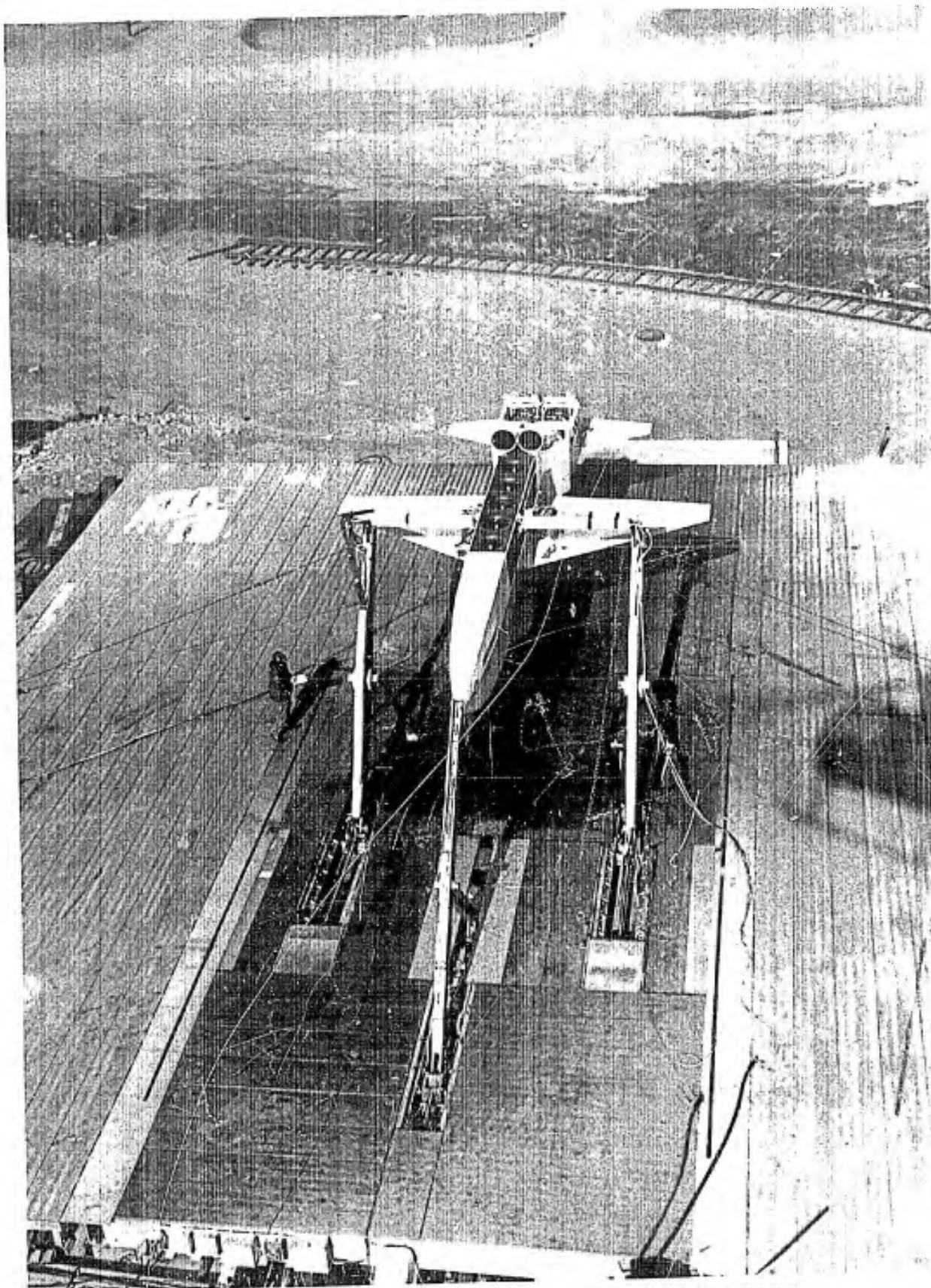
FIGURE 2   TEST VEHICLE MOUNTED ON NASA-AMES VTO STAND
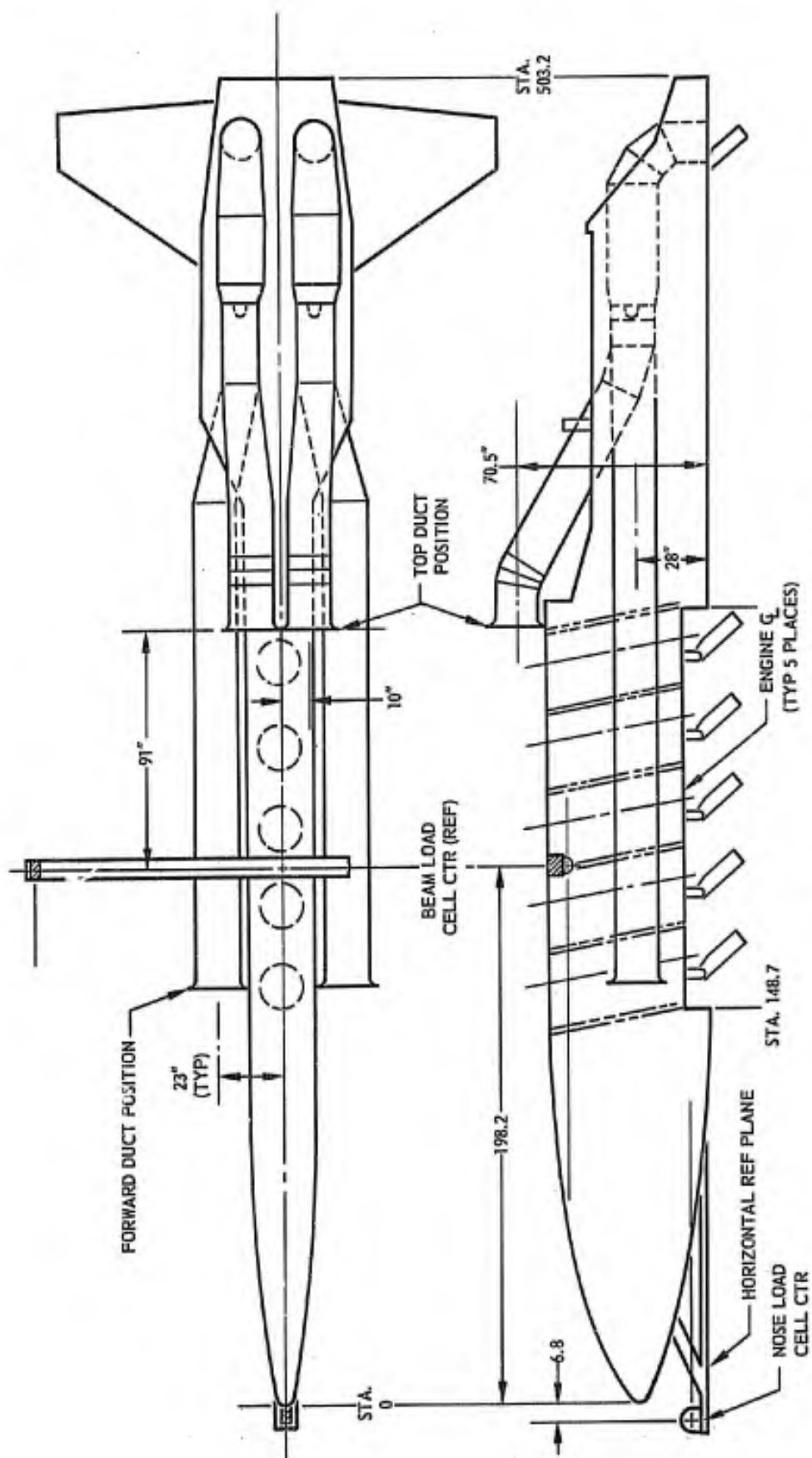
FIGURE 3 TEST MODEL LIFT/CRUISE ENGINE INLET LOCATIONS

FIGURE 4 TEST VEHICLE AT CLOSE GROUND PROXIMITY
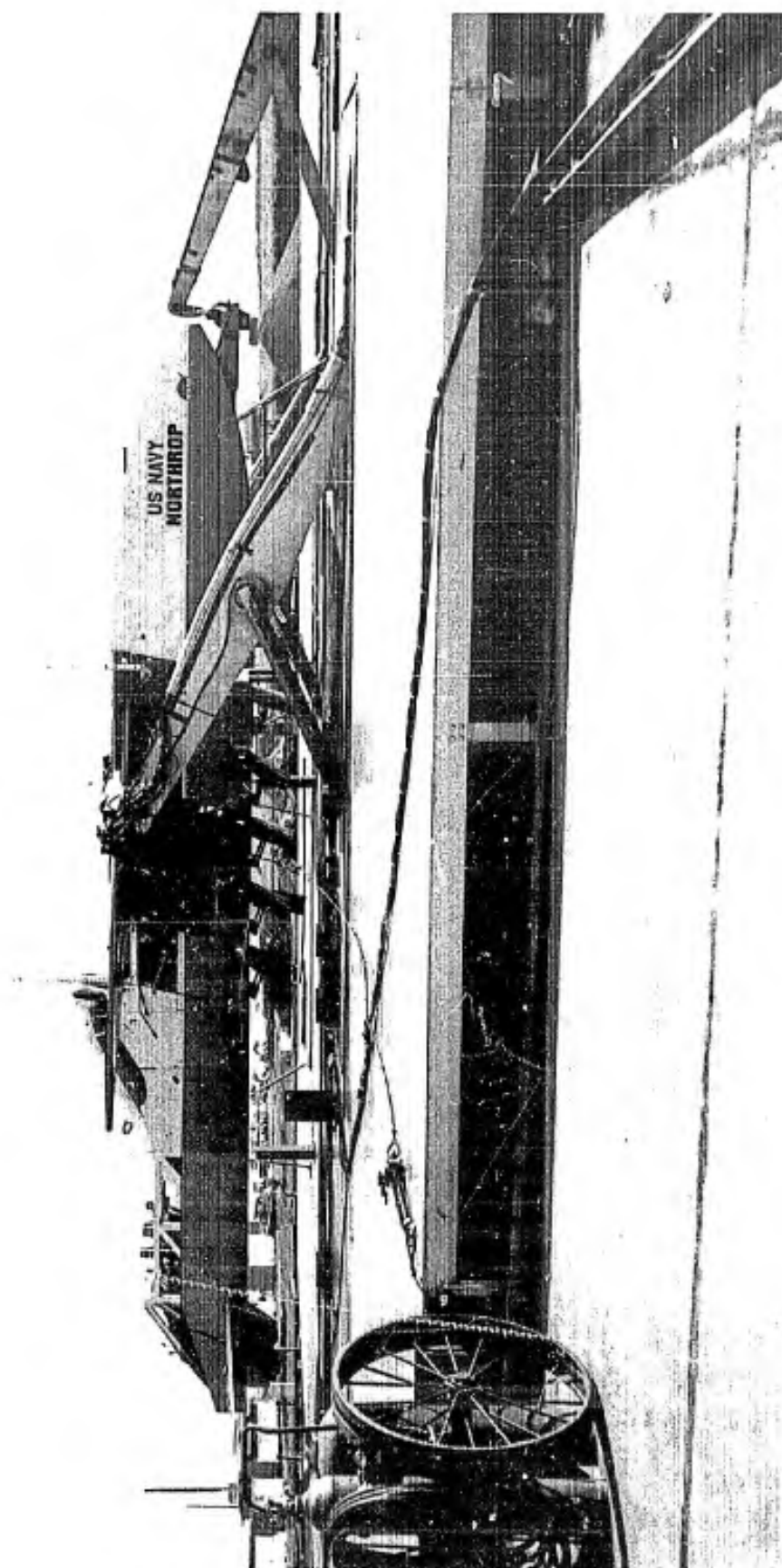
NASA-AMES PHOTO
A-36642

FIGURE 5   TEST VEHICLE WITH FORWARD LOCATION OF LIFT/CRUISE ENGINE INLET
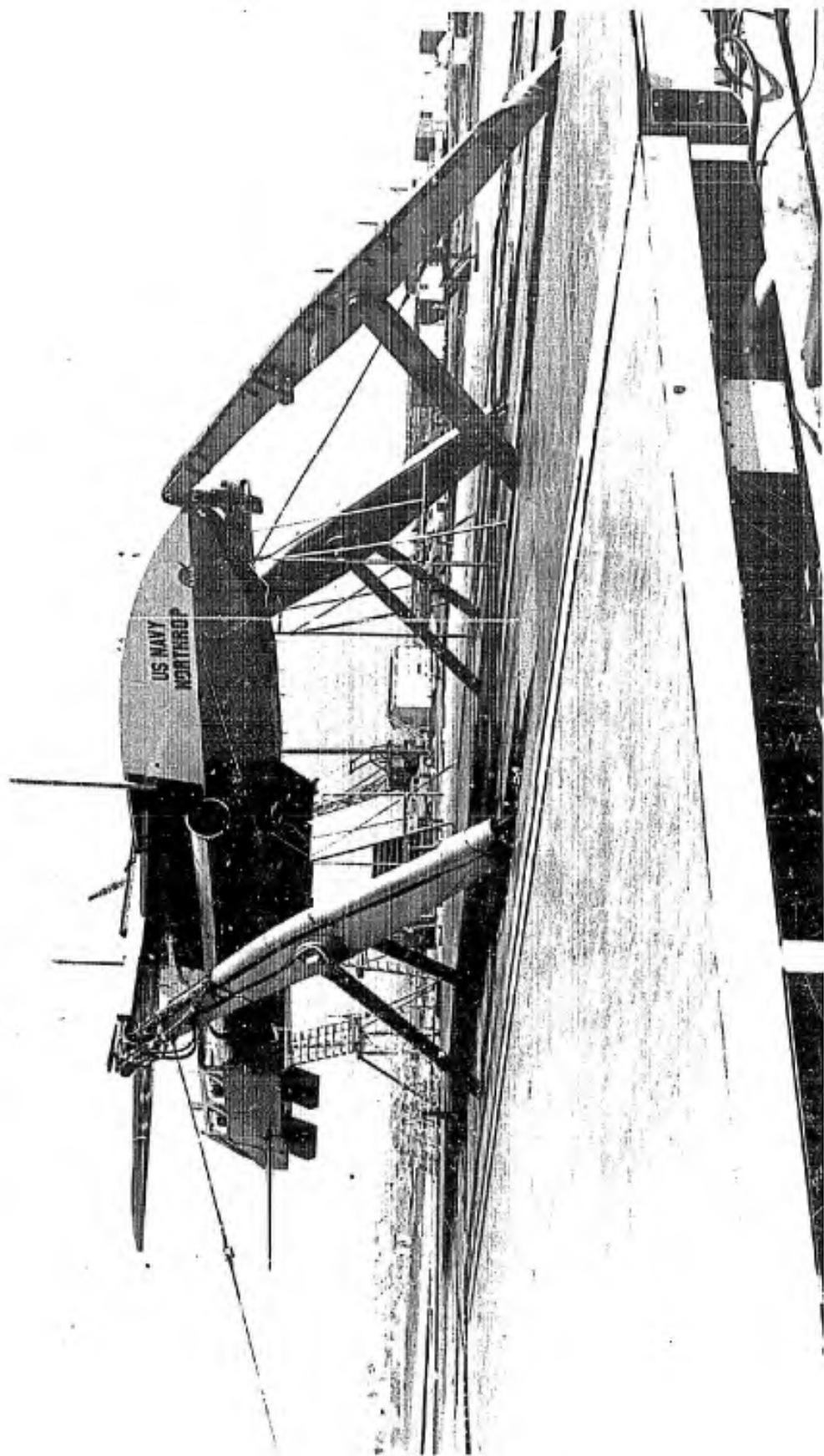
NASA-AMES PHOTO
A-36684
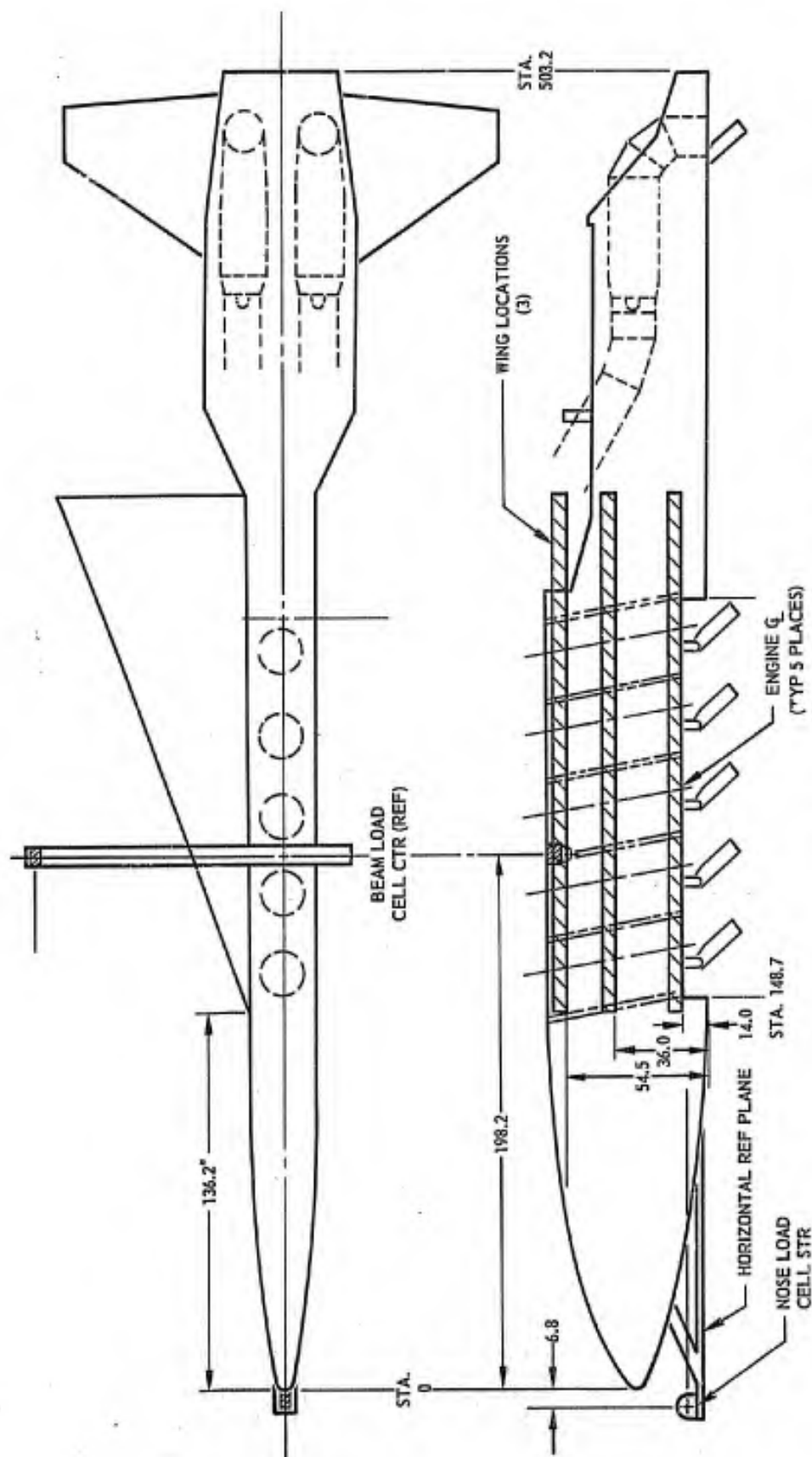
FIGURE 6 TEST MODEL – DELTA-WING LOCATIONS
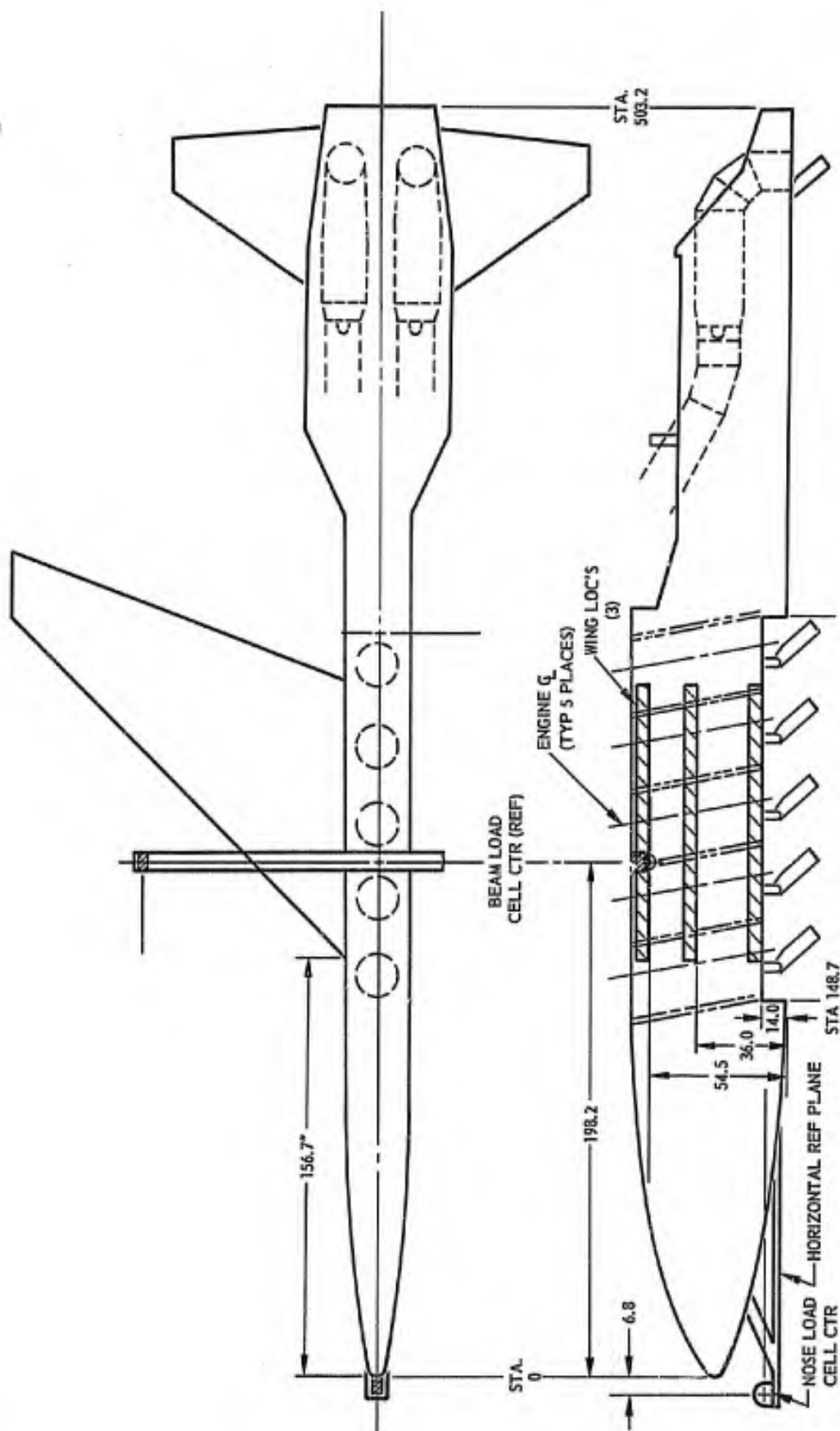
FIGURE 7 TEST MODEL – SWEPT-WING LOCATIONS

66
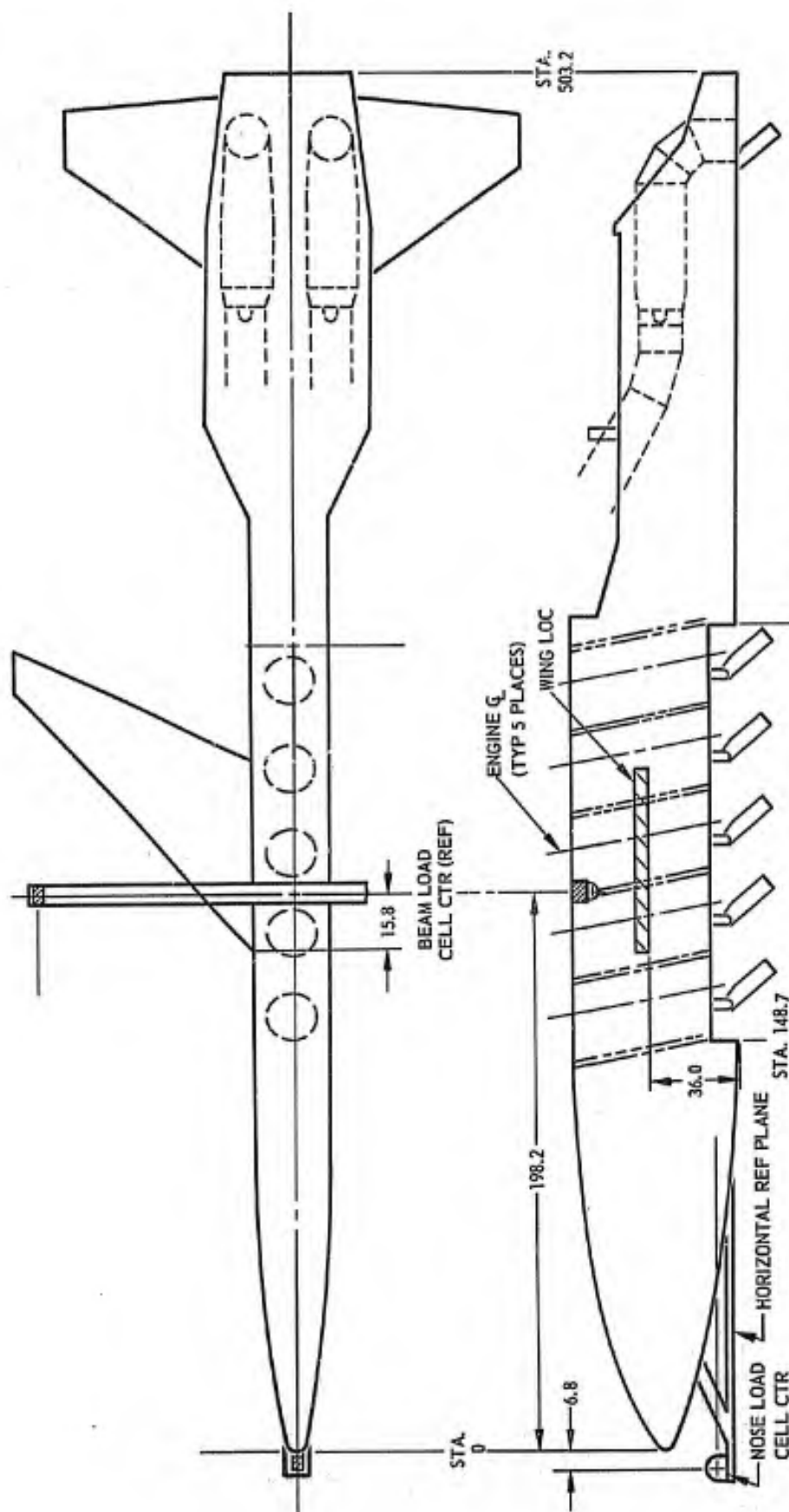
FIGURE 8   TEST MODEL — HALF-SIZE SWEPT-WING LOCATIONS

67
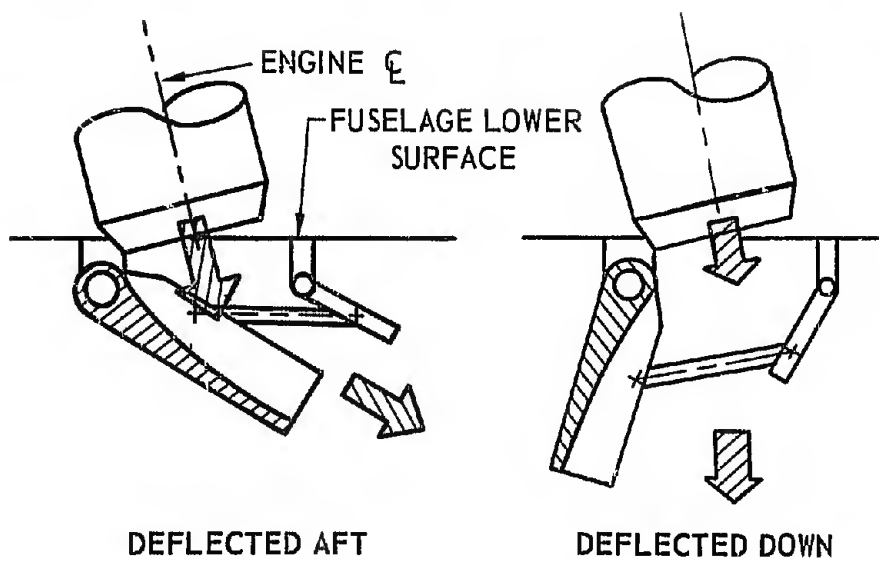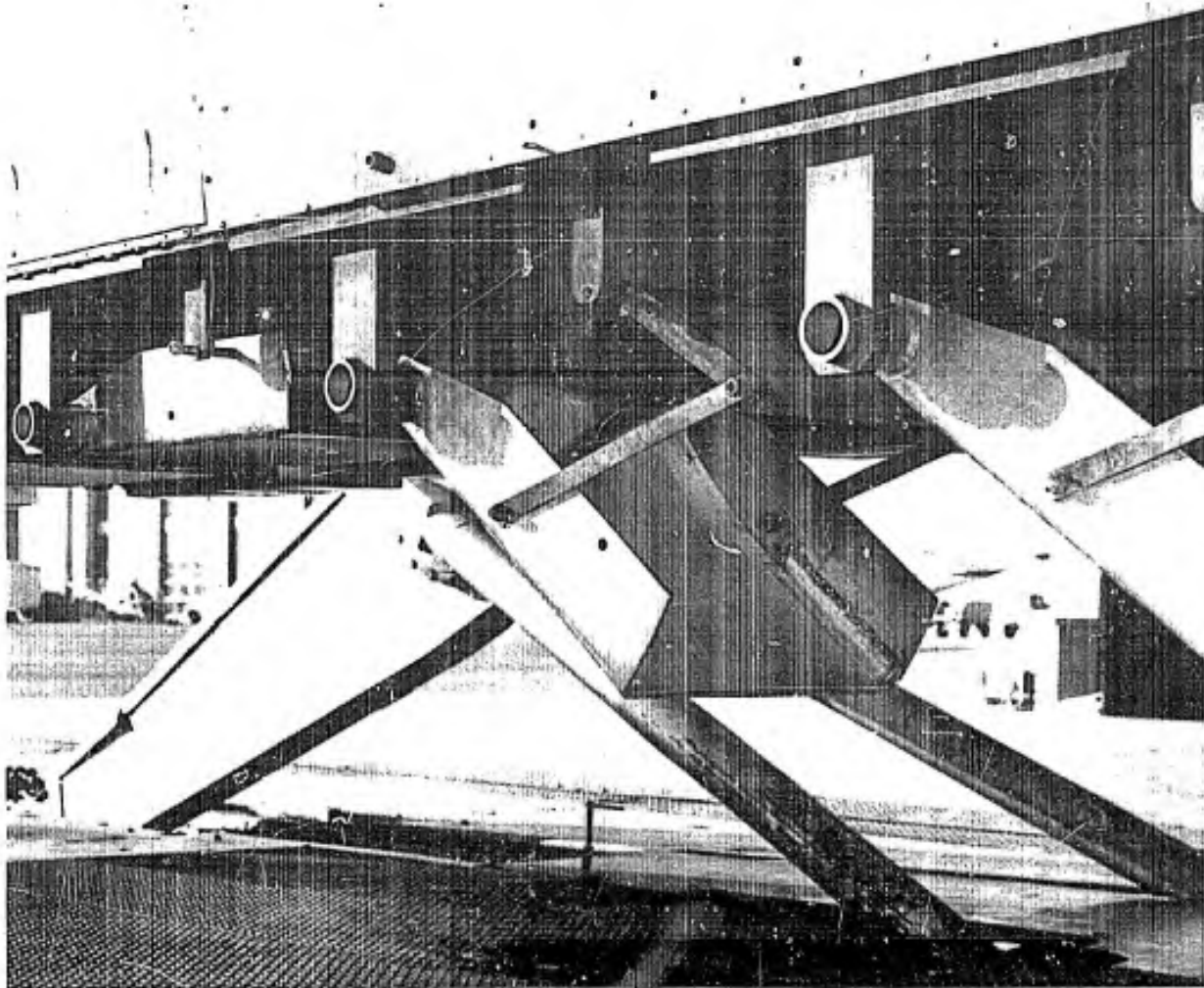
FIGURE 9   DEFLECTOR DOOR ARRANGEMENT
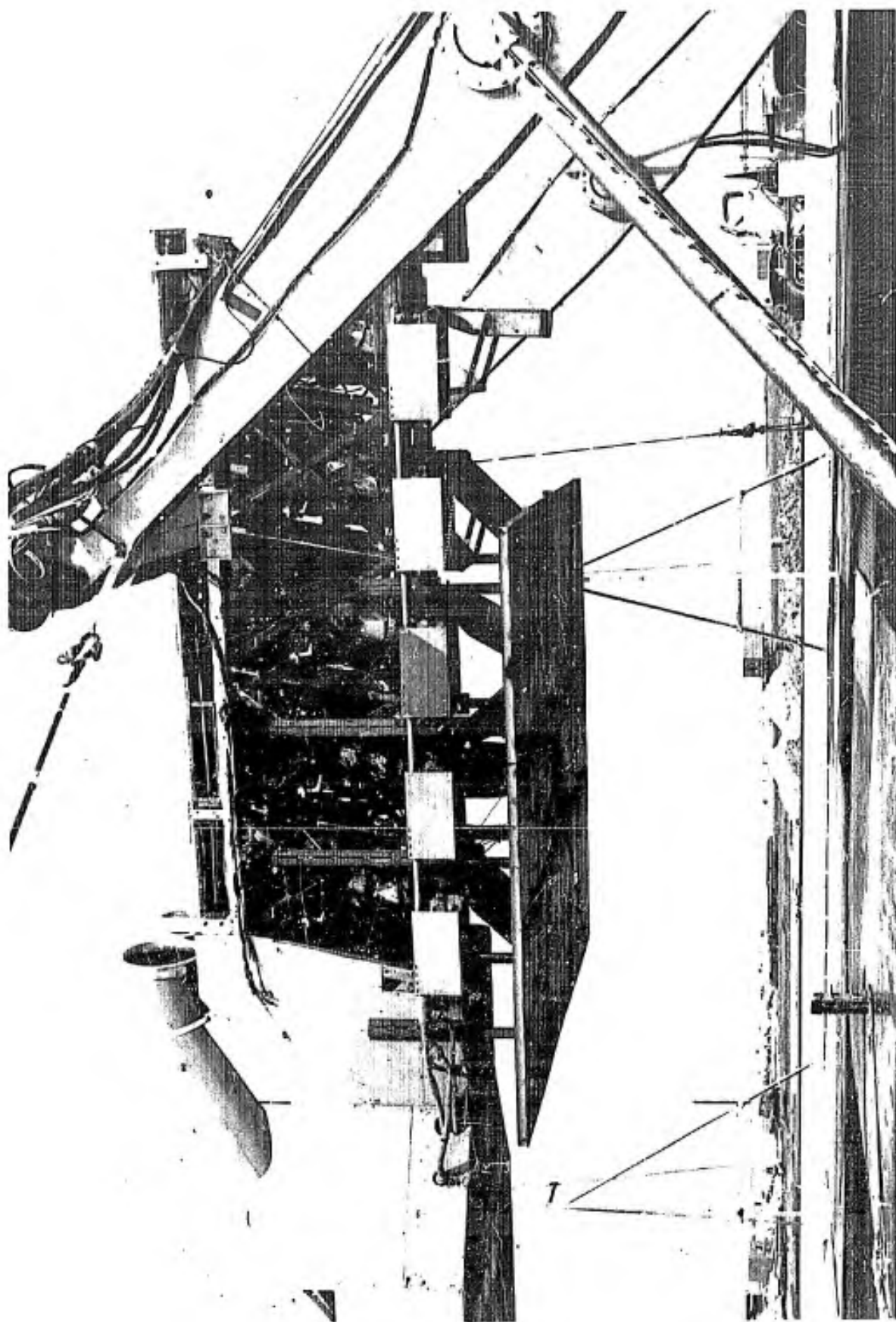
FIGURE 10   10 X 10-FOOT FLAT PLATE MOUNTED ON THE TEST VEHICLE

TOWABLE TRAILER

FUSELAGE STRUT (TYP)

NOSE STRUT

MODEL SUPPORT BEAM (TYP)

GROUND PLANE

16'

TOGGLE MECHANISM

14.8' (MAX)

FIXED POINT (TYP)

TRAILER MOVEMENT MECHANISM
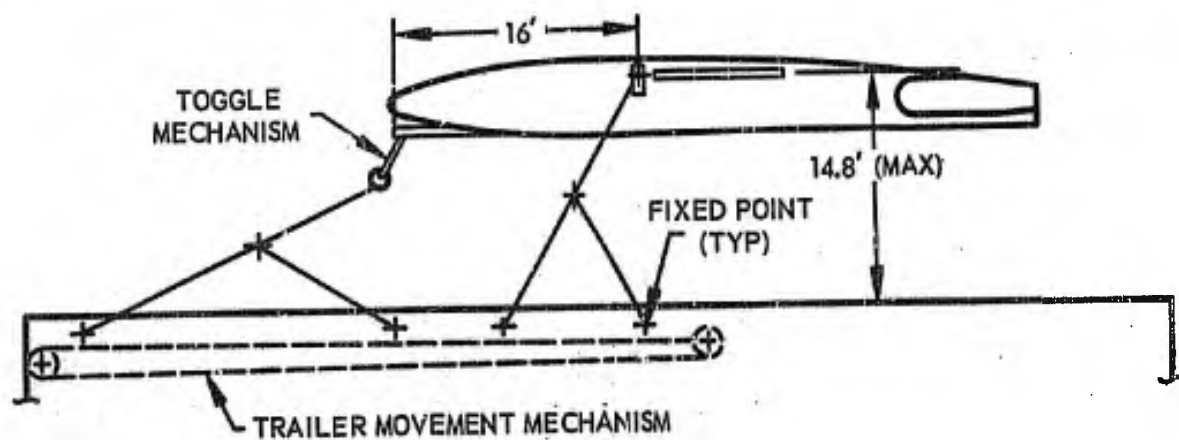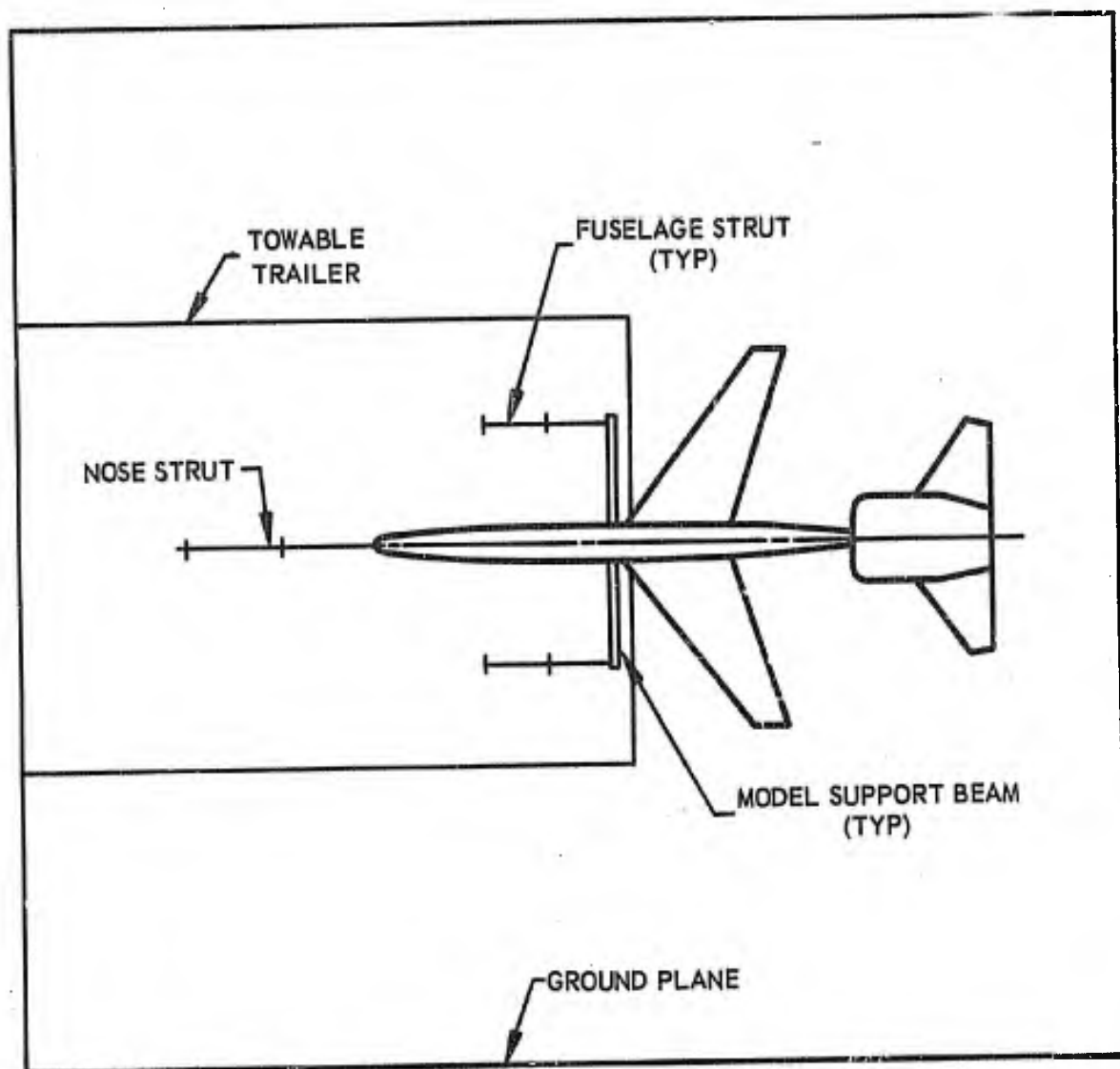
FIGURE 11   NASA-AMES VTO THRUST STAND

LEFT

4.63
2.27
.69

AFT   FWD

– – – – – ENGINE 1 ONLY
————— ALL ENGINES

RIGHT
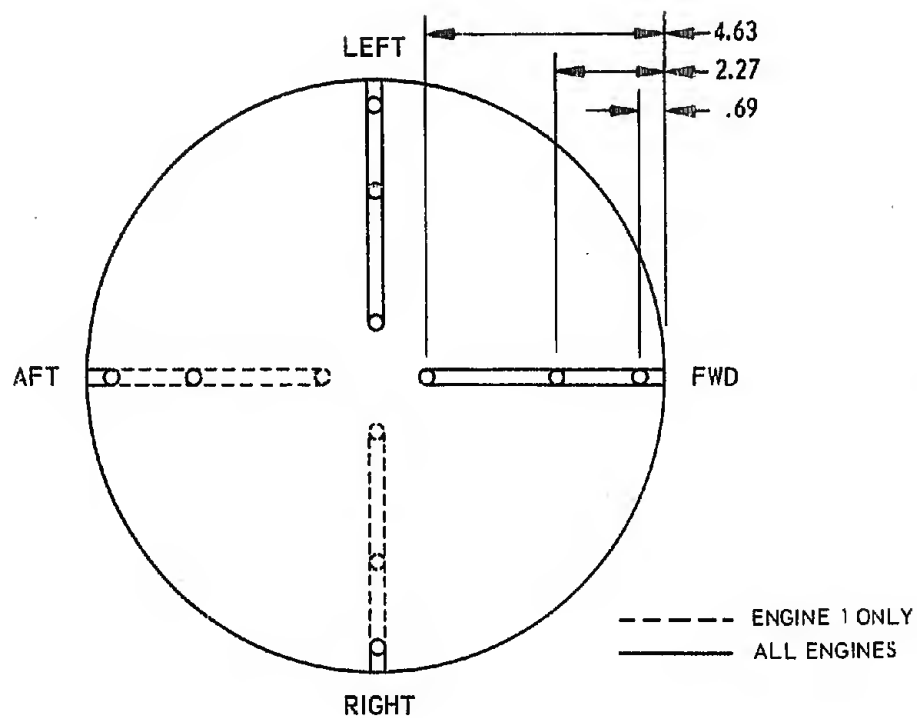
TYPICAL THERMOCOUPLE RAKE INSTALLATION

O TOTAL PRESSURE
⊛ STATIC PRESSURE

90° TYPICAL

D   B

45° TYPICAL

4.87"   6.64"
         5.89"

AFT ENG   FWD END
                                         C̲L

4.45 D

3.85

16.08 D

F   H
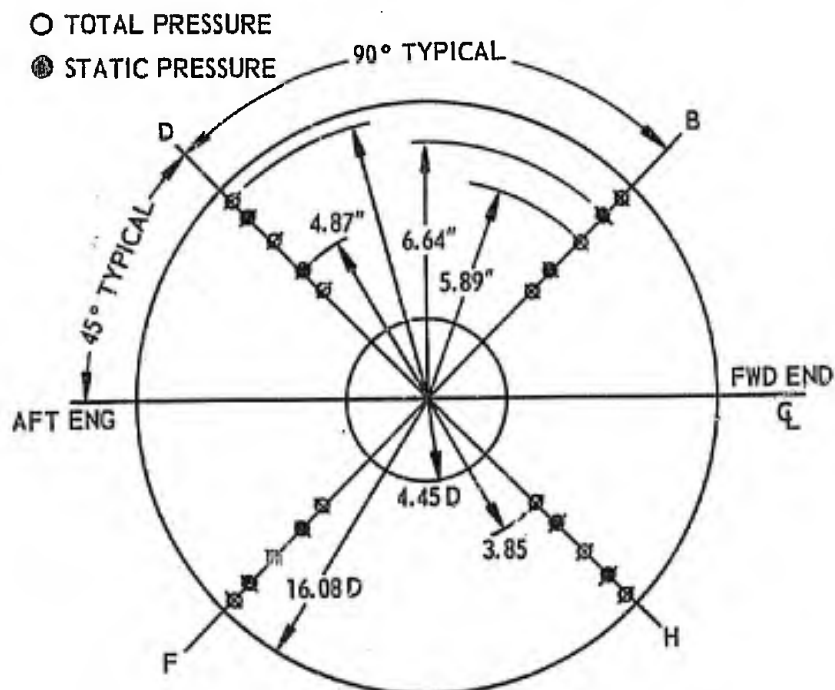
TYPICAL PRESSURE RAKE INSTALLATION

FIGURE 12   INLET INSTRUMENTATION

71
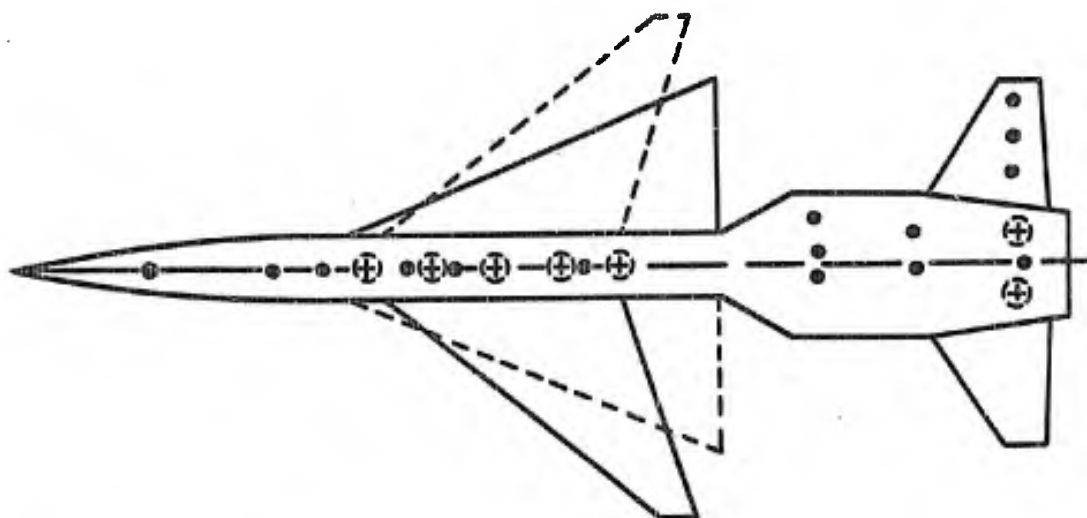
VEHICLE UNDERSIDE STATIC PRESSURE TAPS
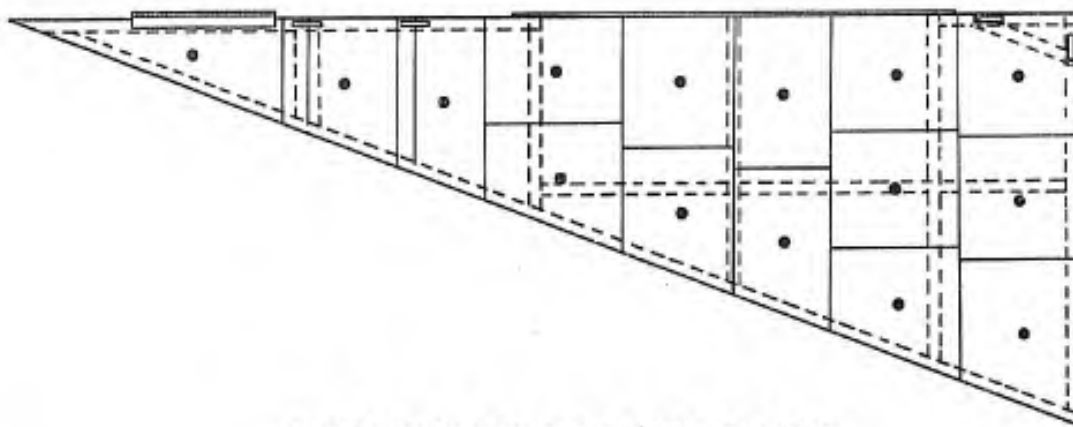
DELTA WING PRESSURE TAP LOCATION
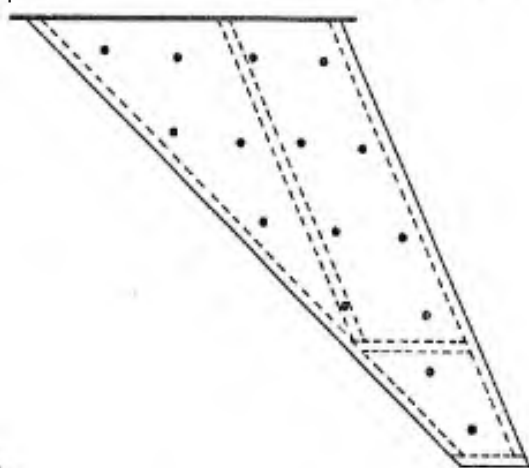
HALF-SIZE SWEPT WING PRESSURE
TAP LOCATION
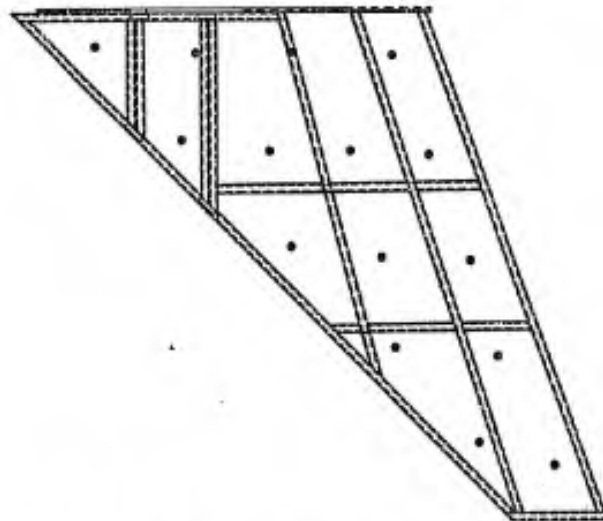
SWEPT WING PRESSURE TAP LOCATION

FIGURE 13   VEHICLE STATIC PRESSURE TAPS

FIGURE 14   VEHICLE PROXIMITY INSTRUMENTATION

73
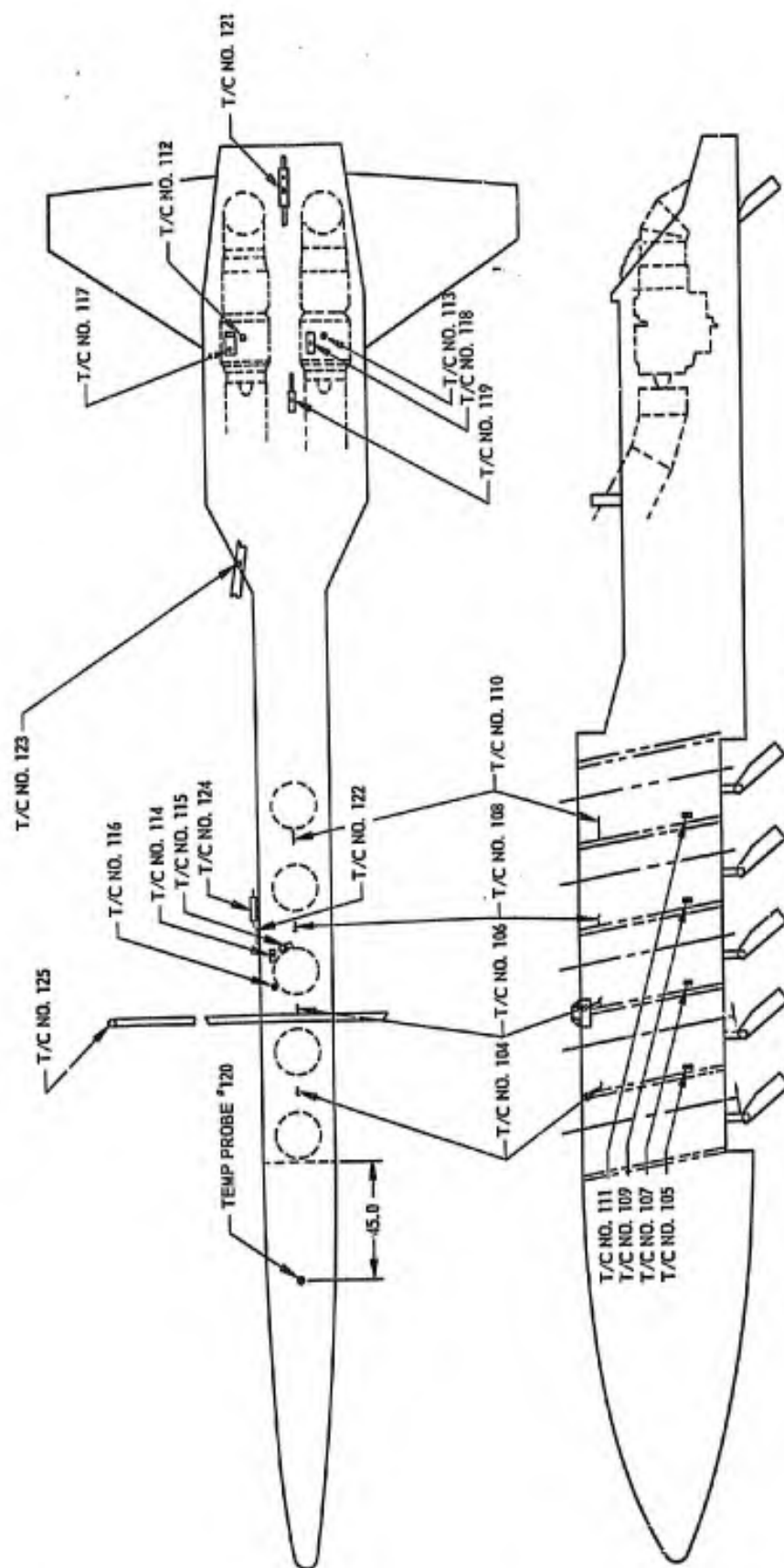
FIGURE 15   VEHICLE TEMPERATURE SURVEY
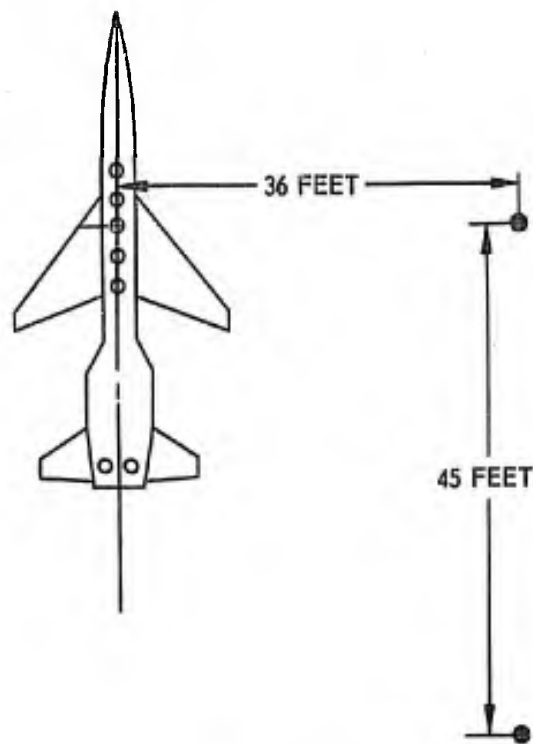
FIGURE 16   ANEMOMETER POSITIONS
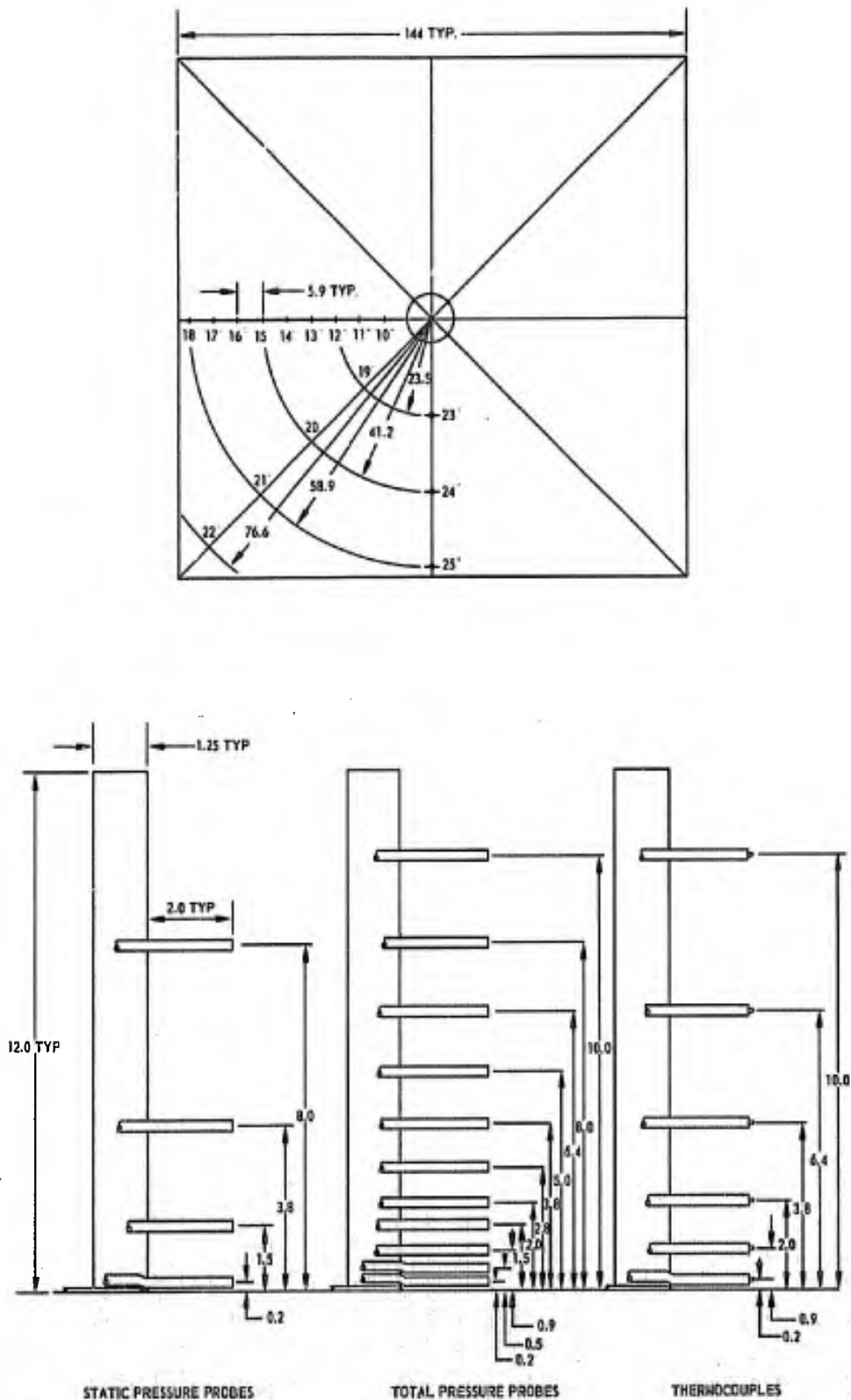
FIGURE 17   SINGLE-ENGINE TESTS INSTRUMENTATION

L.H. (upper left)
○ 142
○ 142
○ 142

AFT ○62 ○67 ○161   ○161 ○142 ○141 FWD

○ 154
○ 172
○ 175
R.H.

CONFIG. = E_x
ENGINE NO. = 1
H/D = 2.5
$\alpha = 0°$
$T_\infty = 72°$

L.H. (upper right)
○ 133
○ 143
○ 160

AFT ○6 ○82 ○93   ○153 ○136 ○112 FWD

○ 111
○ 84
○ 73
R.H.

CONFIG. = E_1
ENGINE NO. = 1
H/D = 6.0
$\alpha = 4°$
$T_\infty = 73°$

L.H. (lower left)
○ 142
○ 142
○ 128

AFT ○103 ○101 ○91   ○73 ○65 ○36 FWD

○ 36
○ 73
○ 63
R.H.

CONFIG. = C_2
ENGINE NO. = 1
H/D = 2.5
$\alpha = 1°$
$T_\infty = 63°$
(STALL)

L.H. (lower right)
○ 79
○ 82
○ 101

AFT ○71 ○79 ○109   ○146 ○147 ○148 FWD

○ 155
○ 106
○ 174
R.H.

CONFIG. = E_2
ENGINE NO. = 1
H/D = 8.7
$\alpha = 0°$
$T_\infty = 64°$
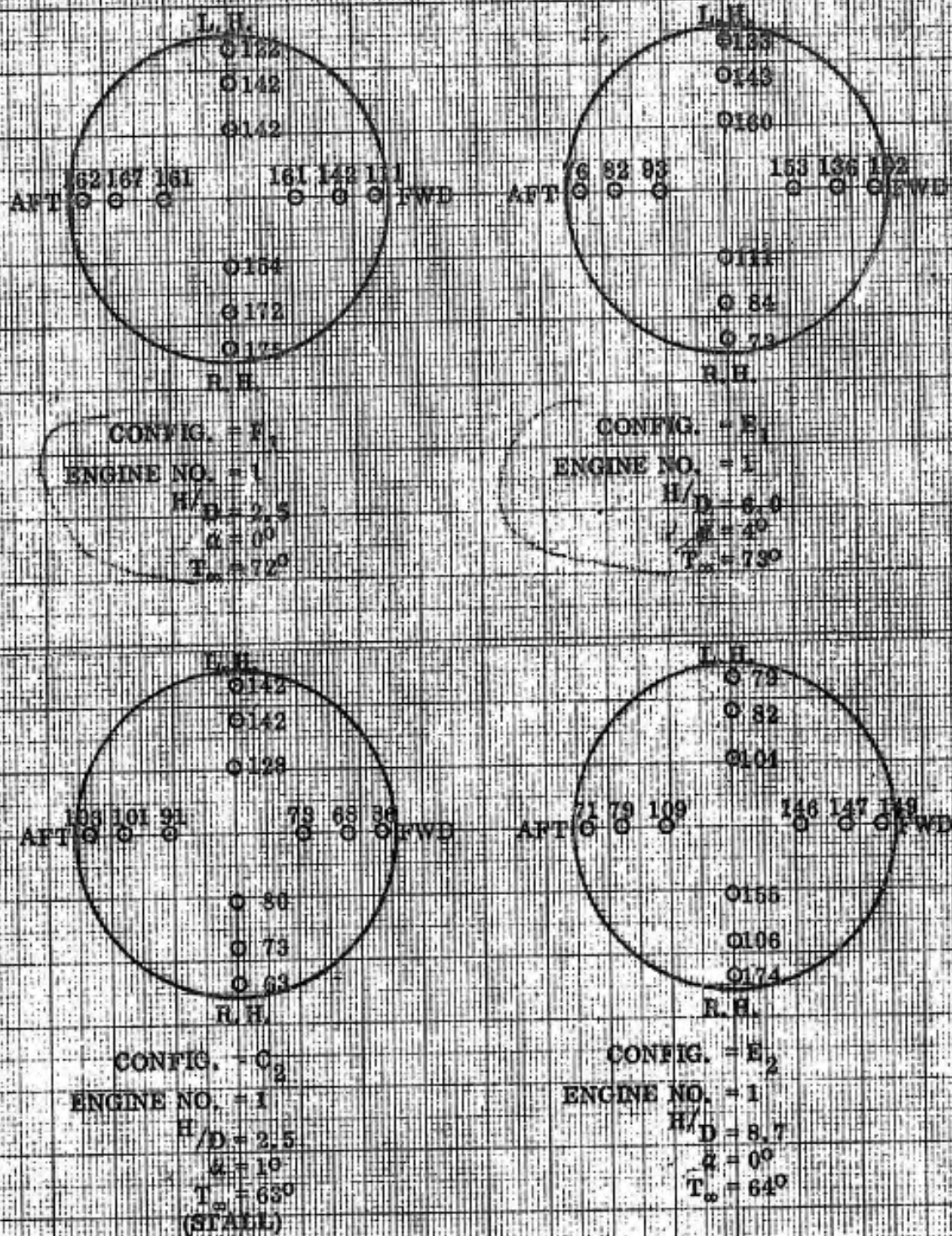
FIGURE 18. TYPICAL LIFT ENGINE INLET TEMPERATURE DISTORTION OF INGESTION PRONE CONFIGURATION

77
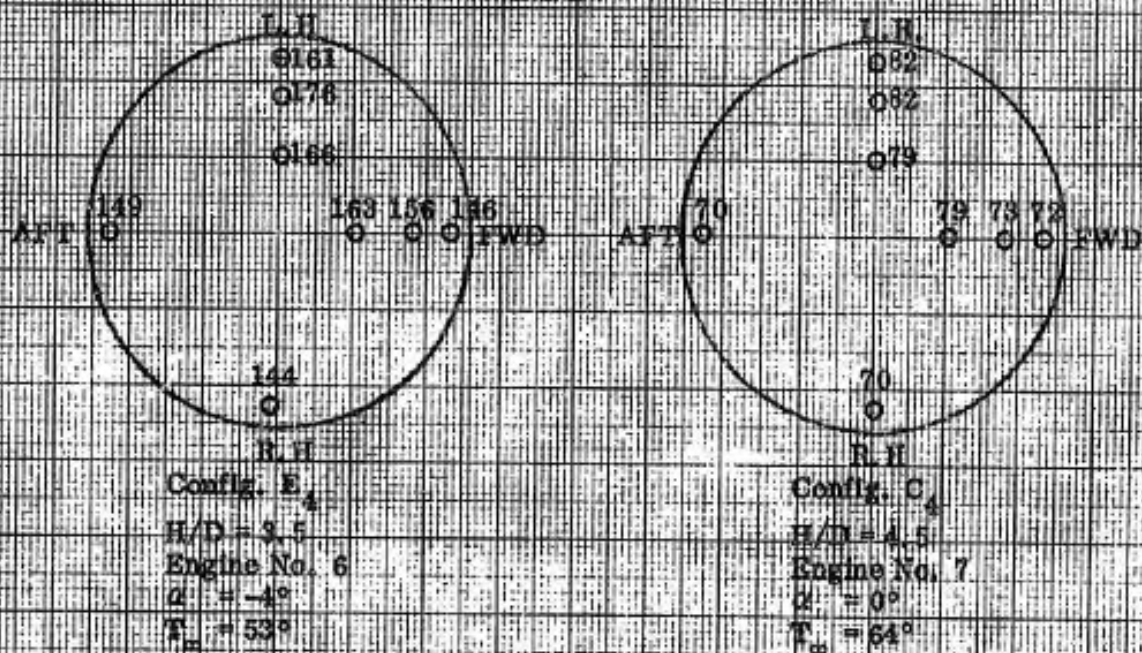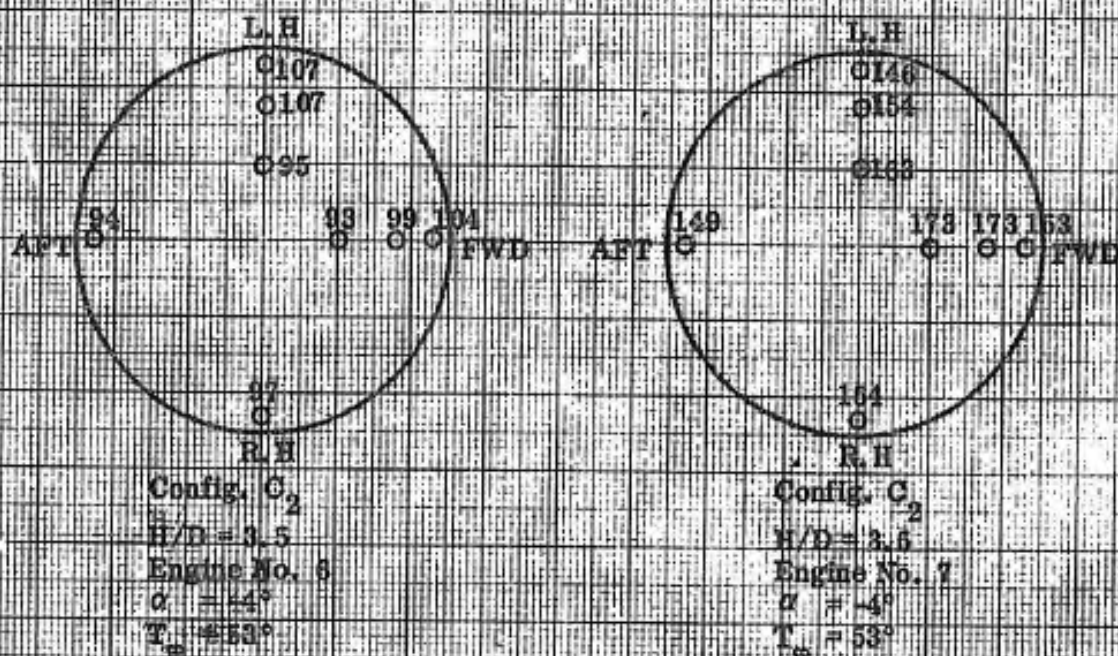
FIGURE 19. TYPICAL LIFT/CRUISE ENGINE
INLET TEMPERATURE DISTORTION
FOR INGESTION PRONE CONFIGURATION
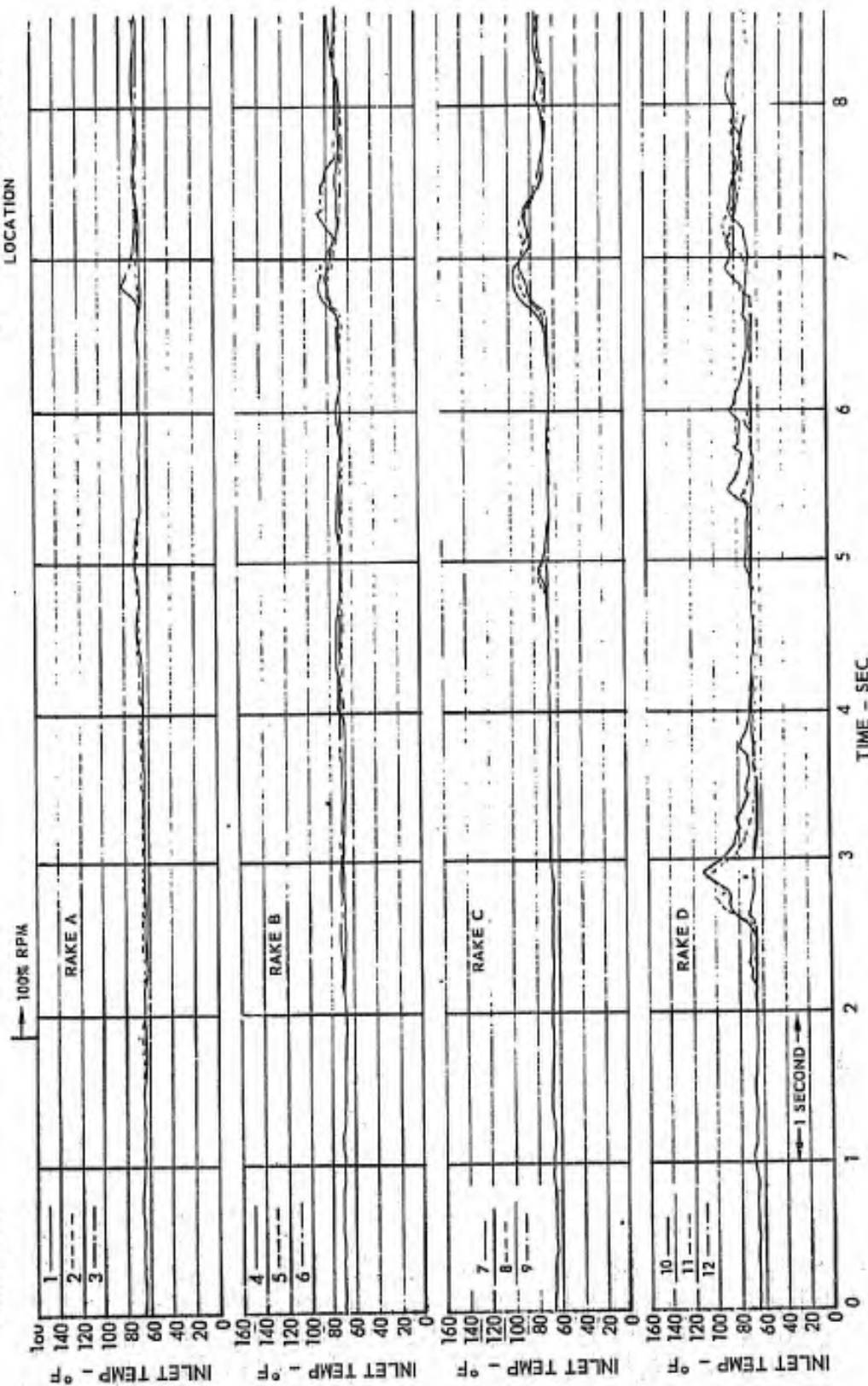
FIGURE 20 (a)   ENGINE INLET TEMPERATURE TRACE

79

FIGURE 20 (b) ENGINE INLET TEMPERATURE TRACE
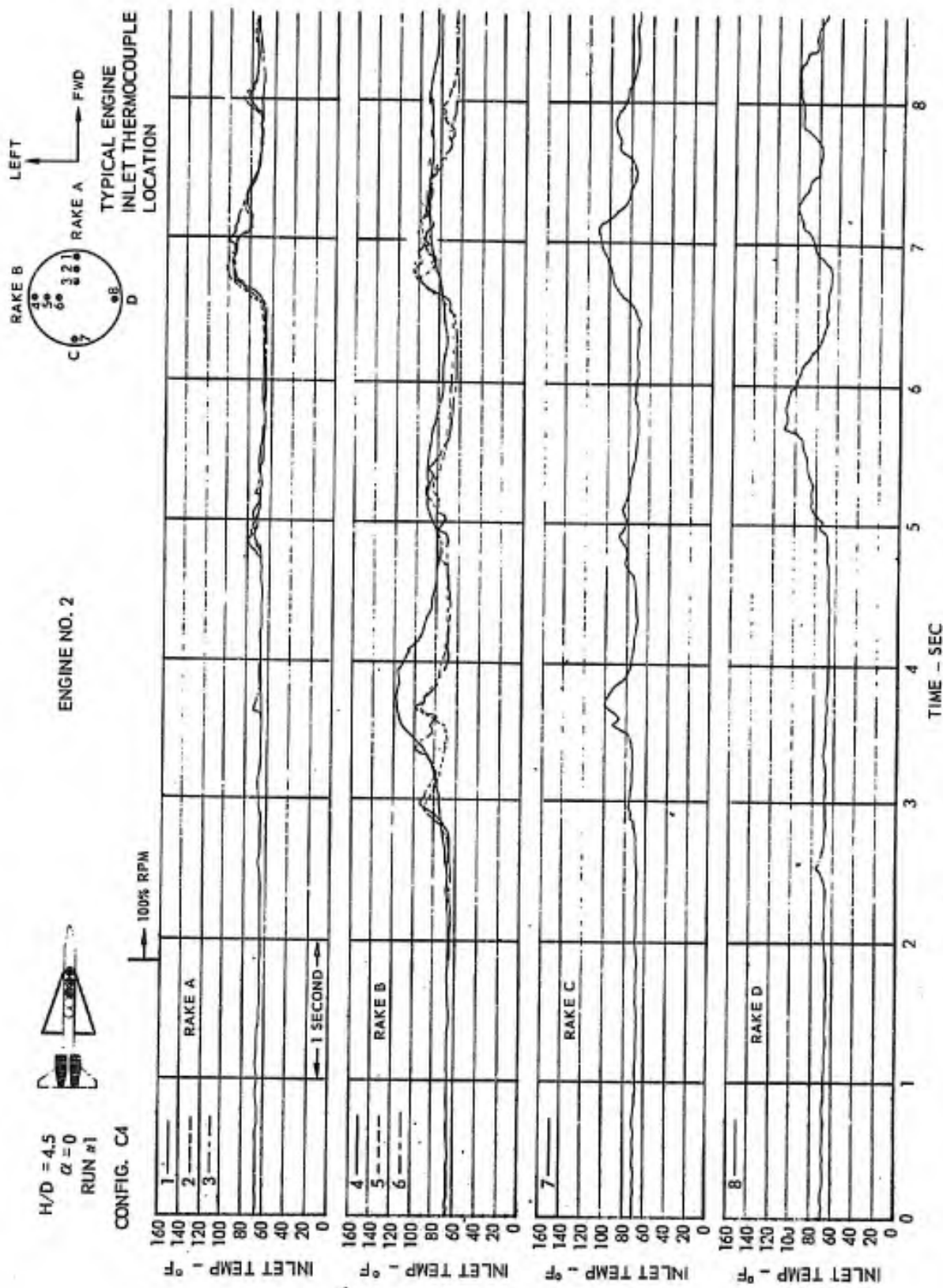
FIGURE 20 (c)   ENGINE INLET TEMPERATURE TRACE

81

FIGURE 20 (d) ENGINE INLET TEMPERATURE TRACE

82
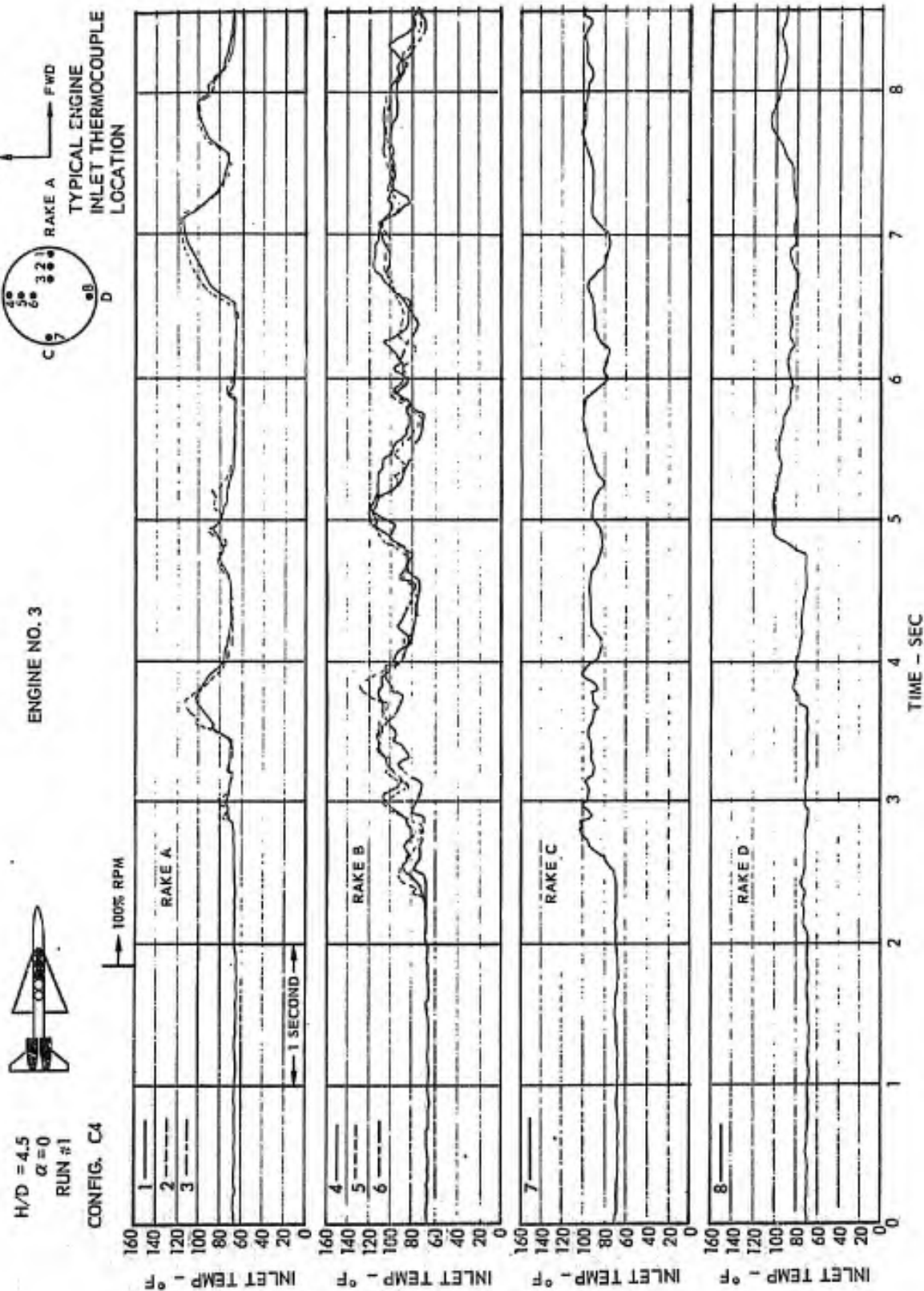
FIGURE 20 (e)   ENGINE INLET TEMPERATURE TRACE
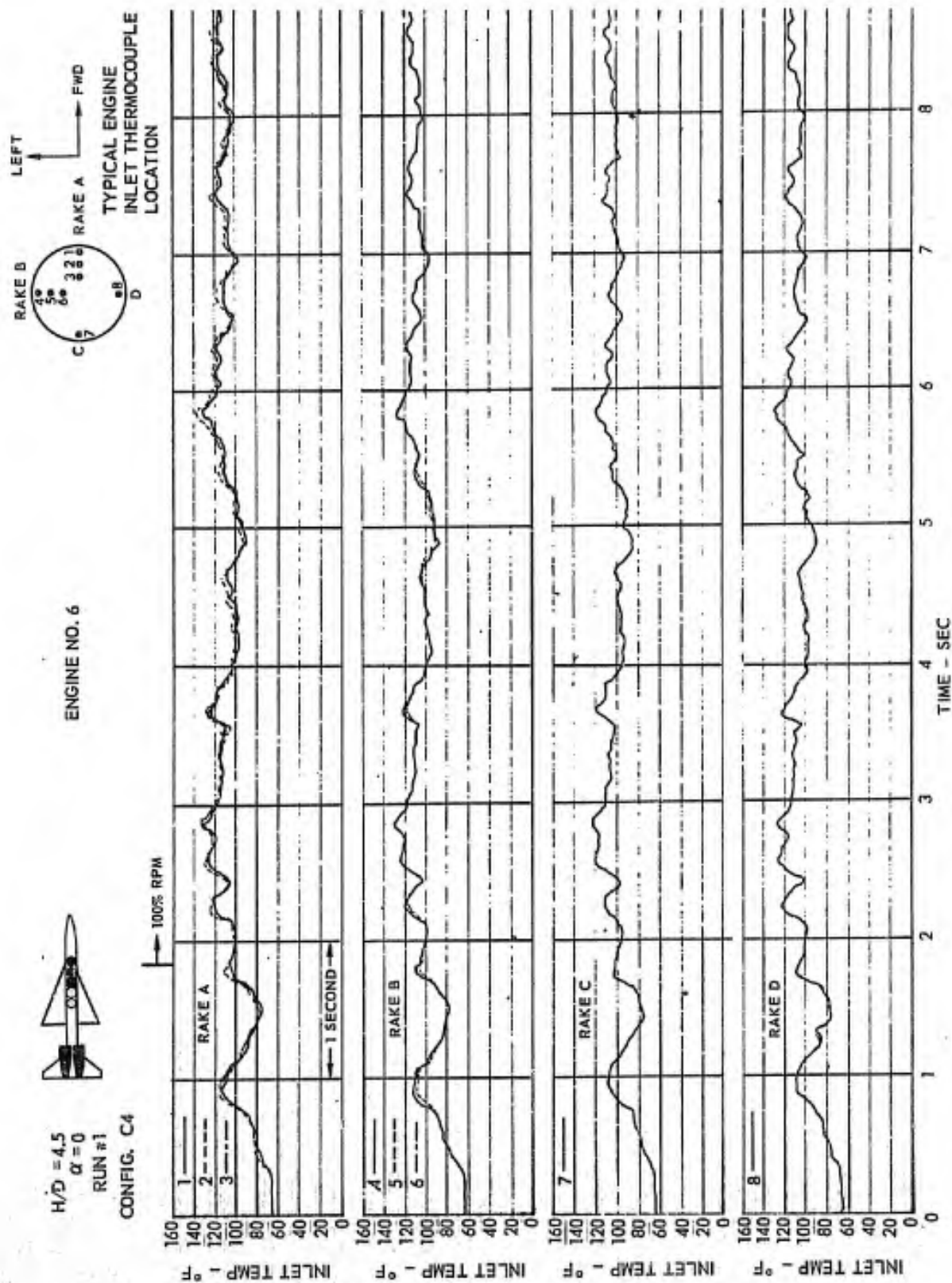
FIGURE 20 (f)   ENGINE INLET TEMPERATURE TRACE

84
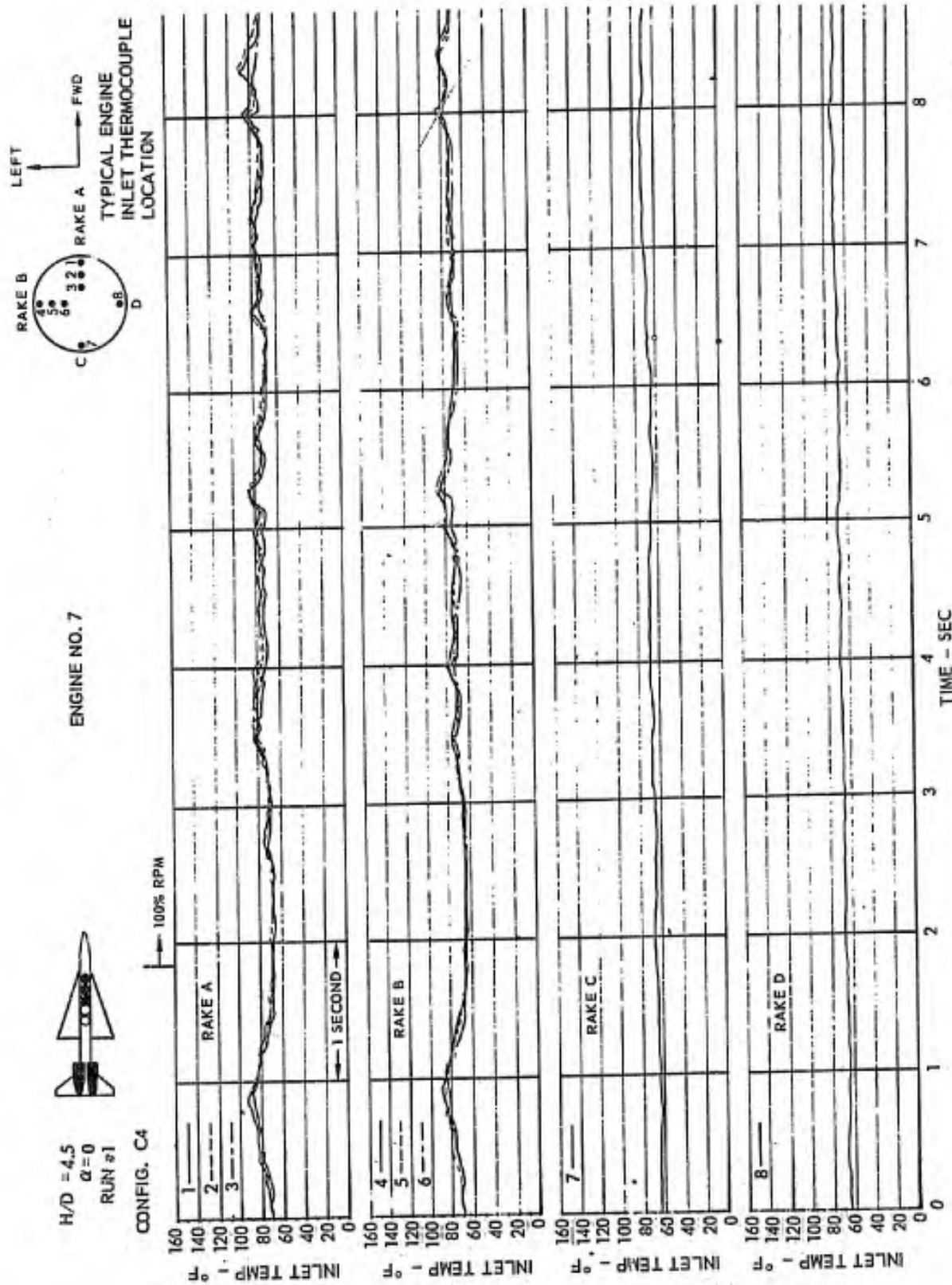
FIGURE 20 (g)   ENGINE INLET TEMPERATURE TRACE

85
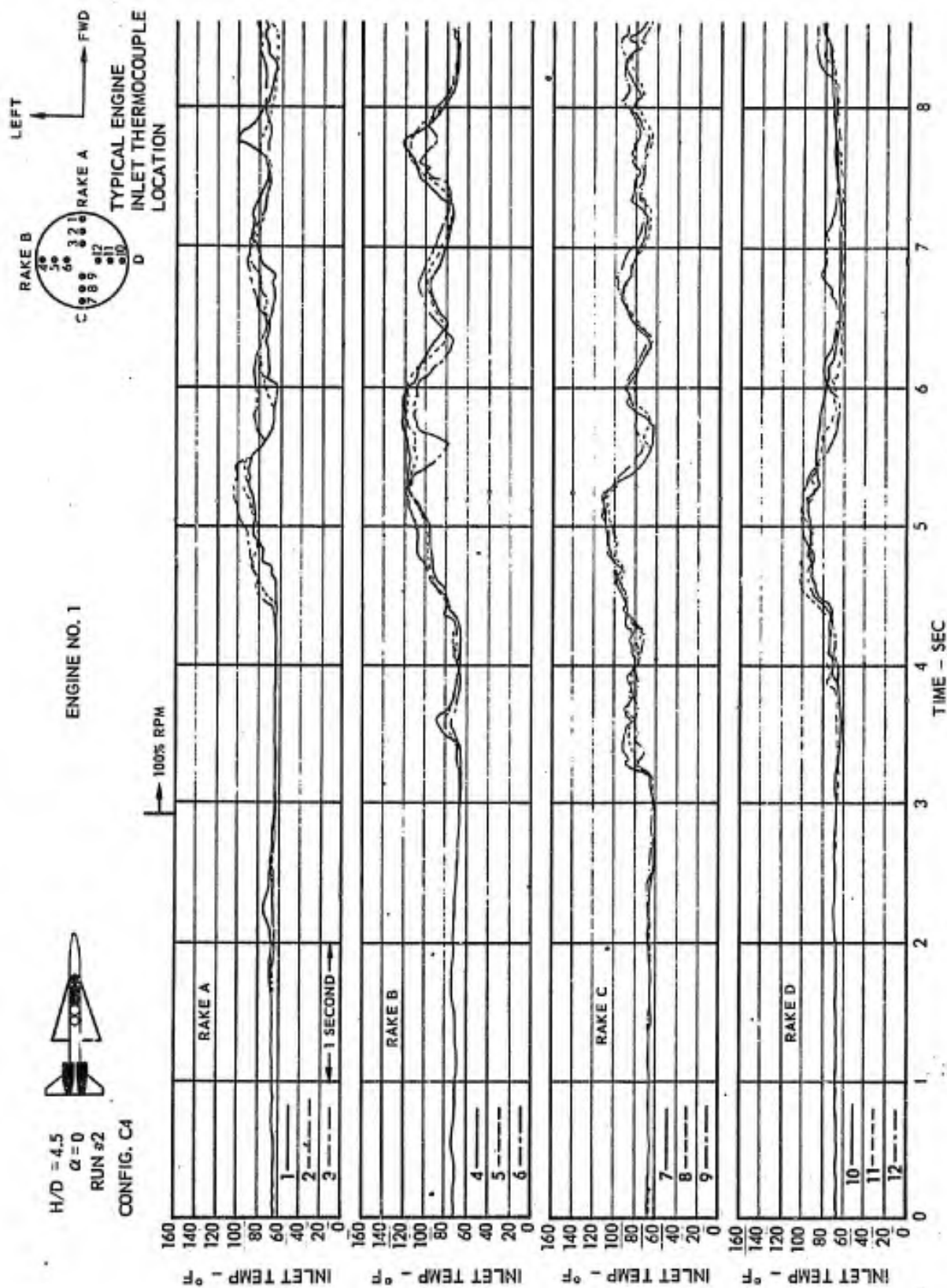
FIGURE 20 (h) ENGINE INLET TEMPERATURE TRACE

FIGURE 20 (i) ENGINE INLET TEMPERATURE TRACE

87

FIGURE 20 (j)   ENGINE INLET TEMPERATURE TRACE

88

FIGURE 20 (k)   ENGINE INLET TEMPERATURE TRACE
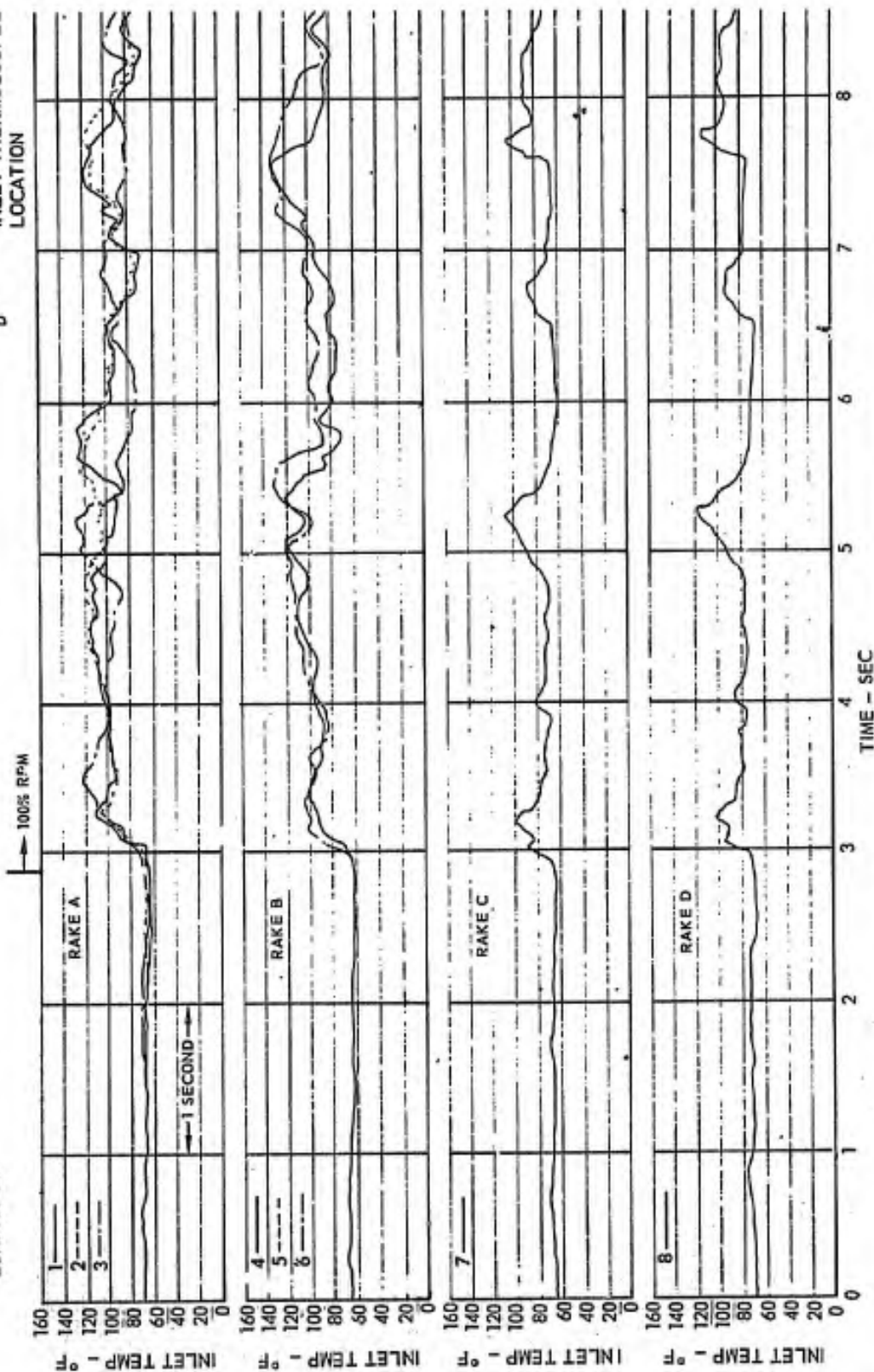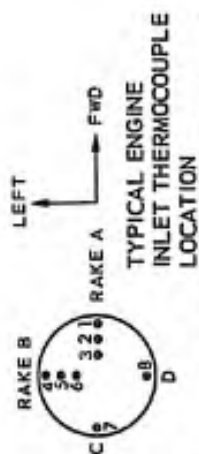
ENGINE NO. 2 (CONTINUED)

CONFIG. C4

H/D = 4.5
α = 0
RUN #2

RAKE B   LEFT
          ↑
       4●   → FWD
       5●
       6●   3●2● 1
          RAKE A
       C●7   ●8
            D

TYPICAL ENGINE
INLET THERMOCOUPLE
LOCATION

RAKE A

RAKE B

RAKE C

RAKE D

← 1 SECOND →

TIME – SEC

INLET TEMP – °F
INLET TEMP – °F
INLET TEMP – °F
INLET TEMP – °F

89

FIGURE 20 (I) ENGINE INLET TEMPERATURE TRACE
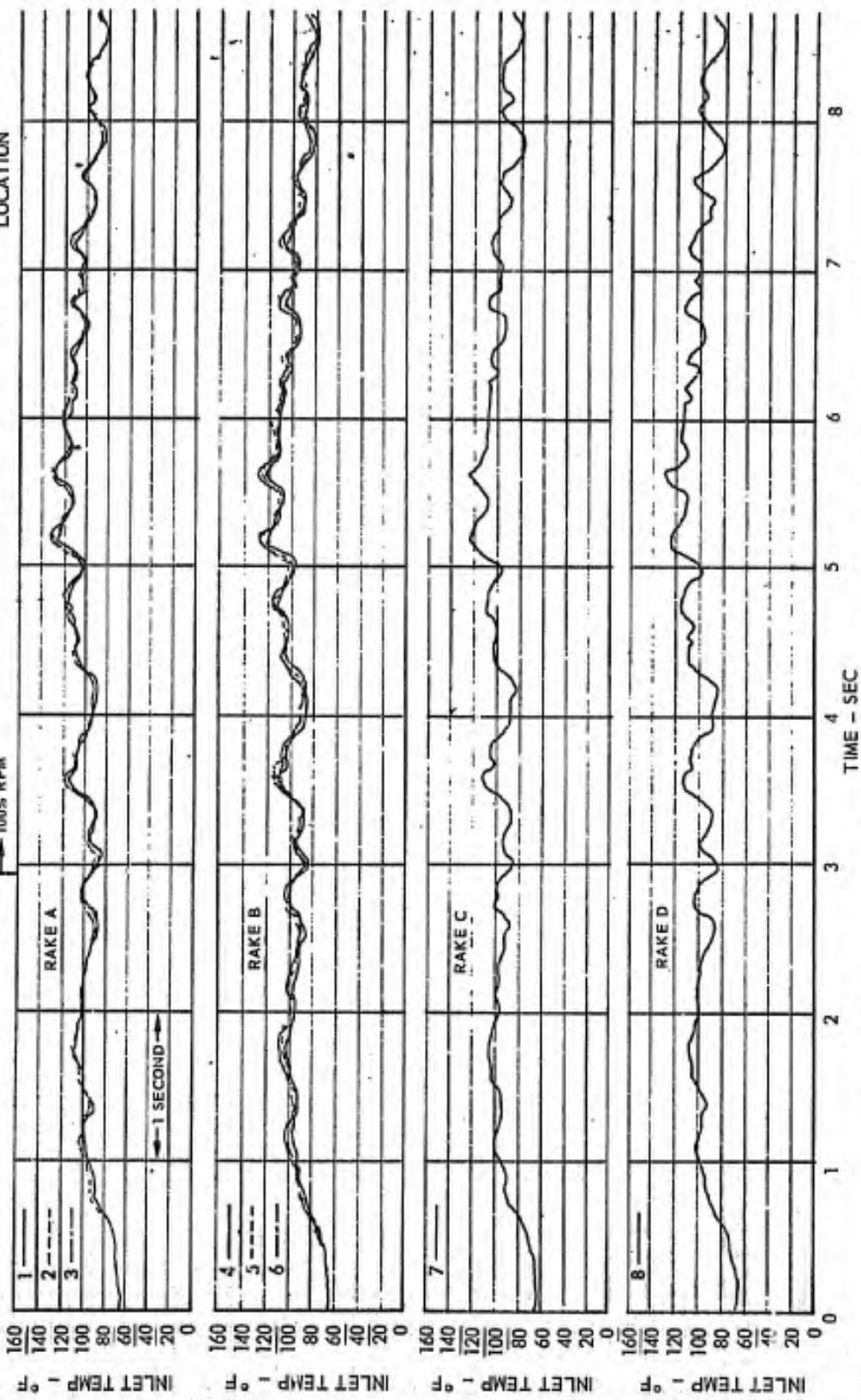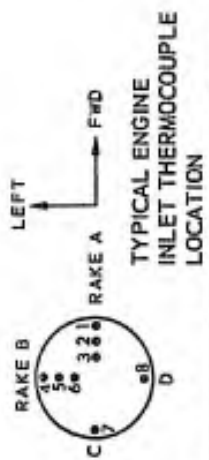
FIGURE 20 (m)   ENGINE INLET TEMPERATURE TRACE

91

FIGURE 20 (n)   ENGINE INLET TEMPERATURE TRACE
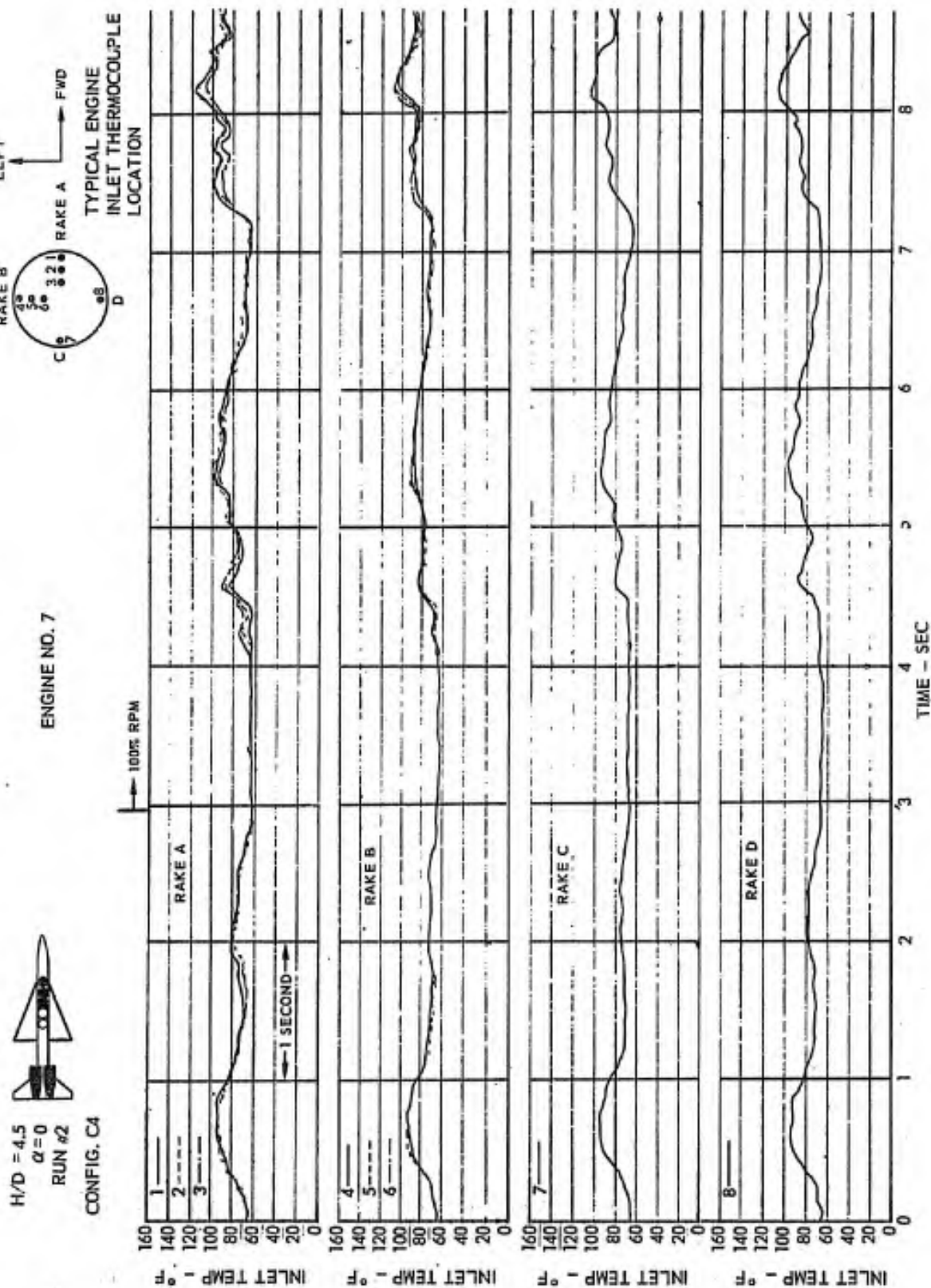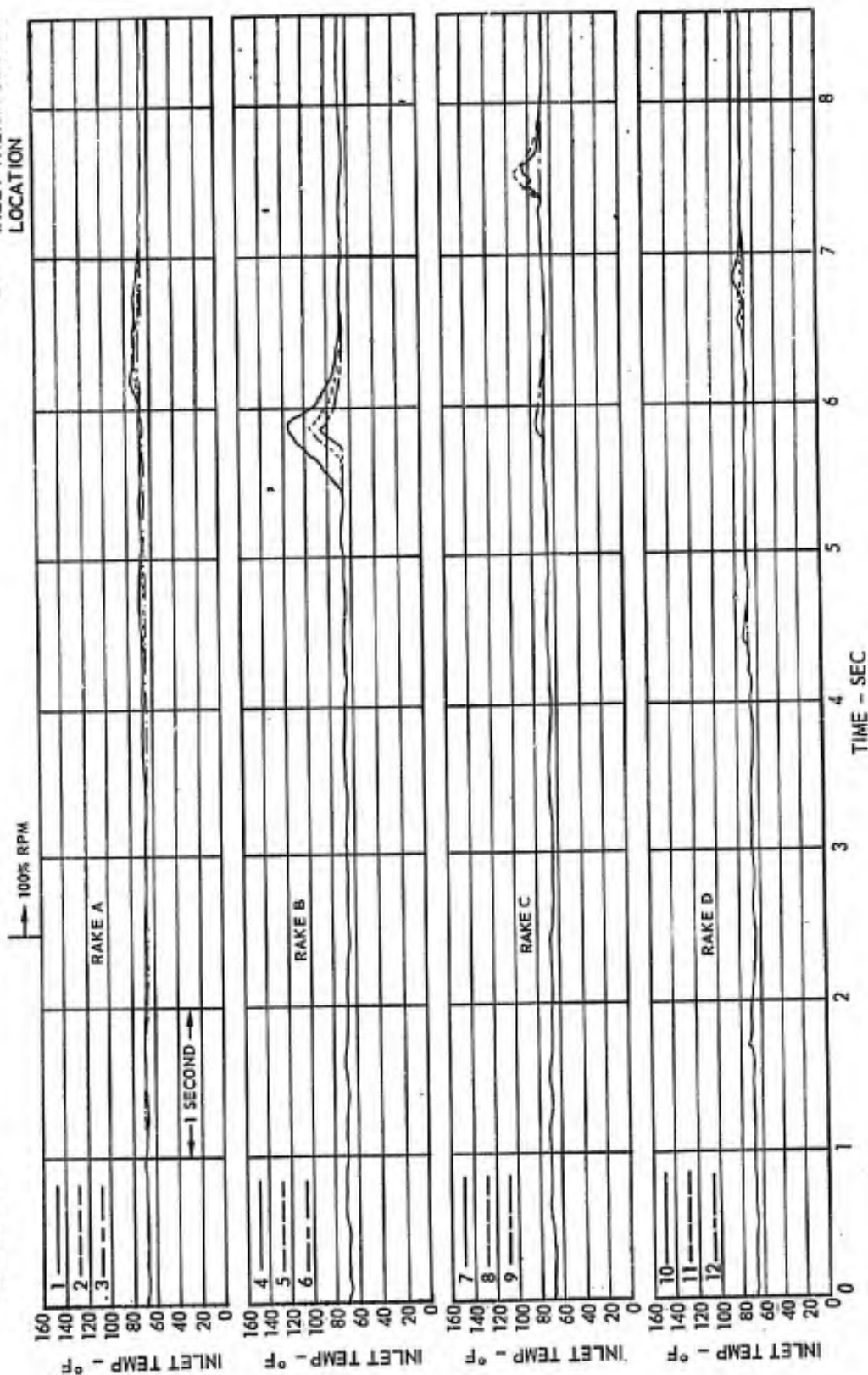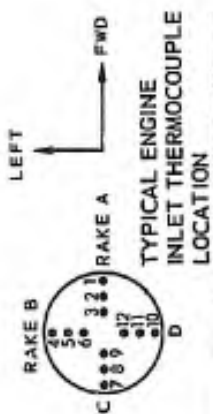
FIGURE 20 (o)   ENGINE INLET TEMPERATURE TRACE

H/D = 4.5
α = 0
RUN #3
CONFIG. C4

ENGINE NO. 1

TYPICAL ENGINE
INLET THERMOCOUPLE
LOCATION
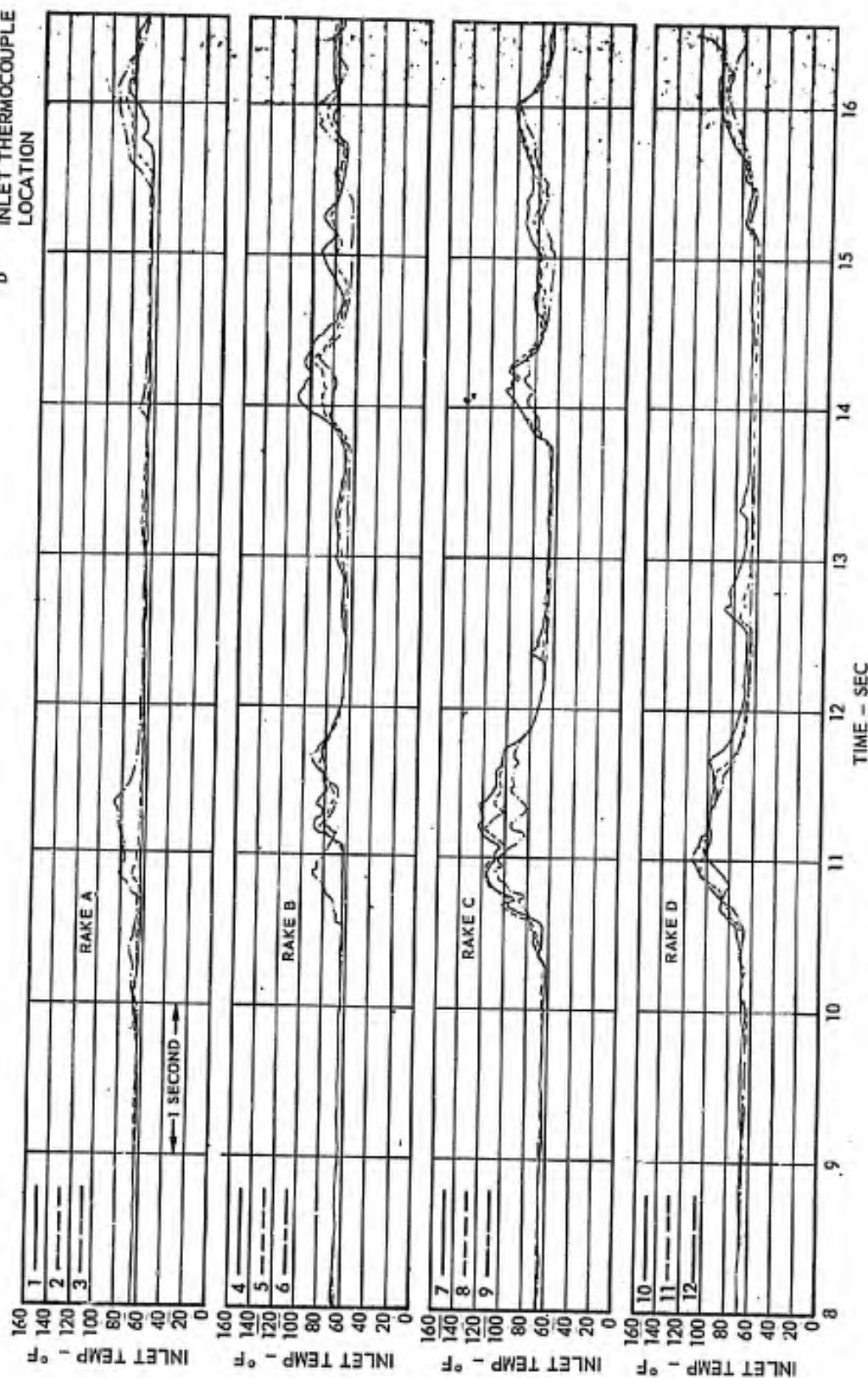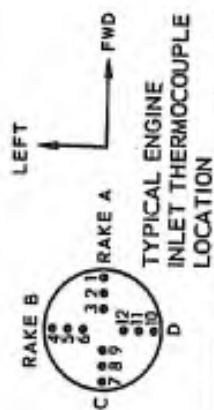
FIGURE 20 (p)   ENGINE INLET TEMPERATURE TRACE

ENGINE NO. 1 (CONTINUED)

TYPICAL ENGINE
INLET THERMOCOUPLE
LOCATION

H/D = 4.5
α = 0
RUN #3
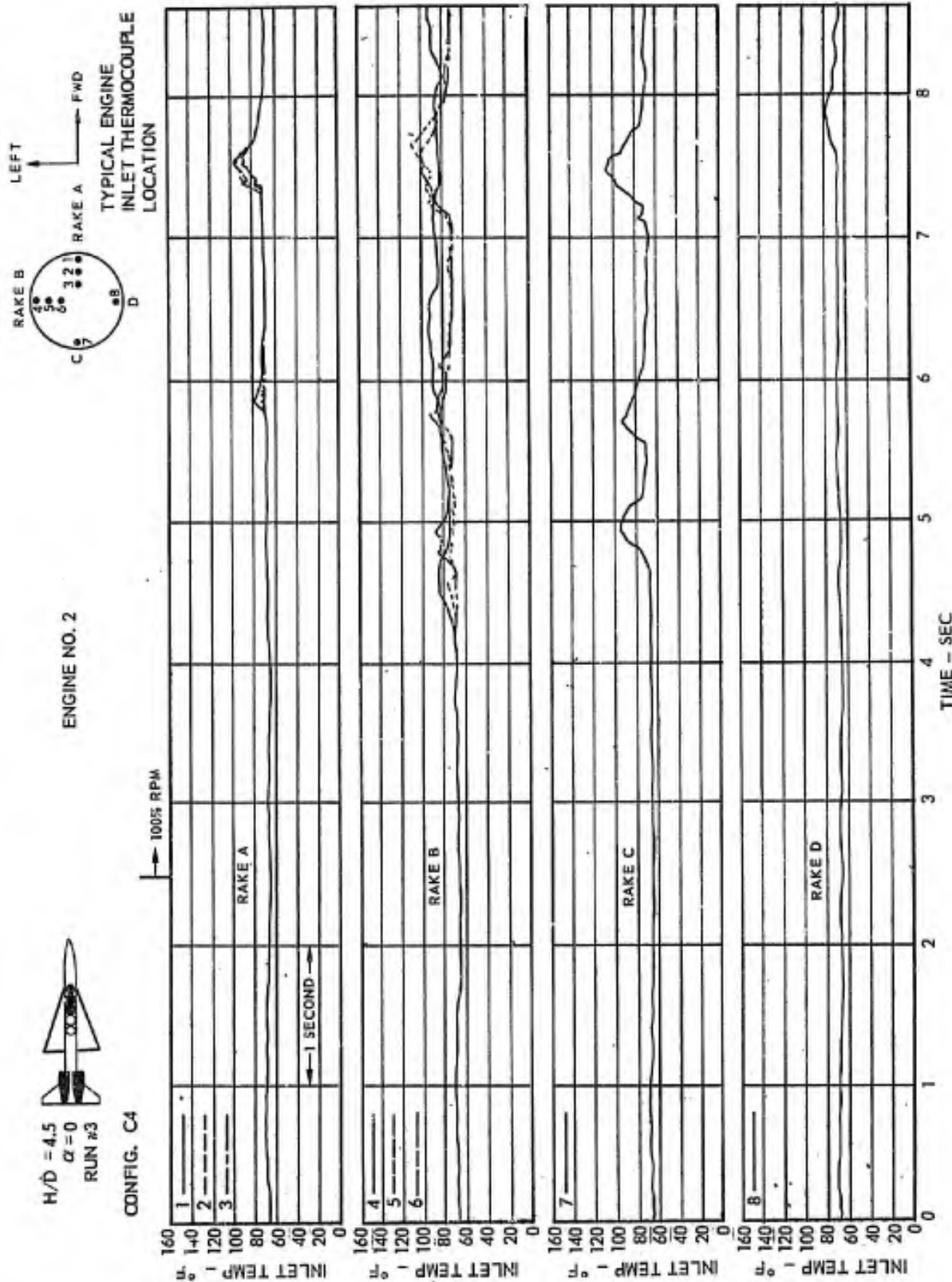
CONFIG. C4

FIGURE 20 (q) ENGINE INLET TEMPERATURE TRACE

95

FIGURE 20 (r)   ENGINE INLET TEMPERATURE TRACE
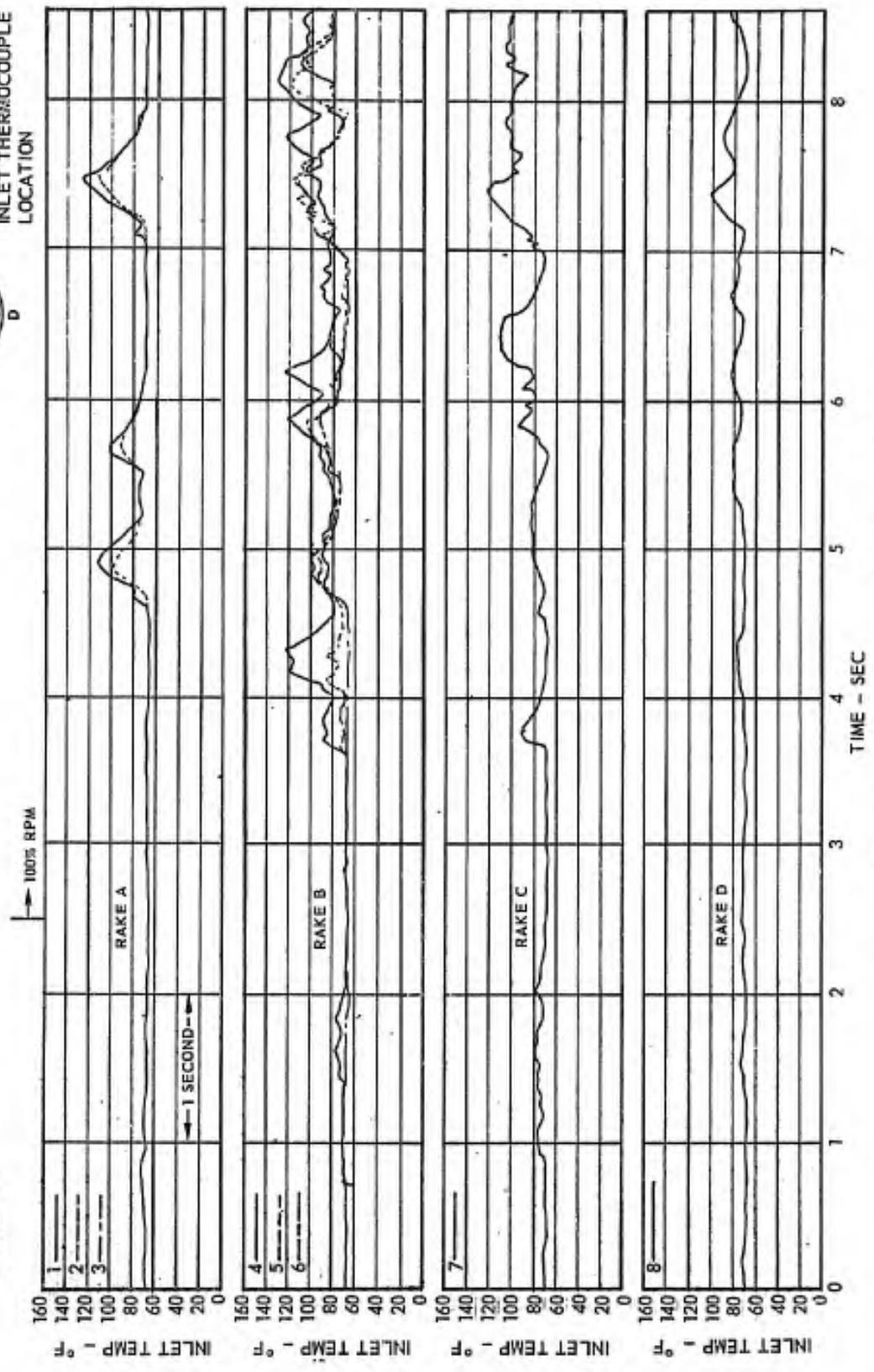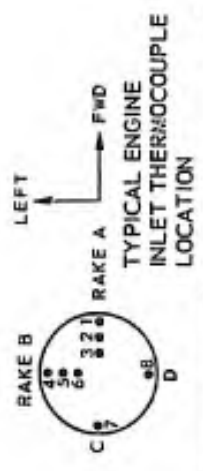
FIGURE 20 (s) ENGINE INLET TEMPERATURE TRACE
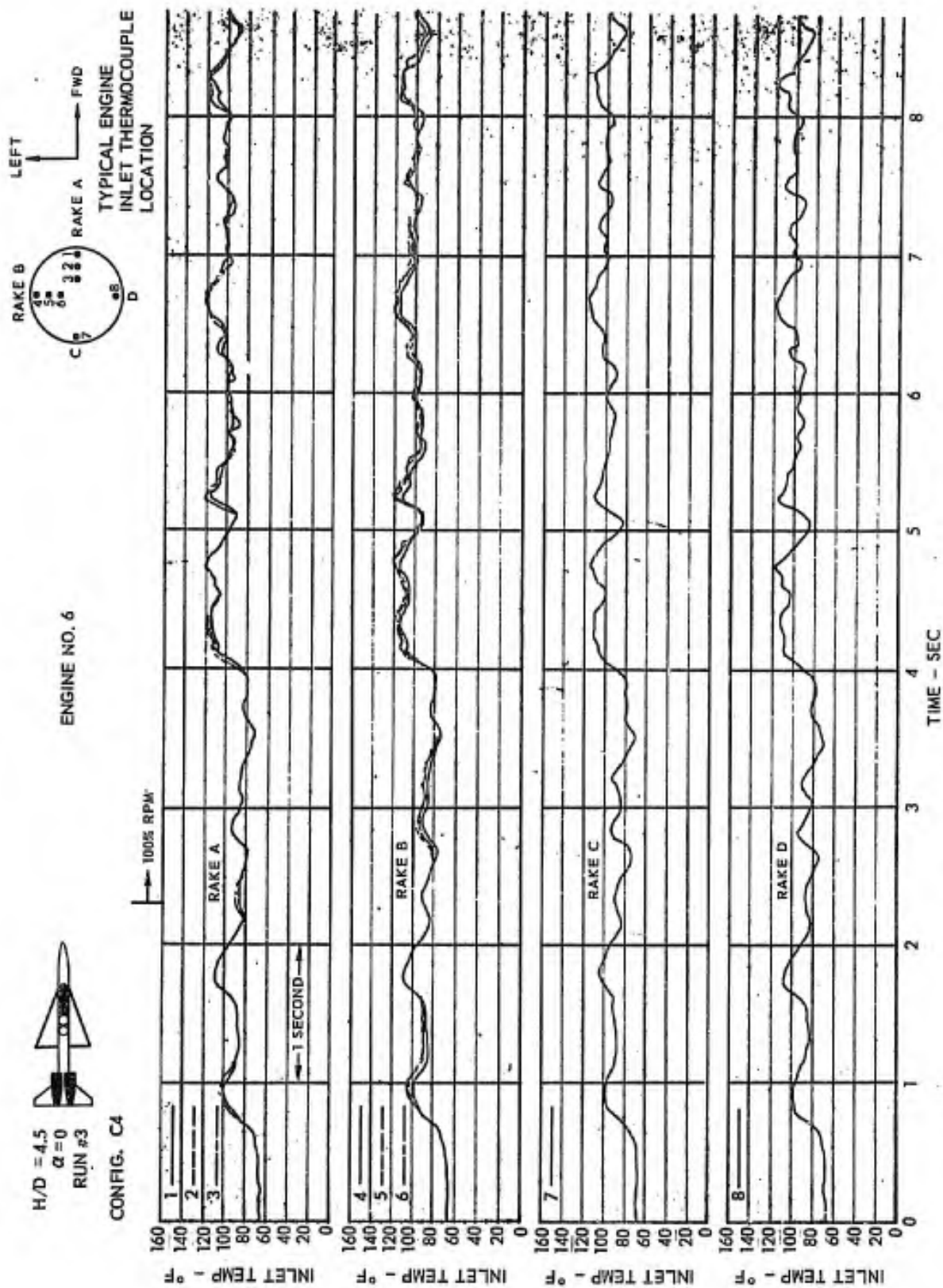
FIGURE 20 (t) ENGINE INLET TEMPERATURE TRACE
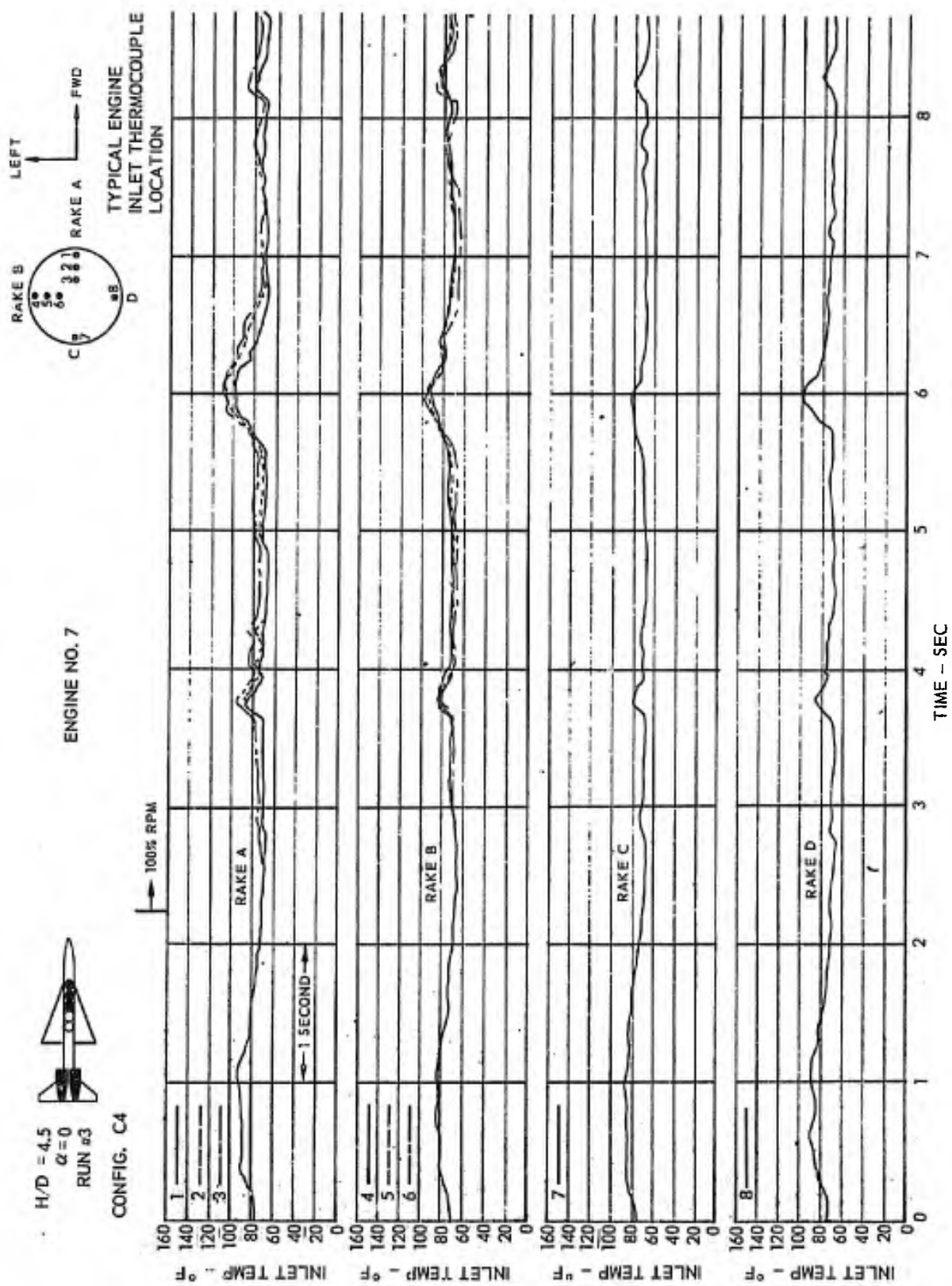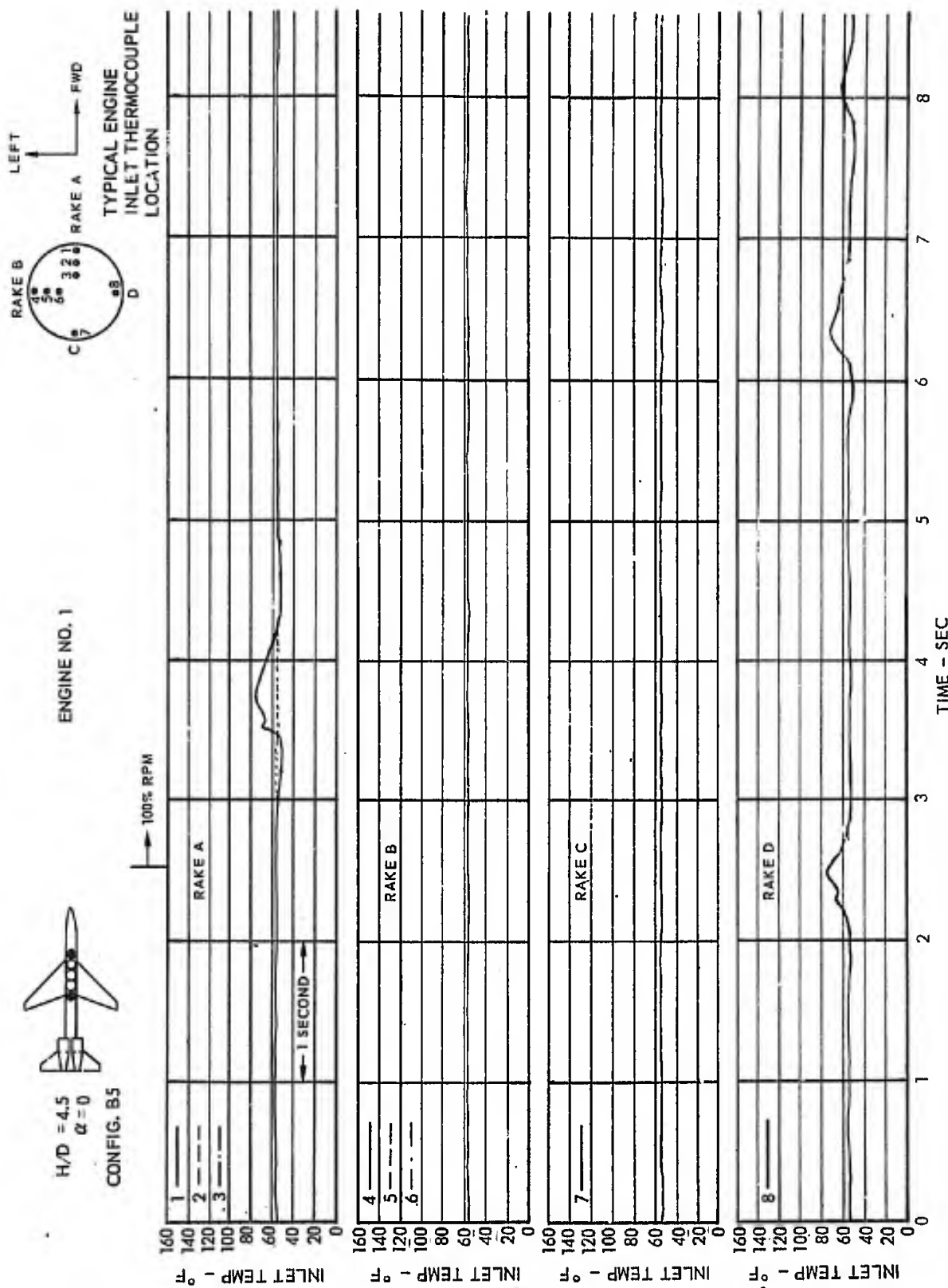
FIGURE 20 (v)   ENGINE INLET TEMPERATURE TRACE
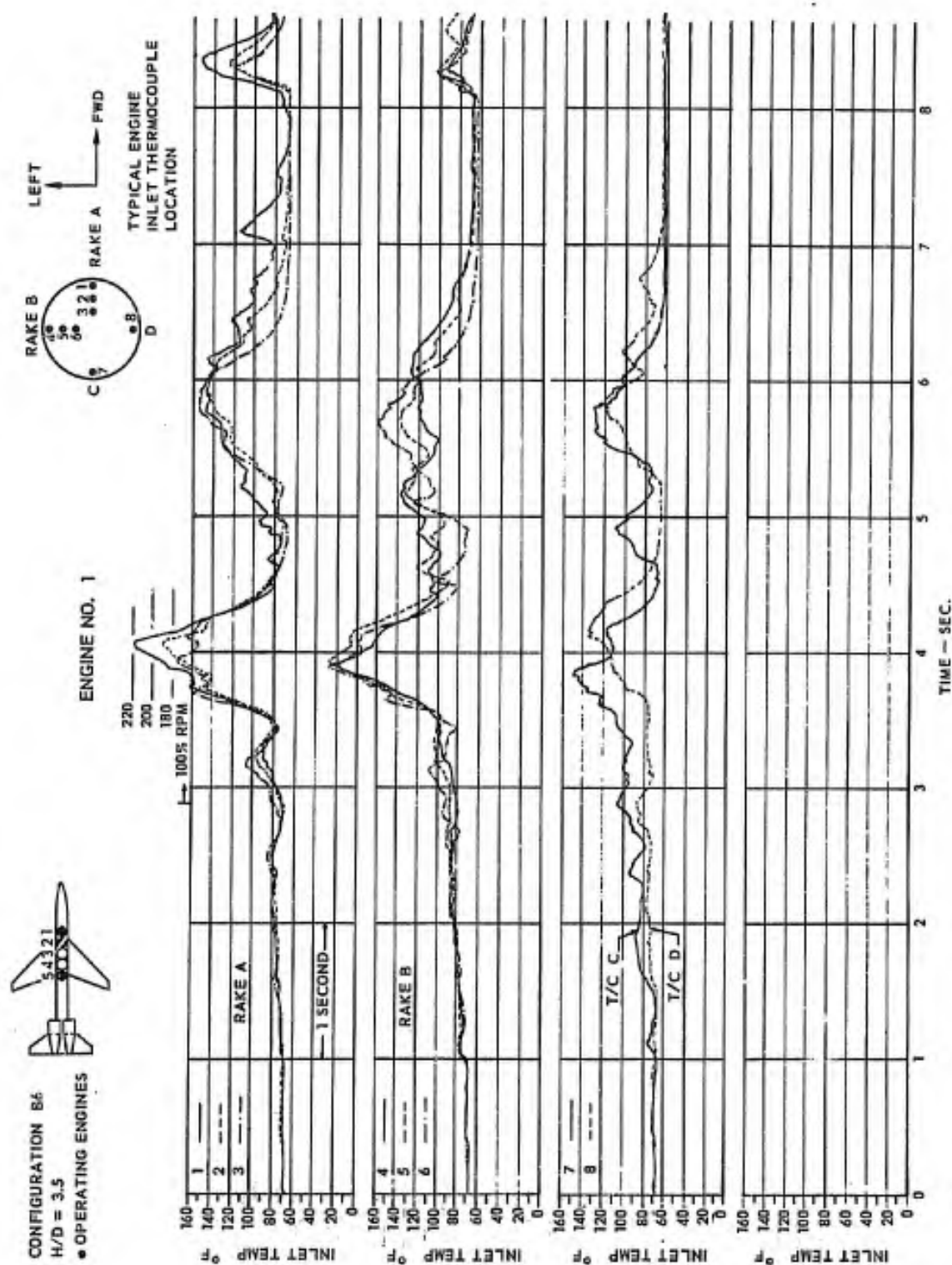
FIGURE 21 (a)   ENGINE INLET TEMPERATURE TRACE
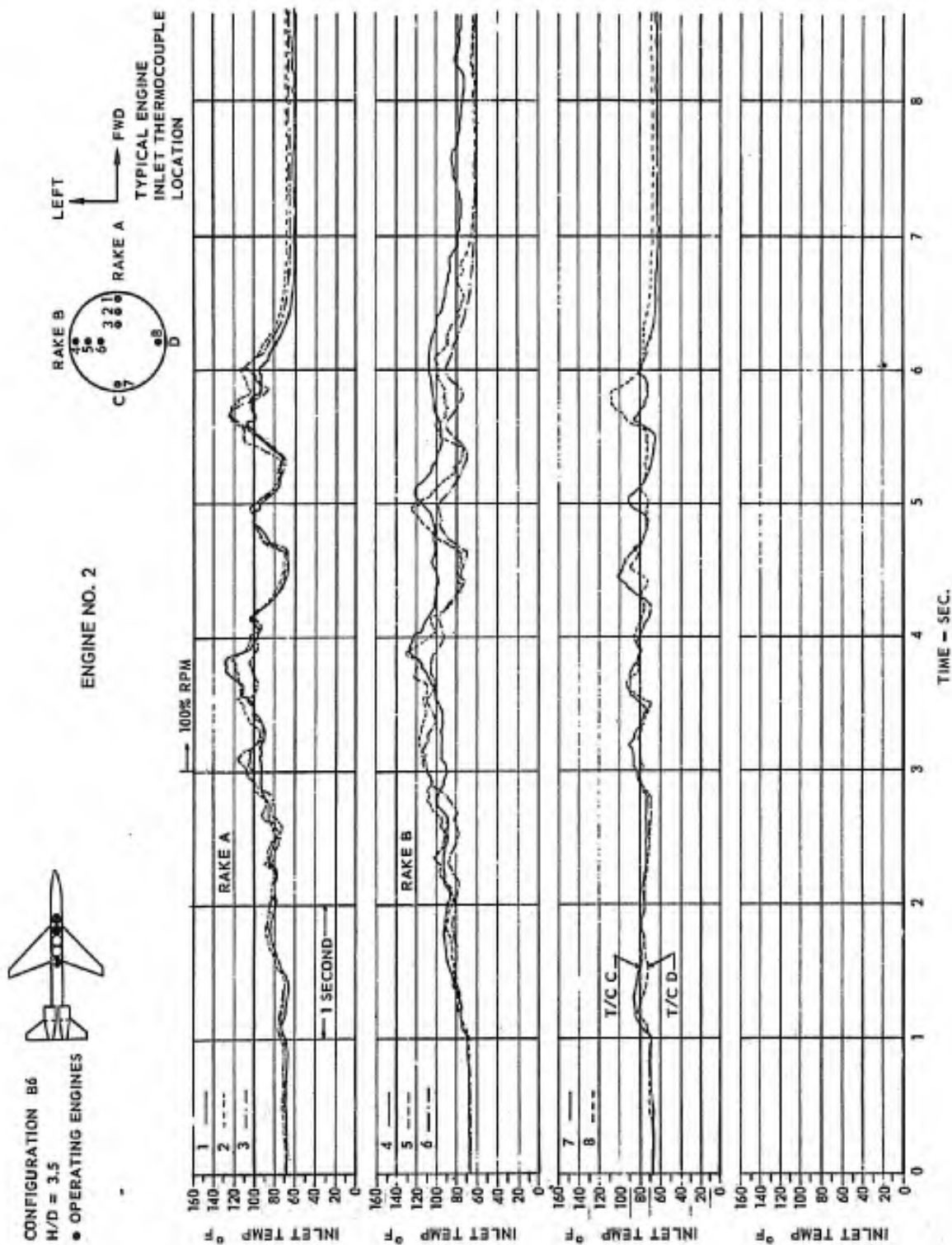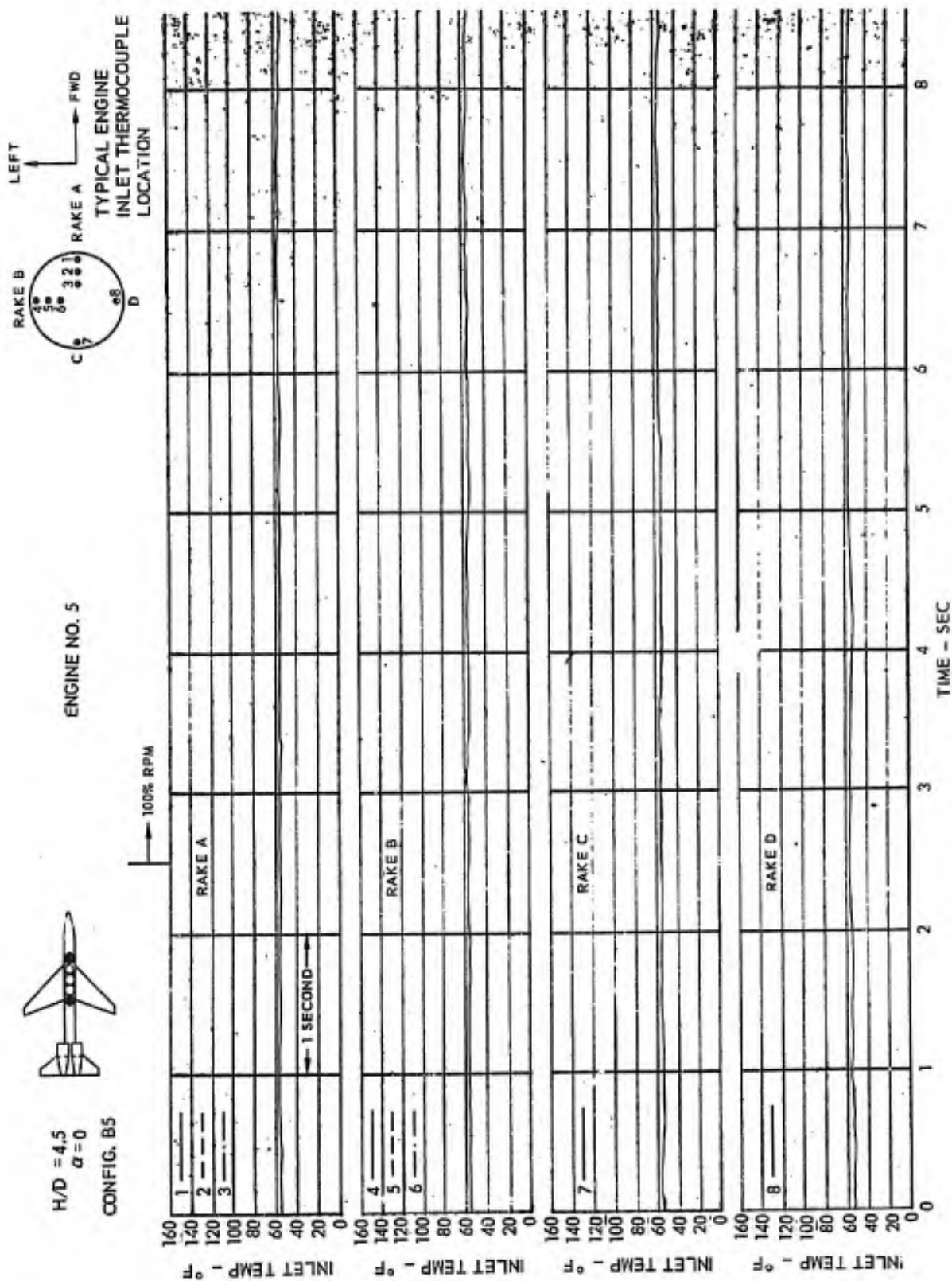
FIGURE 21 (b)   ENGINE INLET TEMPERATURE TRACE
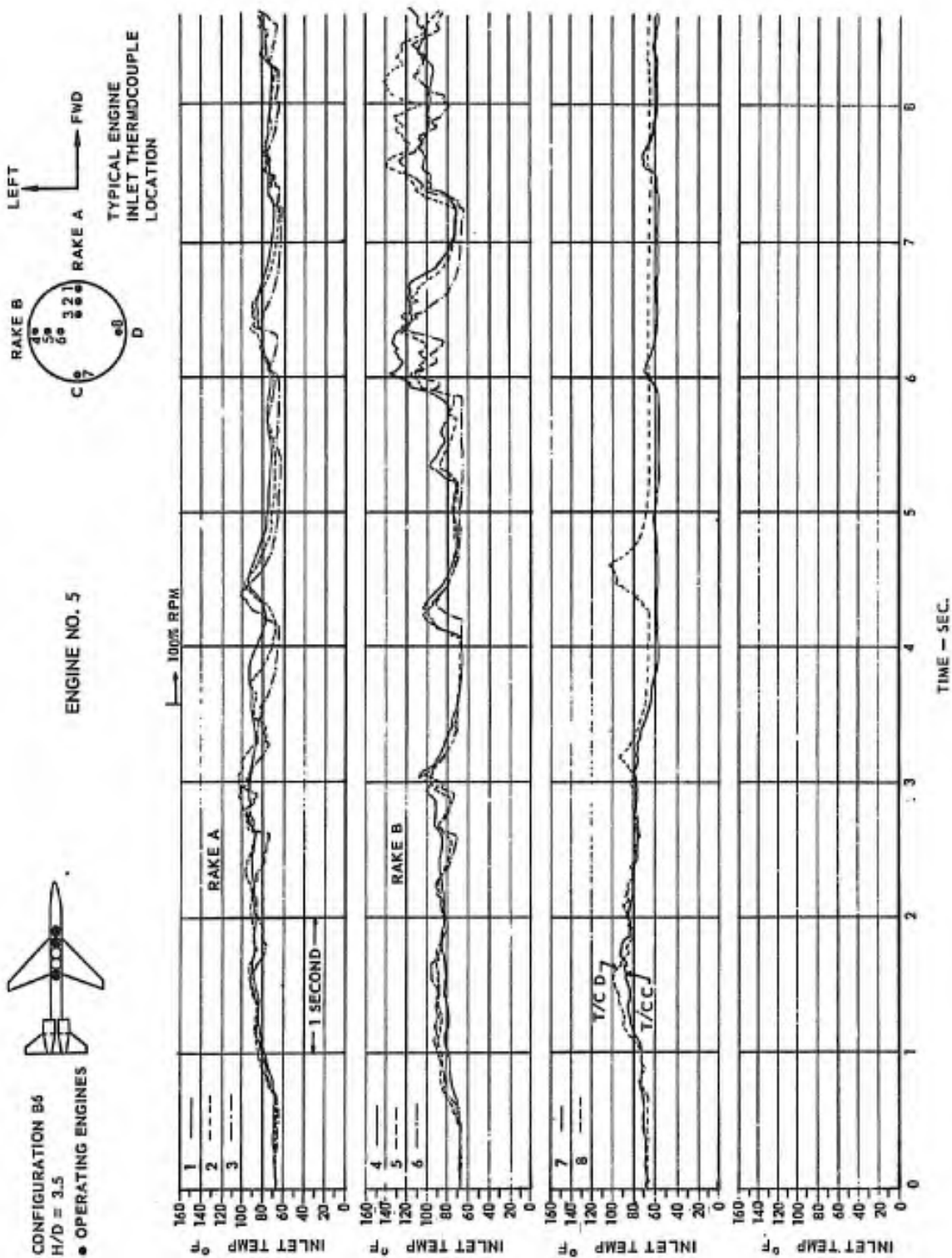
FIGURE 21 (c)   ENGINE INLET TEMPERATURE TRACE
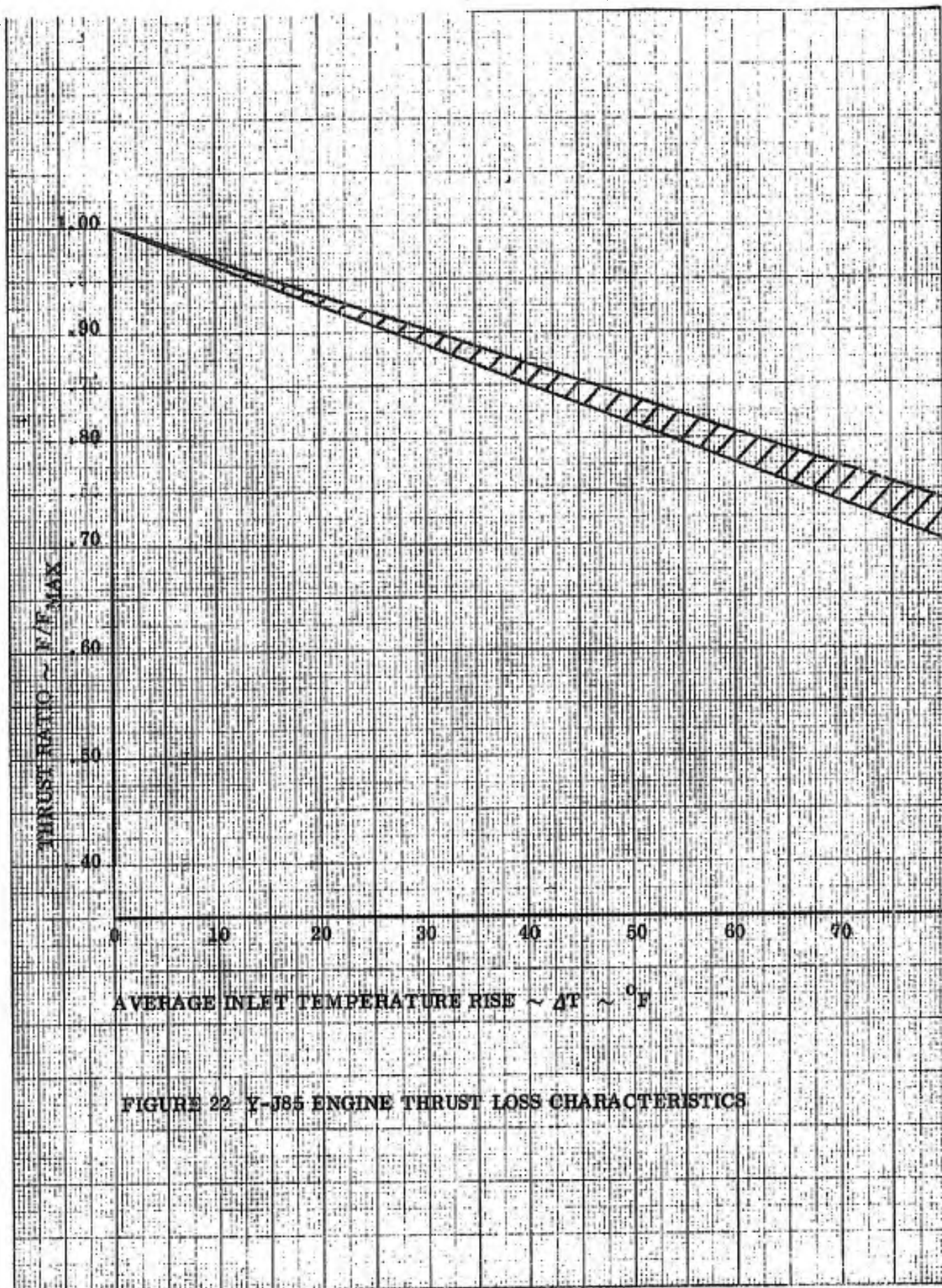
FIGURE 22 Y-J85 ENGINE THRUST LOSS CHARACTERISTICS

FIGURE 23. TYPICAL THRUST & TEMPERATURE
TIME HISTORY
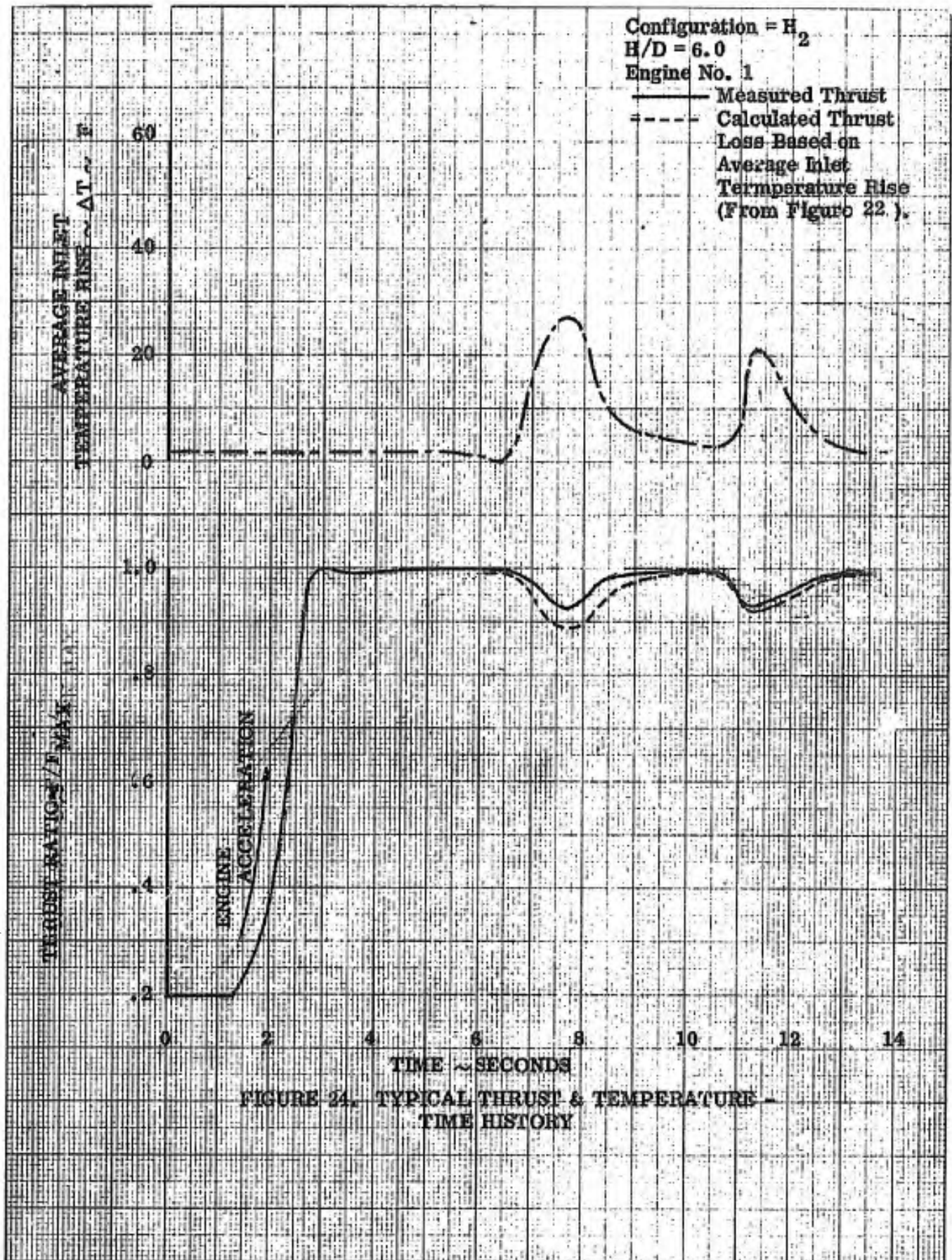
FIGURE 24. TYPICAL THRUST & TEMPERATURE - TIME HISTORY

105
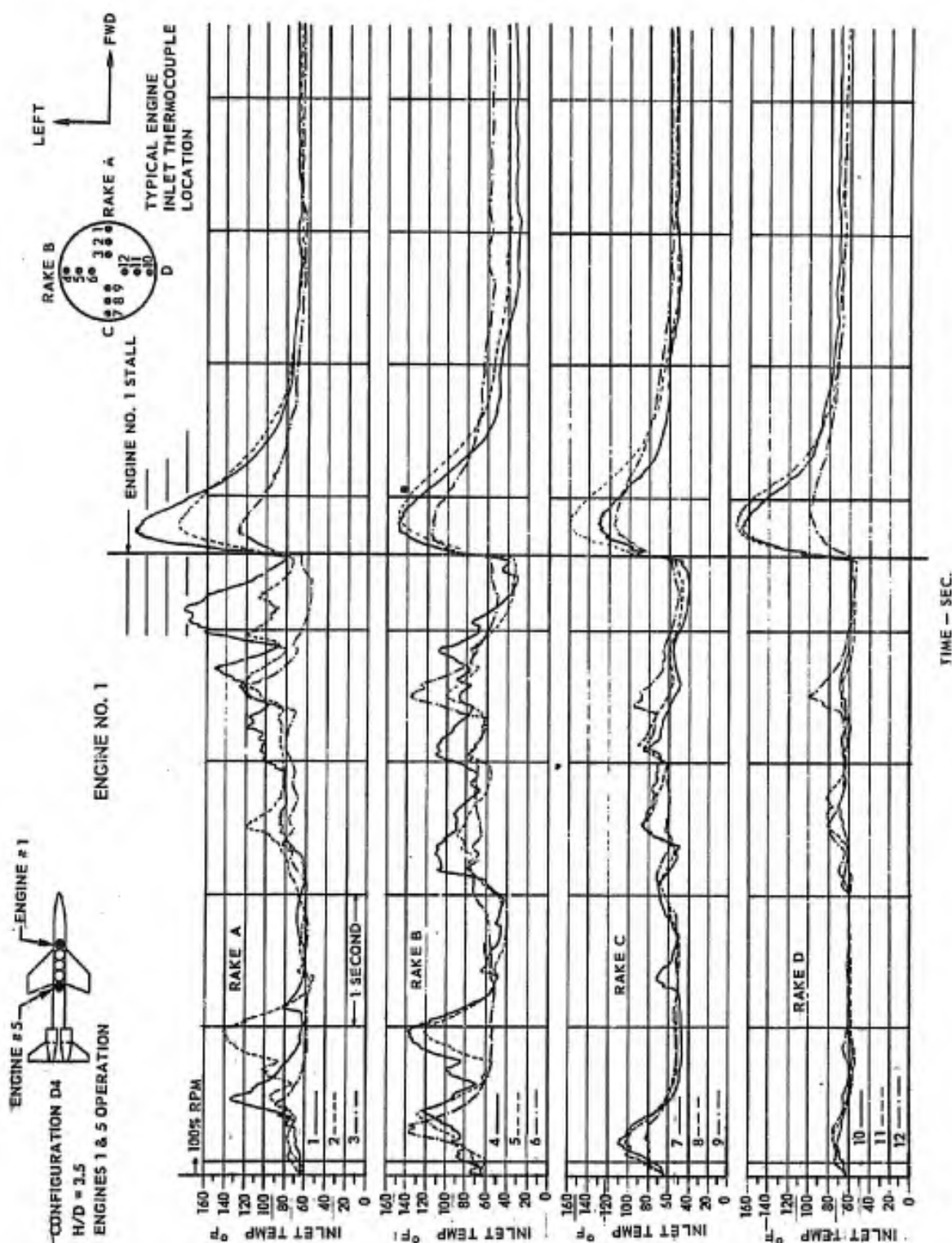
FIGURE 25 TYPICAL INLET TEMPERATURE RISE LEADING TO ENGINE STALL

106

PITCH ATTITUDE = 0

CONFIGURATION B$_1$

(a)

CONFIGURATION B$_2$

(b)

Symbol	Engine
⊙	1
Χ	2
▣	3
Y	4
+	5
☆	6
L	7

CONFIGURATION B$_3$

(c)

INLET TEMPERATURE RISE ~ °F

H/D
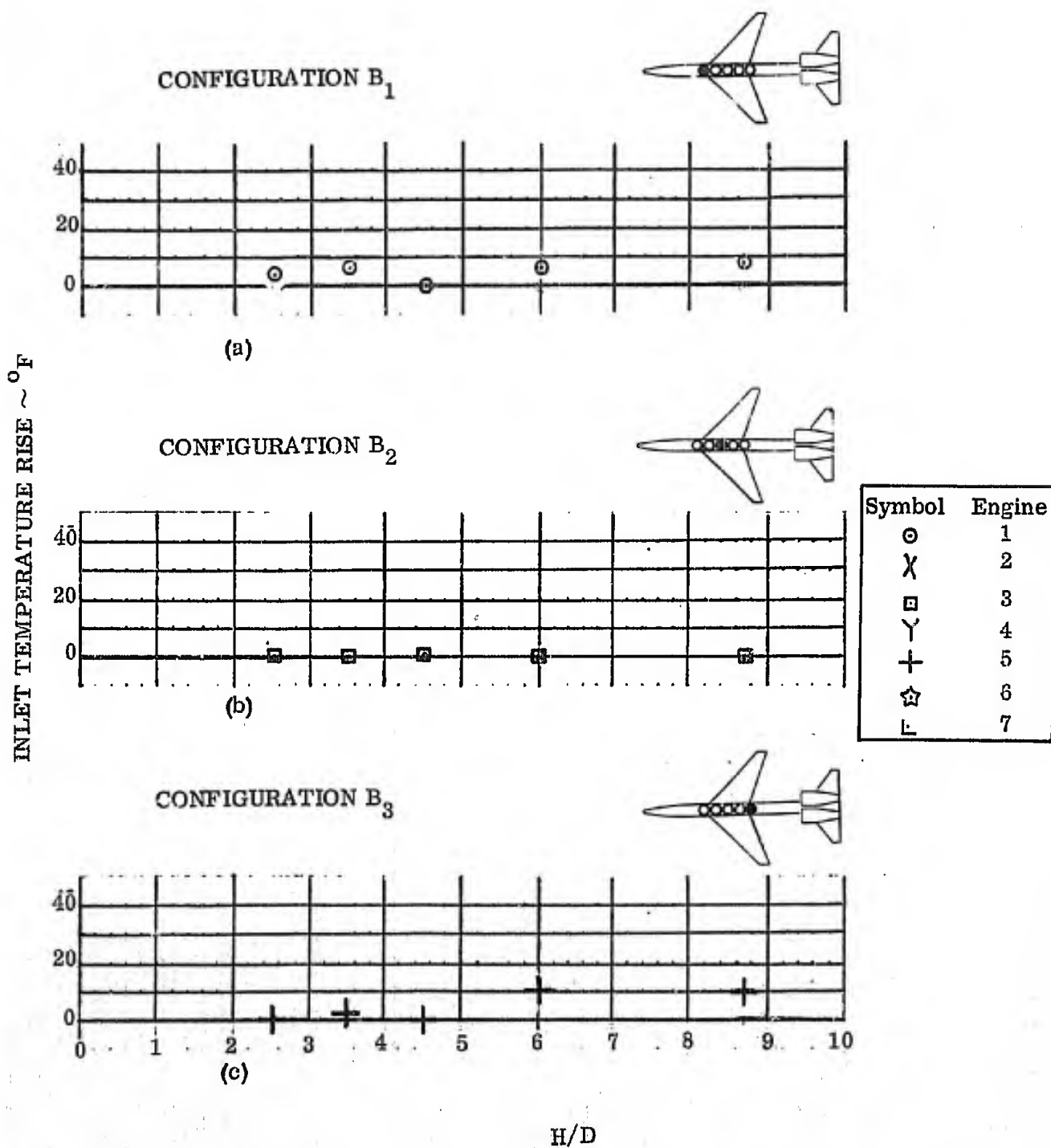
FIGURE 26 HOT GAS INGESTION DURING SINGLE ENGINE OPERATION

107

PITCH ATTITUDE = 0

CONFIGURATION D$_1$

(a)

INLET TEMPERATURE RISE ~ ^{o}F
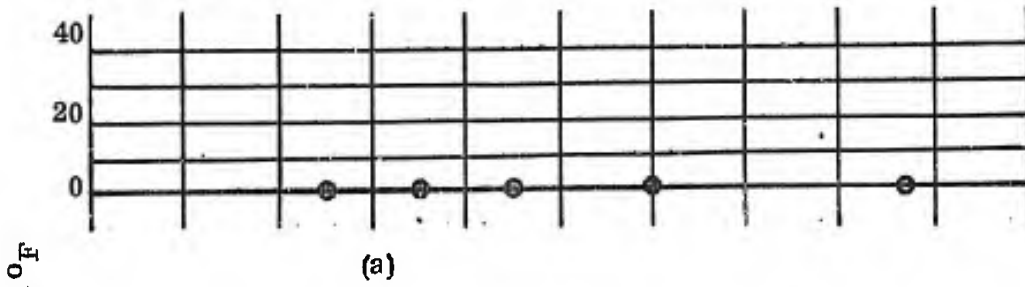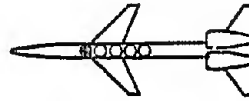
Symbol	Engine
⊙	1
X	2
□	3
Y	4
+	5
☆	6
L	7

CONFIGURATION D$_2$

(b)

H/D
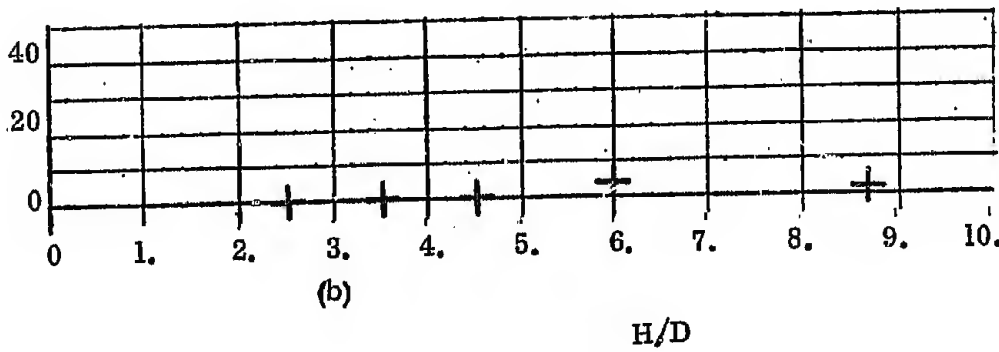
FIGURE 27 HOT GAS INGESTION DURING SINGLE ENGINE OPERATION

PITCH ATTITUDE = 0

CONFIGURATION D$_3$

(a)

Symbol	Engine
⊙	1
X	2
⊡	3
Y	4
+	5
☆	6
L	7

CONFIGURATION D$_4$

(b)

INLET TEMPERATURE RISE ~ ^{o}F

H/D
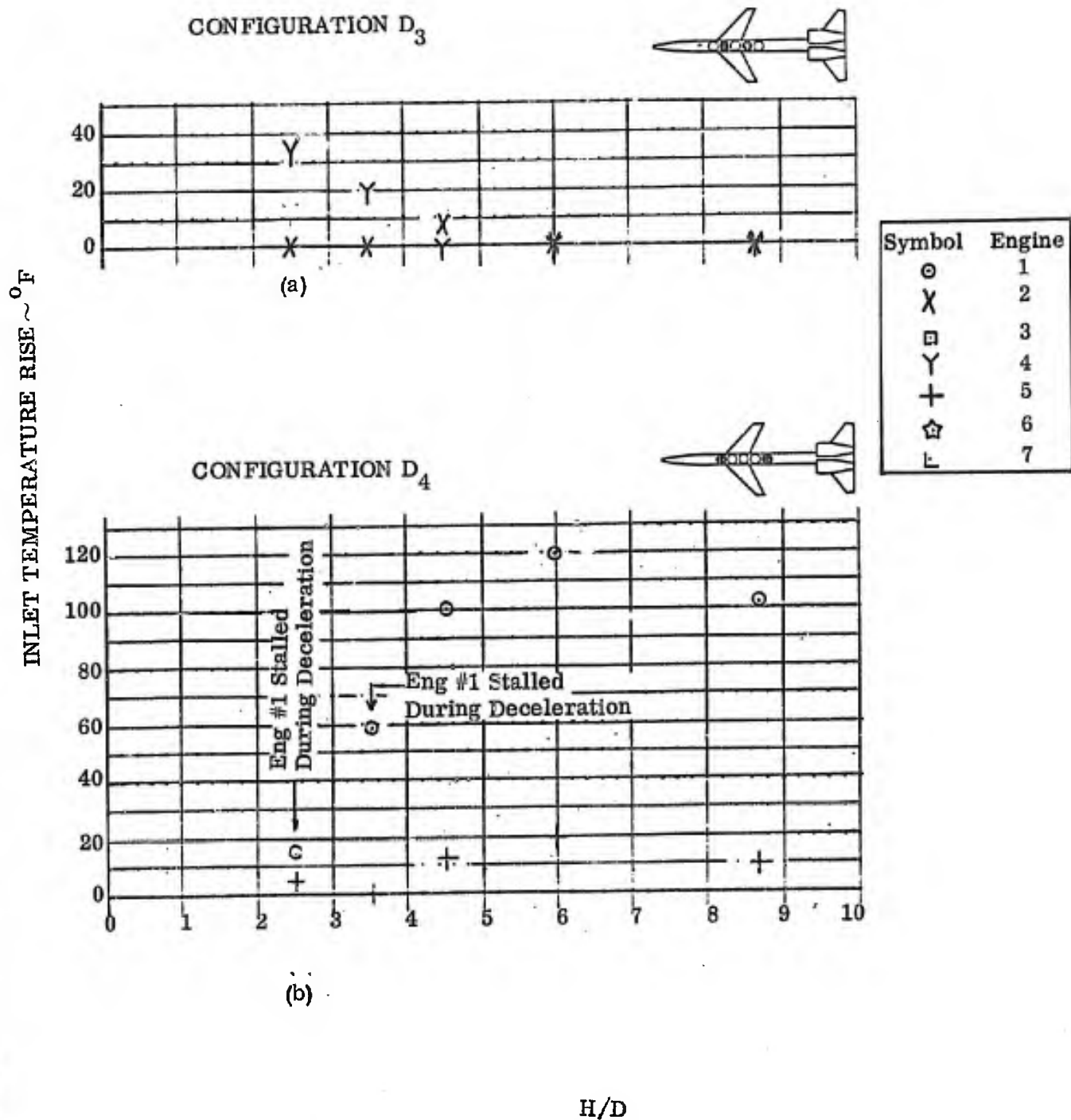
FIGURE 28 EFFECT OF ENGINE SEPARATION ON INGESTION

109

PITCH ATTITUDE = 0

CONFIGURATION B$_4$

(a)

Symbol	Engine
⊙	1
X	2
□	3
Y	4
+	5
✩	6
L	7

CONFIGURATION B$_5$

(b)

H/D
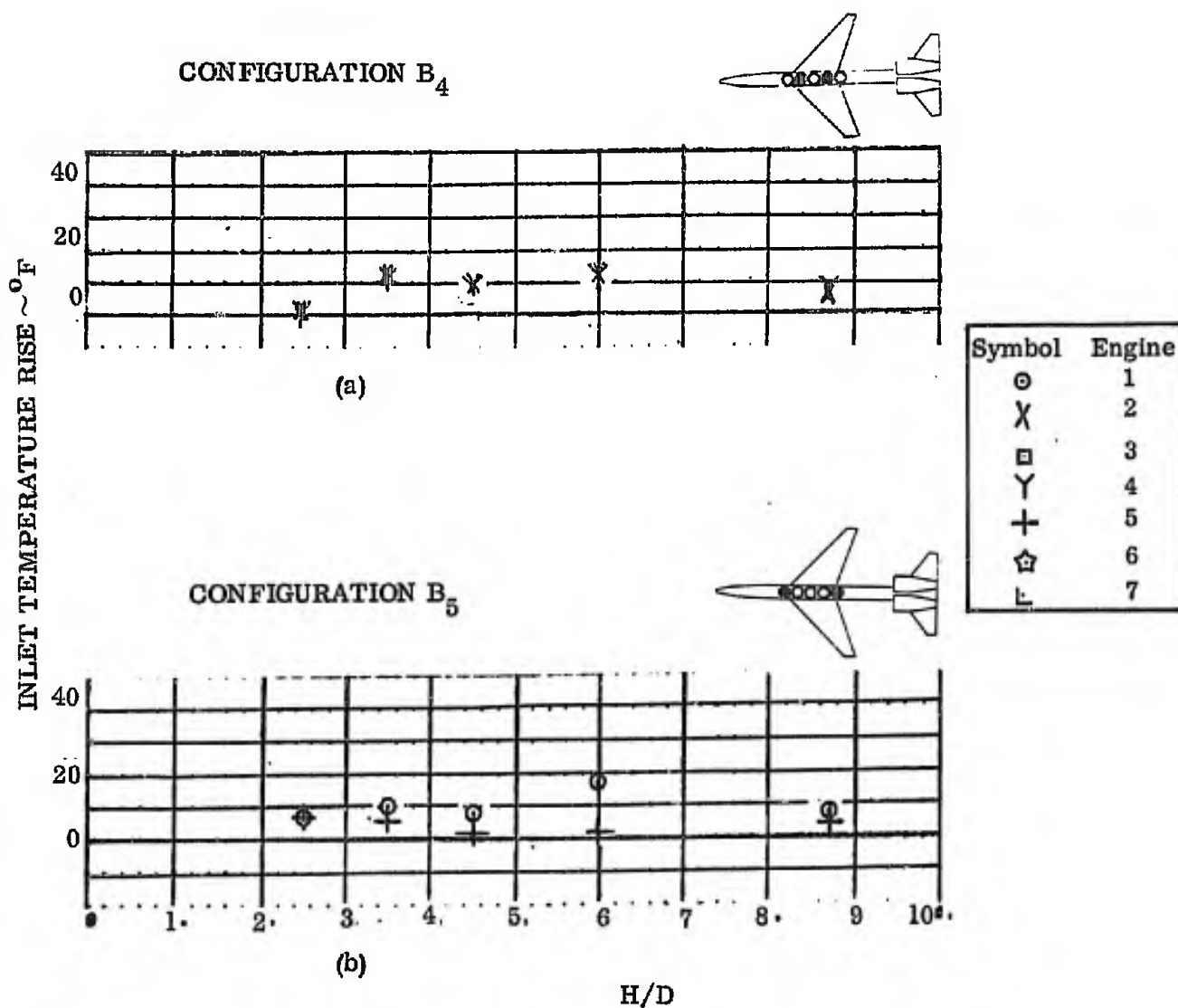
FIGURE 29 EFFECT OF ENGINE SEPARATION ON INGESTION

110

PITCH ATTITUDE = 0

CONFIGURATION B$_5$

(a)

Symbol	Engine
⊙	1
X	2
□	3
Y	4
+	5
☆	6
L	7

CONFIGURATION B$_6$

(b)

INLET TEMPERATURE RISE ~ $^\circ$F
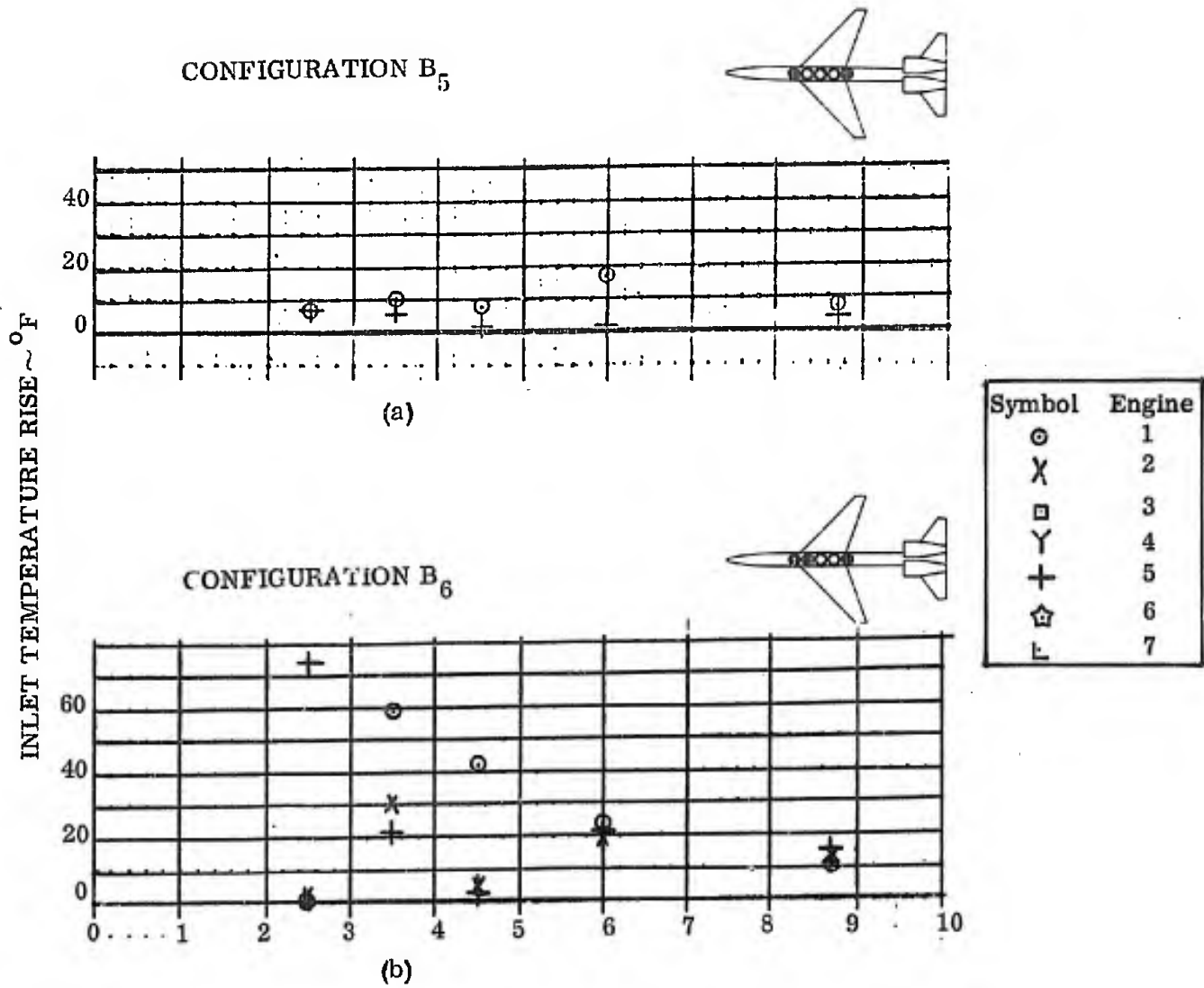
FIGURE 30 EFFECT OF LIFT ENGINE ARRANGEMENT ON INLET TEMPERATURE RISE

PITCH ATTITUDE = 0

CONFIGURATION B$_7$

Symbol	Engine
⊙	1
X	2
⊡	3
Y	4
+	5
☆	6
Ⴑ	7

(a)

H/D
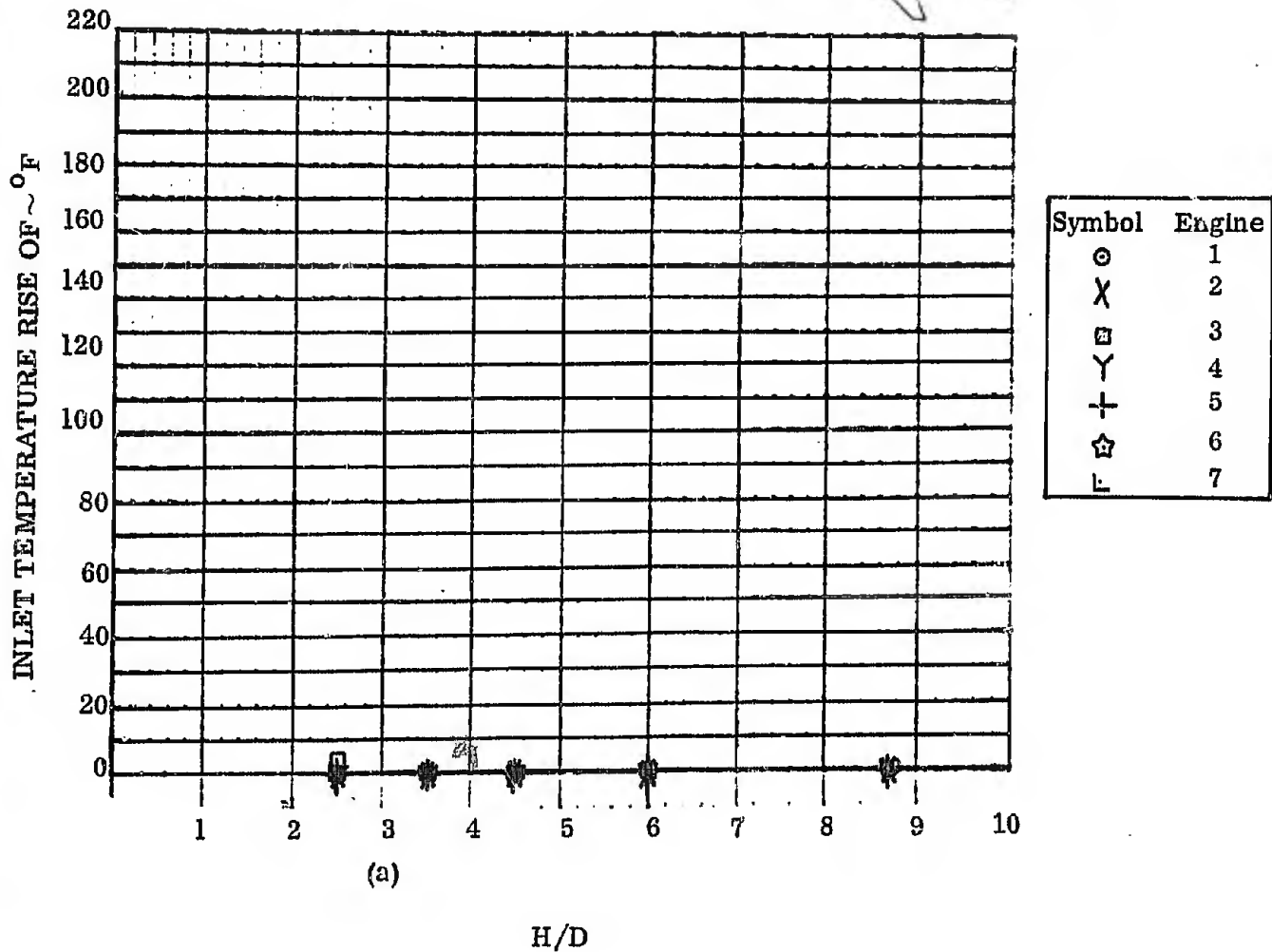
FIGURE 31 EFFECT OF SPACING ON INLET TEMPERATURE RISE
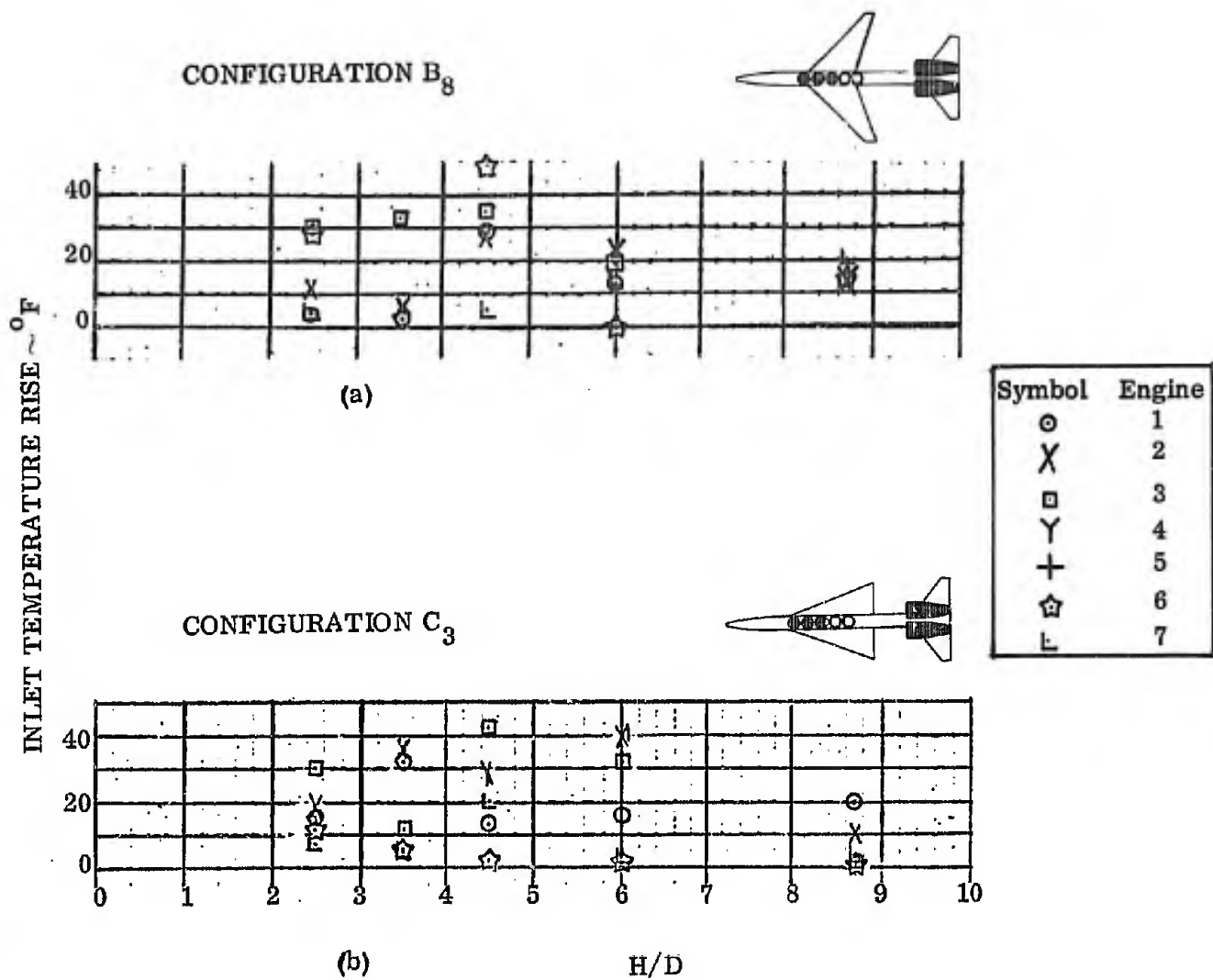
PITCH ATTITUDE = 0

CONFIGURATION B$_8$

(a)

INLET TEMPERATURE RISE, $^{\circ}$F

Symbol	Engine
⊙	1
X	2
▫	3
Y	4
+	5
☆	6
⌐	7

CONFIGURATION C$_3$

(b)

H/D

FIGURE 52 INFLUENCE OF WING GEOMETRY ON GAS INGESTION

113

PITCH ATTITUDE = 0

CONFIGURATION E₁

(a)

INLET TEMPERATURE RISE ~ °F

Symbol	Engine
⊙	1
X	2
⊡	3
Y	4
+	5
☆	6
L	7

CONFIGURATION G₁

(b)
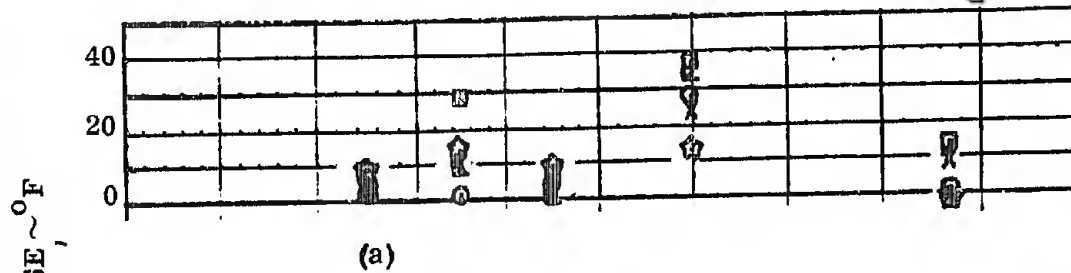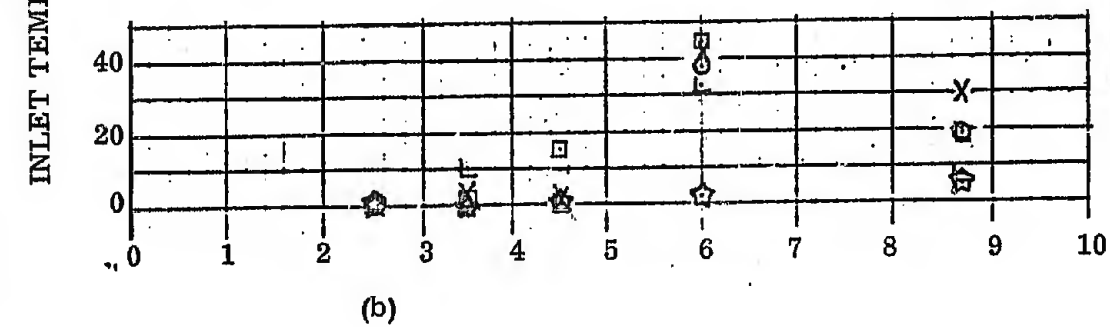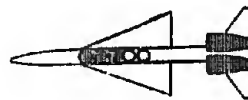
H/D

FIGURE 33 INFLUENCE OF WING GEOMETRY ON GAS INGESTION
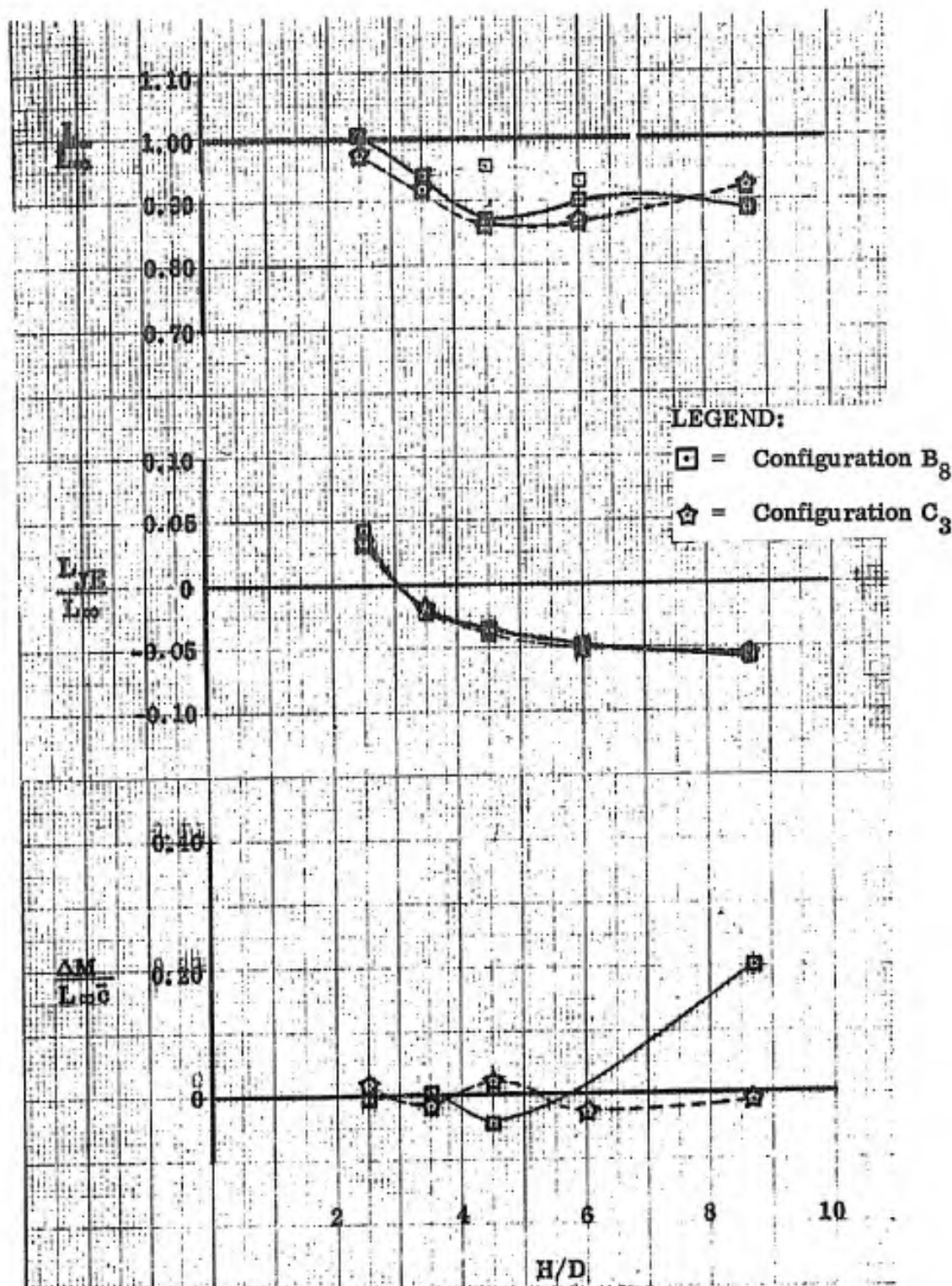
FIGURE 34   INFLUENCE OF WING GEOMETRY ON JET-INDUCED FORCE & MOMENT

115
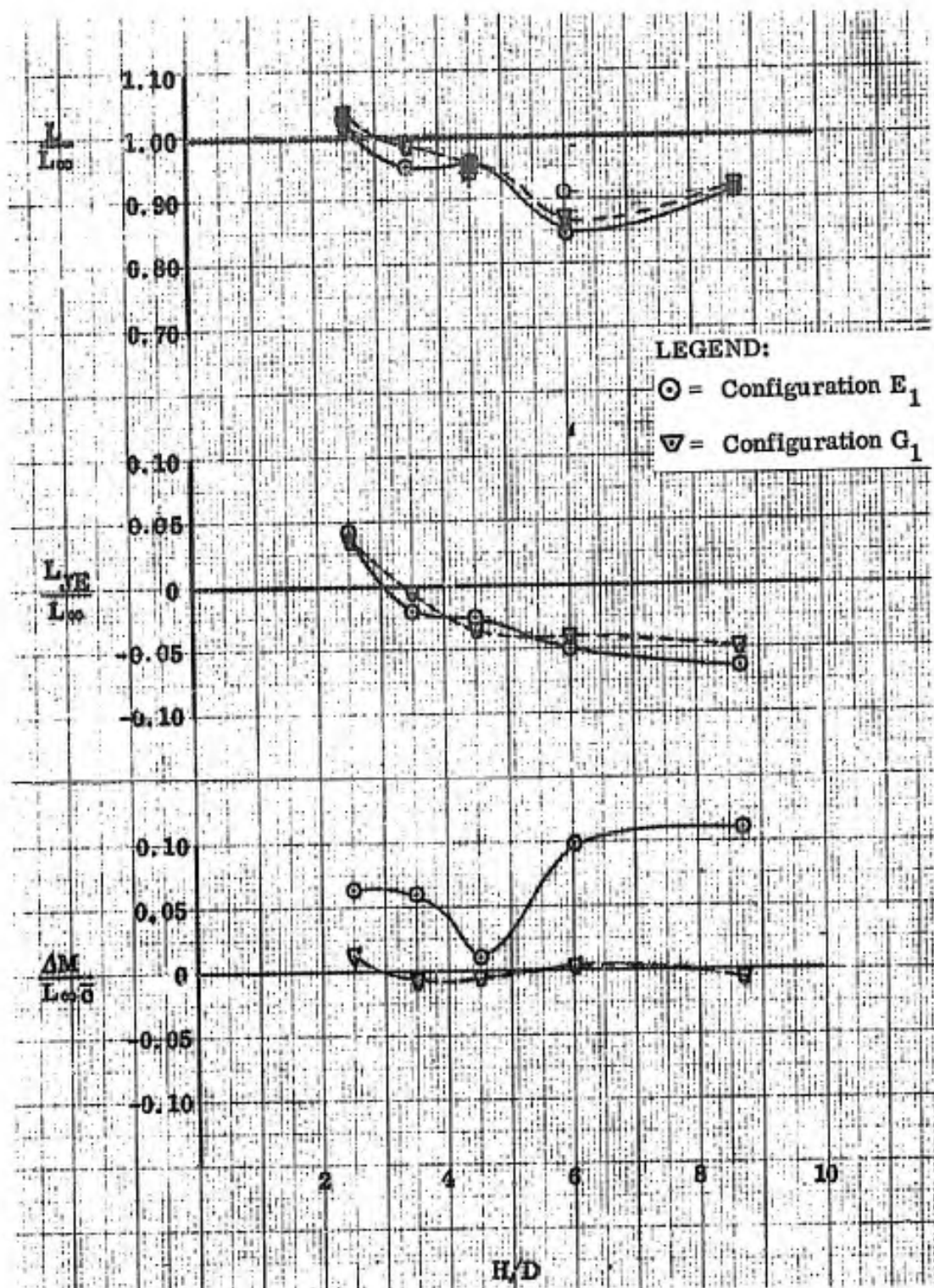
FIGURE 35   INFLUENCE OF WING GEOMETRY ON JET-INDUCED FORCE & MOMENT

116
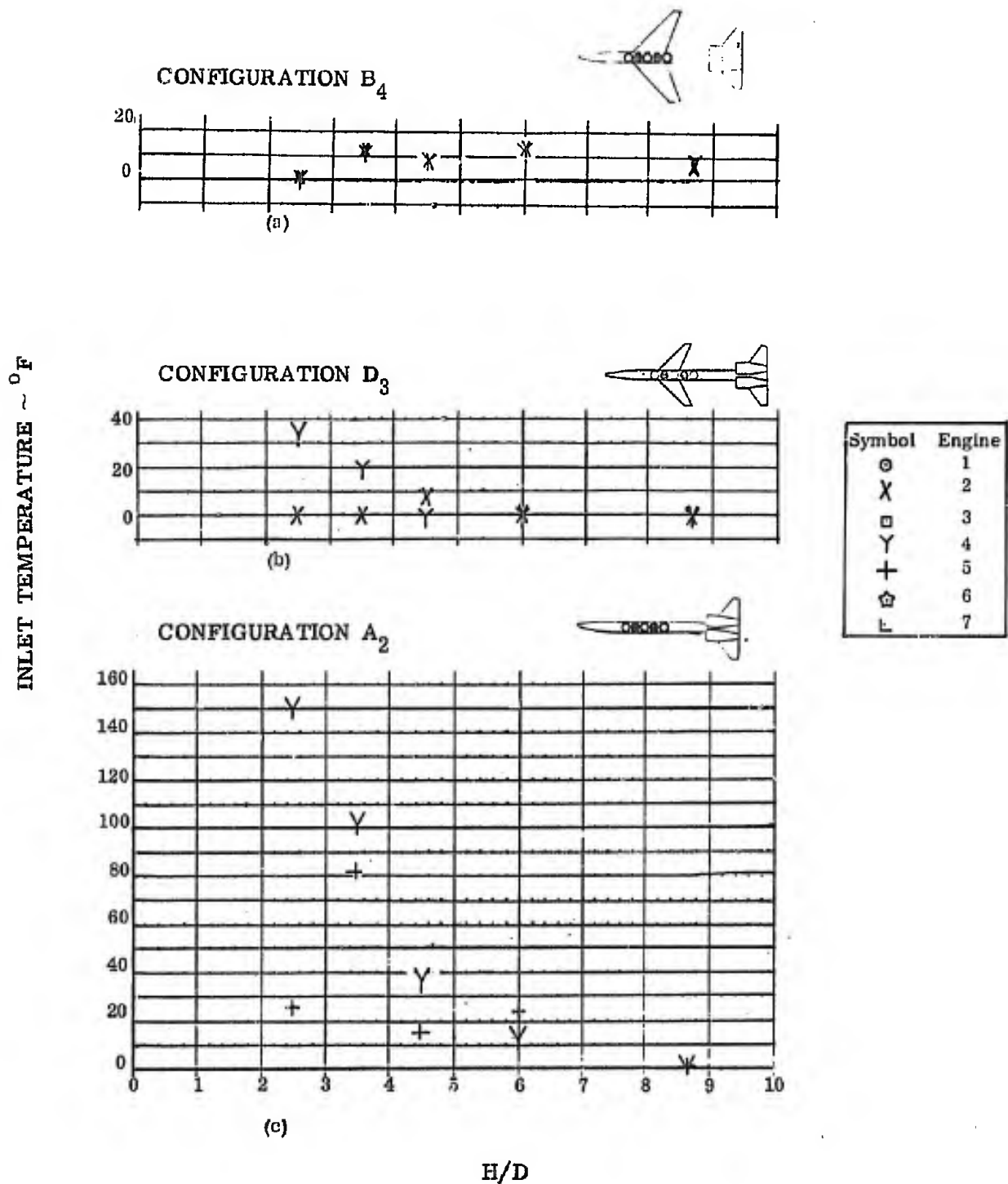
PITCH ATTITUDE = 0

FIGURE 36   EFFECT OF WING SIZE ON GAS INGESTION

117

PITCH ATTITUDE = 0

CONFIGURATION B$_5$

(a)

CONFIGURATION D$_4$

Symbol	Engine
☉	1
X	2
⊡	3
Y	4
+	5
☆	6
L	7

Eng #1 Stalled During Deceleration

Eng #1 Stalled During Deceleration
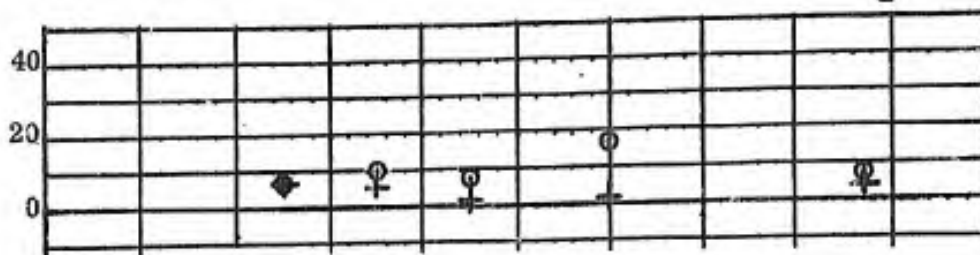
INLET TEMPERATURE RISE ～ $^\circ$F
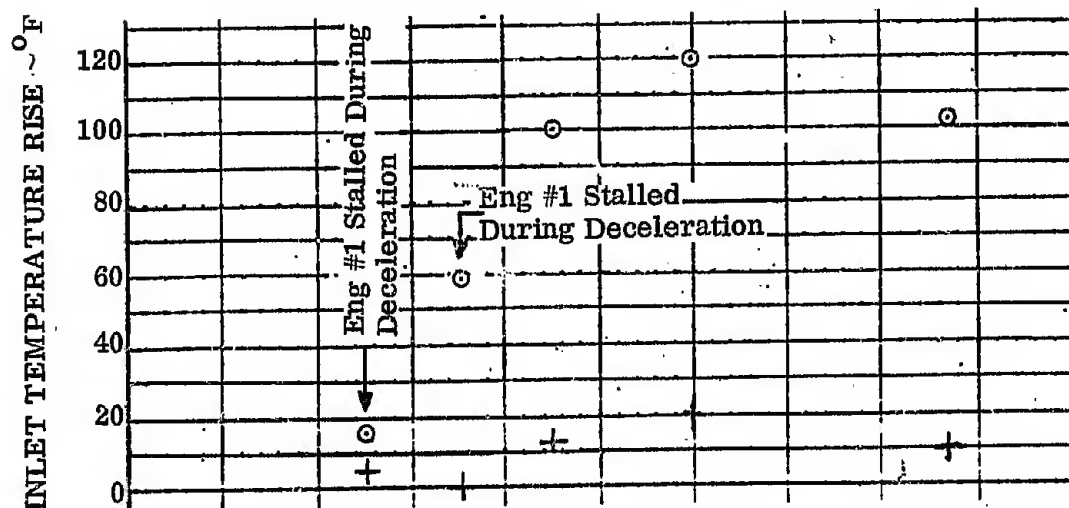
(b)

CONFIGURATION A$_3$

H/D

(c)
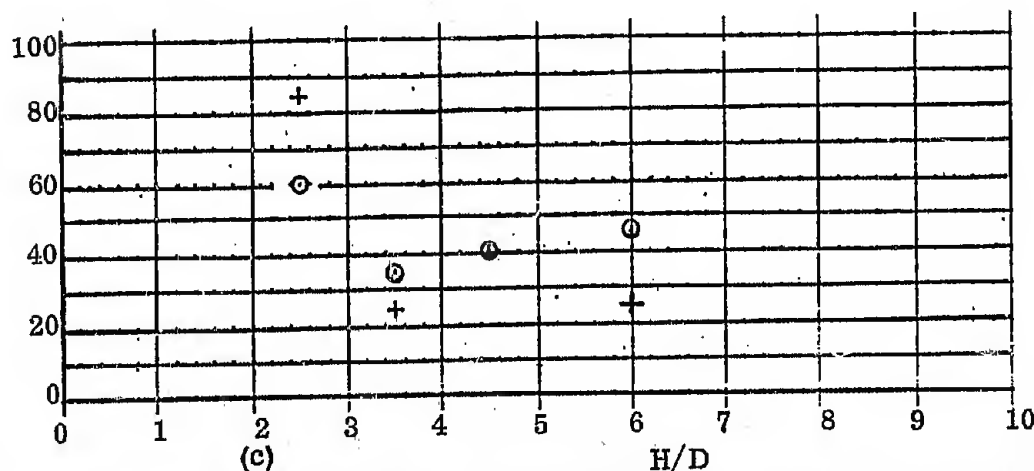
FIGURE 37 INFLUENCE OF WING SIZE AND LOCATION ON GAS INGESTION

118

FIGURE 38 (a)   ENGINE INLET TEMPERATURE TRACE

119

FIGURE 38 (b)   ENGINE INLET TEMPERATURE TRACE

120
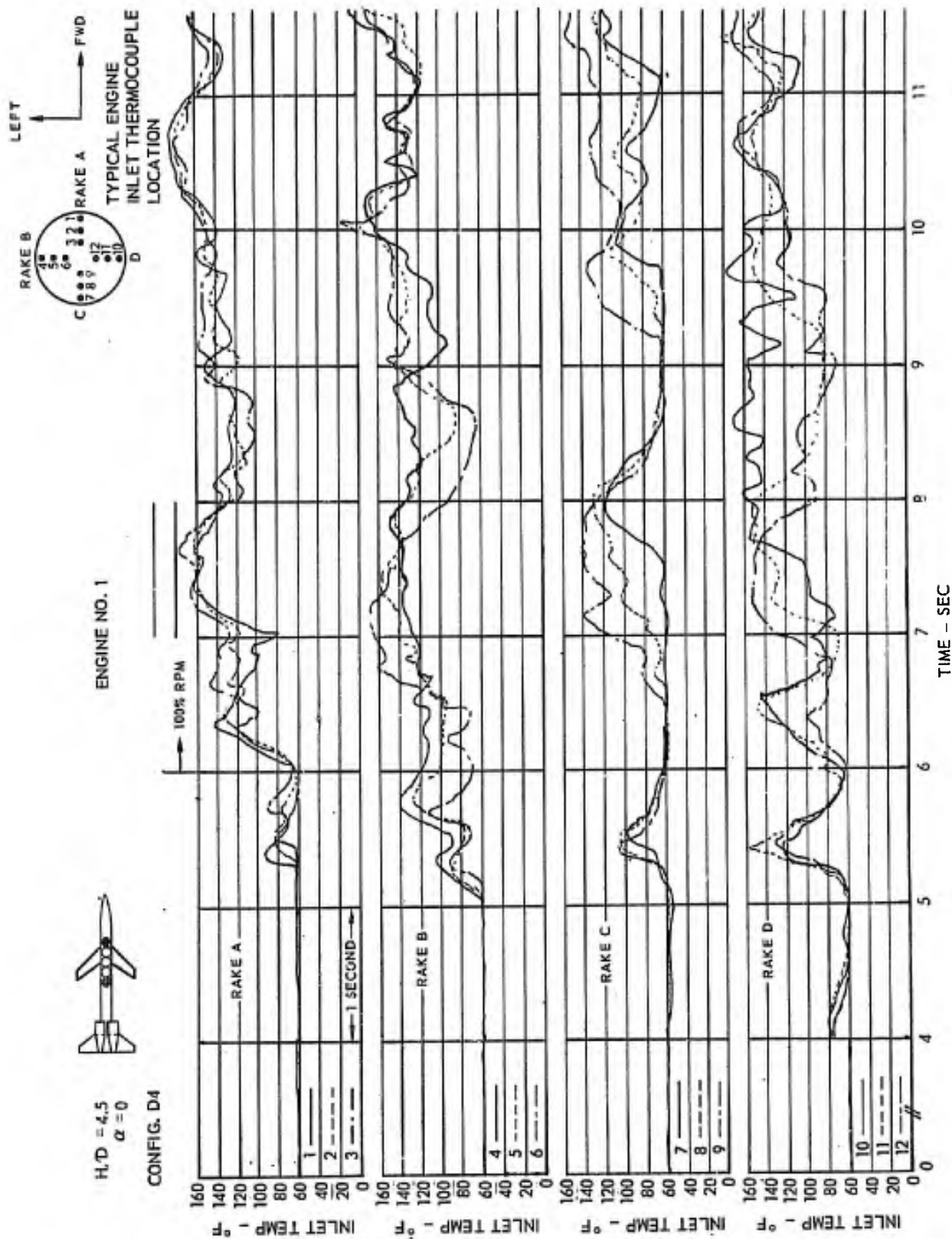
FIGURE 39 (a) ENGINE INLET TEMPERATURE TRACE

121
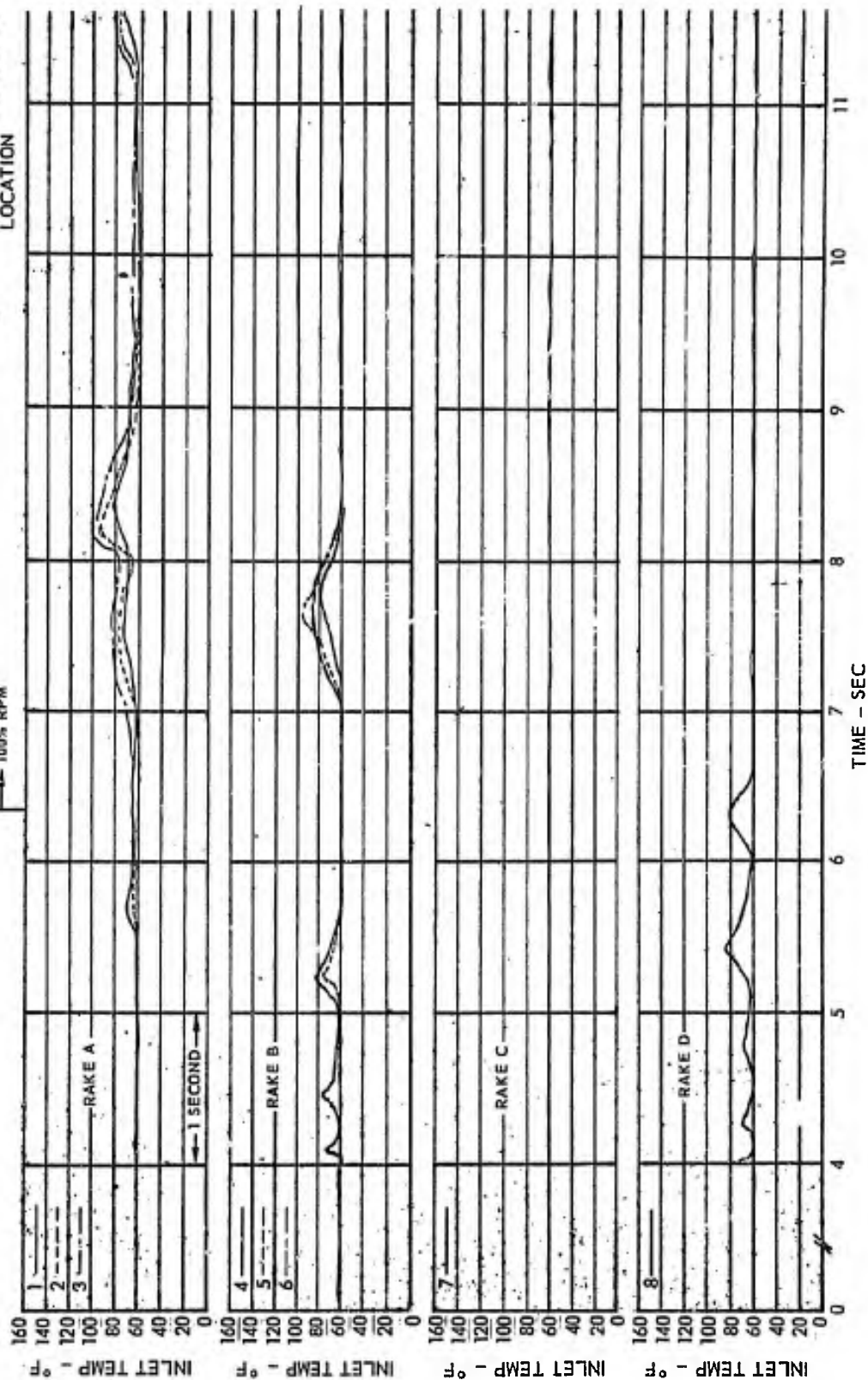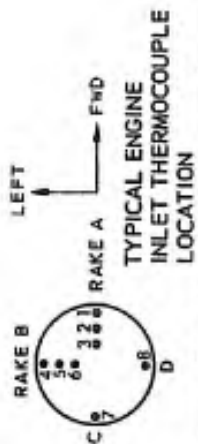
FIGURE 39 (b)   ENGINE INLET TEMPERATURE TRACE
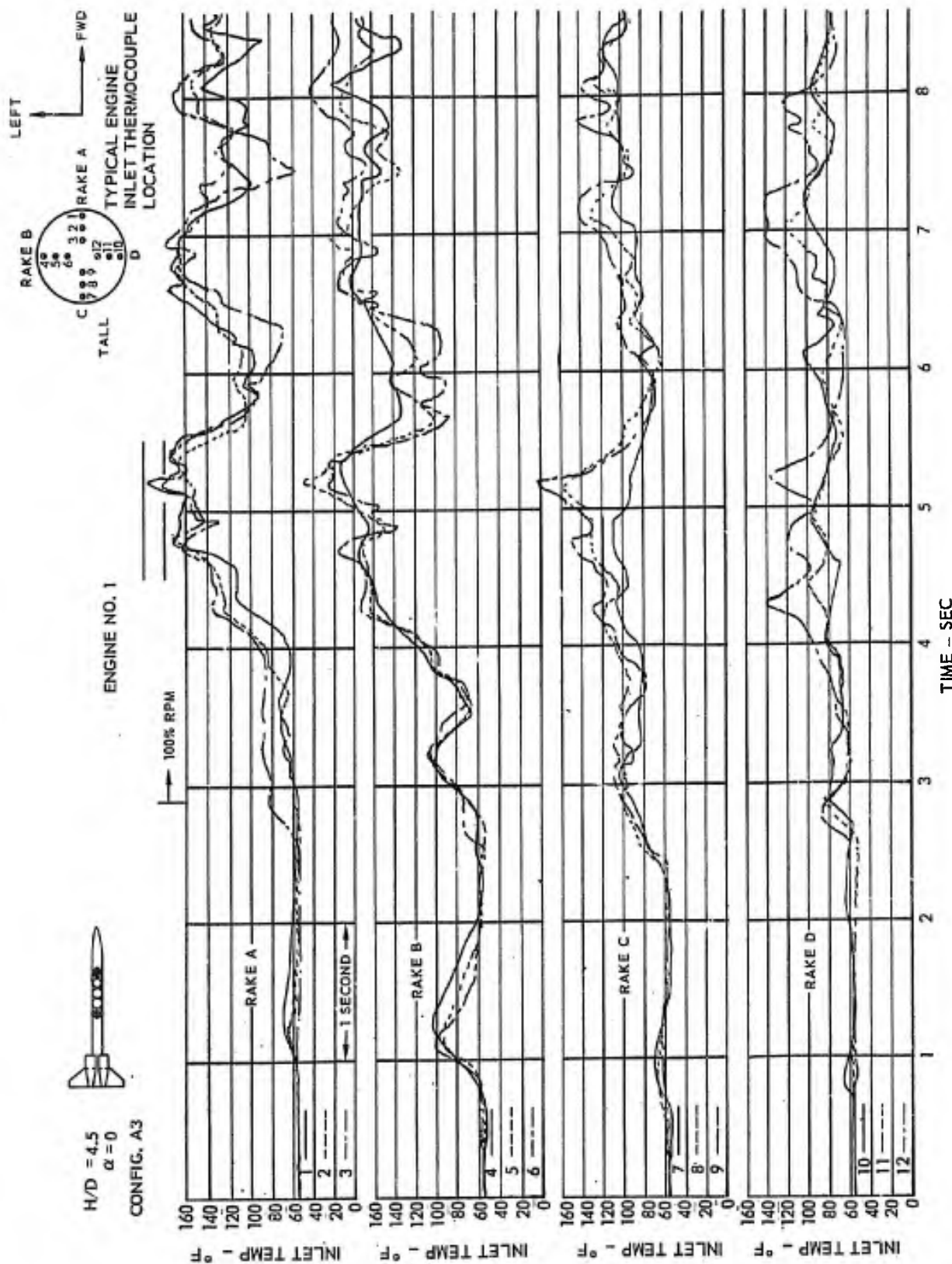
FIGURE 40 (a)   ENGINE INLET TEMPERATURE TRACE

123
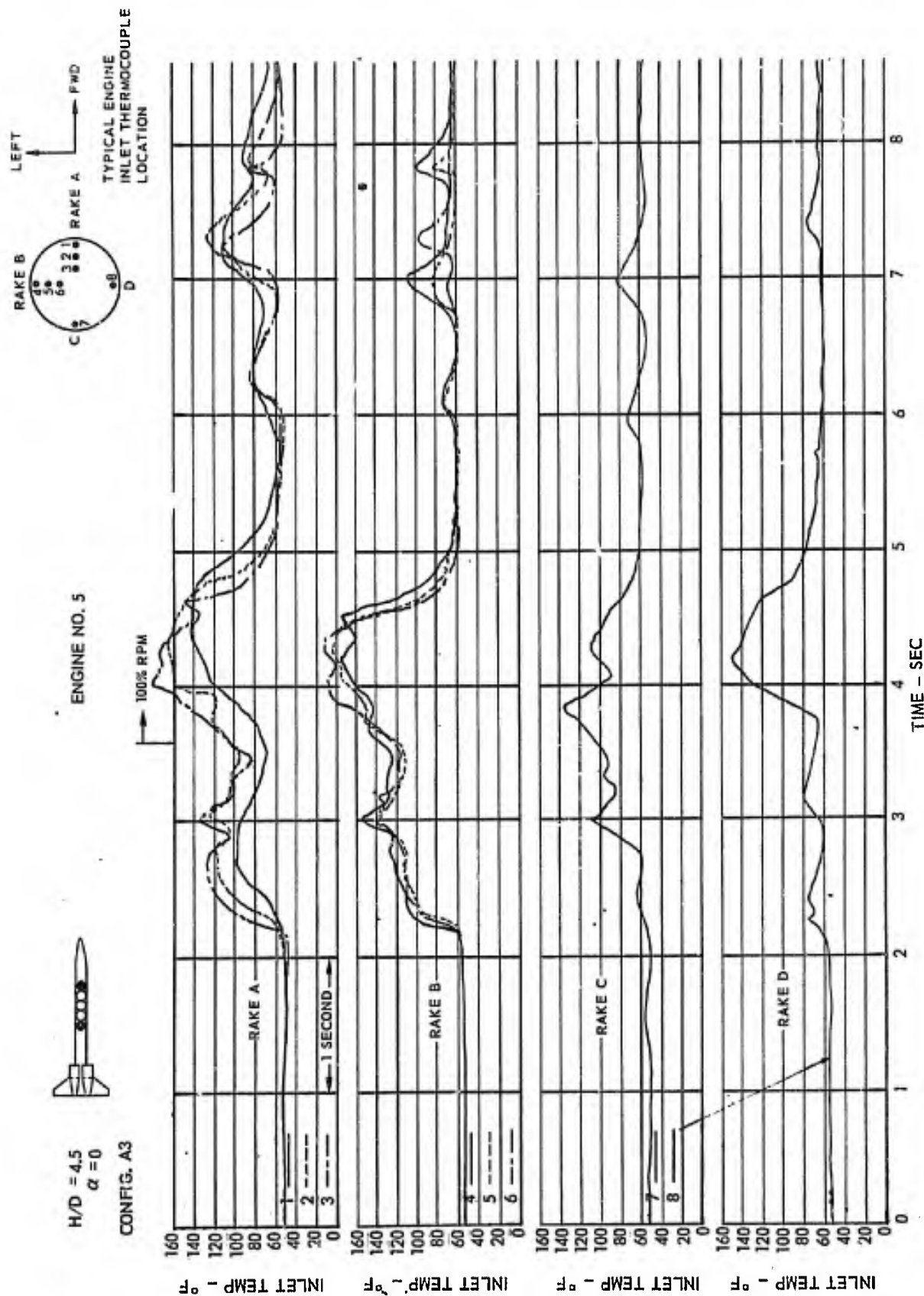
FIGURE 40 (b) ENGINE INLET TEMPERATURE TRACE

124

PITCH ATTITUDE = 0

CONFIGURATION B$_9$

MID WING
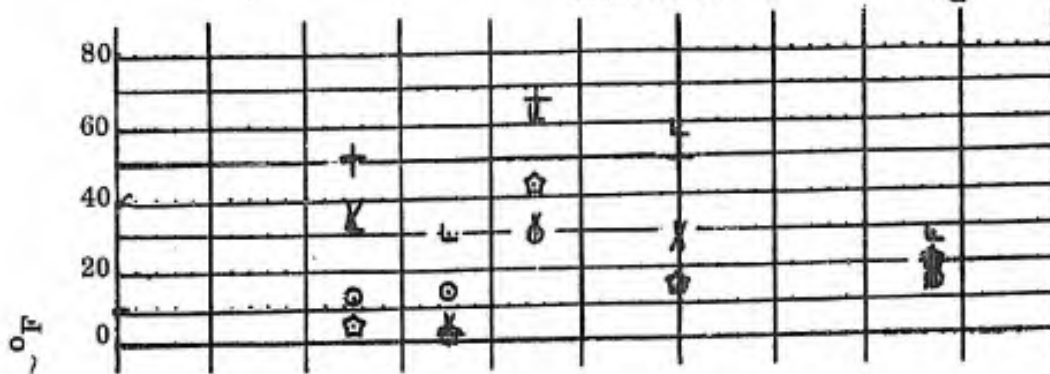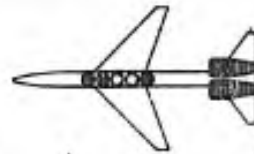
(a)

CONFIGURATION E$_2$

HIGH WING

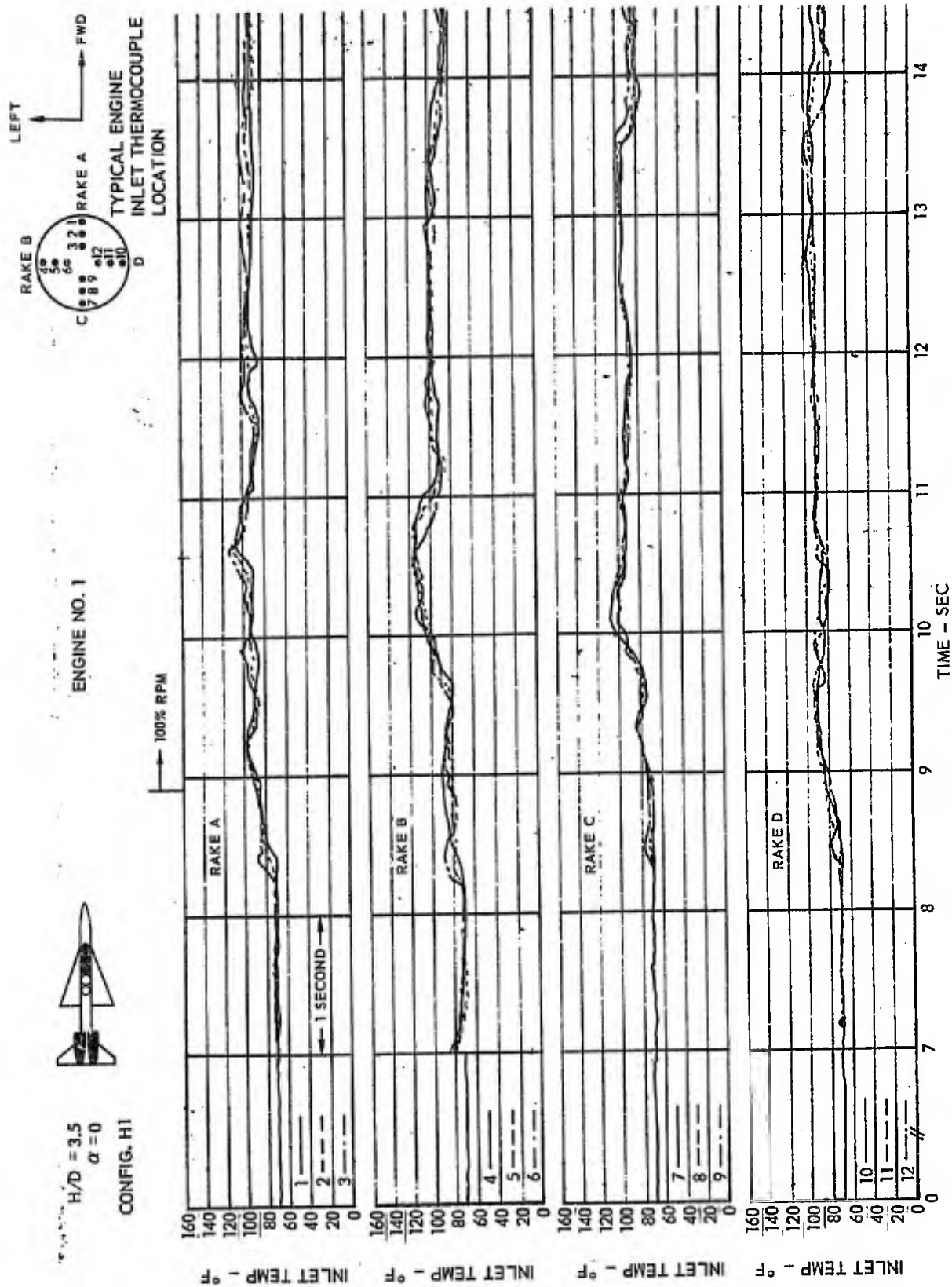INLET TEMPERATURE RISE ~ ^{o}F

Stall on Eng #5 prior to 100% RPM

Stall on Eng #5 1 1/2 Sec after 100% RPM

Stall on Engs #1 & 5 3 Sec & 3 1/2 Sec after 100% RPM

(b)   H/D

Symbol	Engine
⊙	1
X	2
⊡	3
Y	4
+	5
☆	6
Γ	7

FIGURE 41   INFLUENCE OF WING HEIGHT ON GAS INGESTION

125
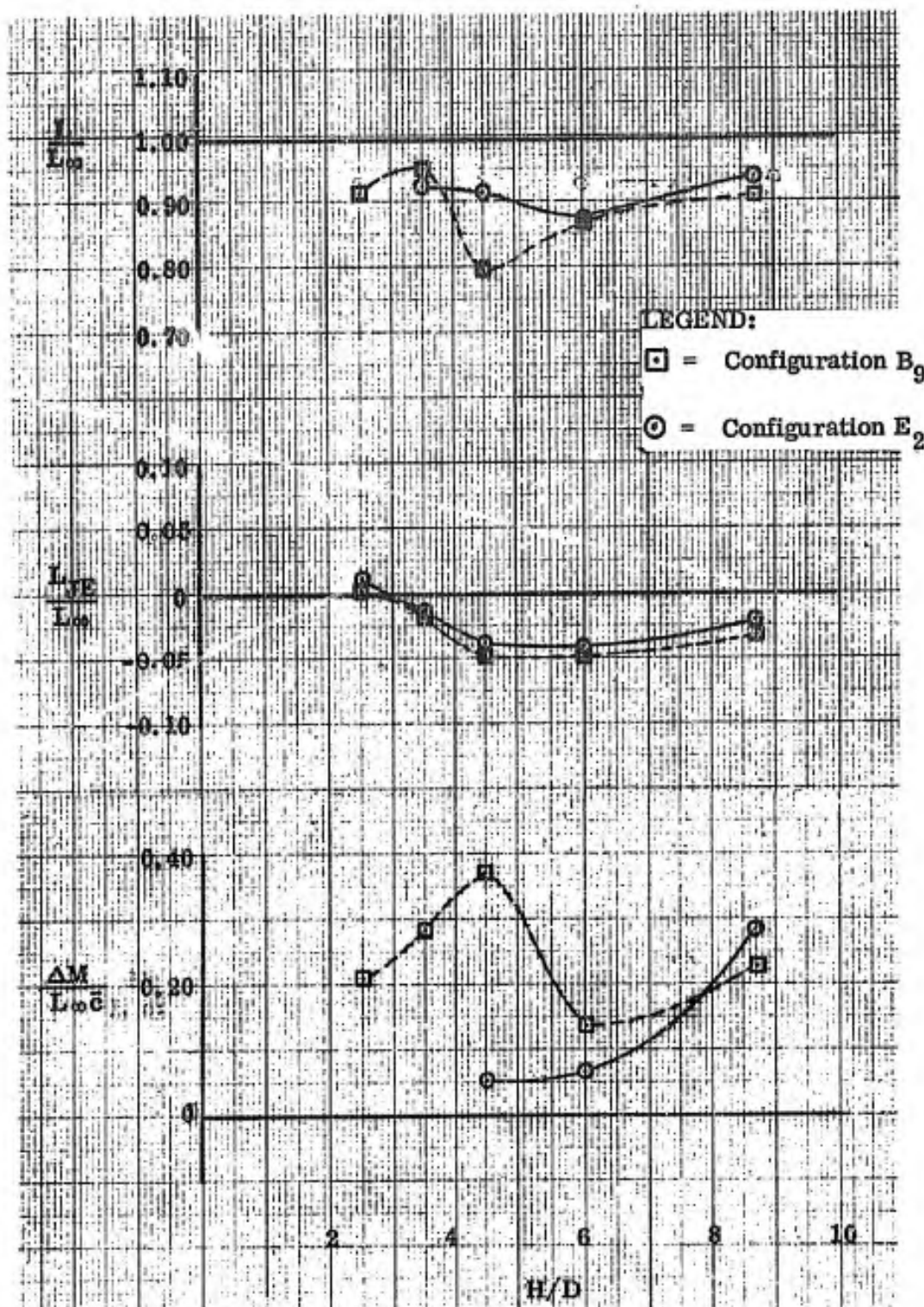
FIGURE 42   INFLUENCE OF WING HEIGHT ON JET-INDUCED FORCE & MOMENT

PITCH ATTITUDE = 0

CONFIGURATION B_{10}

MID WING

(a)
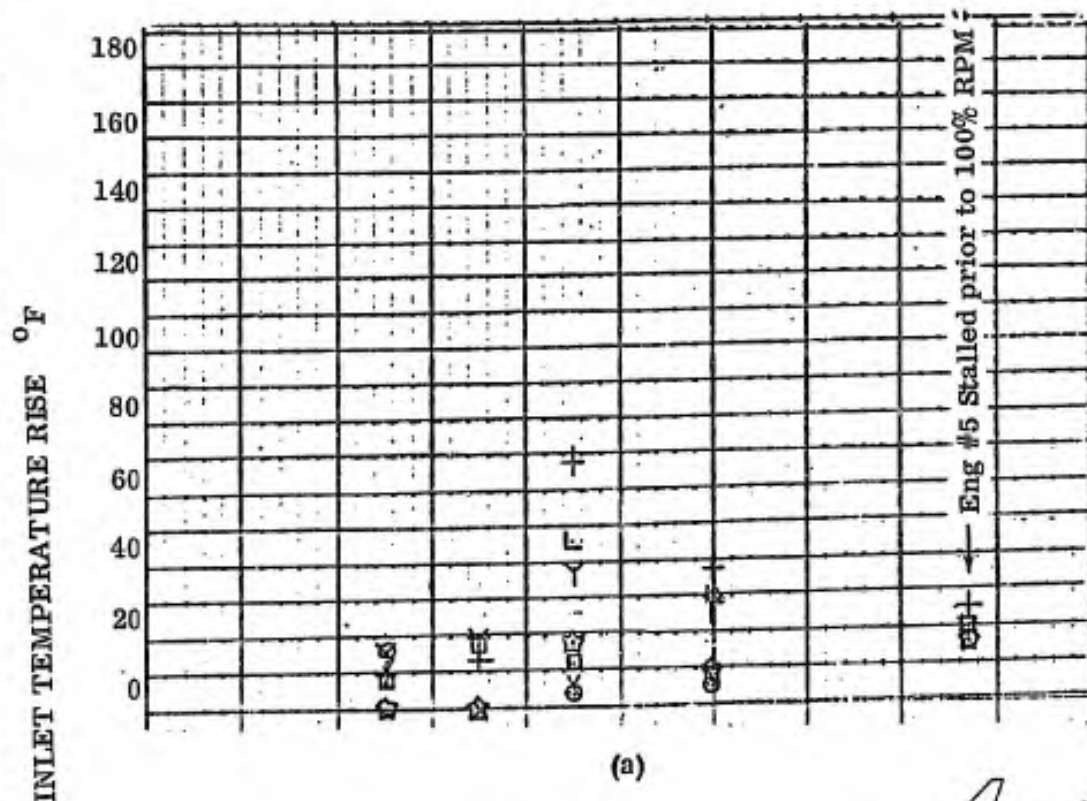
CONFIGURATION E_3

HIGH WING

(b)

H/D
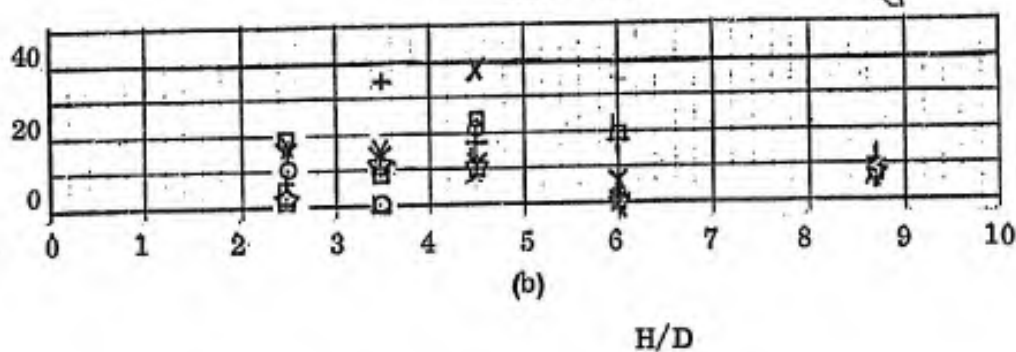
FIGURE 43 INFLUENCE OF WING HEIGHT ON GAS INGESTION

127
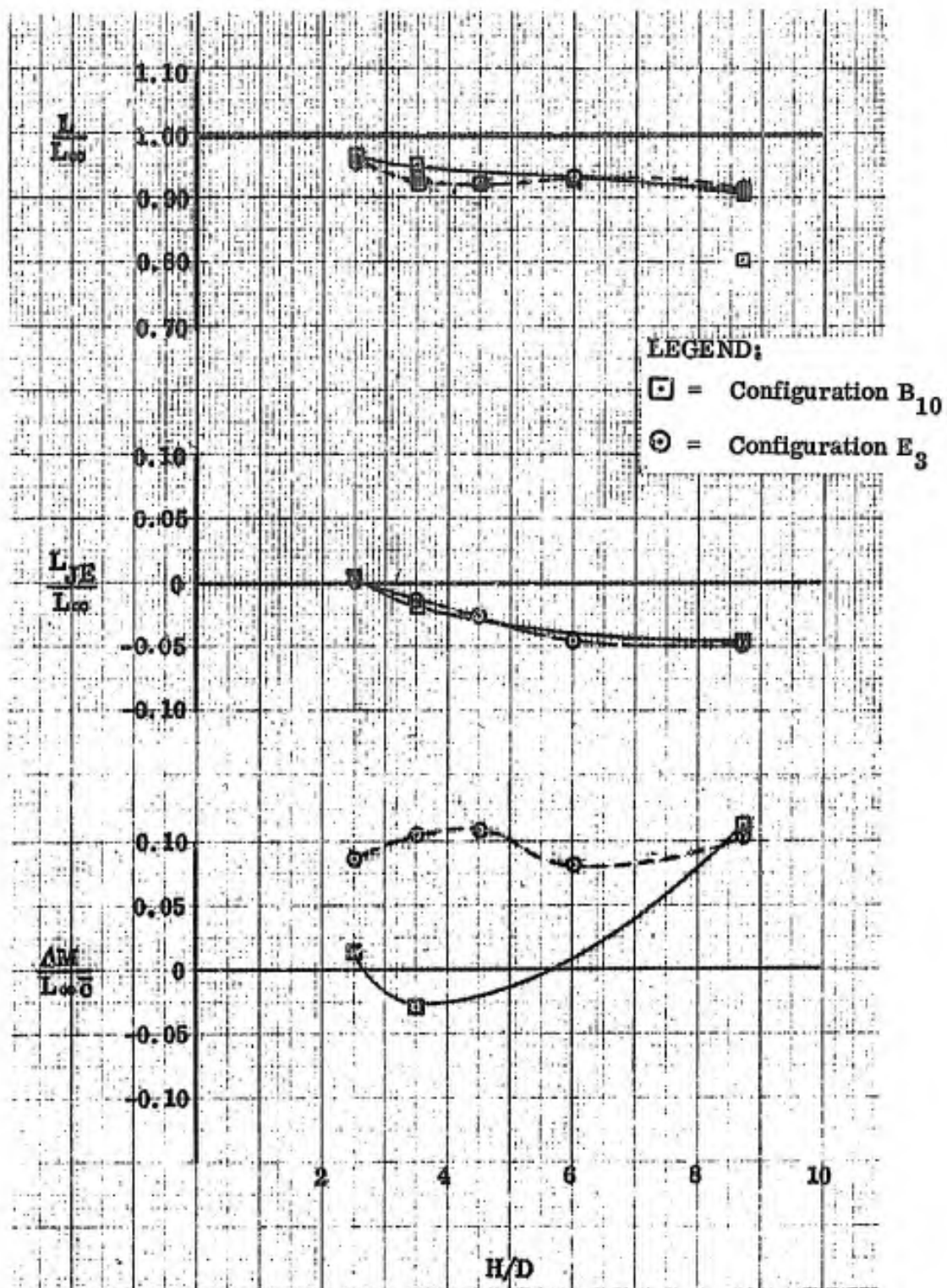
FIGURE 44   INFLUENCE OF WING HEIGHT ON JET-INDUCED FORCE & MOMENT

128

PITCH ATTITUDE = 0

CONFIGURATION H$_1$

LOW WING
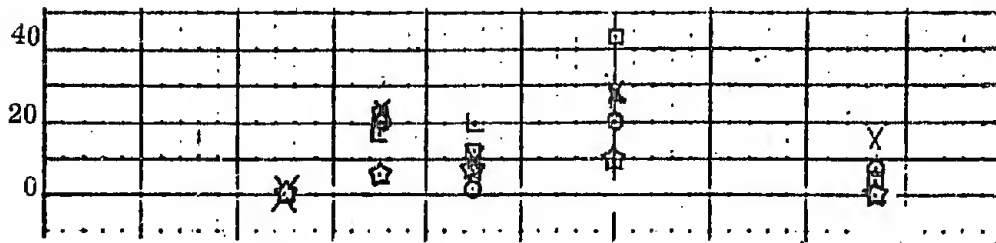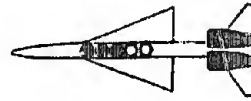
(a)

CONFIGURATION C$_3$

MID WING

(b)
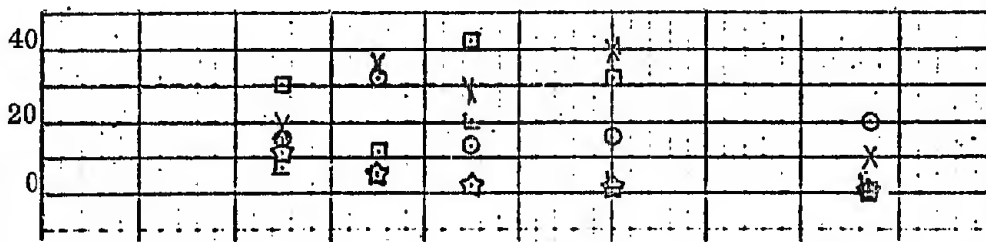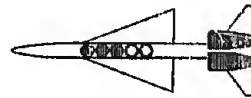
Symbol	Engine
⊙	1
Ⓧ	2
□	3
Y	4
+	5
☆	6
Ⅼ	7

CONFIGURATION G$_1$

HIGH WING

(c)

H/D

INLET TEMPERATURE RISE ~ $^\circ$F
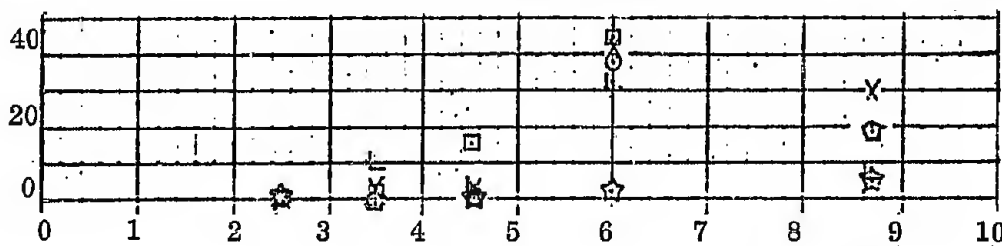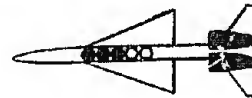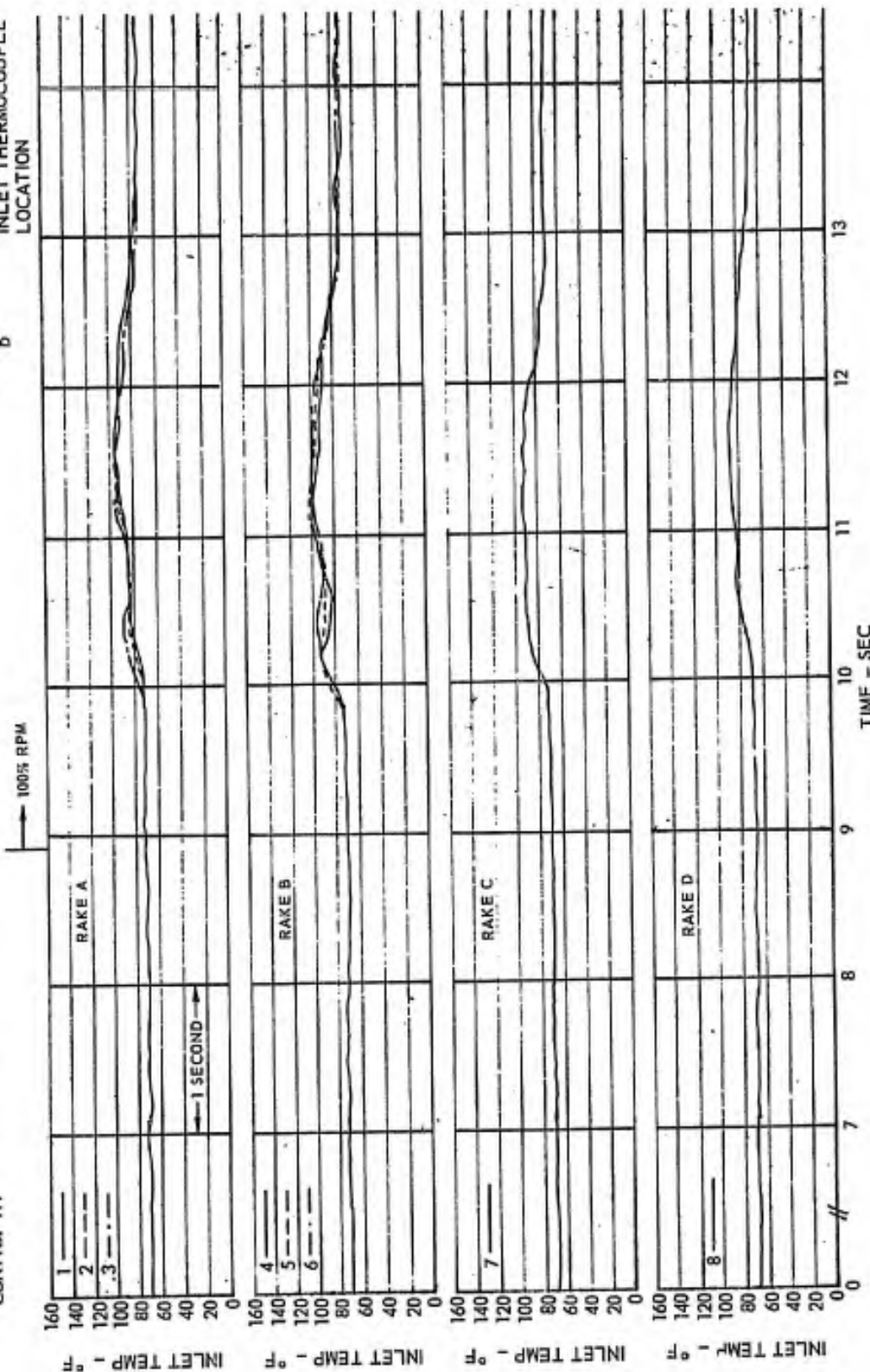
FIGURE 45   INFLUENCE OF WING HEIGHT ON GAS INGESTION

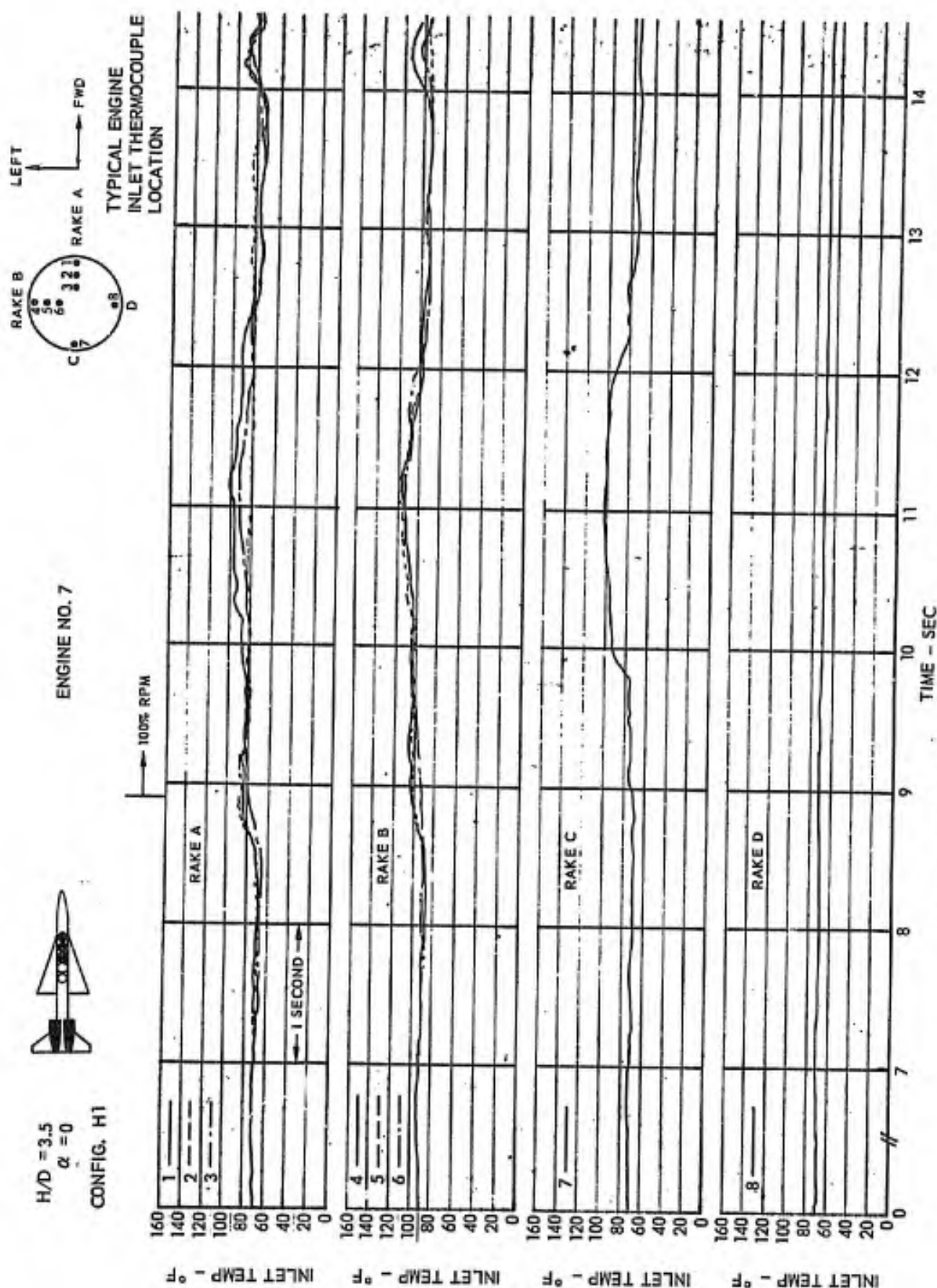FIGURE 46 (a)   ENGINE INLET TEMPERATURE TRACE
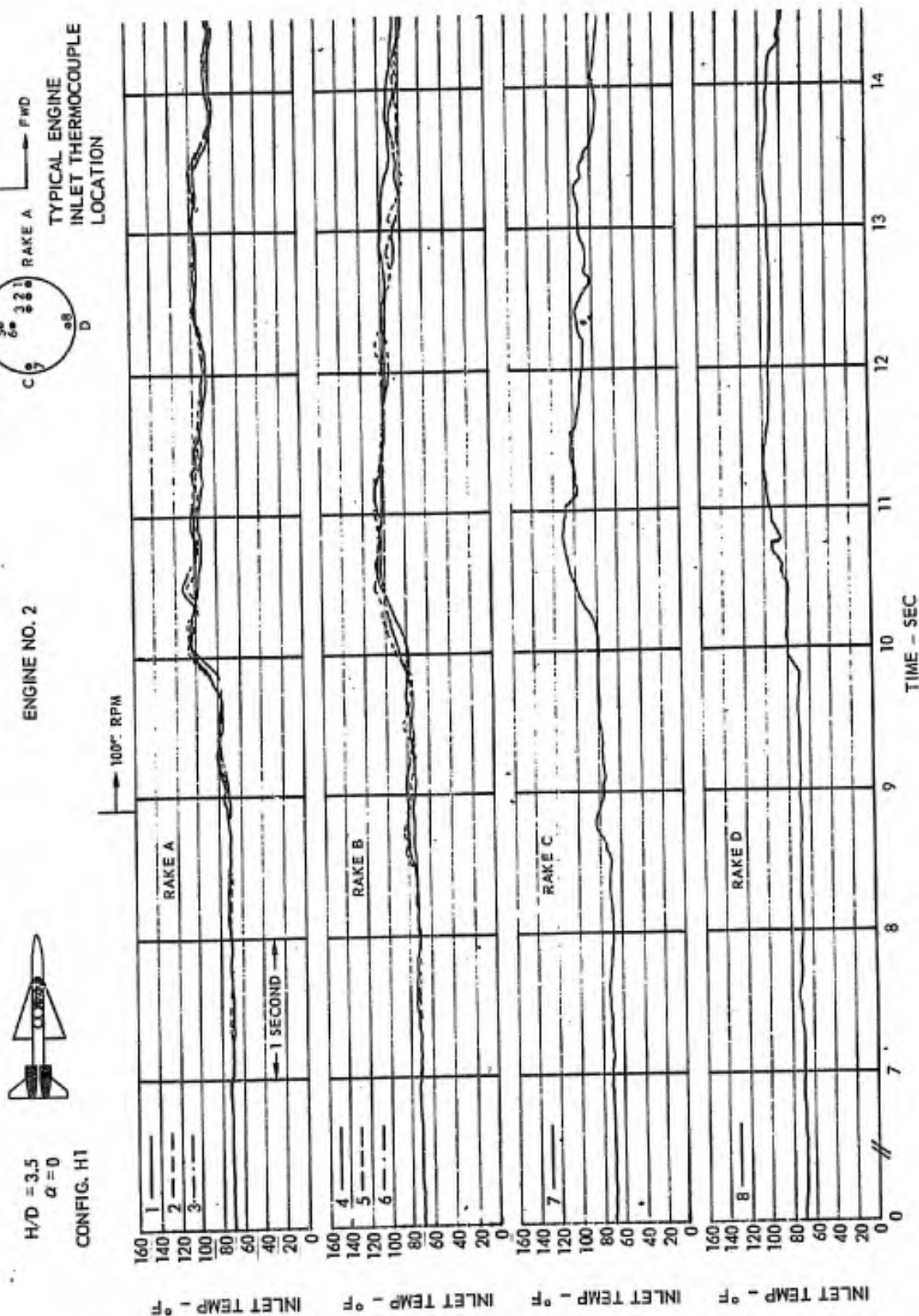
FIGURE 46 (b)   ENGINE INLET TEMPERATURE TRACE
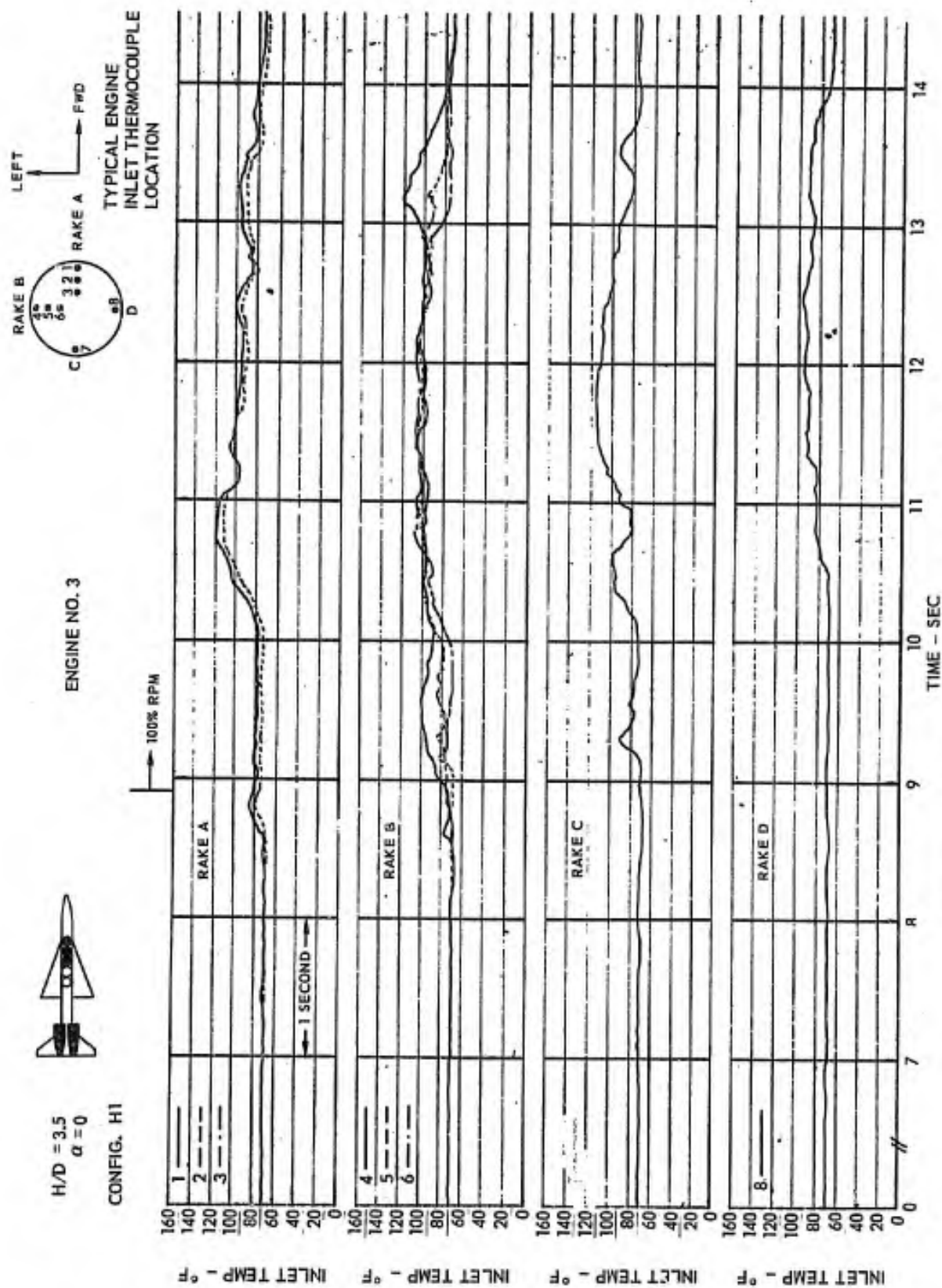
FIGURE 46 (c)   ENGINE INLET TEMPERATURE TRACE

FIGURE 46 (d)   ENGINE INLET TEMPERATURE TRACE

133

FIGURE 46 (e)   ENGINE INLET TEMPERATURE TRACE

134

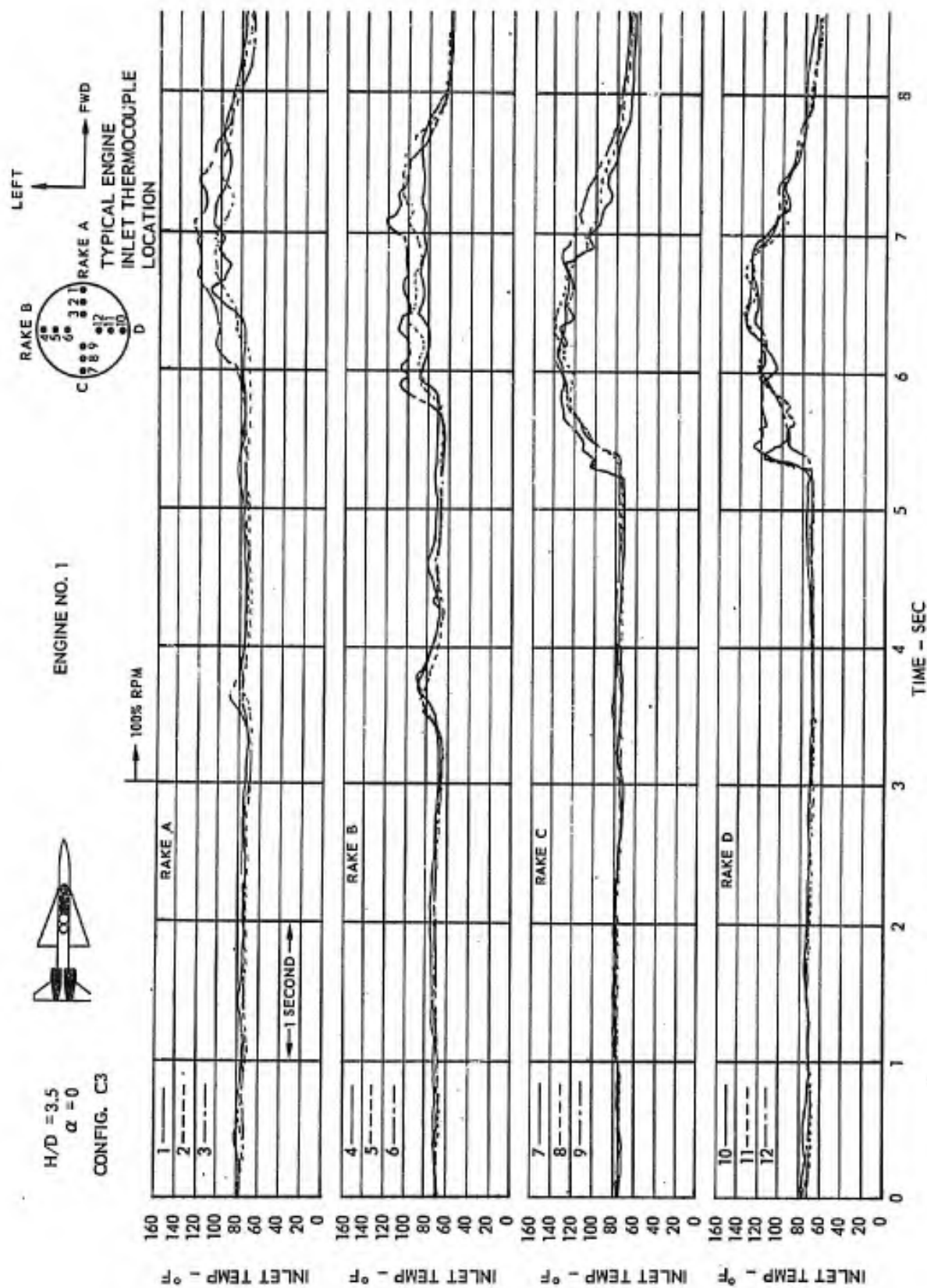FIGURE 47 (a)   ENGINE INLET TEMPERATURE TRACE

135

FIGURE 47 (b)   ENGINE INLET TEMPERATURE TRACE
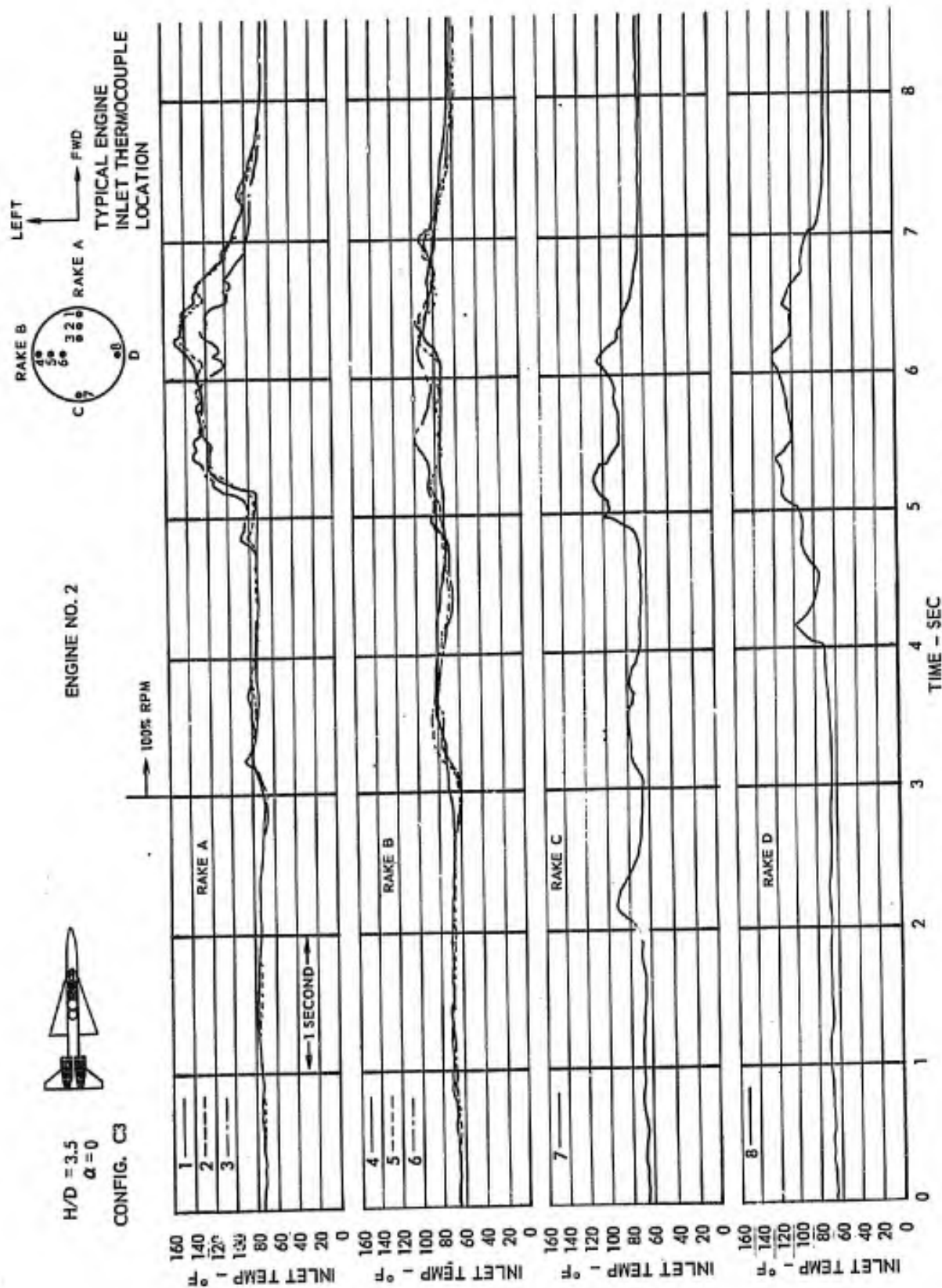
FIGURE 47 (c) ENGINE INLET TEMPERATURE TRACE
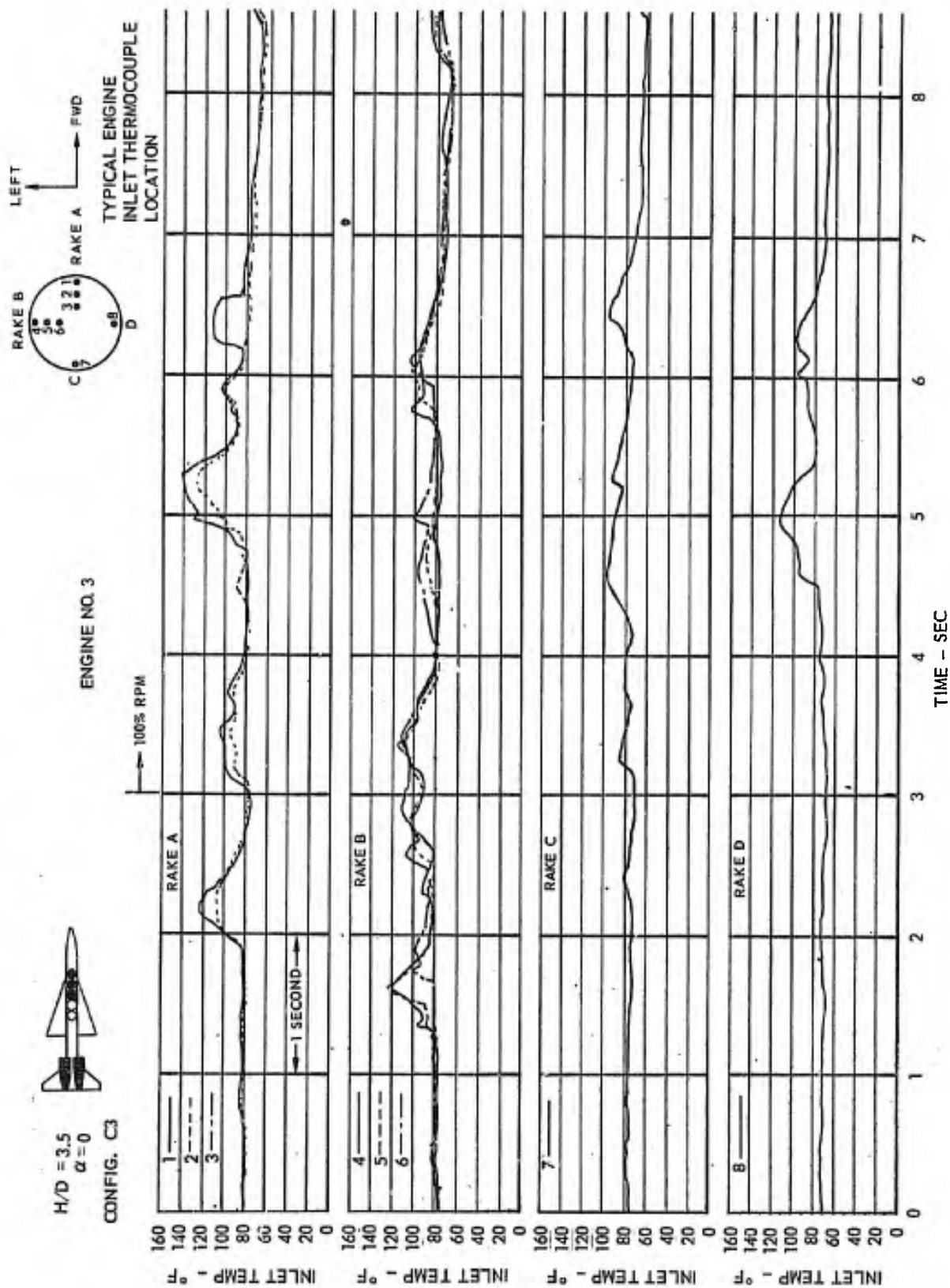
137

FIGURE 47 (d)   ENGINE INLET TEMPERATURE TRACE

PITCH ATTITUDE = 0

CONFIGURATION H$_2$

LOW WING

(a)

CONFIGURATION C$_4$

MID WING

Symbol	Engine
⊙	1
χ	2
▫	3
Y	4
+	5
☆	6
L	7

(b)

CONFIGURATION G$_2$

HIGH WING

(c)

H/D
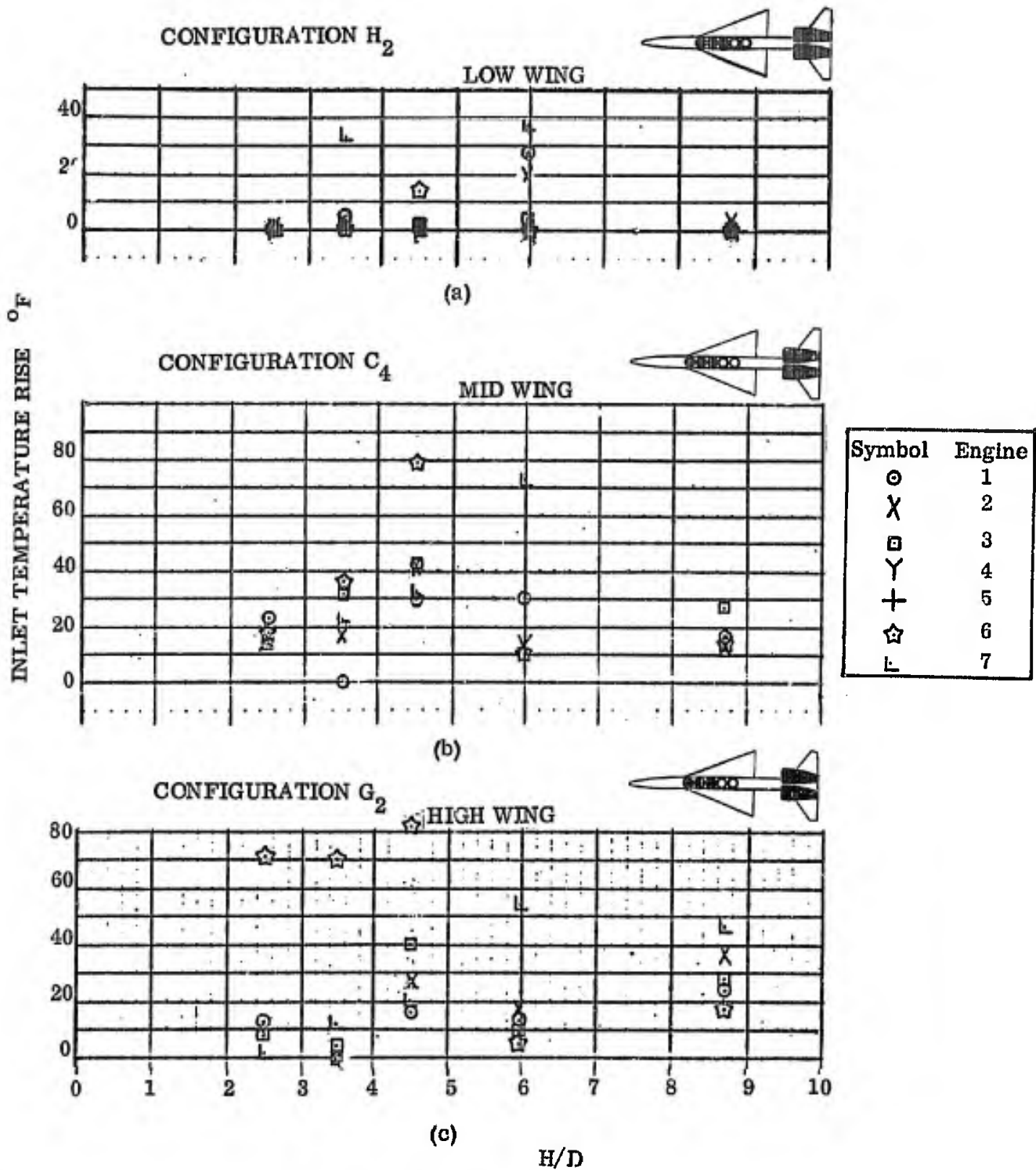
INLET TEMPERATURE RISE °F

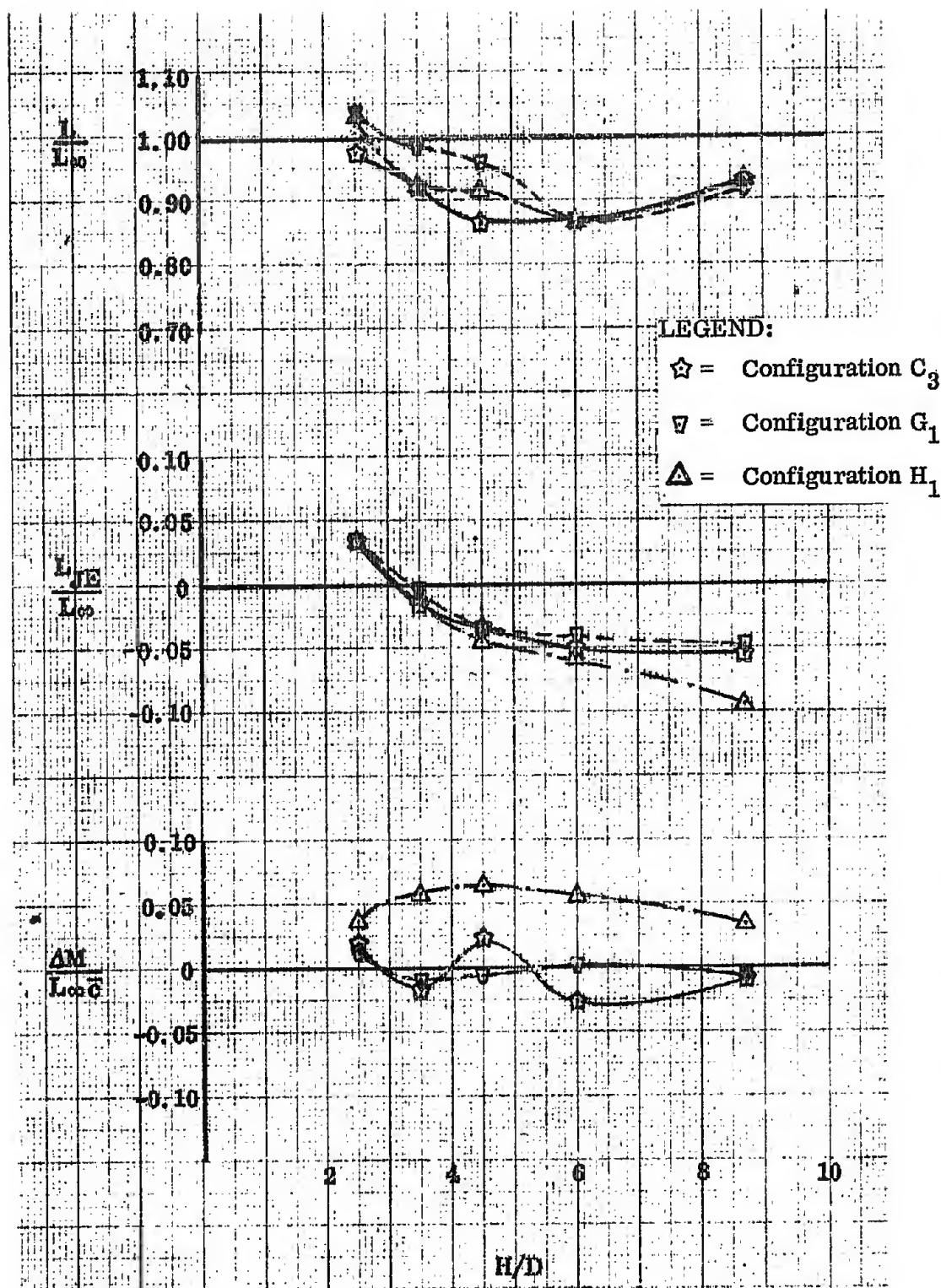FIGURE 48 INFLUENCE OF WING HEIGHT ON GAS INGESTION

139

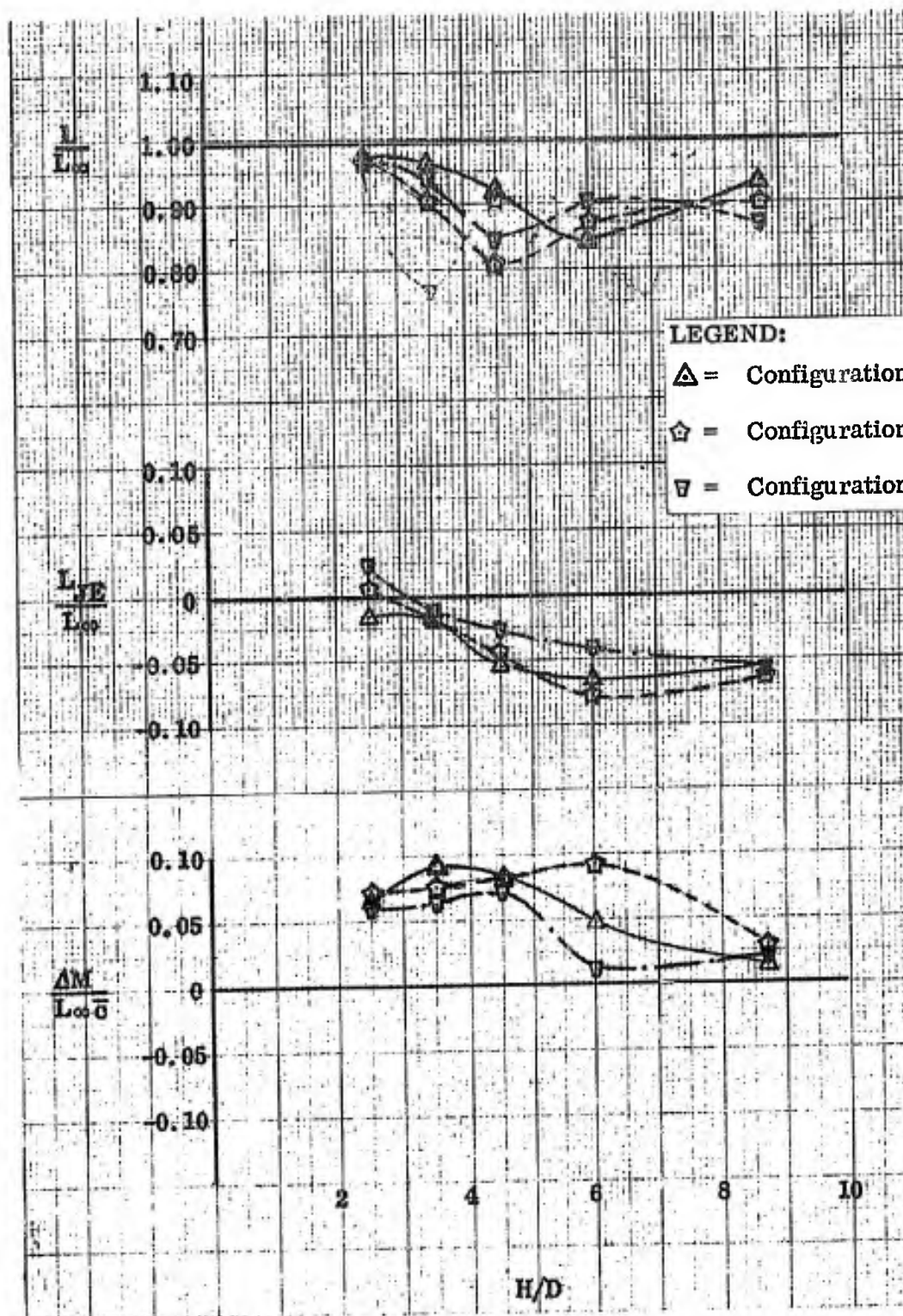FIGURE 49   INFLUENCE OF WING HEIGHT ON JET-INDUCED FORCE & MOMENT

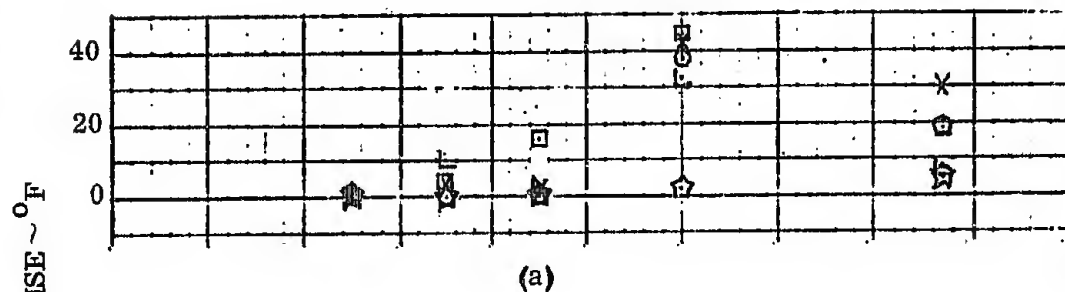FIGURE 50   INFLUENCE OF WING HEIGHT ON JET-INDUCED FORCE & MOMENT
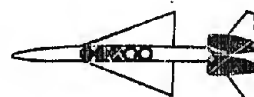
PITCH ATTITUDE = 0

CONFIGURATION G_1

TOP INLET

(a)

Symbol	Engine
⊙	1
X	2
▣	3
Y	4
+	5
☆	6
Ⅼ	7

CONFIGURATION G_2

FORWARD INLET

(b)

INLET TEMPERATURE RISE ~ ^oF
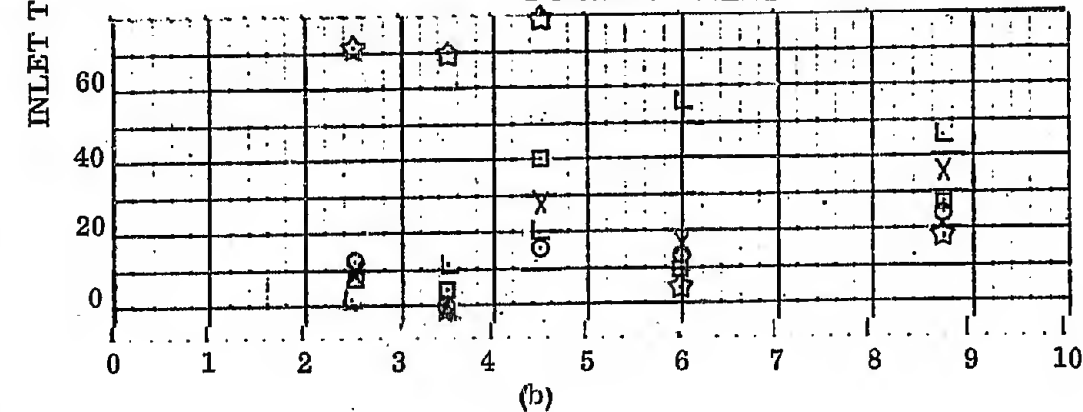
H/D

FIGURE 51 INFLUENCE OF LIFT/CRUISE ENGINE INLET LOCATION ON INGESTION

PITCH ATTITUDE = 0

CONFIGURATION E_3

TOP INLET

(a)

CONFIGURATION E_5

FORWARD INLET

INLET TEMPERATURE RISE $^\circ F$

H/D

(b)
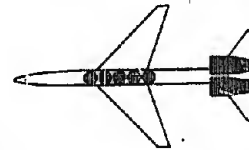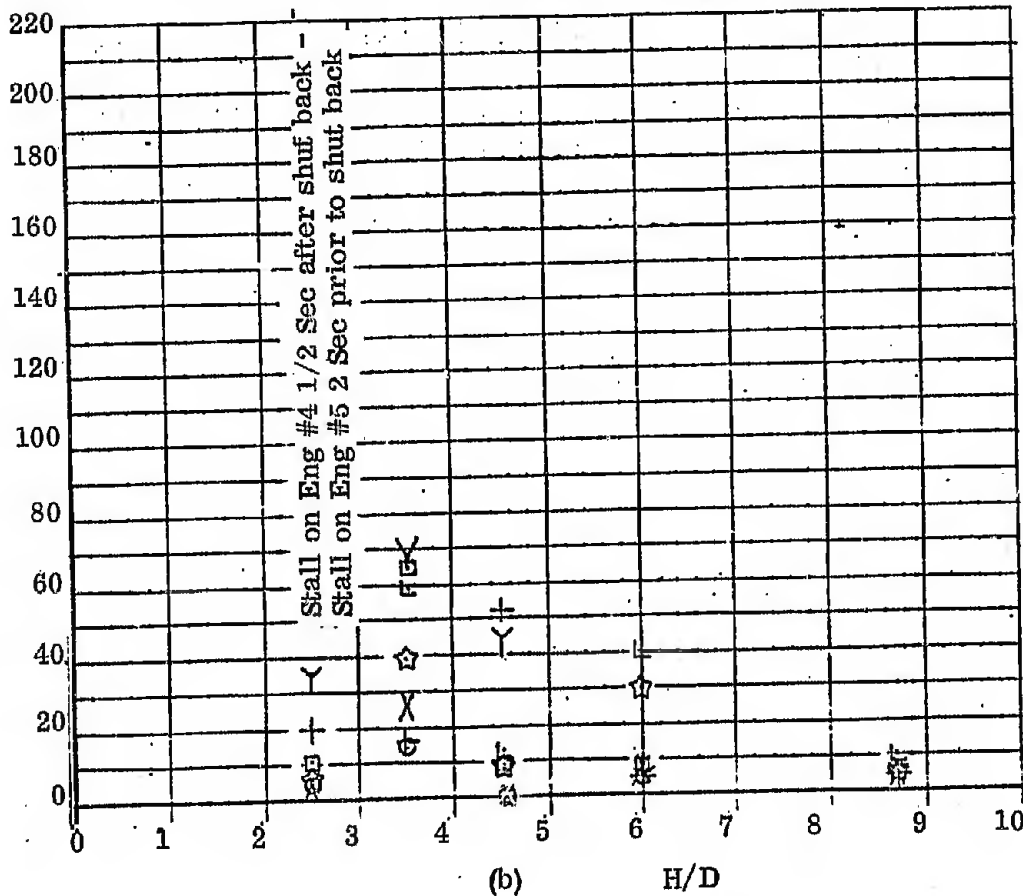
Symbol	Engine
⊙	1
X	2
⊡	3
Y	4
+	5
☆	6
L	7

FIGURE 52   INFLUENCE OF LIFT/CRUISE ENGINE-INLET LOCATION ON INGESTION
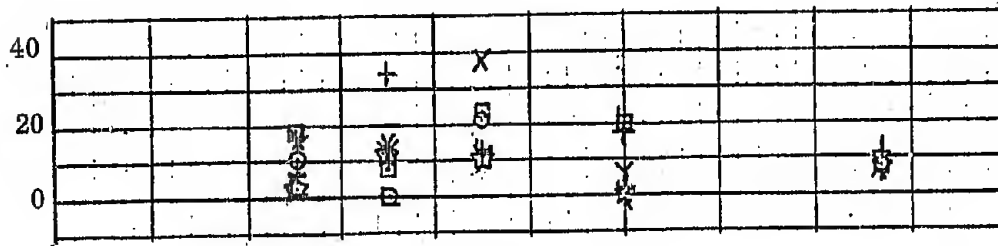
143
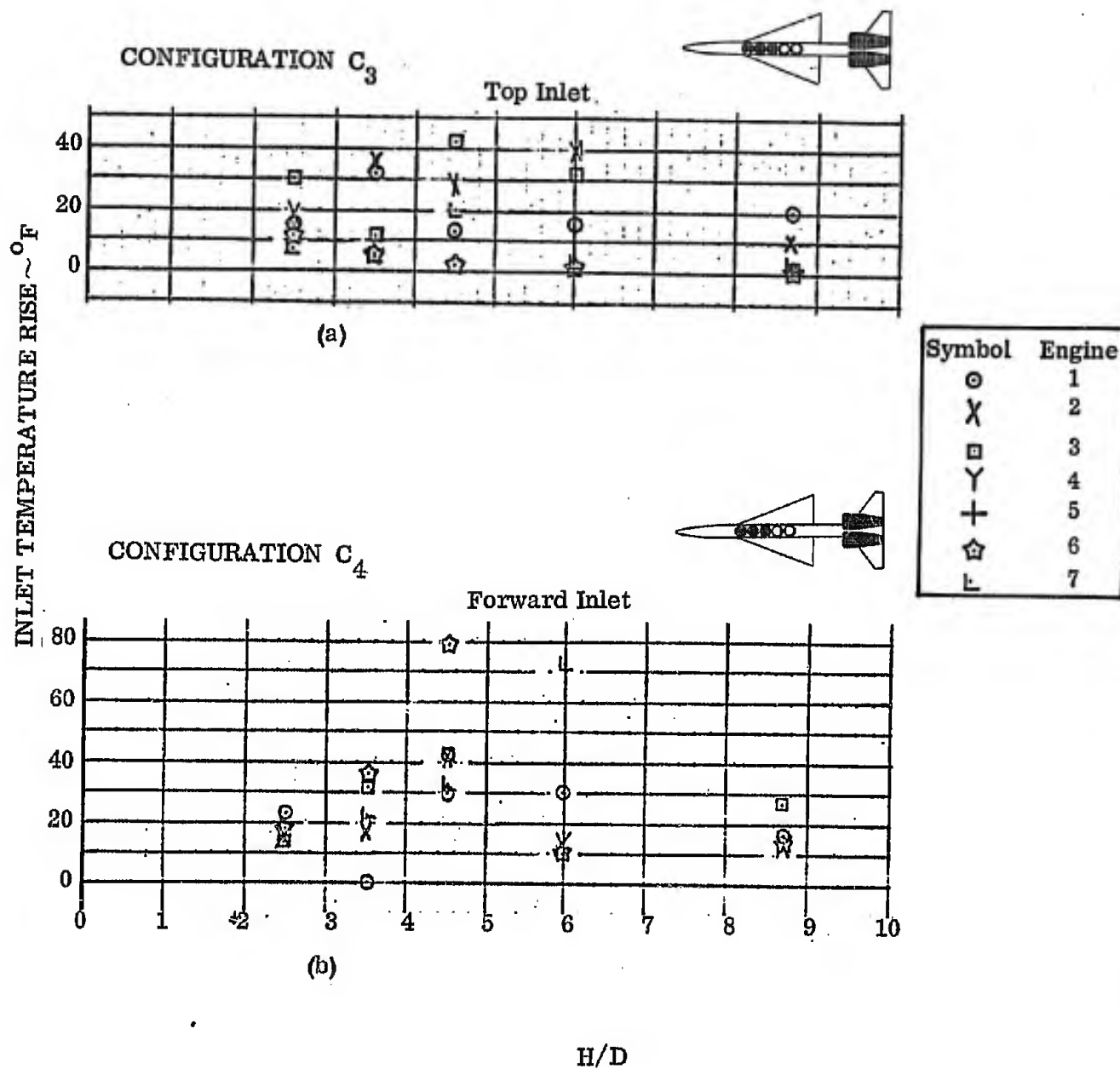
FIGURE 53 INFLUENCE OF LIFT/CRUISE ENGINE-INLET LOCATION ON INGESTION

PITCH ATTITUDE = 0

CONFIGURATION E$_1$

TOP INLET

(a)

CONFIGURATION E$_4$

FORWARD INLET

(b)

Symbol	Engine
⊙	1
X	2
▫	3
Y	4
+	5
☆	6
L	7

H/D

FIGURE 54 INFLUENCE OF LIFT/CRUISE ENGINE-INLET LOCATION ON INGESTION

PITCH ATTITUDE = 0

CONFIGURATION H₁   TOP INLET

(a)

CONFIGURATION H₂   FORWARD INLET

(b)

H/D

Symbol	Engine
⊙	1
Χ	2
□	3
Y	4
+	5
☆	6
L	7

INLET TEMPERATURE RISE ~ °F
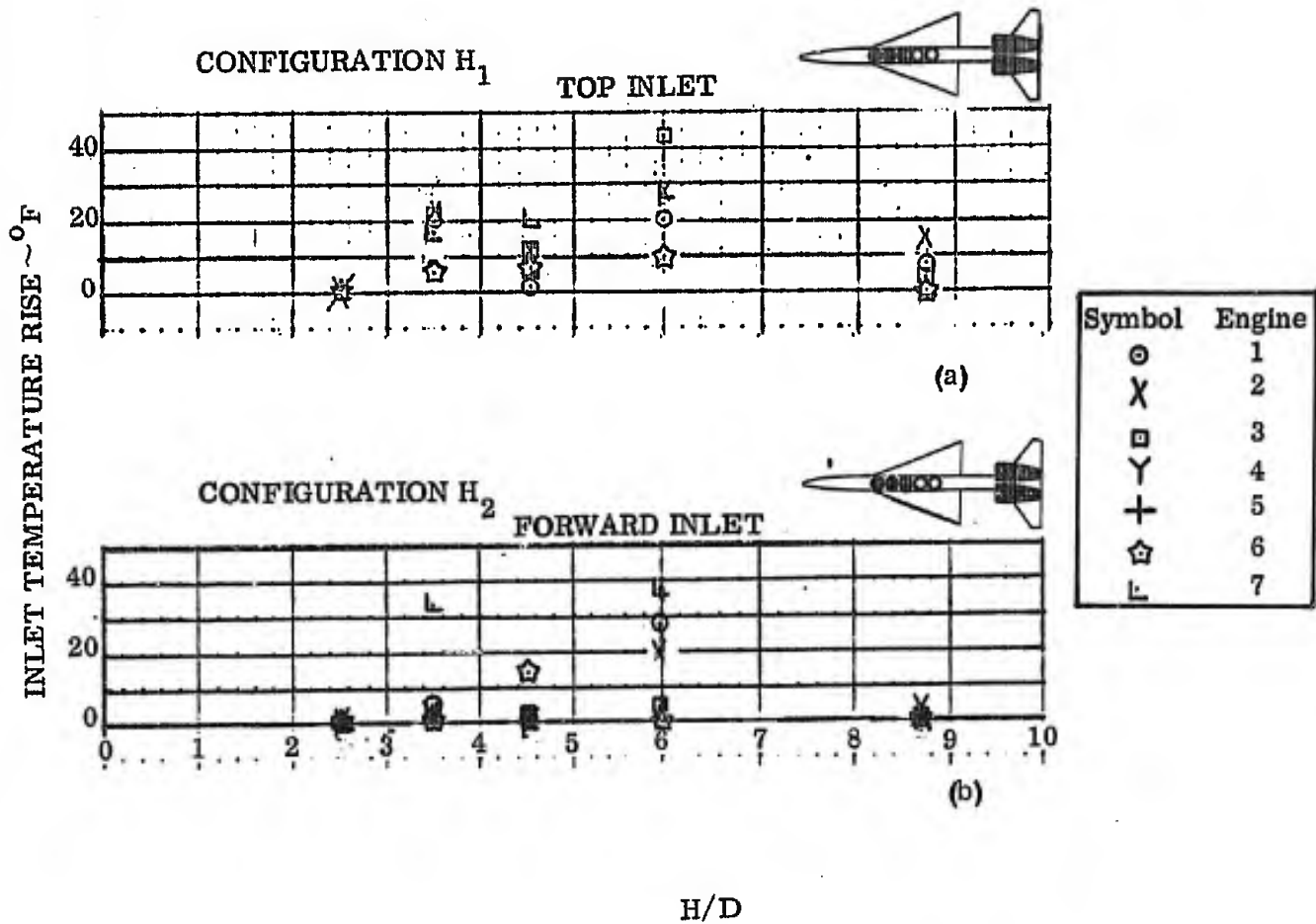
FIGURE 55 INFLUENCE OF LIFT/CRUISE ENGINE INLET LOCATION ON INGESTION

146
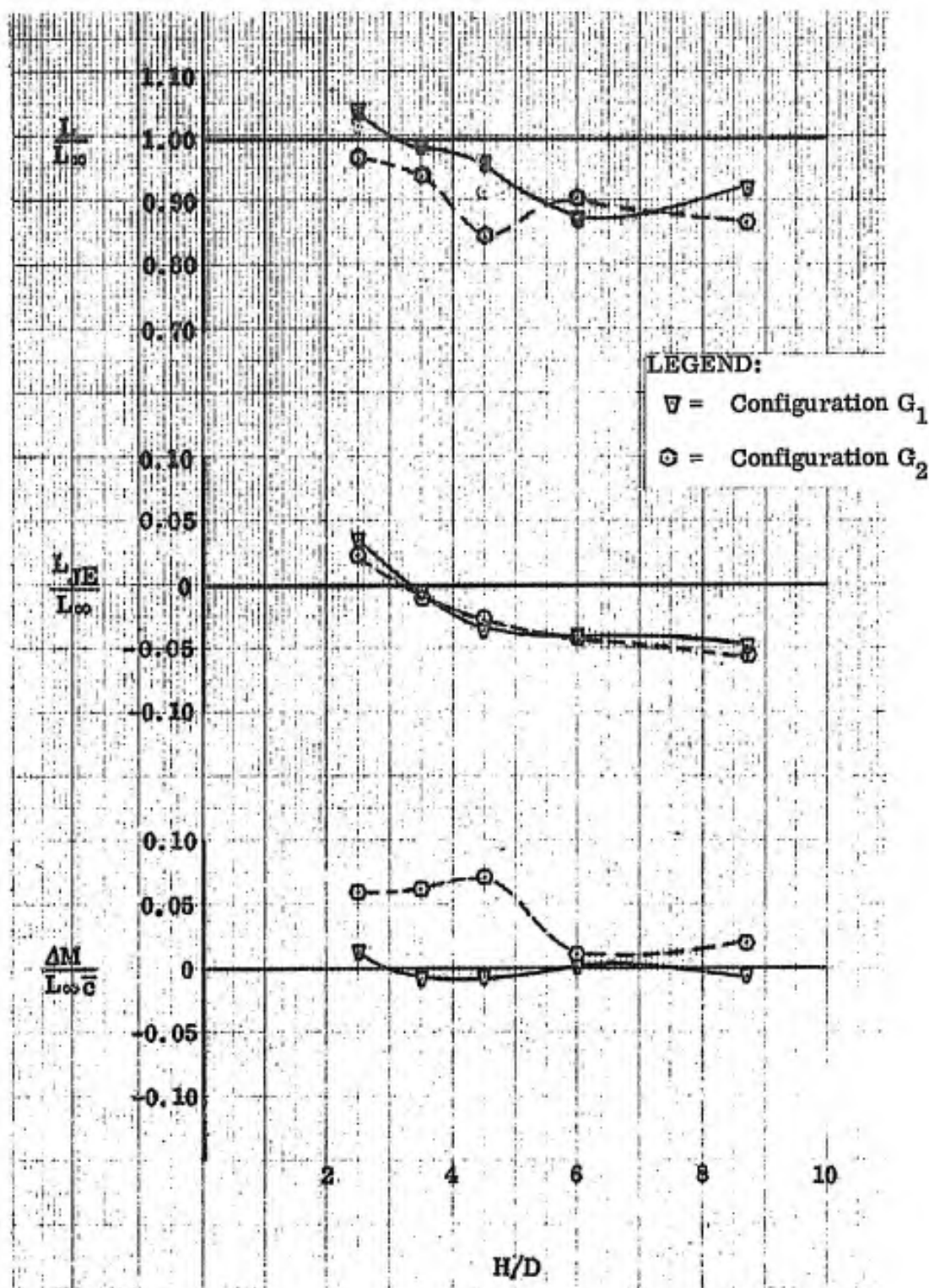
FIGURE 56 INFLUENCE OF LIFT/CRUISE ENGINE INLET LOCATION
ON JET-INDUCED FORCE & MOMENT

PITCH ATTITUDE = 0

CONFIGURATION C_1

(a)

CONFIGURATION C_2

INLET TEMPERATURE ~ $^\circ$F

Engine #1 Stalled At Max.

(b)

Symbol	Engine
⊙	1
X	2
▣	3
Y	4
+	5
☆	6
L	7

CONFIGURATION C_3

(c)

H/D
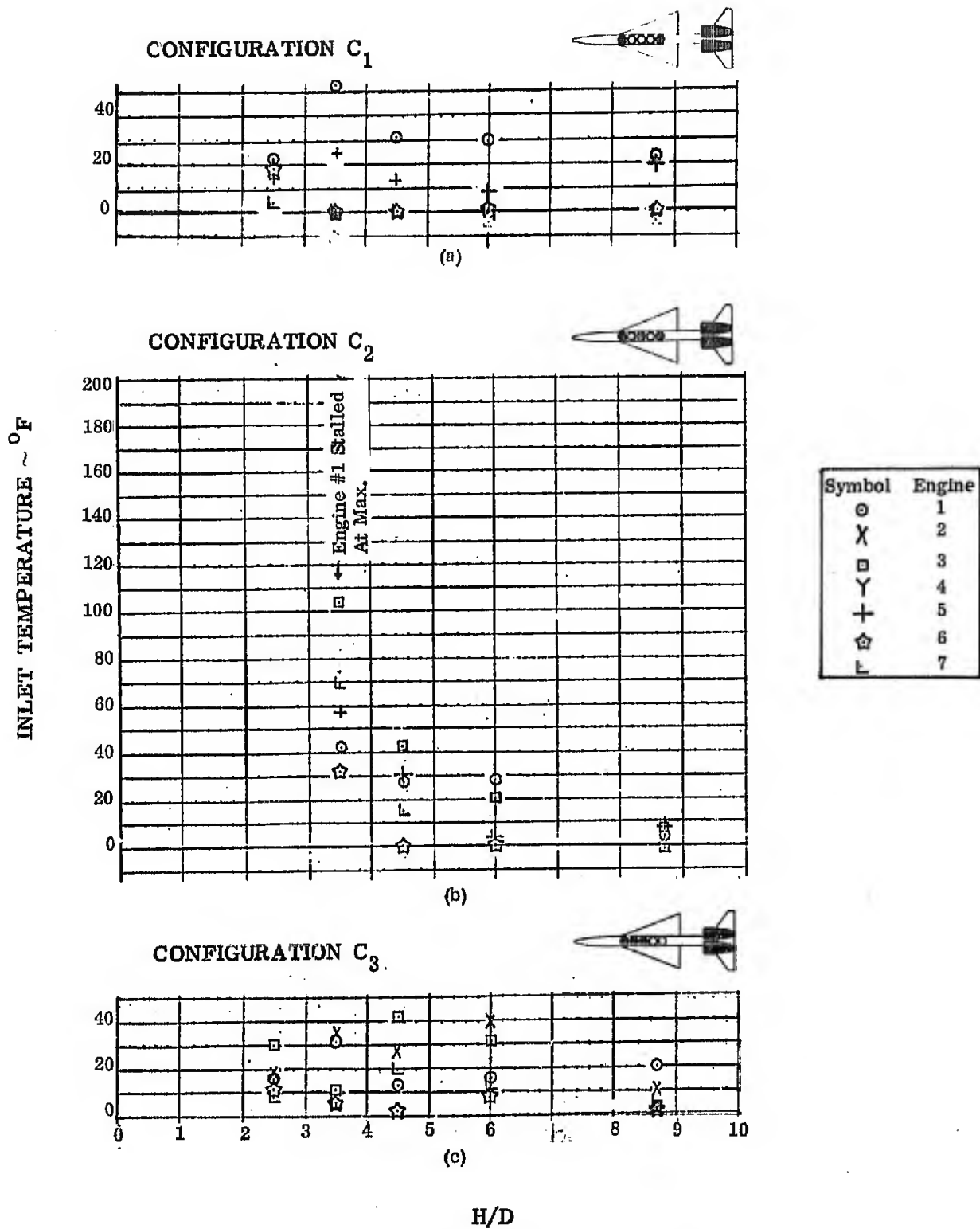
FIGURE 57   EFFECT OF ENGINE ARRANGEMENT ON GAS INGESTION

FIGURE 58   EFFECT OF ENGINE ARRANGEMENT ON INGESTION

PITCH ATTITUDE = 0

CONFIGURATION F_1

(a)

Symbol	Engine
⊙	1
✕	2
▣	3
Y	4
+	5
☆	6
L	7

INLET TEMPERATURE RISE ~ °F
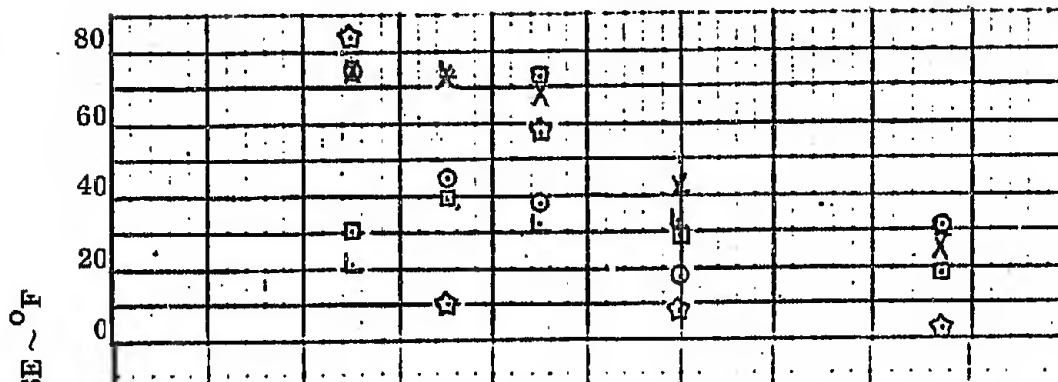
CONFIGURATION F_2

(b)

H/D

FIGURE 59   EFFECT OF ENGINE ARRANGEMENT ON INGESTION

150
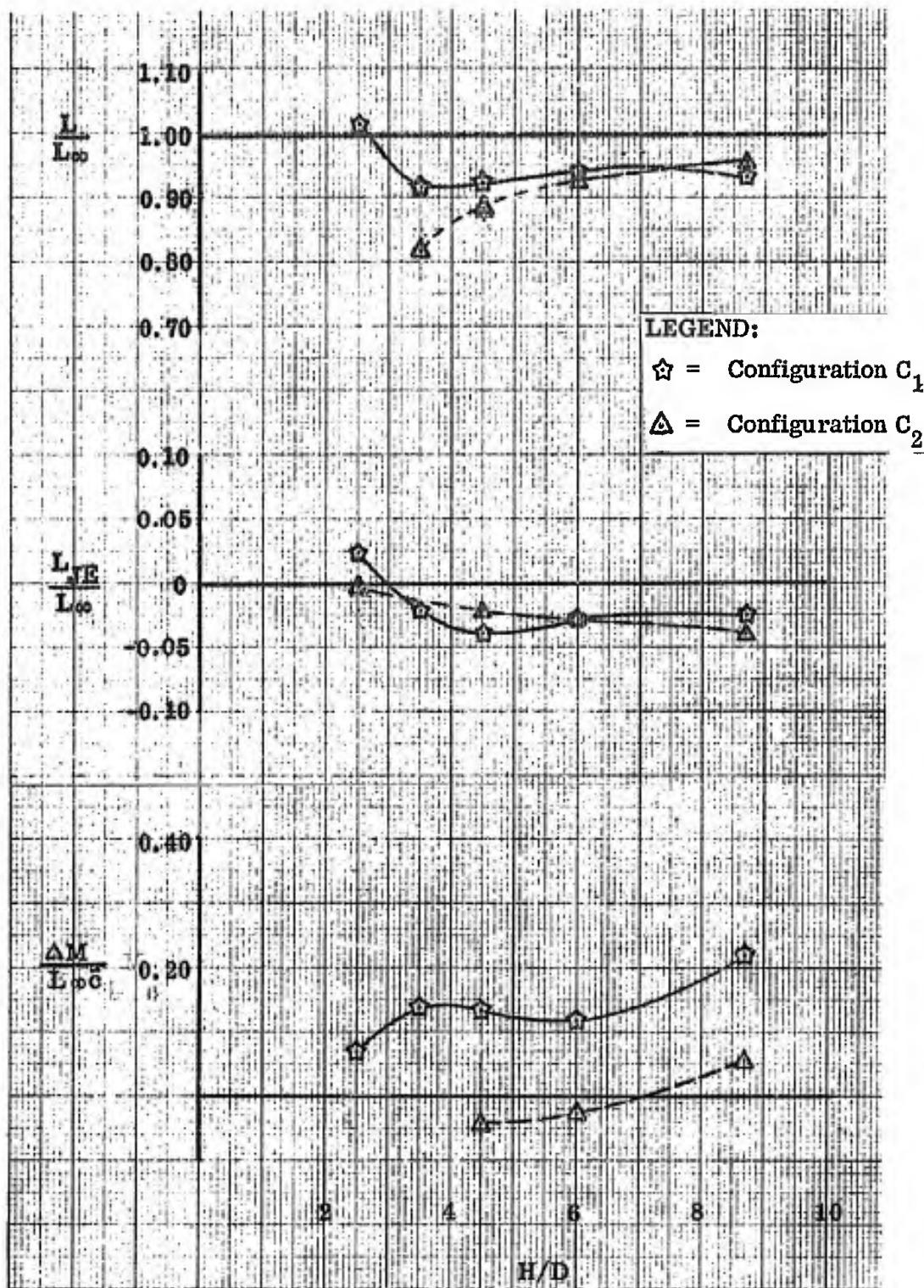
FIGURE 60   EFFECT OF ENGINE ARRANGEMENT ON JET-INDUCED FORCE & MOMENT

151
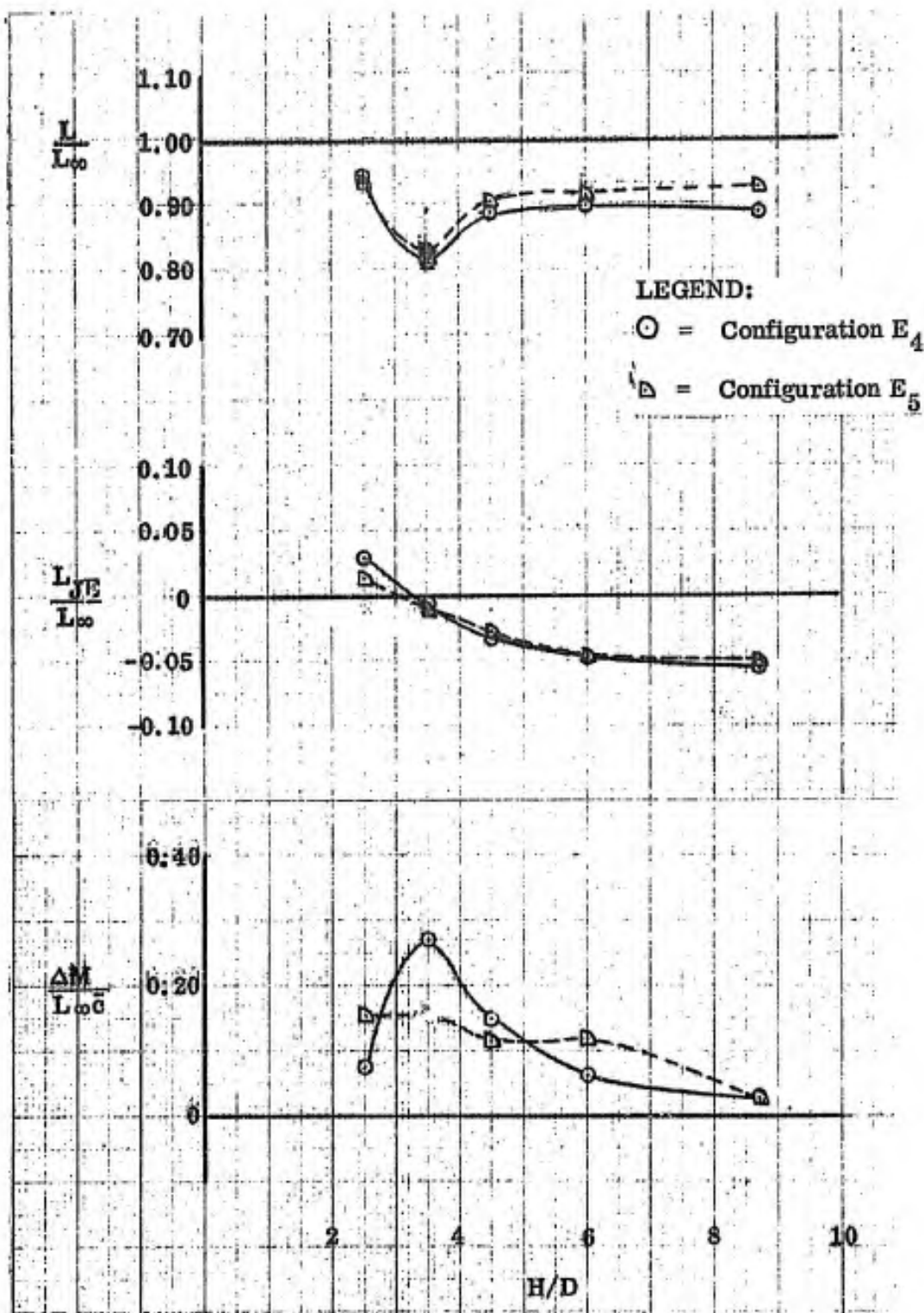
FIGURE 61 EFFECT OF ENGINE ARRANGEMENT ON JET-INDUCED FORCE & MOMENT
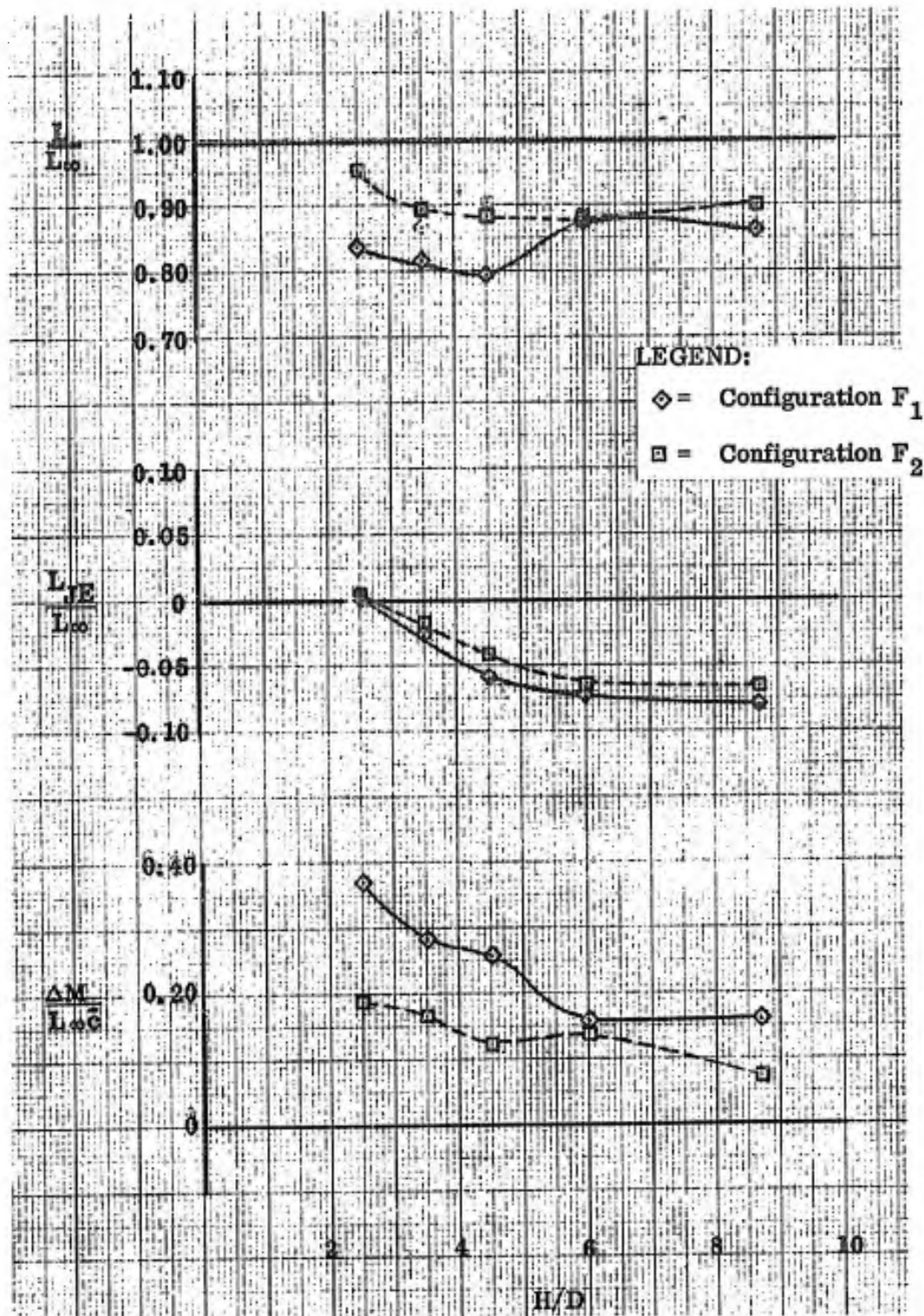
FIGURE 62   EFFECT OF ENGINE ARRANGEMENT ON JET-INDUCED FORCE & MOMENT

153

CONFIGURATION B$_6$

PITCH ATTITUDE ~ α = 0

(a)

PITCH ATTITUDE ~ α = -4°

INLET TEMPERATURE RISE $^\circ$F

Eng #5 Stall 1 Sec after 100%

Symbol	Engine
⊙	1
X	2
⊡	3
Y	4
+	5
☆	6
L	7

(b)

PITCH ATTITUDE ~ α = +4

H/D
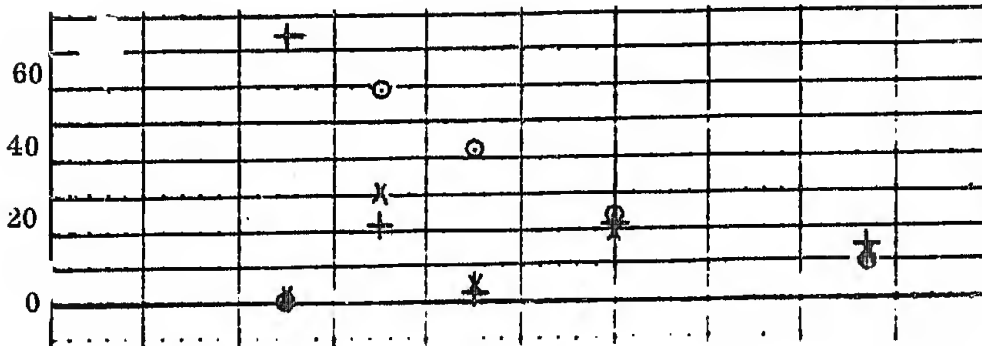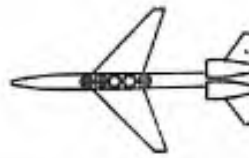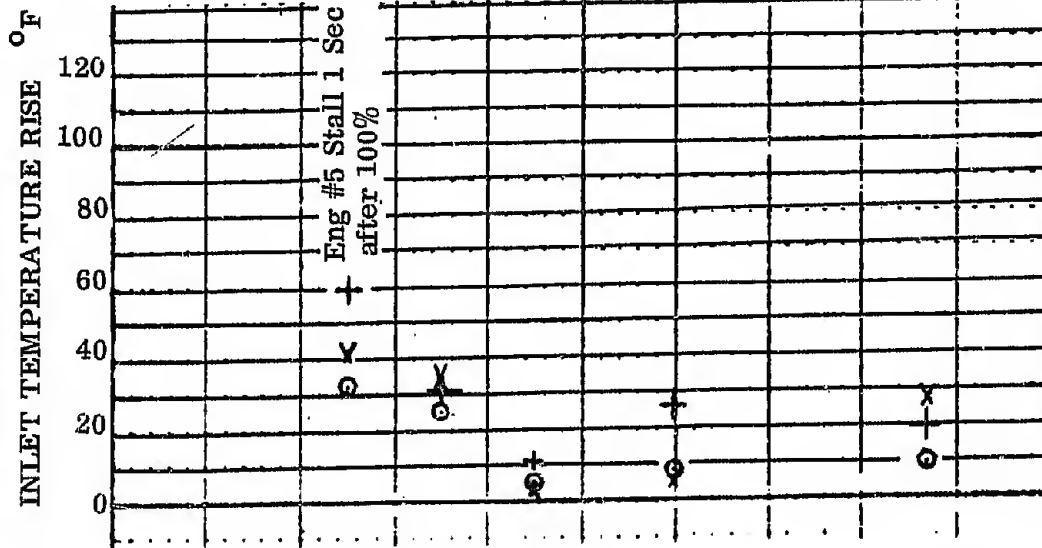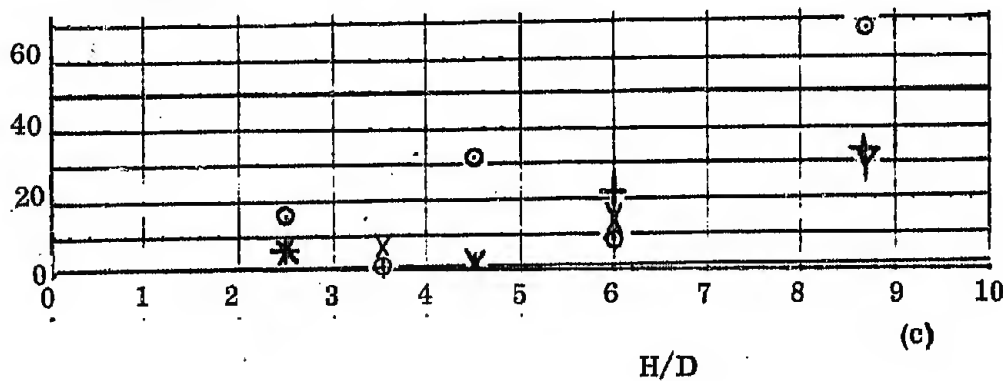
(c)

FIGURE 63 PITCH ATTITUDE VARIATION EFFECTS
ON INGESTION CHARACTERISTICS

154

CONFIGURATION B_8

PITCH ATTITUDE $\alpha = 0$

(a)

PITCH ATTITUDE $\alpha = -4^0$

(b)

Symbol	Engine
⊙	1
X	2
▣	3
Y	4
+	5
☆	6
L	7

PITCH ATTITUDE $\alpha = +4$

Eng #3 stalled
prior to 100%

H/D

(c)

INLET TEMPERATURE ~ ^0F

FIGURE 64   PITCH ATTITUDE VARIATION EFFECTS ON INGESTION CHARACTERISTICS

CONFIGURATION C_2

PITCH ATTITUDE $\alpha = 0$

(a)

PITCH ATTITUDE $\alpha = -4^o$

Stall on Eng 1
8 Sec after 100%

Symbol	Engine
⊙	1
X	2
□	3
Y	4
+	5
☆	6
L	7

(b)

INLET TEMPERATURE RISE ^{o}F

PITCH ATTITUDE $\alpha = +4^o$

Eng #1 stalled
at Max

H/D

(c)
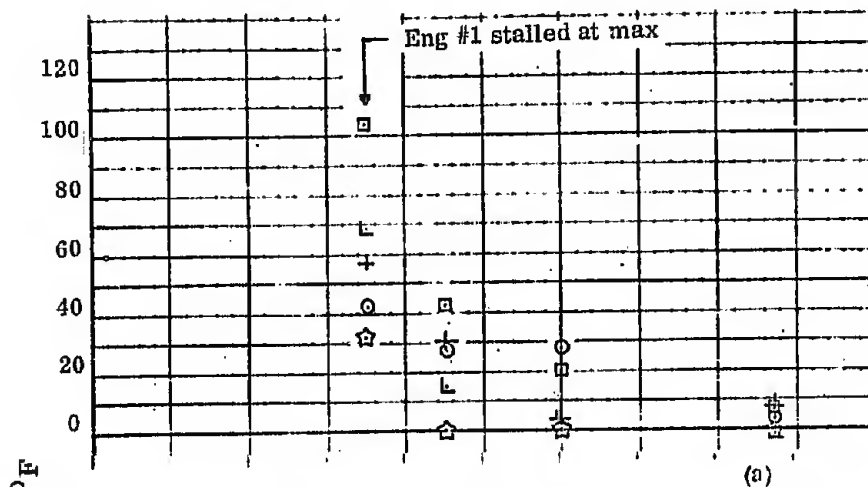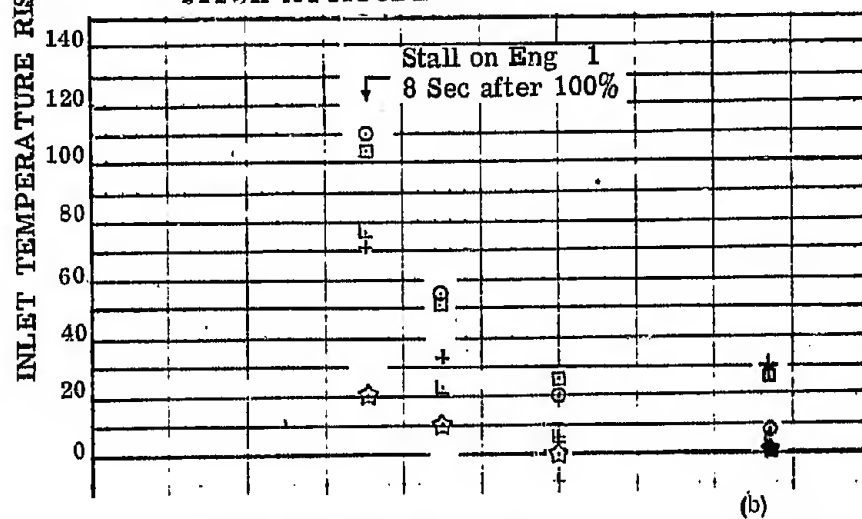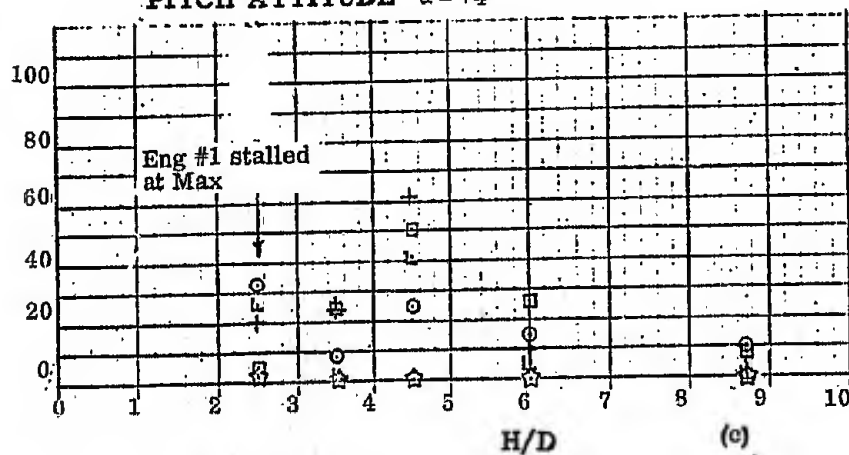
FIGURE 65   PITCH ATTITUDE VARIATION EFFECTS ON INGESTION CHARACTERISTICS

156

CONFIGURATION E$_1$

PITCH ATTITUDE $\alpha = 0$

(a)

PITCH ATTITUDE $\alpha = -4^o$

(b)
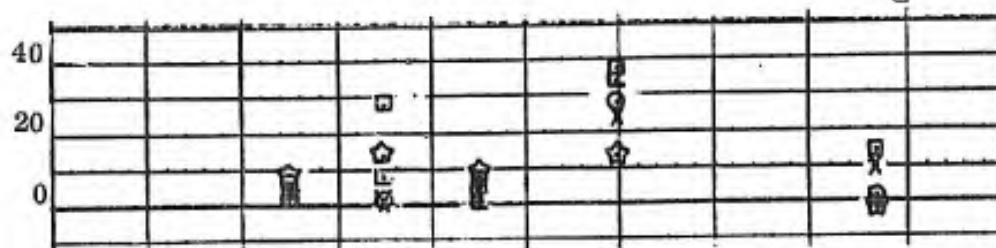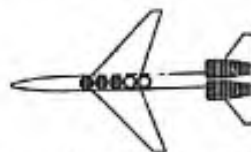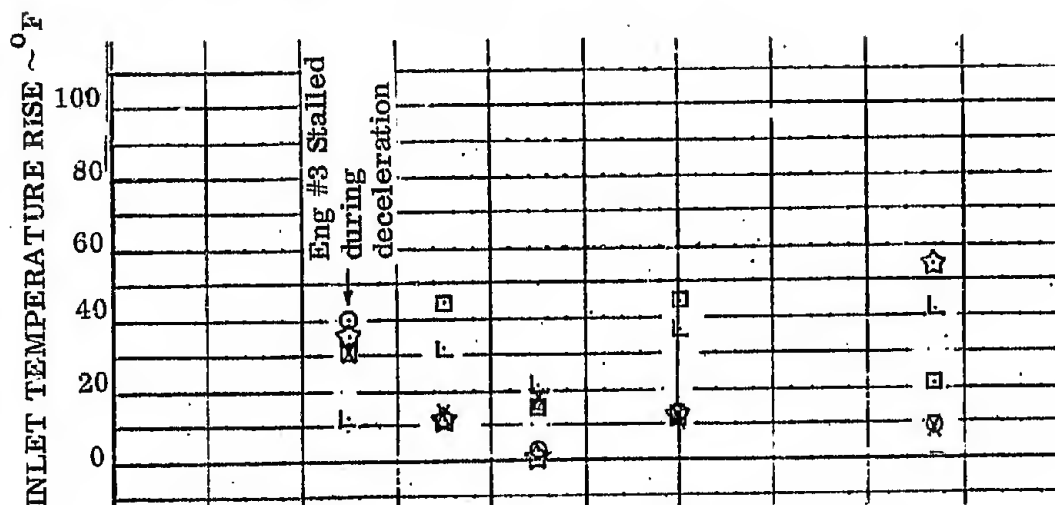
Symbol	Engine
⊙	1
X	2
▫	3
Y	4
+	5
☆	6
L	7

PITCH ATTITUDE $\alpha = +4^o$
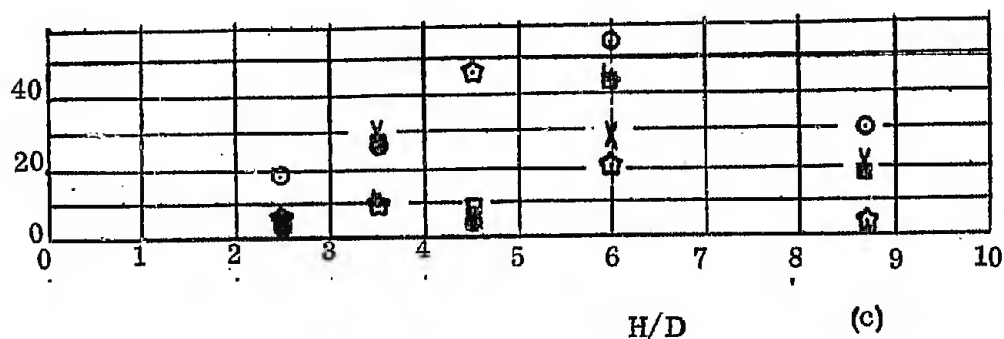
H/D   (c)

FIGURE 66 PITCH ATTITUDE VARIATION EFFECTS ON INGESTION CHARACTERISTICS

157

CONFIGURATION E$_4$

PITCH ATTITUDE $\alpha = 0$

(a)

PITCH ATTITUDE $\alpha = -4^o$

(b)

Symbol	Engine
⊙	1
X	2
□	3
Y	4
+	5
☆	6
L	7

PITCH ATTITUDE $\alpha = +4^o$

(c)

H/D
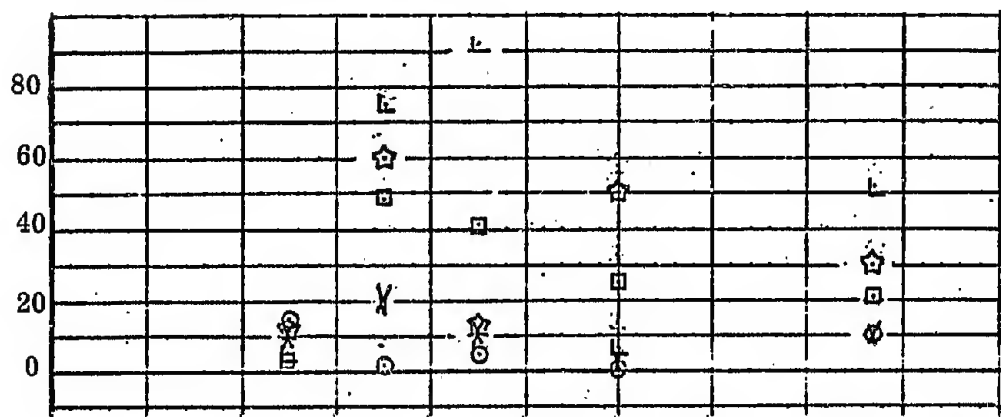
INLET TEMPERATURE RISE ~ ^{o}F
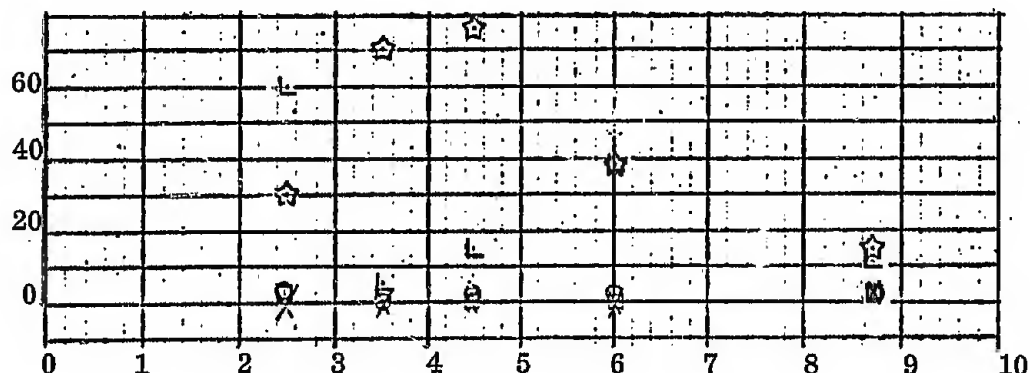
FIGURE 67 PITCH ATTITUDE VARIATION EFFECTS ON INGESTION CHARACTERISTICS

158

FIGURE 68. NEAR-FIELD TEMPERATURE SURVEY

159

FIGURE 69. NEAR-FIELD TEMPERATURE SURVEY

FIGURE 79. NEAR-FIELD TEMPERATURE SURVEY
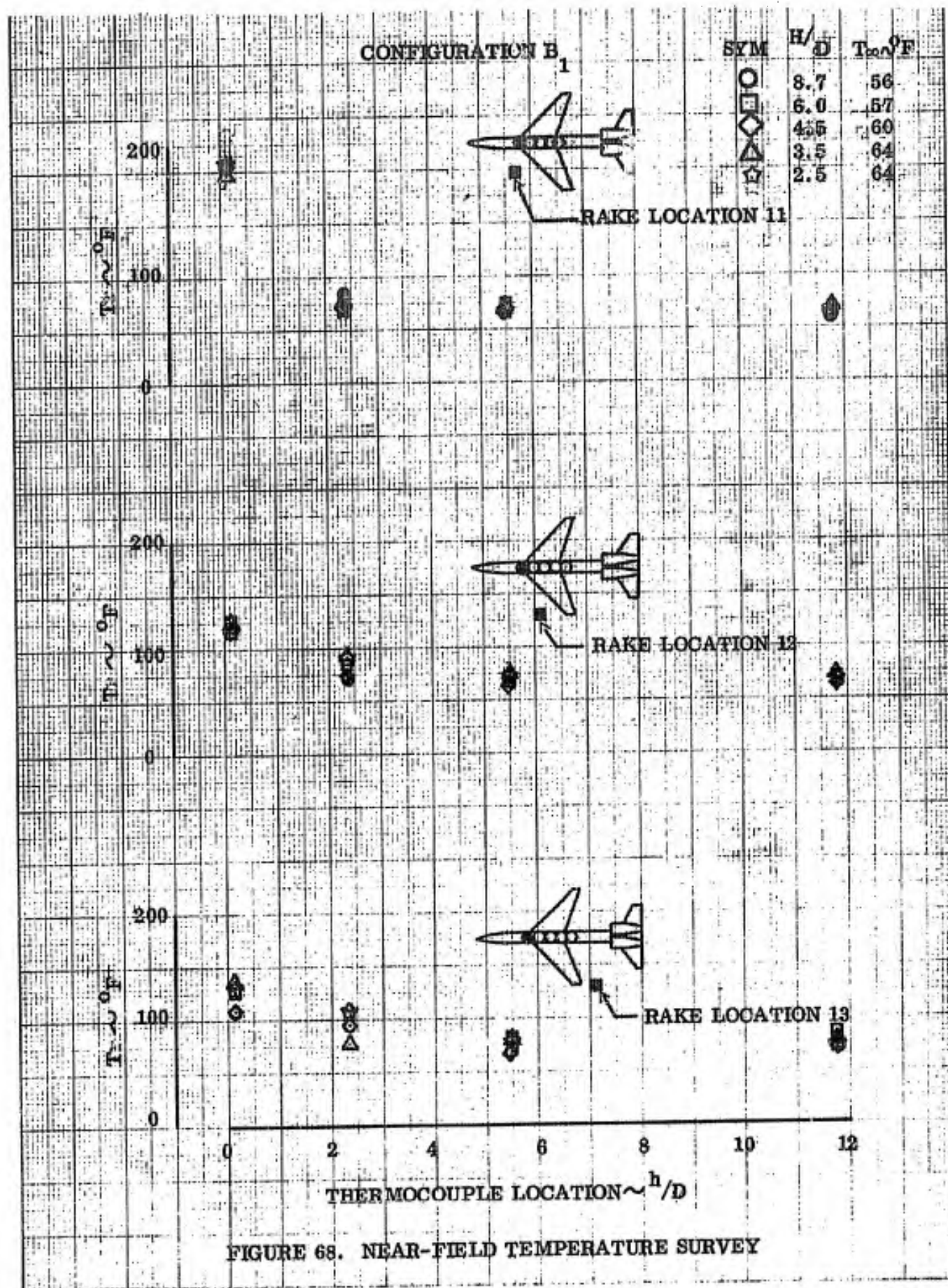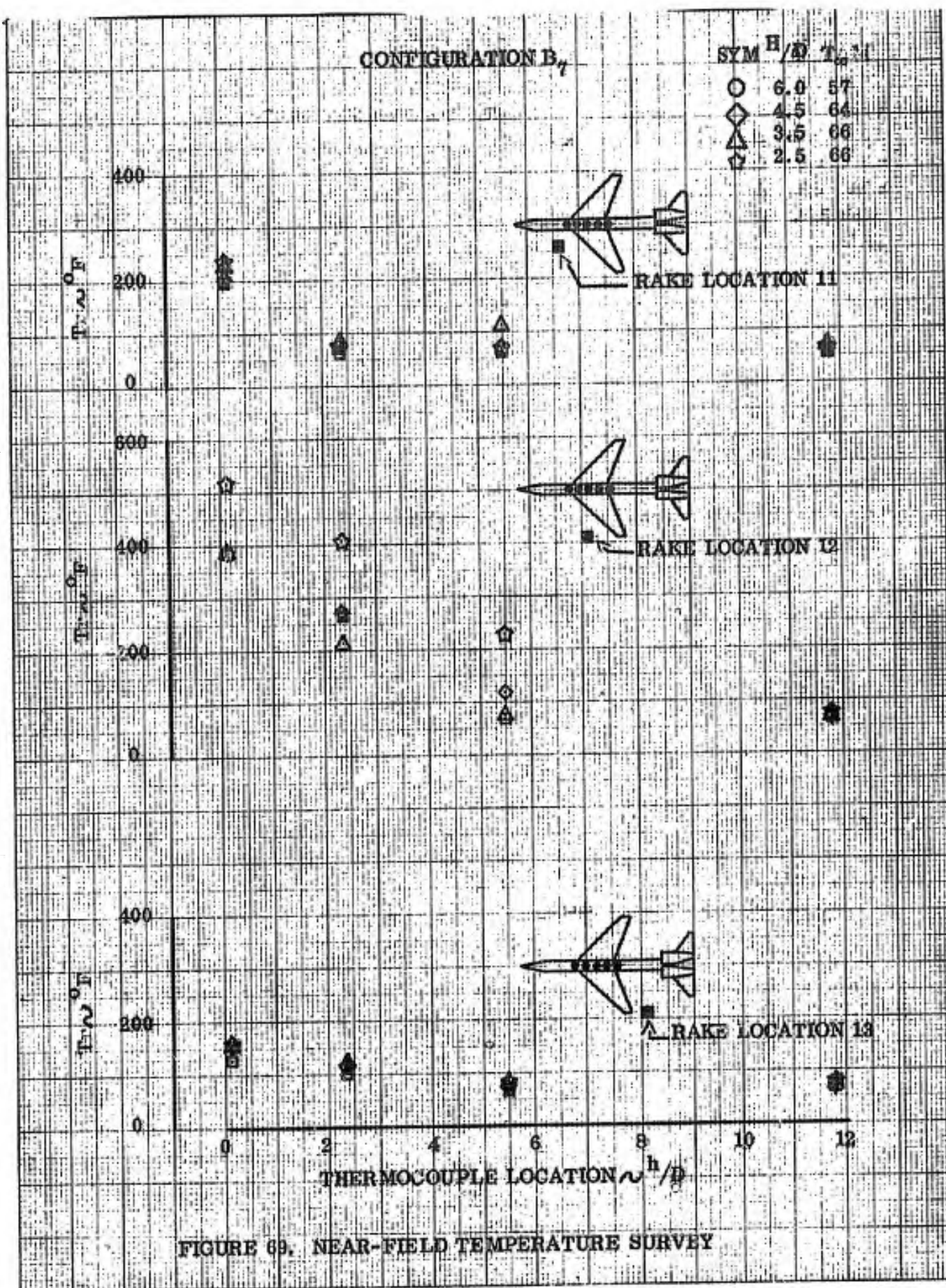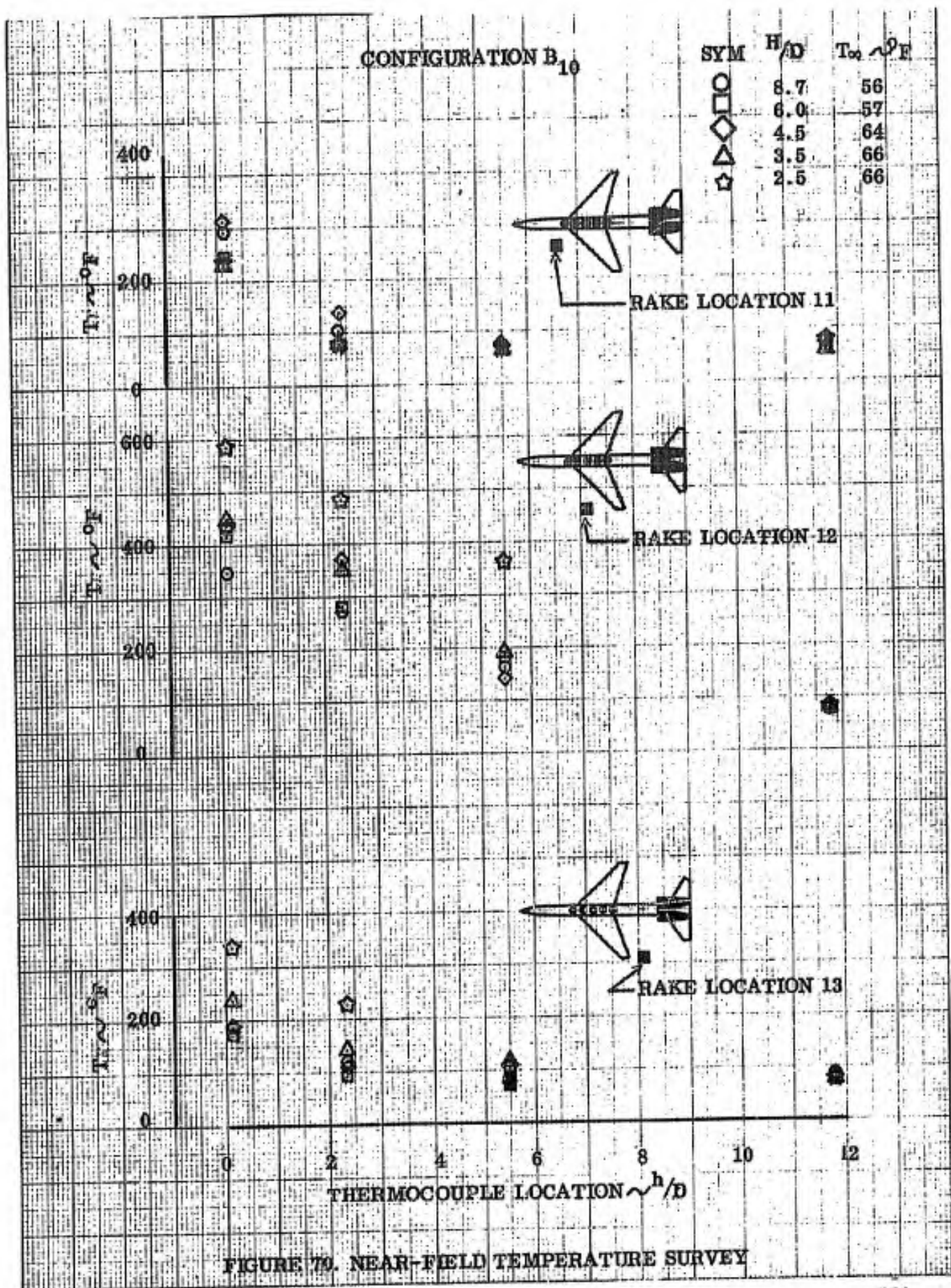
FIGURE 71. NEAR FIELD TEMPERATURE ENVIRONMENT
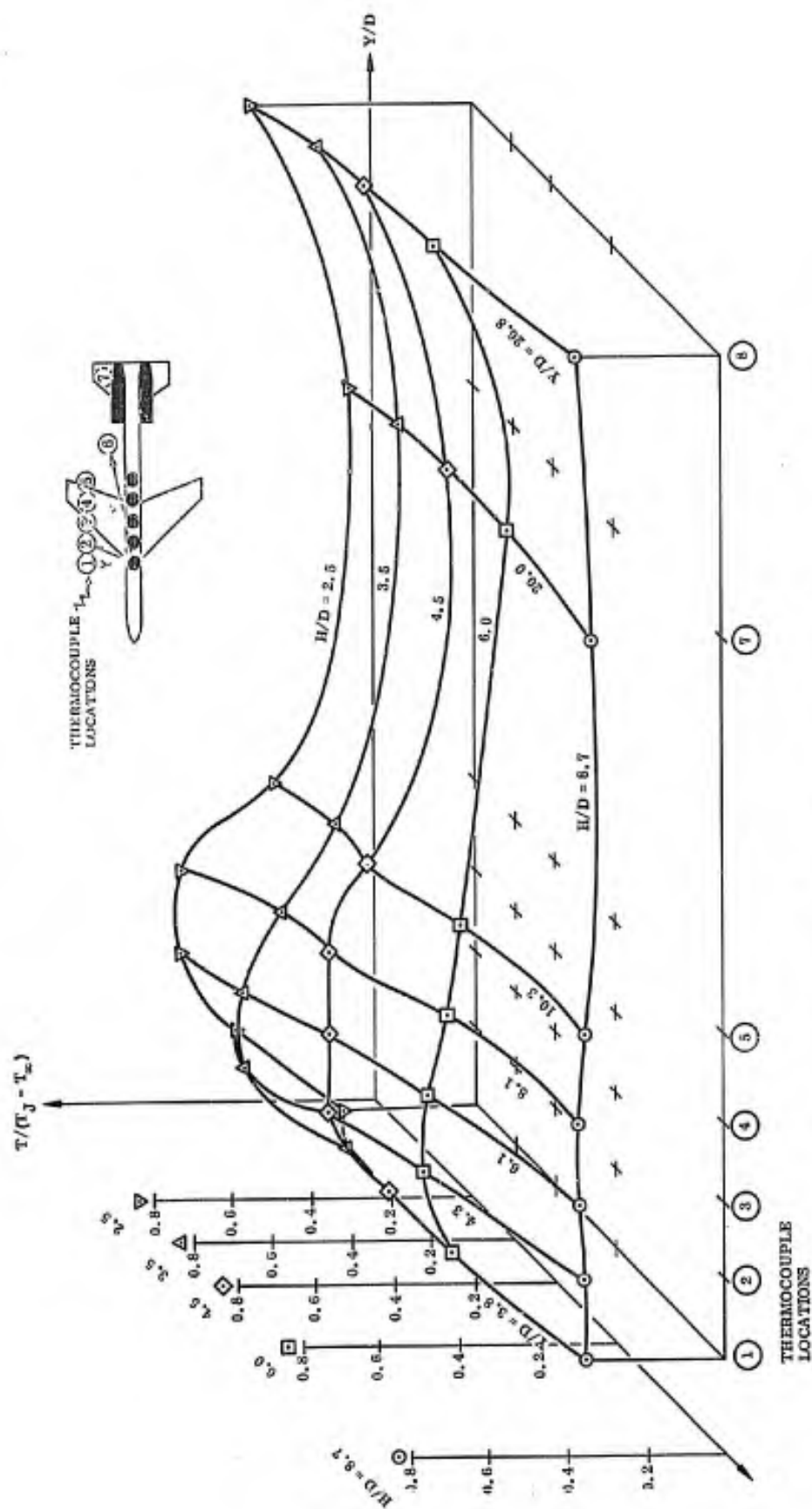
162

CONFIGURATION B₁₀

THERMOCOUPLE LOCATIONS

FIGURE 72. NEAR FIELD TEMPERATURE ENVIRONMENT

163

INLET TEMPERATURE RISE ~ °F

CONFIGURATION B$_2$

40

20

0

(a)
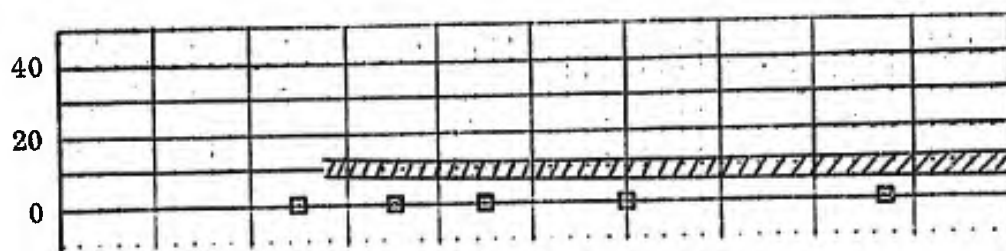
Symbol	Engine
☉	1
✕	2
⊡	3
Y	4
✛	5
☆	6
L	7

▨▨▨ Small-Scale data
Reference 7

INLET TEMPERATURE RISE ~ °F

CONFIGURATION B$_5$

40

20

0

1   2   3   4   5   6   7   8   9   10

(b)

H/D
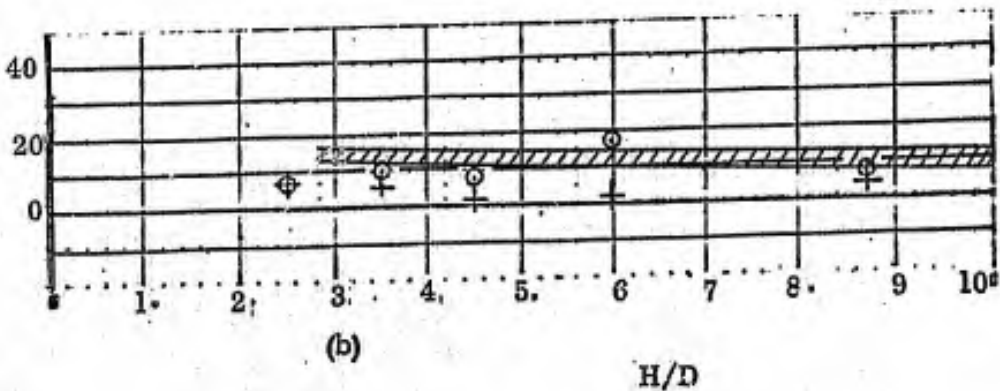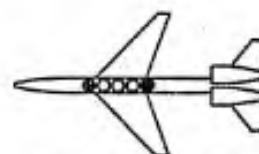
Figure 73. Comparison of Small Scale and
Full Scale Exhaust Gas Ingestion

164
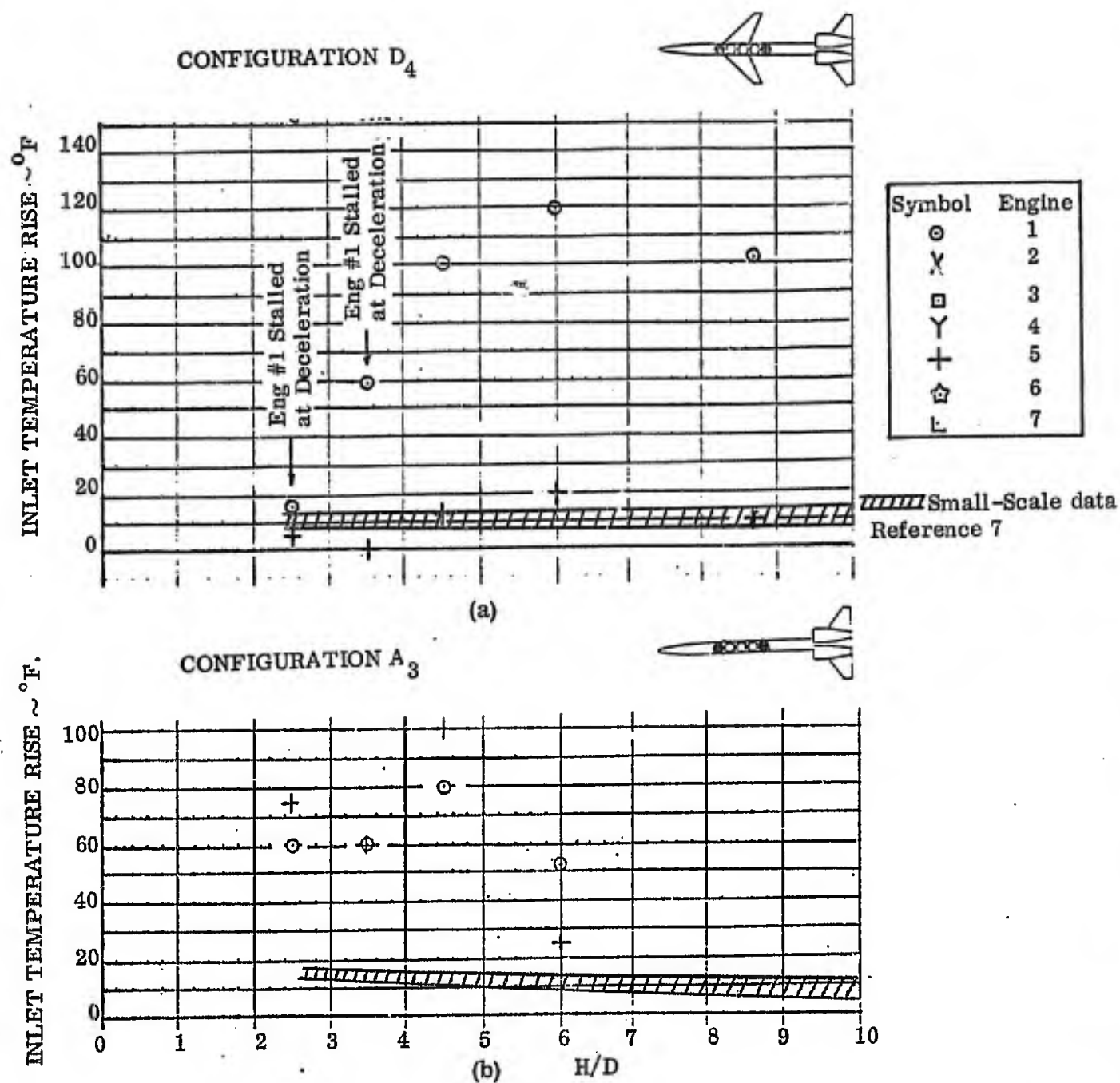
Figure 74. Comparison of Small Scale and Full Scale
Exhaust Gas Ingestion
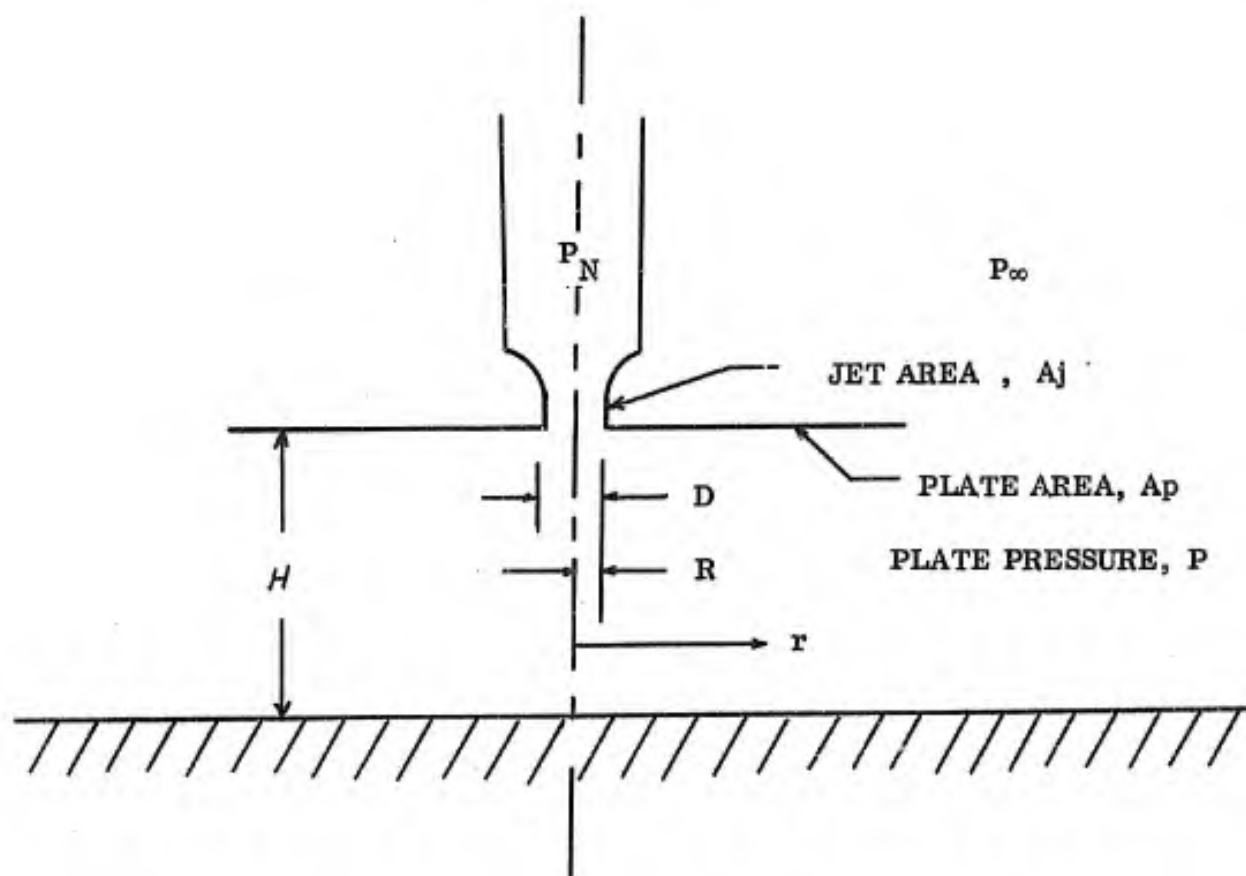
FIGURE 75. TEST CONFIGURATION AND NOMENCLATURE
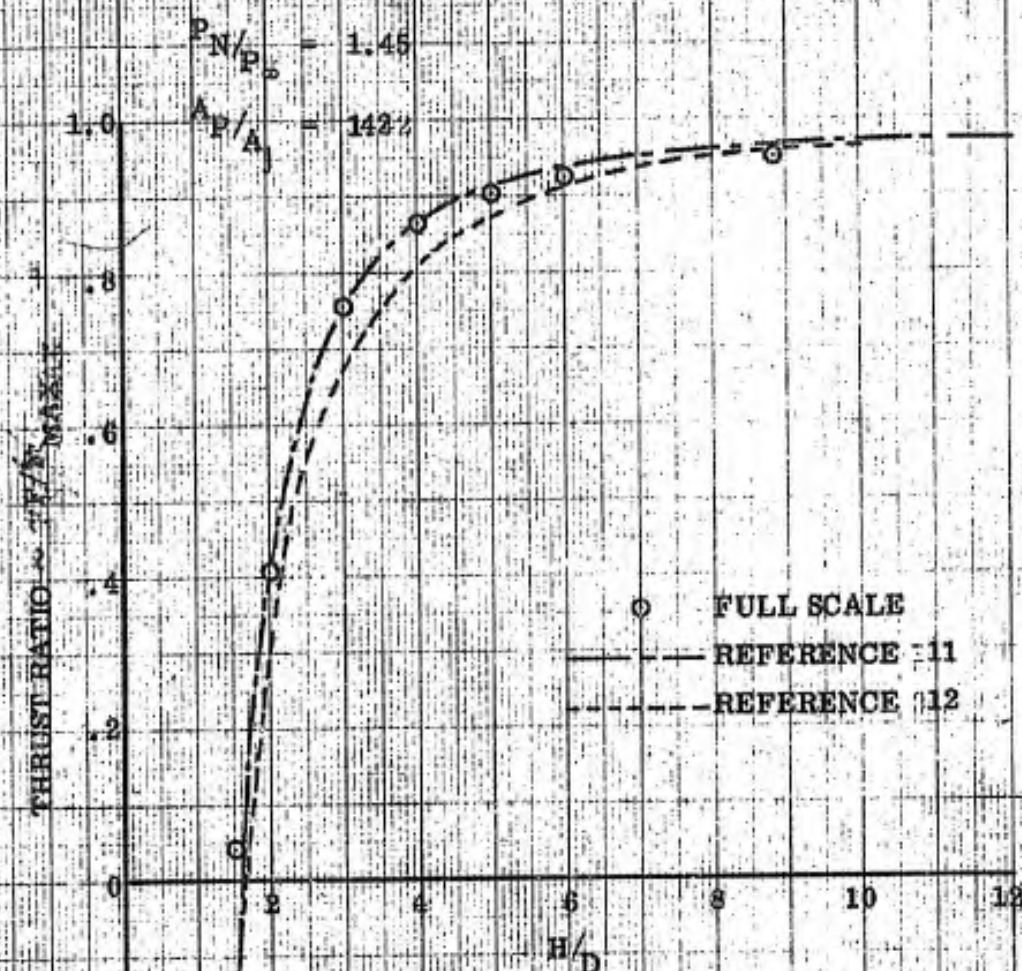
FIGURE 76. THRUST RATIO AS A FUNCTION OF H/D

167
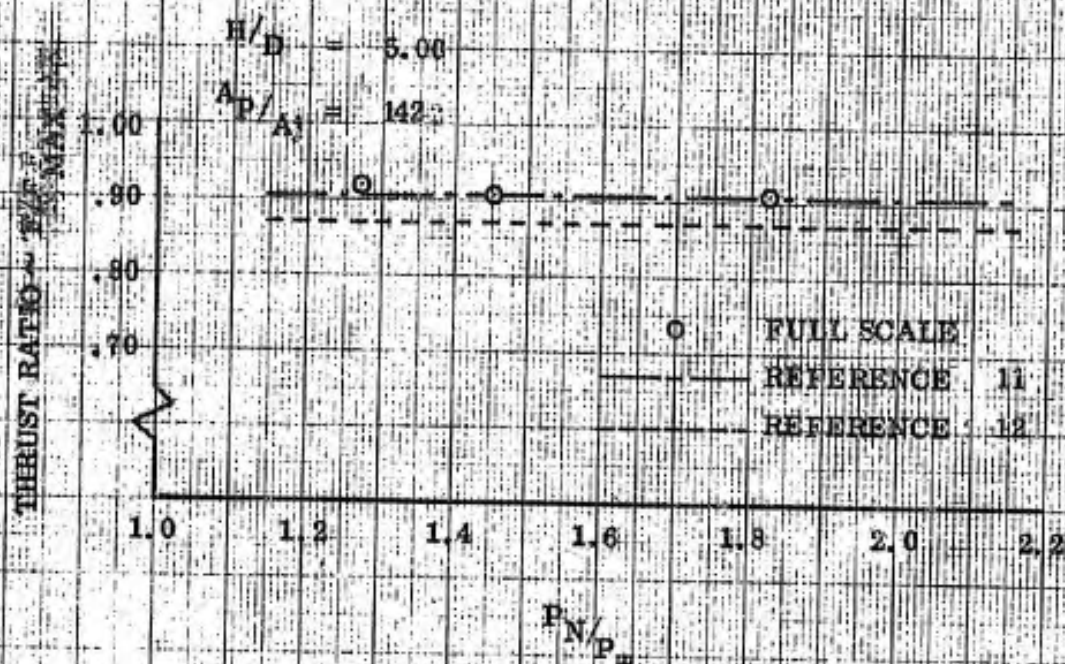
FIGURE 77. THRUST RATIO AS A FUNCTION OF NOZZLE PRESSURE RATIO

168
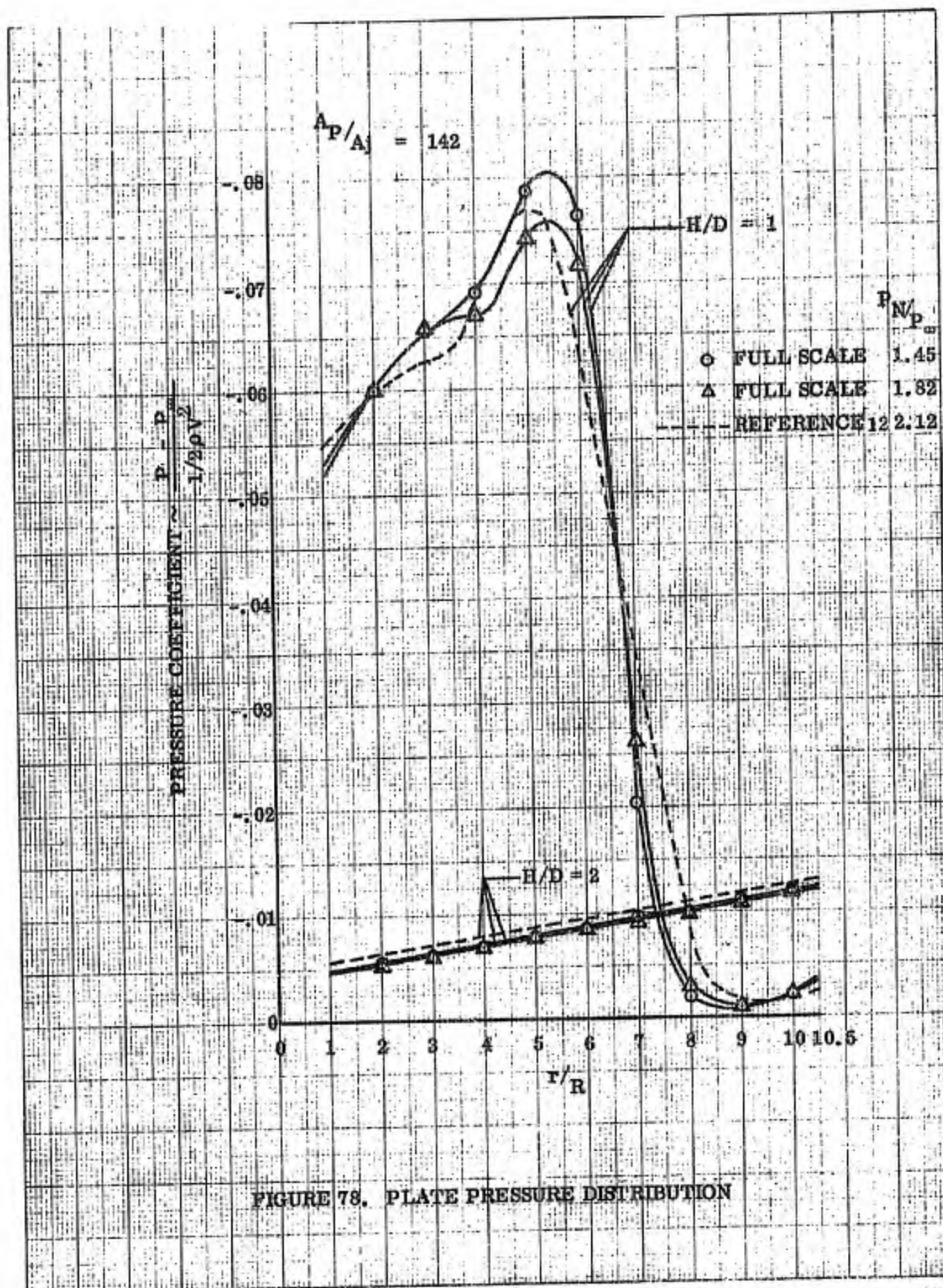
FIGURE 78. PLATE PRESSURE DISTRIBUTION

169
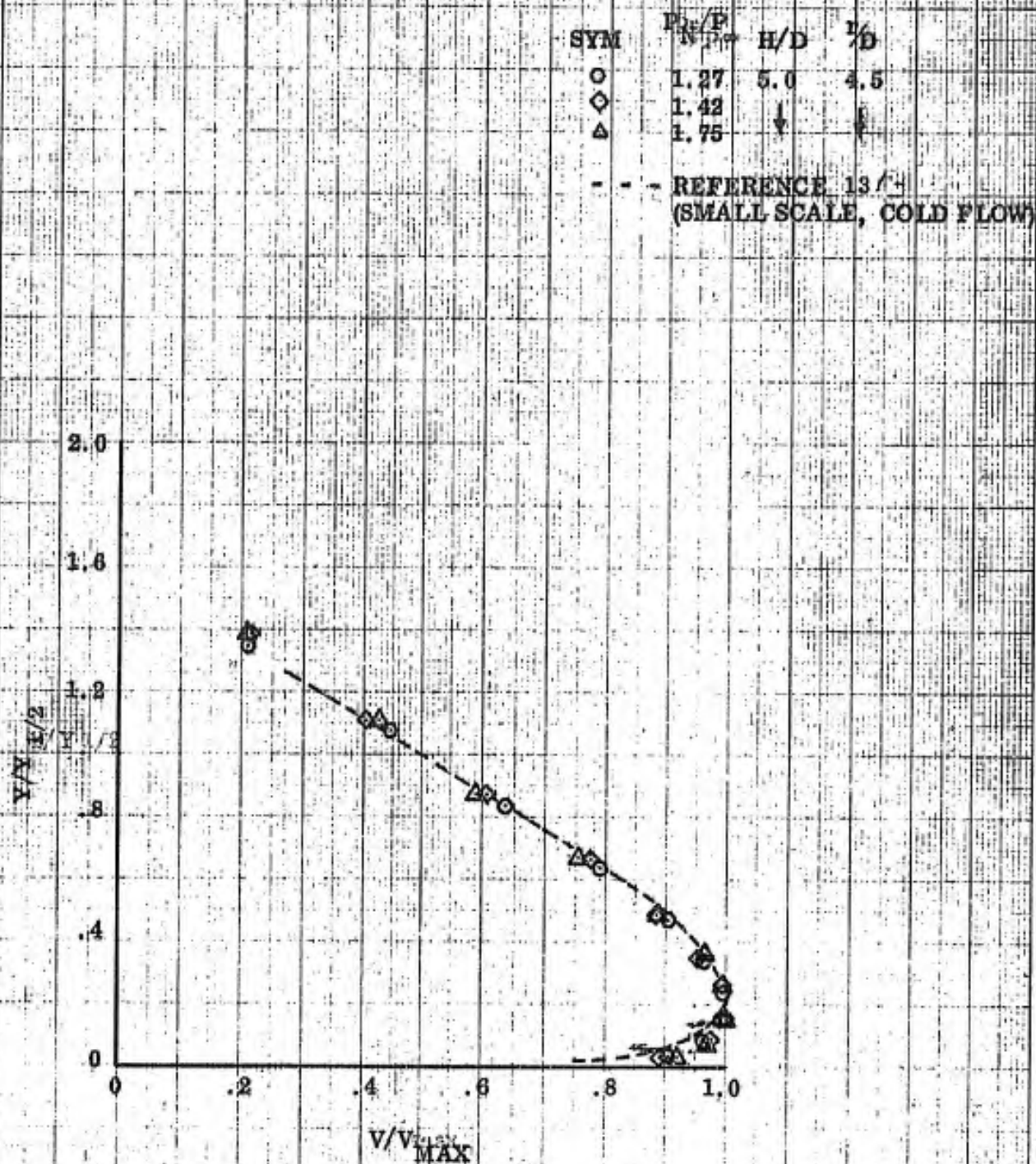
FIGURE 79. GROUND JET VELOCITY PROFILES

SYM	P_N/P_∞	H/D	r/D
O	1.27	5.0	4.5
◇	1.42	↓	↓
△	1.75	

$$\frac{T - T_\infty}{T_{MAX} - T_\infty}$$

Y/Y 1/2

FIGURE 80.   GROUND JET TEMPERATURE PROFILES

SYM P_N/P_∞ H/D
○   ≅ 1.27   5.0
◇   ≅ 1.45   ↓
△   ≅ 1.75   ↓

- - - REFERENCE 9
(SMALL SCALE, $T_o = 1200^\circ F$
H/D = 5.0)

— — REFERENCE 14
(LARGE SCALE, COLD FLOW,
H/D = 4.0)
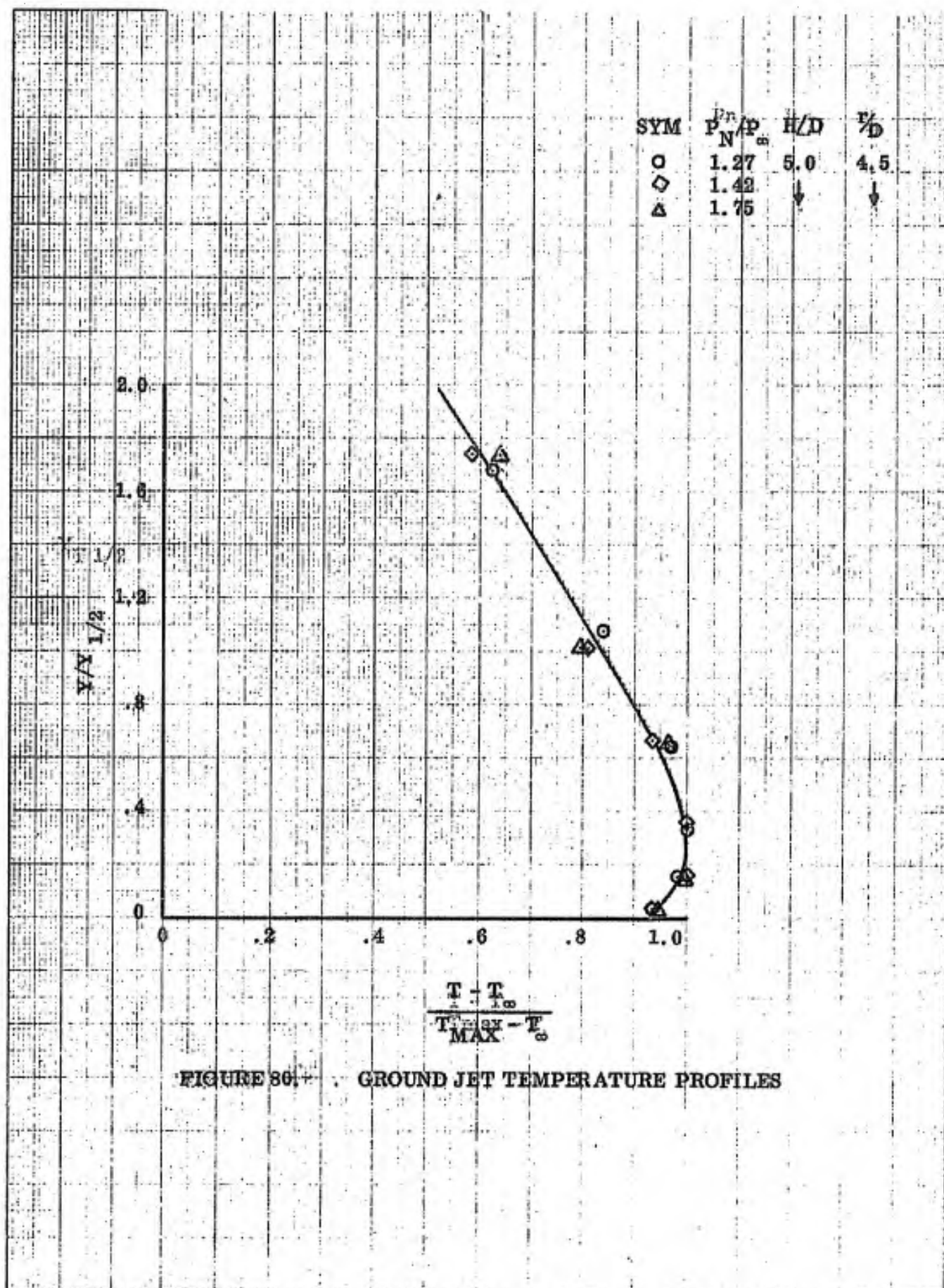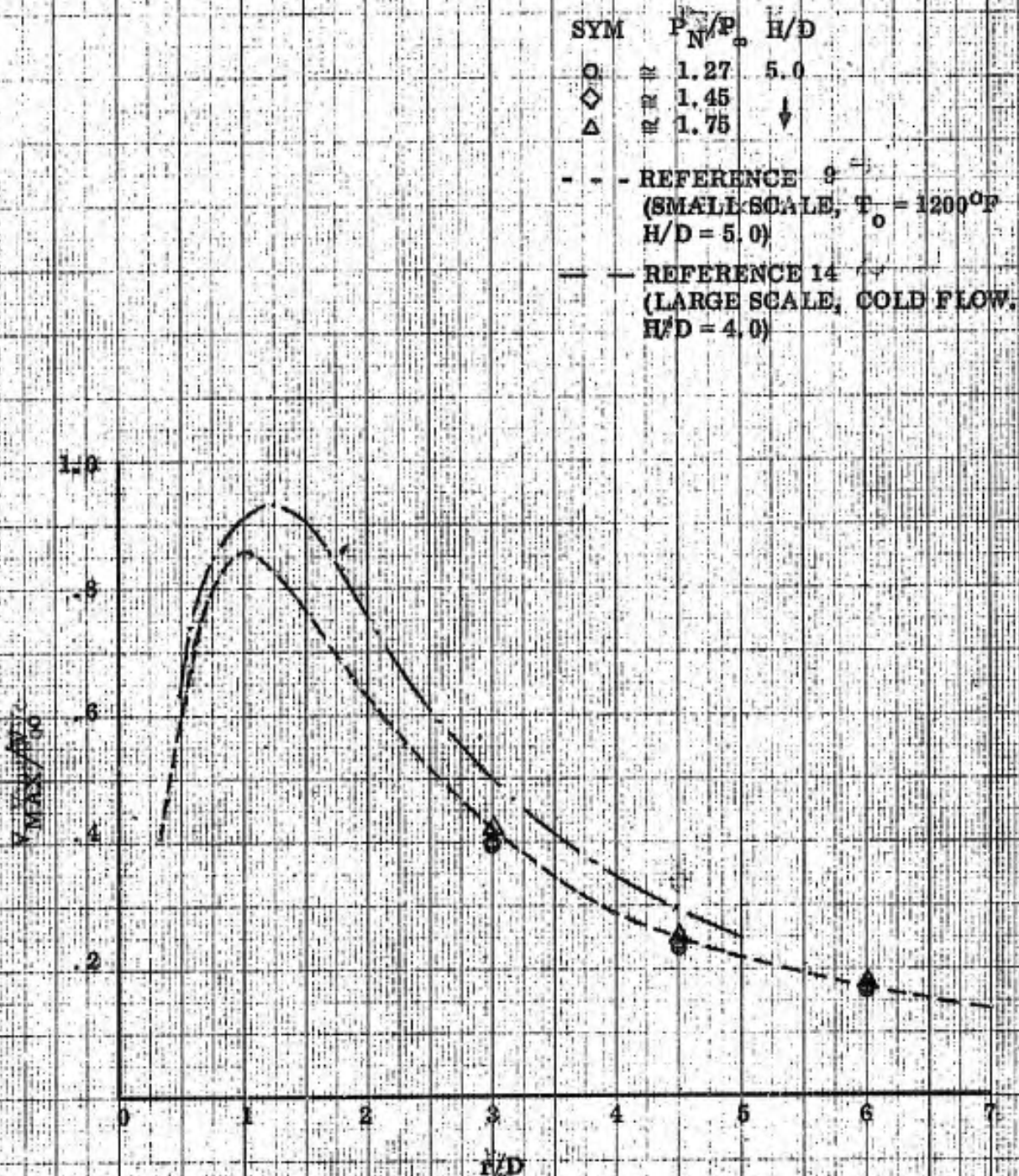
FIGURE 8E.   VARIATION OF MAXIMUM LOCAL VELOCITY NEAR THE GROUND
WITH RADIAL DISTANCE FROM JET CENTERLINE

172
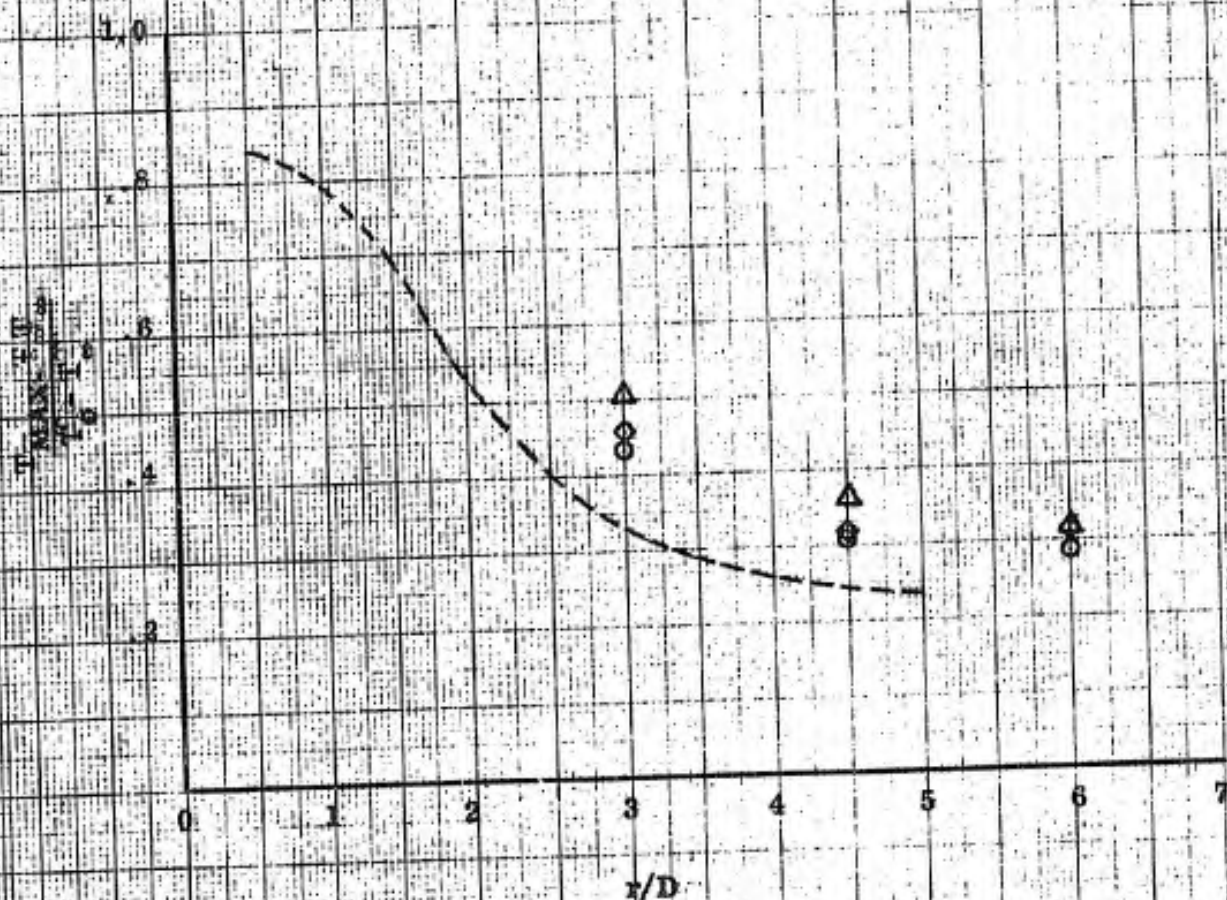
FIGURE 32. VARIATION OF MAXIMUM TEMPERATURE NEAR THE GROUND WITH RADIAL DISTANCE FROM JET CENTERLINE

173
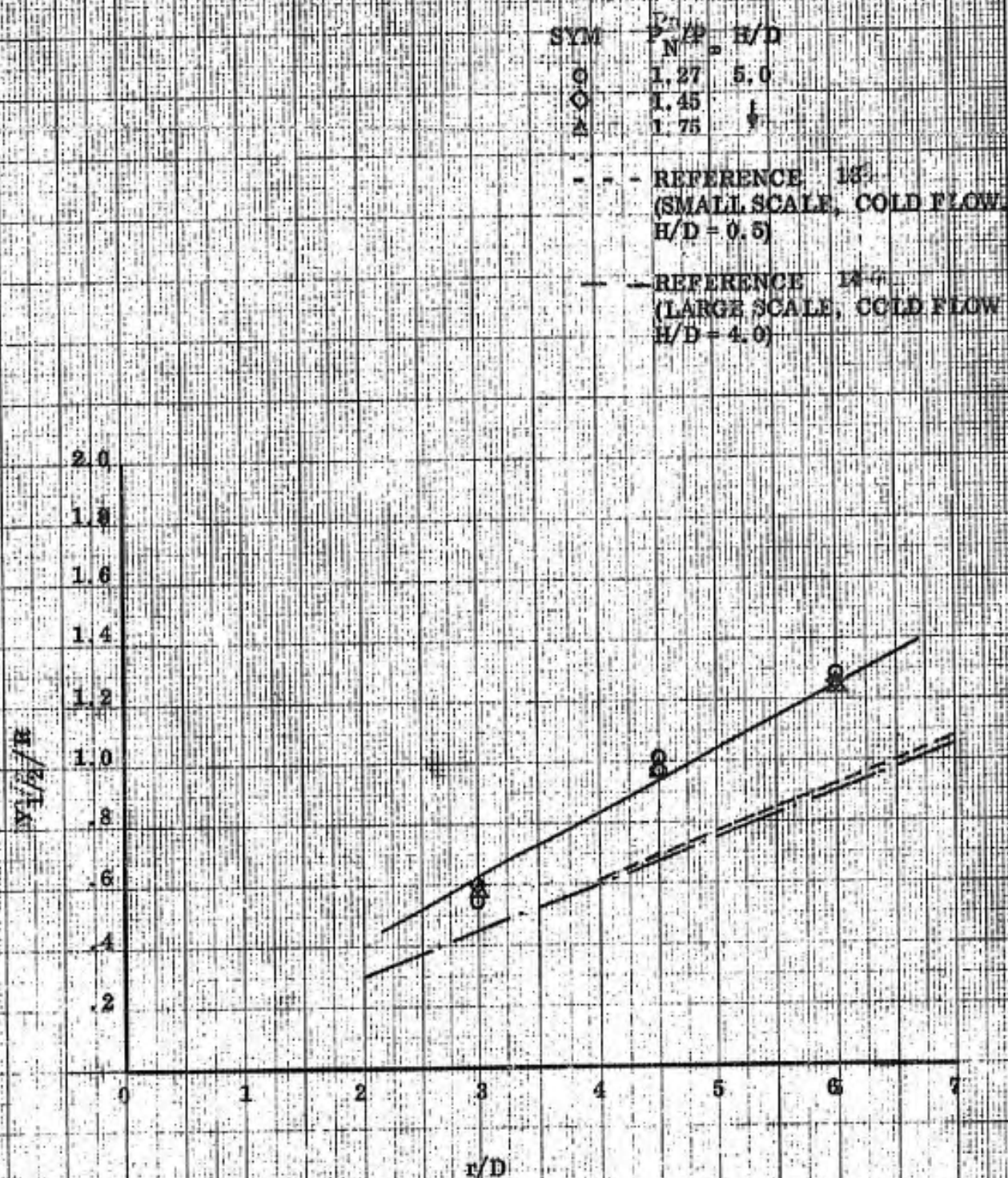
FIGURE 83. GROUND JET GROWTH WITH RADIAL DISTANCE FROM JET CENTERLINE

APPENDIX "A"*

RESPONSE OF BARE WIRE THERMOCOUPLES
TO TEMPERATURE VARIATIONS IN A JET ENGINE INTAKE

INTRODUCTION

Recent full scale VTOL exhaust gas ingestion tests performed by Norair and others have indicated engine inlet air temperature histories of a highly transient character for many of the configurations tested. Considering the transient character of these data, highly responsive thermocouples are required to reproduce the actual temperature transients experienced within the inlets. In general, however, thermocouples of small enough thermal mass to follow the actual temperature transients are costly to fabricate and may not withstand the hostile vibration and acoustic environment within an engine inlet. Considering these practical factors, along with the generally large number of thermocouples required to define the inlet temperature fields for multijet configurations, it may be necessary to accept a temperature pick-up which sacrifices thermal response.

Depending upon the particular objective of the investigation, damped thermal response may or may not represent a serious compromise in the test objective. For instance, for determining the thrust degradation resulting from exhaust gas ingestion for a particular airplane configuration, measurements of short duration temperature pulses of the order of a few milliseconds are not required due to the relatively slow response of the engine to changes in inlet temperature. For evaluations of this type, some damping of the instantaneous temperature field is acceptable, in fact, there is some merit to matching the response of the temperature read-out circuit to the response of the engines for experimental correlations of this type.

On the other hand, for configurations in which exhaust gas ingestion is severe enough to result in engine stall caused by sharp localized temperature pulses within the engine inlet, then undamped measurements of these temperature pulses are obviously important. This means selection of a highly responsive temperature pick-up and a recorder with response equal to or greater than that of the temperature pick-up.

Although an example is pointed out above for a case in which instantaneous temperature determination is not important and for an example in which instantaneous temperature determination is important, it is not the purpose of this note to discuss what one should be measuring since there is no unique answer to this question. Rather, the purpose of this note is to aid one in the selection of a particular temperature pick-up once the desired response is established, or, if the desired response results in wire gage too fine to withstand the environment, to provide data from which the actual response may be determined so that the data may be interpreted accordingly. If in following the latter course, one feels that the instantaneous temperature is highly

---

*Appendix Authors: G. R. Hall and J. A. Bogdanovic, Internal Aerodynamics & Propulsion Research, Northrop Corporation, Norair Division

A-1

important, it is still possible to reconstruct the actual input temperature history, given the output temperature history and temperature pick-up response characteristics. This can be accomplished by use of compensating amplifiers either directly in the instrumentation circuit or through various data playback techniques, or by manual reconstruction of the true temperature input through step-by-step calculations based on the differential equation governing the thermal response of the temperature pick-up in conjunction with the measured output.

ANALYSIS

Consider a thermocouple wire oriented normal to an approaching airflow. Neglecting radiation, heat loss from the ends of the wire by conduction, and assuming the radial temperature gradient through the wire is negligible, the following heat balance may be written

$$\dot{g} = hA (T_g - T_w) = wc \frac{dT_w}{dt} \tag{1}$$

where h = convection coefficient

          A = wire surface area

          T_g = recovery temperature of the air

          T_w = wire temperature

          w = weight of the wire

          c = heat capacity of the wire

          t = time

For typical bare thermocouple wire sizes projected approximately 1/8" - 1/4" beyond the supporting probe, and whose temperature is within a few hundred degrees of ambient temperature, the assumptions stated above, namely, (1) neglecting radiation, (2) neglecting conduction heat loss from the ends of the wire and (3) neglecting the radial thermal gradient, have been checked by numerical calculations and were found to be good engineering approximations for an analysis of the thermal response of the thermocouple junction.

CASE I: Step Input - Consider the case for which T_w is in equilibrium with the air temperature at $t < 0$ ($T_w = T_{g_1}$). At $t = 0$, the air temperature is suddenly changed to the value T_{g_2} and remains constant for $t > 0$. The solution to to equation (1) is then given by

$$\frac{T_w - T_{g_1}}{T_{g_2} - T_{g_1}} = 1 - e^{-\lambda t} \tag{2}$$

where $\lambda \equiv \frac{hA}{Wc}$

CASE II: Sine Wave Input -- Consider the case in which the air temperature varies
sinusoidally with time.   That is, let Tg of equation (1) be given by

$$Tg = T_o + A_o \; SIN \; \omega t$$

For this case the particular solution to equation (1) may be shown to be given
by

$$\frac{T_w - T_o}{\lambda_o} = \frac{1}{\sqrt{1 + \left(\frac{\omega}{\lambda}\right)^2}} \; SIN\left(\omega t + SIN^{-1} \frac{-\omega/\lambda}{\sqrt{1 + \left(\frac{\omega}{\lambda}\right)^2}}\right) \tag{3}$$

The amplitude ratio is then given by

$$\frac{A_w}{A_o} = \frac{1}{\sqrt{1 + \left(\frac{\omega}{\lambda}\right)^2}} \tag{4}$$

where

$$A_w \equiv \left(T_w - T_o\right) MAX$$

and the phase lag angle φ is

$$\varphi = SIN^{-1} \frac{-\omega/\lambda}{\sqrt{1 + \left(\frac{\omega}{\lambda}\right)^2}} \tag{5}$$

For the purpose of evaluating λ in equations (2) through (5), the convection coefficient,
h, may be determined from experimental data of reference 1 which gives $Nu = f(R_{e_d})$
for flow across wires. For the iron-constantan thermocouple response results pre-
sented in Fig. A-1 through A-4, values of $\rho = 486 \; lb/ft^3$ and $c = .12 \; BTU/lb°F$ were
used. It is seen from equation (2) that the thermocouple time constant is simply the
inverse of λ.

RESULTS

The results of the analysis were compared to experimental data obtained for the
response of a 30-gage (d = .010" diameter) iron-constantan thermocouple subjected to
a step change in air temperature. The step change in air temperature was achieved
by thrusting the thermocouple, which was initially in thermal equilibrium with the
ambient environment, into a uniform stream of hot gas at 230°F issuing from a 4-by-
4-inch-square duct. The output of the thermocouple was monitored on an oscilloscope
and the thermal response was documented with an oscilloscope camera. Data were
obtained for hot air flow velocities of V = 100, 200, and 300 feet/second.

Figure A-1 shows the comparison of the theoretical calculations with the experimental data for a step change in air temperature from T_{g_1} to T_{g_2} at $t = 0$. The solid curve is the theoretical calculation as given by equation (2) with the numerical value of λ calculated for the actual conditions of the experiment. The experimental data are represented by the symbols, each of which is an average of duplicate data which were within 2 percent of each other for all data points measured. Although continuous traces of the experimental data were obtained, the agreement between the experimental data and the theoretical calculations is too close to allow definition of two discrete curves. As a result, points were measured from the continuous trace experimental data at 100 m.s. time intervals for the comparison shown in Fig. A-1.

The near perfect agreement of the calculated curves and the experimental data must be considered somewhat fortuitous. In reviewing the various inputs to the analysis in detail, one may have expected disagreement between the analysis and the experimental data in the neighborhood of 10-20 percent if the anticipated differences between the analysis and the experiment had accumulated in a more unfavorable way. Even with an unfavorable accumulation of differences, however, the analysis must be considered as a good indication of the actual thermocouple response.

Figs. A-2 through A-4 show some numerical results of the analysis which are of particular interest for the response of thermocouples within the inlet to a jet engine. The results given are for iron-constantan thermocouples of various wire gage sizes oriented normal to an airstream with a velocity of 400 feet/second at standard pressure and temperature. The curves are also considered indicative of the response for other wire orientations and indicative of the response for chromel-alumel thermocouples since the response depends only upon the value of λ, which for chromel-alumel thermocouples is within a few percent of the value for iron-constantan thermocouples for the same wire size and flow conditions. The data of Fig. A-2, which give the response to a step change in air temperature, indicate a time constant to approximately 100 m.s. and a 99 percent rise time of approximately one-half second for the 30 gage (d = .010" diameter) thermocouple wire used in recent exhaust gas ingestion tests performed by Norair and others.

Figs. A-3 and A-4 show, respectively, the amplitude ratio, A_w/A_o (equation 4) and the phase lag angle, φ (equation 5) as a function of frequency for a gas temperature which varies sinusoidally with time. From Fig. A-3, it is seen that flat response for the 30 gage (.010" wire) is limited to frequencies of less than a few tenths of a cycle/second while at 15 cps the input signal is attentuated 90 percent.

REFERENCE

1. "Physical Measurements in Gas Dynamics and Combustion," Volume IX of High Speed Aerodynamics and Jet Propulsion, Princeton University Press, 1954.
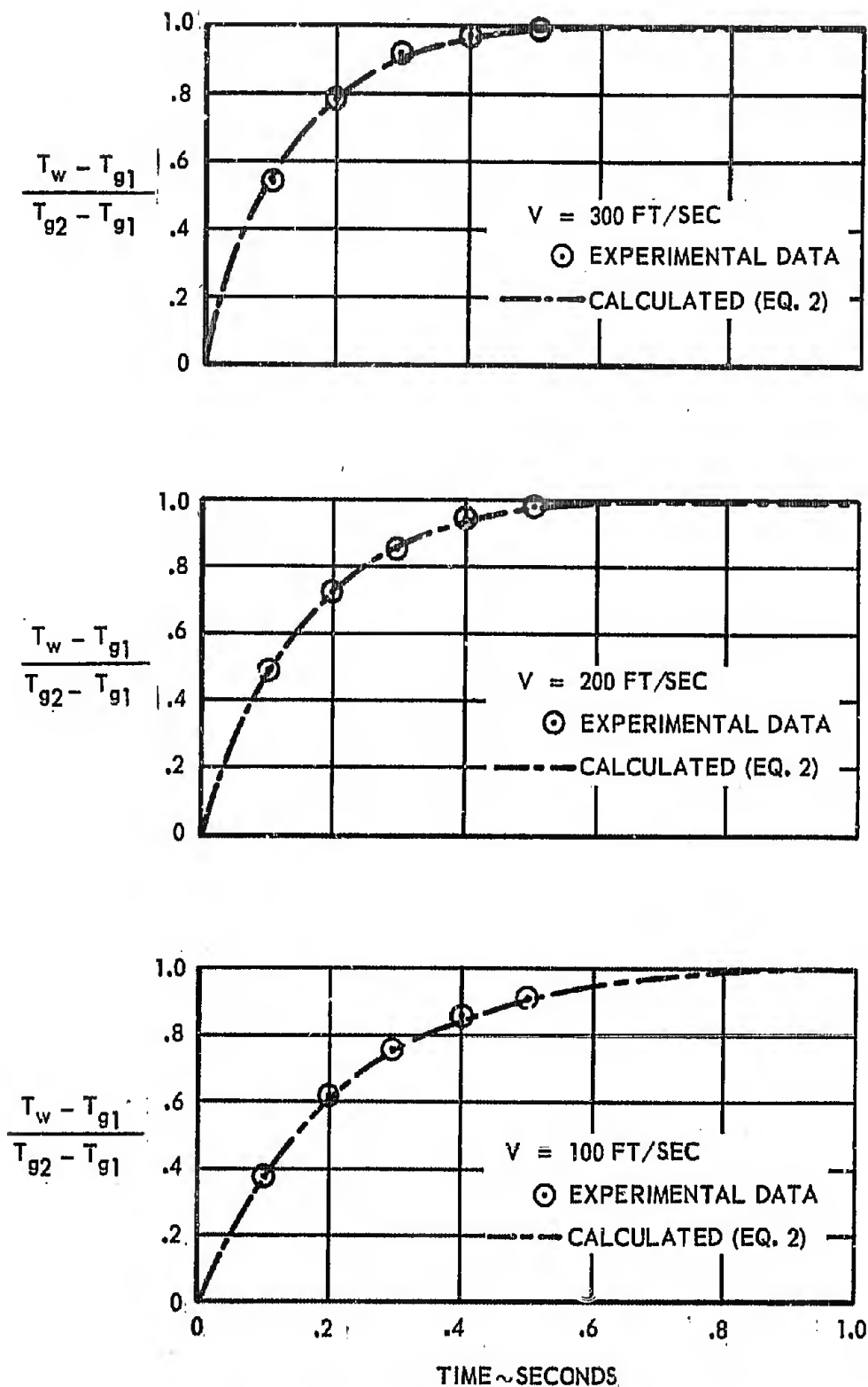
FIGURE A-1 COMPARISON OF THEORETICAL RESPONSE TO EXPERIMENTALLY DETERMINED RESPONSE FOR A STEP CHANGE IN GAS TEMPERATURE FROM T_{g1} TO T_{g2}.
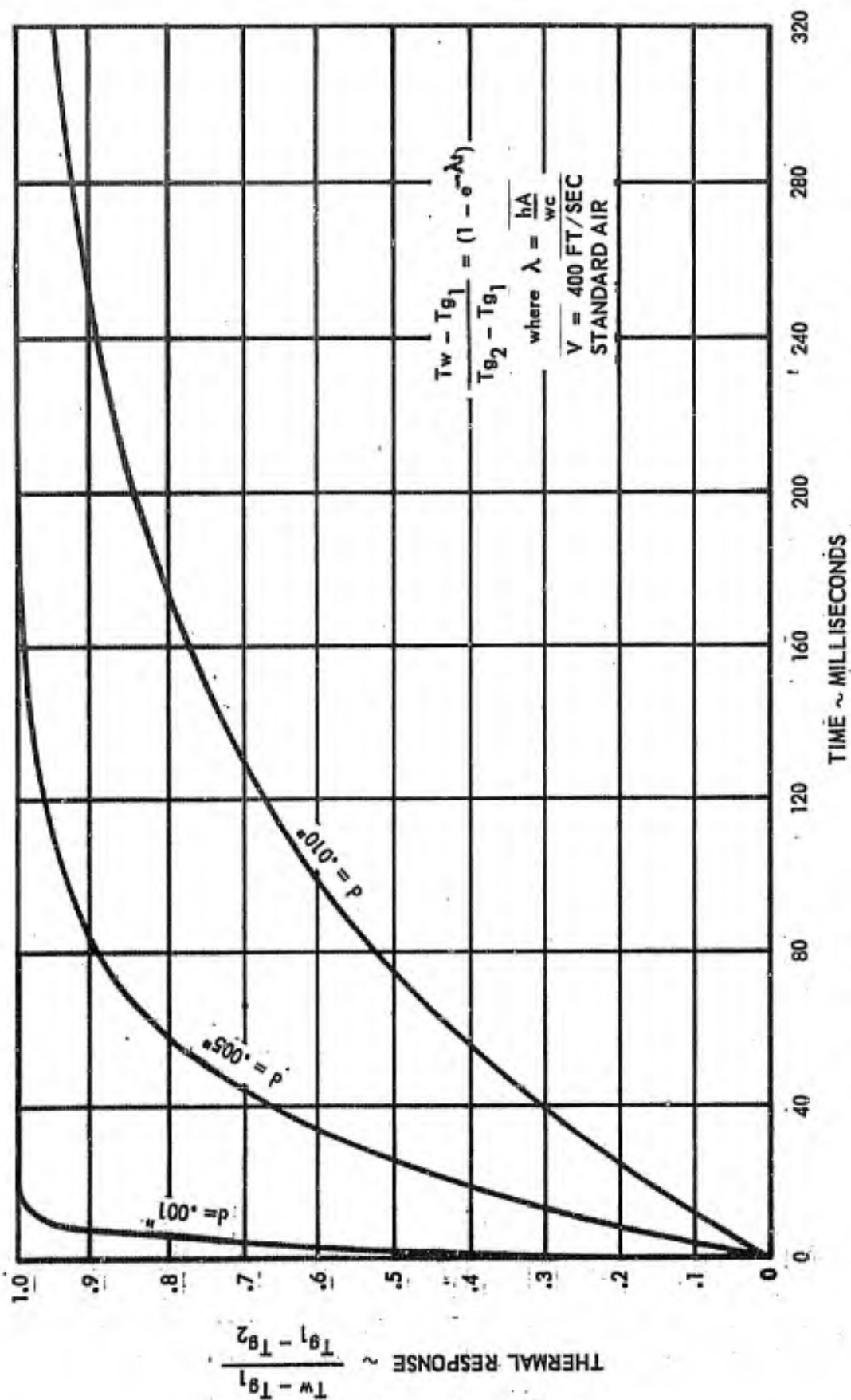
FIGURE A-2 RESPONSE OF IRON-CONSTANTAN THERMOCOUPLE TO STEP CHANGE IN GAS TEMPERATURE FROM T_{g1} TO T_{g2}.

The figure plots THERMAL RESPONSE $\sim \dfrac{T_w - T_{g_1}}{T_{g_1} - T_{g_2}}$ versus TIME $\sim$ MILLISECONDS for curves $d = .001"$, $d = .005"$, and $d = .010"$, with the relation:

$$\frac{T_w - T_{g_1}}{T_{g_2} - T_{g_1}} = (1 - e^{-\lambda_t})$$

$$\text{where } \lambda = \frac{hA}{wc}$$

$$V = 400 \text{ FT/SEC}$$
$$\text{STANDARD AIR}$$

FIGURE A-3 RESPONSE CHARACTERISTICS OF IRON-CONSTANTAN THERMOCOUPLE TO
A SINUSOIDAL VARIATION OF GAS TEMPERATURE
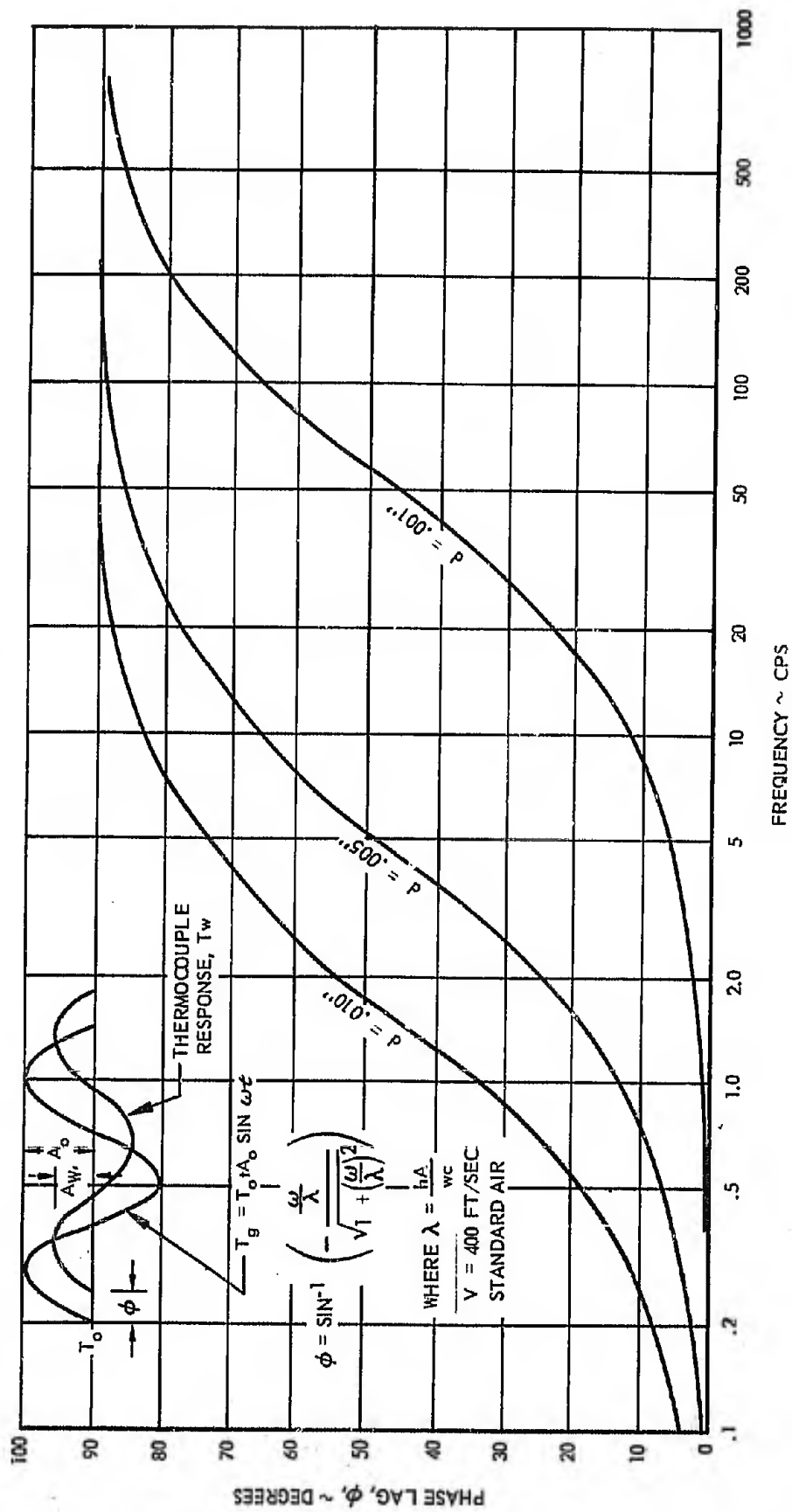
FIGURE A-4   PHASE LAG CHARACTERISTICS OF IRON-CONSTANTAN THERMOCOUPLE
FOR A SINUSOIDAL VARIATION IN GAS TEMPERATURE

DOCUMENT CONTROL DATA - R&D

(Security classification of title, body of abstract and indexing annotation must be entered when the overall report is classified)

1. ORIGINATING ACTIVITY (Corporate author)	2a. REPORT SECURITY CLASSIFICATION
Norair Division Northrop Corporation Hawthorne, California	Unclassified
	2b. GROUP Not Applicable

3. REPORT TITLE

Parametric Investigation of VTOL Hot Gas Ingestion and Induced Jet Effects in Ground Proximity

4. DESCRIPTIVE NOTES *(Type of report and inclusive dates)*

Final Report

5. AUTHOR(S) *(Last name, first name, initial)*

Lavi, Rahim

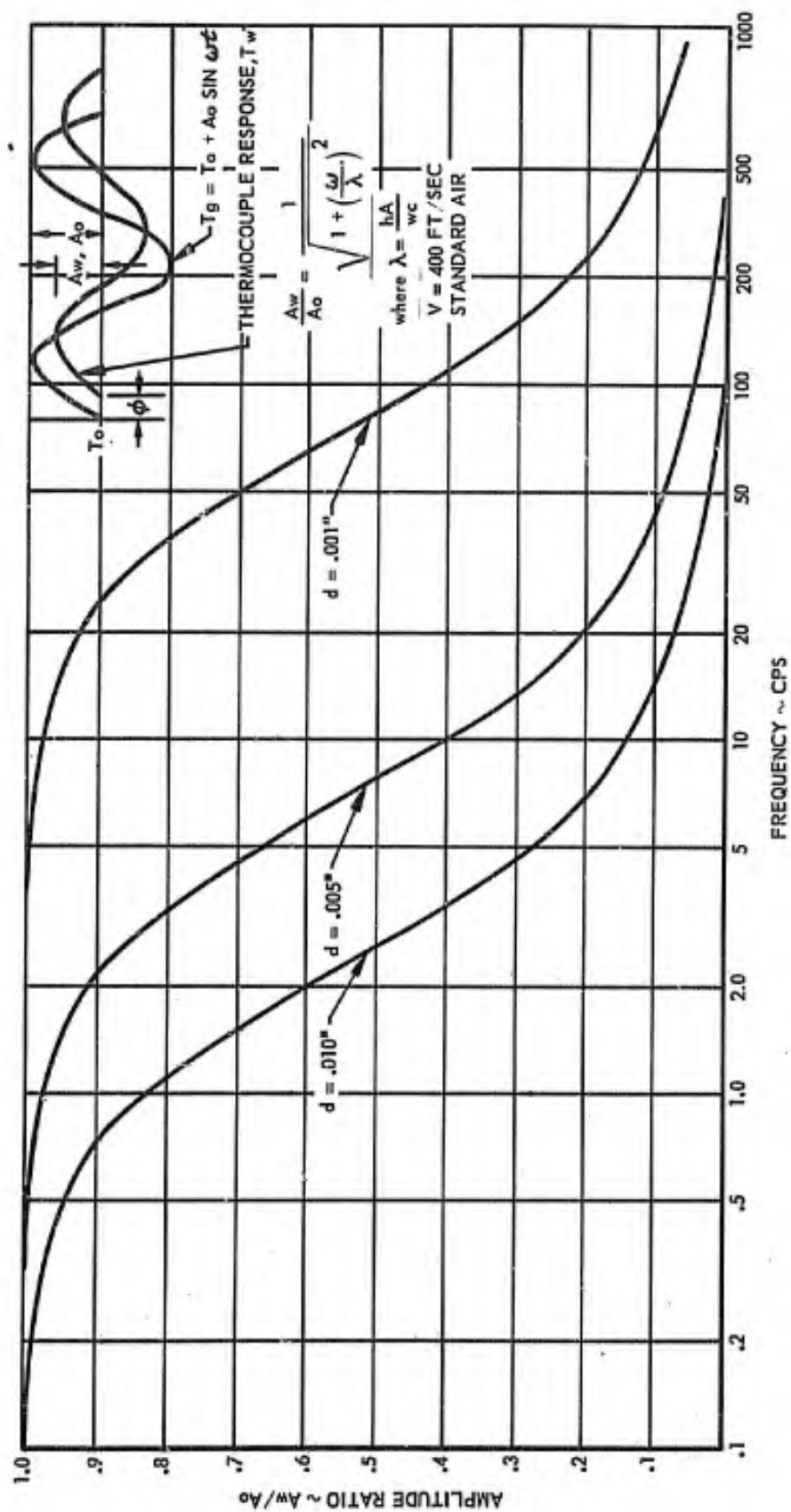| 6. REPORT DATE 14 February 1967	7a. TOTAL NO. OF PAGES 194	7b. NO. OF REFS 15
8a. CONTRACT OR GRANT NO. NOw 66-0316-f	**9a. ORIGINATOR'S REPORT NUMBER(S)**	
b. PROJECT NO. (Not Applicable)	NOR 67-32	
c.	**9b. OTHER REPORT NO(S)** *(Any other numbers that may be assigned this report)*	
d.	Not Applicable	

10. AVAILABILITY/LIMITATION NOTICES

Qualified requesters may obtain copies of this report from DDC

11. SUPPLEMENTARY NOTES	12. SPONSORING MILITARY ACTIVITY
(Not applicable)	U.S. Naval Air Systems Command

13. ABSTRACT A large-scale VTOL test bed designed around the Ames Lift Engine Pod was used for ground-proximity tests at the Ames Research Center VTOL test facility, under sponsorship of the Naval Air Systems Command. Objectives were to obtain parametric data on gas ingestion and jet effects experienced by jet-powered VTOL configurations. Results showed that ingestion and induced-lift effects are configuration-and time-dependent; for many configurations the degree of ingestion experienced cannot be tolerated in operational aircraft. This contrasts with results of recent small-scale tests. Wing geometry, size, location; engine arrangement; lift/cruise engine location and pitch attitude have strong influences on ingestion tendencies and jet-induced effects. Near-field temperature environment appears to be influenced by engine arrangement and number of operating engines. Rapid inlet temperature rise with a high temperature distortion at the compressor face sometimes resulted in engine stall. Hot gases expelled from the engine subsequent to stall occasionally caused stalling of adjacent engines. Large induced force levels and moments resulted from near-ground operation of many configurations. Positive-and negative-induced lift were measured. Aerodynamic suckdown results with a single jet-fundamental geometry configuration are in agreement with empirical correlation of small-scale tests. Results showed that transient measurements with rapid-response thermocouple and recording equipment needed for realistic assessment of VTOL environment and inlet temperature rise caused by ingestion.

DD FORM 1 JAN 64 1473

14. KEY WORDS	LINK A		LINK B		LINK C	
	ROLE	WT	ROLE	WT	ROLE	WT

INSTRUCTIONS

1. **ORIGINATING ACTIVITY:** Enter the name and address of the contractor, subcontractor, grantee, Department of Defense activity or other organization *(corporate author)* issuing the report.

2a. **REPORT SECURITY CLASSIFICATION:** Enter the overall security classification of the report. Indicate whether "Restricted Data" is included. Marking is to be in accordance with appropriate security regulations.

2b. **GROUP:** Automatic downgrading is specified in DoD Directive 5200.10 and Armed Forces Industrial Manual. Enter the group number. Also, when applicable, show that optional markings have been used for Group 3 and Group 4 as authorized.

3. **REPORT TITLE:** Enter the complete report title in all capital letters. Titles in all cases should be unclassified. If a meaningful title cannot be selected without classification, show title classification in all capitals in parenthesis immediately following the title.

4. **DESCRIPTIVE NOTES:** If appropriate, enter the type of report, e.g., interim, progress, summary, annual, or final. Give the inclusive dates when a specific reporting period is covered.

5. **AUTHOR(S):** Enter the name(s) of author(s) as shown on or in the report. Enter last name, first name, middle initial. If military, show rank and branch of service. The name of the principal author is an absolute minimum requirement.

6. **REPORT DATE:** Enter the date of the report as day, month, year; or month, year. If more than one date appears on the report, use date of publication.

7a. **TOTAL NUMBER OF PAGES:** The total page count should follow normal pagination procedures, i.e., enter the number of pages containing information.

7b. **NUMBER OF REFERENCES:** Enter the total number of references cited in the report.

8a. **CONTRACT OR GRANT NUMBER:** If appropriate, enter the applicable number of the contract or grant under which the report was written.

8b, 8c, & 8d. **PROJECT NUMBER:** Enter the appropriate military department identification, such as project number, subproject number, system numbers, task number, etc.

9a. **ORIGINATOR'S REPORT NUMBER(S):** Enter the official report number by which the document will be identified and controlled by the originating activity. This number must be unique to this report.

9b. **OTHER REPORT NUMBER(S):** If the report has been assigned any other report numbers *(either by the originator or by the sponsor)*, also enter this number(s).

10. **AVAILABILITY/LIMITATION NOTICES:** Enter any limitations on further dissemination of the report, other than those imposed by security classification, using standard statements such as:

  (1) "Qualified requesters may obtain copies of this report from DDC."

  (2) "Foreign announcement and dissemination of this report by DDC is not authorized."

  (3) "U. S. Government agencies may obtain copies of this report directly from DDC. Other qualified DDC users shall request through

     _____ ."

  (4) "U. S. military agencies may obtain copies of this report directly from DDC. Other qualified users shall request through

     _____ ."

  (5) "All distribution of this report is controlled. Qualified DDC users shall request through

     _____ ."

If the report has been furnished to the Office of Technical Services, Department of Commerce, for sale to the public, indicate this fact and enter the price, if known.

11. **SUPPLEMENTARY NOTES:** Use for additional explanatory notes.

12. **SPONSORING MILITARY ACTIVITY:** Enter the name of the departmental project office or laboratory sponsoring *(paying for)* the research and development. Include address.

13. **ABSTRACT:** Enter an abstract giving a brief and factual summary of the document indicative of the report, even though it may also appear elsewhere in the body of the technical report. If additional space is required, a continuation sheet shall be attached.

It is highly desirable that the abstract of classified reports be unclassified. Each paragraph of the abstract shall end with an indication of the military security classification of the information in the paragraph, represented as *(TS)*, *(S)*, *(C)*, or *(U)*.

There is no limitation on the length of the abstract. However, the suggested length is from 150 to 225 words.

14. **KEY WORDS:** Key words are technically meaningful terms or short phrases that characterize a report and may be used as index entries for cataloging the report. Key words must be selected so that no security classification is required. Identifiers, such as equipment model designation, trade name, military project code name, geographic location, may be used as key words but will be followed by an indication of technical context. The assignment of links, rules, and weights is optional.

GPO 886-551